Cajal-Retzius cells:

Investigations on cannabinoid type 1 receptor function in the Reelin signaling system

Dissertation

Zur Erlangung des Grades

“Doktor der Naturwissenschaften“

Am Fachbereich Biologie der

Jennifer Sitta

geb. am 14.7.1987 in Ludwigshafen am Rhein

Mainz, 2021

Dekan: Prof. Dr. Eckhard Thines

1. Berichterstatter:

2. Berichterstatter:

Tag der mündlichen Prüfung 22.9.22

Table of Contents

Summary

Cajal-Retzius cells are the first-born neurons in the developing cortex and arise from mostly three different regions: The neuroepithelium of the pallium, including the cortical hem and pallial septum, and the lateral region of the pallial-subpallial boundary. From these regions, they start to migrate tangentially from E10.5 on to cover the entire marginal zone of the cortex. By secreting the glycoprotein Reelin they can regulate the radial migration of pyramidal neurons and the formation of the six-layered cortex. Reelin acts as a stop signal for neurons arriving at the marginal zone via a cofilin-mediated mechanism. Most of these cells undergo apoptosis within the second postnatal week. Nearly at the same time of cortical development, the endocannabinoid (eCB) lipid signaling system with its major constituent, the cannabinoid type 1 receptor (CB1), evolves. CB1 has been shown to be another essential regulator of the cerebral cortex development. CB1 deficiency leads to reduced proliferation, premature stop of migration, and impaired differentiation of pyramidal neurons. Here we focus on the putative function of CB1 in Cajal-Retzius cells. In addition, there is an interesting aspect on the role of CB1 in the Reelin signal "receiving" pyramidal cells, as the downstream signaling cascades of CB1 and Reelin may converge at the level of cytoskeleton regulation, and CB1 is also expressed in pyramidal cells. As CB1 and Reelin are co-expressed to a certain extent in Cajal-Retzius cells during the time when the cerebral cortex develops its layered structure, this leads to the notion of a possible modulation of Reelin activity by CB1. During cortex development, CB1 is not only expressed in Cajal-Retzius cells but also in pyramidal neurons and interneurons.

One of the aims of this thesis was to clarify the function of CB1 within the Reelin-expressing Cajal-Retzius cells. To do so a Reelin Cre-mouse line was needed so that CB1 expression can specifically be modulated (inactivated or overexpressed) in the Reelin-expressing cell population. With the help of the CRISPR/Cas9 system, we were able to introduce a Cre-recombinase gene via homology directed repair into the genomic locus of the Reelin gene without interfering with proper Reelin function. The founders were analyzed via genotyping and sequencing for correct insertion of the HDR construct. To verify the correct function of Cre and Reelin, the Reelin-Cre mice were crossed with ROSA26-floxed-stop-YFP (yellow fluorescent protein) reporter mice. The transgenic offspring (Reelin $^{TG/wt}$ x ROSA 26-YFP $^{Stop\ fl/fl}$) showed YFP expression exclusively within Reelin and Cre expressing cells. Reelin expression was not altered in transgenic mice.

Further experiments with Reelin-Cre x CB1 fl/fl mice showed that CB1 RNA-expression was gone in mutant (Reelin-Cre-CB1 KO) mice and so confirmed the proper function of our newly created Reelin-Cre mouse line. Cortex layer analysis of Ctip2 and Satb2-expressing neurons could show an alteration

in neuronal migration and positioning in Reelin-Cre-CB1 KO mice when compared to Reelin-Cre-CB1 WT animals.

Zusammenfassung

Cajal-Retzius Zellen sind die ersten Neuronen, welche im sich entwickelnden Cortex des pränatalen Gehirns entstehen. Sie werden hauptsächlich an drei Stellen gebildet: Dem Neuroepithelium des Palliums, zu welcher der kortikale Saum und das palliale Septum gehören, und lateral an der pallialen-subpallialen Grenze (auch „anti-hem“ genannt). Am Entstehungsort beginnend, migrieren Cajal-Retzius-Zellen bereits bei einem embryonalem Alter von E10.5 tangential, um sich nach kurzer Zeit über die gesamte Marginalzone des Cortex anzusiedeln. Durch die Sekretion des Glykoproteins Reelin können Cajal-Retzius Zellen die radiale Migration der Pyramidalneuronen und die Formation des 6-schichtigen Cortex regulieren. Reelin agiert als ein Stopp-Signal für von der ventrikulären Zone zur Marginalzone heraufwandernde Neurone über einen Cofilin-vermittelnden Signalweg. Ein Großteil der Cajal-Retzius Zellen unterläuft innerhalb der ersten zwei Wochen nach der Geburt des Mausembryos Apoptose. Fast zur selben Zeit wie die Entwicklung von Cajal-Retzius-Zellen, entsteht das Endocannabinoid System mit seinen Hauptkomponenten, dem Cannabinoid-Rezeptor Typ 1 (CB1). CB1 ist ebenfalls ein essentieller Regulationsfaktor in der Entwicklung des cerebralen Cortex. Ein Mangel an CB1 führt zu einer verminderten Proliferationsrate, den verfrühten Stopp der Migration von Zellen und einer eingeschränkten Differenzierung der Pyramidalneuronen. Während der Cortexentwicklung wird CB1 nicht nur in Cajal-Retzius-Zellen, sondern auch in Pyramidalneuronen und Interneuronen exprimiert.

In dieser Arbeit fokussieren wir uns auf die mögliche Funktion von CB1 innerhalb der Cajal-Retzius Zellpopulation („Reelin Signal-sendende“ Zellen). Zusätzlich dazu gibt es interessante Aspekte der Rolle von CB1 auf die Reelin Signal-erhaltende Zelle, da “downstream” Signalkaskaden von Reelin und CB1 gemeinsame Funktion auf die Regulation des Zytoskeletts haben könnten. Während der Cortexentwicklung, genau zu der Zeit, in der sich die einzelnen Cortexschichten bilden, werden CB1 und Reelin in vielen Cajal-Retzius Zellen co-exprimiert. Dies führte zu der Annahme, dass die Wirkung von Reelin von CB1 beeinflusst werden könnte.

Ziel dieser Arbeit war es, die Funktion von CB1 innerhalb der Reelin-exprimierenden Cajal-Retzius Zellpopulation nachzuweisen. Dafür wurde eine Reelin-Cre Mauslinie benötigt, sodass die CB1 Expression Reelin spezifisch inaktiviert oder überexprimiert werden kann. Mit Hilfe des CRISPR/Cas9 Systems ist es in dieser Arbeit gelungen ein Gen für Cre-Rekombinase über homologe Rekombination

in den Reelin Lokus einzuführen, ohne dabei die Funktion des Reelin Gens zu stören. Die Gründermäuse wurden mittels Genotypisierung und DNA-Sequenzierung auf korrekte Insertion des Rekombinationskonstrukts überprüft. Um die einwandfreie Funktion von Reelin und Cre in der Reelin-Cre Maus zu überprüfen, wurde diese mit einer ROSA26-floxed-stop-YFP (yellow fluorescent protein) Reporterlinie gekreuzt. Die transgenen Nachkommen (Reelin $^{TG/wt}$ x ROSA 26-YFP $^{Stop\ fl/fl}$) haben gezeigt, dass YFP exklusiv in Reelin und Cre exprimierenden Zellen vorkommt. Die Reelin-Expression selbst hat sich in diesen Mäusen nicht von den unveränderten Wild-Typ Mäusen unterschieden. Fortführende Experimente mit Reelin-Cre x CB1 fl/fl Mäusen zeigten, dass die CB1-RNA Expression in mutanten Mäusen (Reelin-Cre-CB1 KO) nicht mehr nachzuweisen war, was beweist, dass die Cre-Expression der Reelin-Cre Linie ausreichend ist, um die Expression von CB1 vollständig auszuschalten. Weitergehende Experimente bezüglich der Positionierung der Zellen innerhalb der Cortexschichten zeigten, dass das Migrationsverhalten von Satb2- und Ctip2-exprimierenden Zellen verändert ist und somit ein wahrscheinlicher Einfluss von CB1 in der Reelin-exprimierenden Cajal-Retzius Zellpopulation auf das Positionierungsverhalten neu entstehender Neuronen besteht.

List of abbreviations

Δ^9-THC	Δ^9-Tetrahydrocannabinol
2-AG	2-Arachidonoylglycerol
AEA	N-Arachidonoylethanolamine/ Anandamide
ApoER2	Apolipoprotein E receptor 2
BSA	Bovine serum albumin
BrdU	5-Bromo-2'-deoxyuridine
Cas9	CRISPR associated protein9
CB1	Cannabinoid type 1 receptor
CB2	Cannabinoid type 2 receptor
CNS	Central nervous system
CRc	Cajal-Retzius cells
Cre	Causes recombination
CRISPR	Clustered regularly interspaced short palin-dromic repeat
crRNA	CRISPR ribonucleic acid
CRKL	Crk-like protein
CP	Cortical plate
Ctip2	COUPTF-interacting protein2
Cy3	Cyanine 3
Dab1	Disabled-1
DAPI	4’,6-Diamidino-2-phenylindole
DAGL	Diacylglycerol lipase
DIG	Digoxigenin
DMEM	Dulbeccos’s modified Eagle’s medium
DNA	Deoxyribonucleic acid
DP	Dorsal pallium
Dpc	Days post coitum
DSB	Double strand break
DTT	Dithiothreitol

E	Embryonic day (days after fertilization)
eCB(s)	Endocannabinoid(s)
E.coli	Escherichia Coli
EDTA	Ethylenediaminetetraacetic acid
EGF	Epidermal growth factor
ERK1/2	Extracellular signal-regulated kinase 1/2
ES cells	Embryonic stem cells
EtOH	Ethanol
FAAH	Fatty acid amide hydrolase
FBS	Fetal bovine serum
FCS	Fetal calf serum
FITC	Fluorescein isothiocyanate
Fyn	Proto-oncogene tyrosine-protein kinase
GABA	γ-Aminobutyric acid
GDP	Guanosine diphosphate
GE	Ganglionic Eminence
eGFP/GFP	(enhanced) Green fluorescent protein
GPCRs	G-coupled receptors
gRNA	Guide ribonucleic acid
GSK3β	Glykogensynthase-3β
GTP	Guanosine triphosphate
HA	Hemagglutinin
HCl	Hydrogen chloride
HDR	Homology directed repair
HeNe	Helium–neon laser
HEK	Human embryonic kidney
Iap gene	Alkaline phosphatase isozyme gene
IRES	Internal ribosomal entry site
ISH	*In situ* hybridization

IZ	Intermediate zone
LB	Lysogeny broth
LIF	Leukemia inhibitory factor
LIMK	Lim kinase
LIS1	Lissencephaly 1
LGE	Lateral Ganglionic Eminence
loxP	locus of crossover [x] in P1 bacteriophage
LP	Lateral pallium
MAPK	Mitogen-activated protein kinase
MAGL	Monoacylglycerol lipase
MEF	Mouse Embryonic Fibroblasts
MGE	Marginal Ganglionic Eminence
MP	Medial pallium
mRNA	Messenger ribonucleic acid
mTOR/mTORC	mammalian target of rapamycin/ mammalian target of rapamycin complex1
MZ	Marginal zone
NaCl	Natriumchlorid
NAPE-PLD	N-Acylphosphatidyletanolamine
NHEJ	Non-homologous end joining
NLS	Nucleus localization signal
NP	Neural progenitor
NTP	Nucleoside triphosphate
NudE	Nuclear distribution protein nudE homolog
PAM	Protospacer adjacent motif
PBS	Phosphate-buffered solution
pBS-KS	pBluescript- Ks
PCR	Polymerase Chain Reaction
PE	Perkin Elmer
PFA	Paraformaldehyde

PIK3	Phosphoinositide 3-kinase
PKB	Protein kinase B
PNS	Peripheral nervous system
PP	Preplate
POA	Preoptic area
POD	Peroxidases
RG	Radial glia
RNA	Ribonucleic acid
RNP	Ribonucleoprotein
ROI	Region of interest
Satb2	Special AT-rich sequence-binding protein 2
SCPN	Subcortical projection neurons
SDS-PAGE	Sodium dodecyl sulphate–polyacrylamide gel electrophoresis
sgRNA	Single guide ribonucleic acid
SP	Subplate
Src	Non-receptor tyrosine kinase protein that in humans is encoded by the SRC gene
SSC	Standard saline citrate
SVZ	Subventricular zone
Tbr1	T-box gene 1
TBS	Tris-buffered saline
TNT	Tris-NaCl-Tween buffer
tracrRNA	Trans-activating crispr RNA
UTP	Uridine-5′-triphosphate
VLDLR	Very-low-density-lipoprotein receptor
VZ	Ventricular zone
WT	Wild-type
YFP	Yellow fluorescent protein

1 Introduction

1.1 Development of the cortex

The cerebral cortex brain region, one part of the telencephalon, is responsible for cognitive function, sensory perception and consciousness, abilities which make it undergo a considerable expansion and development during evolution (Finlay & Darlington, 1995). The largest cortical region, the neocortex, forms a six-layered structure consisting of neurons, astrocytes, oligodendrocytes, blood vessels and ependymal cells (Cajal, 1891). The two major types of cortical neurons are GABAergic (γ-aminobutyric acid)-interneurons and glutamatergic pyramidal projection neurons. Whereas interneurons make local connections, projection neurons extend their axons to distant intracortical, subcortical and subcerebral targets. Projection neurons have a pyramidal morphology and are generated from progenitors in the dorsal telencephalon (Anderson, 2002; Gorski et al., 2002; Rakic, 1972; Tan et al., 1998; Ware et al., 1999). GABA containing interneurons are mostly generated from progenitors in the ventral telencephalon, in subpallial regions defined as the ganglionic eminence (GE) and preoptic area (POA) (Gelman & Marín, 2010). They can migrate long distances within the neocortex (Wonders & Anderson, 2006).

Distinct populations of projection neurons, located in different neuronal layers have unique morphology features, express different complements of transcription factors and serve different functions, making the neocortex a complex structured tissue.

1.1.1 Cortical lamination

The cortical lamination occurs between embryonic days E10.5 and E17.5 in mice (Angevine & Sidman, 1961; Rakic, 1974; Rakic & Caviness, 1995a). The neocortex is part of the dorsal pallium and one of the earliest developed parts of the mouse brain. Precise connections are essential for proper brain function. Cortical layers are created by neurons, which exit the cell cycle and migrate to differentiate into distinct neuronal phenotypes (Rakic, 1974). Neurons migrate mainly radially but also tangentially. Radial migration is favored by cortical projection neurons, which migrate along radial glia cells, whereas interneurons migrate mostly tangentially (Hatanaka et al., 2016).After migratory processes have finished, radial glia cells become neuronal progenitors (neocortex), astrocytes (cerebral cortex), or Bergmann-glia (cerebellum) (Hatten, 1999). During early neocortical development stages, projection neurons can also extend their leading processes to the marginal zone and then shorten their leading processes to move their cell bodies to their final position in a radial glia-independent manner. This migration mode is called “somal translocation” (Nadarajah & Parnavelas, 2002).

Locomotion, the radial glia-dependent migration mode, is used by neurons that directionally migrate towards the brain surface. When these neurons reach the primitive cortical zone, the outermost cell-dense region of the cortical plate, they switch into “terminal translocation” mode (Sekine et al., 2012), in which the somata move in a radial glia-independent manner to reach their position beneath the marginal zone (MZ).

At the beginning of cortical development, the earliest born neurons are generated in the ventricular zone (VZ) and migrate to form a layer of differentiated neurons above the VZ, the preplate (PP). Cajal-Retzius cells (CRc) and subplate neurons populate the preplate forming the intermediate zone, which separates the preplate from the proliferative zone. At the same time migrating neurons create the cortical plate, which split the preplate into two layers forming the superficial marginal zone (MZ) and the deep subplate. Whereas Cajal-Retzius cells remain near the pial surface in the MZ, successive waves of migrating neurons form layers within the CP (Fig. 1).

At E13.5, an additional proliferation layer, the subventricular zone (SVZ), forms above the VZ and expands during late corticogenesis. Projection neurons are glutamatergic pyramidal neurons, which are generated from progenitors in both VZ and SVZ in a temporal order between E11.5 and E17.5 of mouse embryonic development. Newborn neurons migrate radially from the VZ, pass through the subplate and stop at the marginal zone to form the cortical plate (CP), which later will give rise to the multilayered cortex. The cortical layers form the six-layered cortex in an inside out manner, which means that later born neurons migrate through earlier born neurons (Angevine & Sidman, 1961; Rakic, 1974).

In a differentiation gradient, neurons migrate radially along radial glia to form the layers VI, V, IV, III/II, to which layer III/II is the closest to the surface (Fig. 2). Neurons migrate through the former layers until they are stopped at the marginal zone by the Reelin signal secreted by CRc (Soriano & Del Río, 2005).

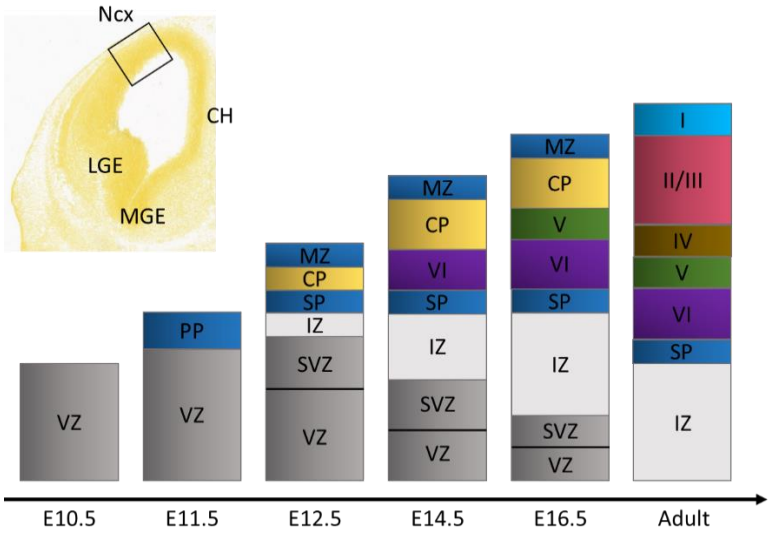

Figure 1 Schematic overview of how progenitors produce projection neurons in an "inside-out" manner.
The earliest born neurons are generated in the ventricular zone (VZ), where they migrate out to form the preplate (PP). The PP later splits into the outer marginal zone (MZ) and the lower subplate (SP) with the cortical plate (CP) in between. Upcoming neurons from the VZ migrate through earlier born neurons and stop at the CP to form the inside-out-pattern. The intermediate zone (IZ), the subventricular zone (SVZ) and the VZ later form the white matter. MGE: marginal ganglionic eminence, LGE: lateral ganglionic eminence, Ncx: Neocortex, CH: Cortical Hem. (Overview image from Allen brain atlas: https://developingmouse.brain-map.org/experiment/siv?id=100074513&imageId=101243192&initImage=hp_yellow).

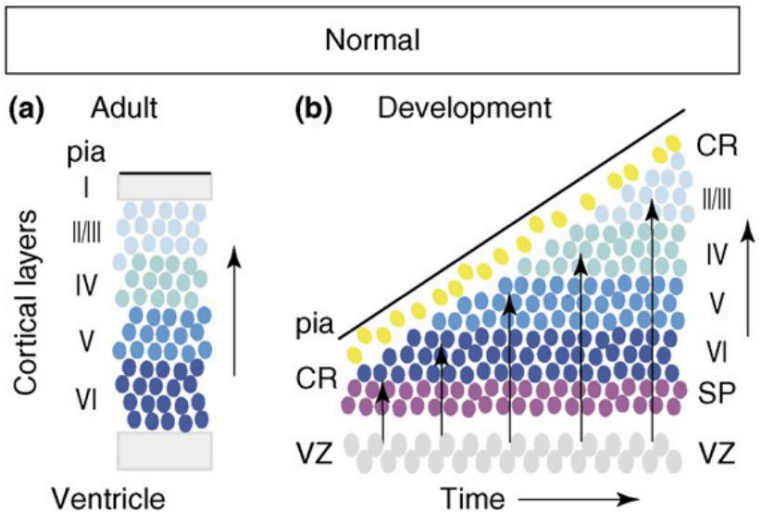

Figure 2 Development of the cortex layers.
Mechanism for inside-out lamination in the neocortex. (a) The cortical plate is divided into six layers (I-VI) counted from the uppermost pial surface to the inner ventricular zone. In between the plates, the projection neurons generated in the VZ migrate towards the pial surface. (b) The temporal development of the layers shows that projection neurons are generated in the ventricular zone and migrate towards the pial surface until they reach the uppermost layer, also called molecular layer, containing the Reelin-expressing Cajal-Retzius cells. To form the typical inside-out-pattern, later generated neurons migrate through earlier born neurons. CR cells (yellow) as well as subplate cells (SP, purple) degenerate after birth and are not shown in (a) anymore. (Figure from Cooper, 2008).

1.1.2 Cortex layer markers

For a better understanding of the mechanisms that control the differentiation and migration of neurons, several transcription factors have been implicated in the development of specific cell types in the cortex (Chenn et al., 2009; Rubenstein et al., 1999) of which some are expressed in specific laminar patterns. Below, the essential layer markers are presented:

The T-Box-gene Tbr1 is a transcription factor that is expressed soon after cortical progenitors begin to differentiate. It is expressed in glutamatergic early-born cortical neurons which are located in the preplate and in layer 6 (Bulfone et al., 1995, 1998; Hevner et al., 2001). The high expression of Tbr1 in the preplate suggests a role in cortical development. As Tbr1 mutants have a reduced expression of Reelin, developmental abnormalities in the laminar organization of the neurons and the guidance of cortical axons, Tbr1 seems to be essential for the differentiation of Cajal-Retzius cells and the developmental roles of early-born cortical neurons (Hevner et al., 2001).

Special AT-rich sequence-binding protein 2 (Satb2) and COUPTF-interacting protein2 (Ctip2) act in the development of the major classes of projections neurons. Satb2 is a transcription factor that is expressed in young upper-layer neurons, located in layer IV-II (Britanova et al., 2008). It regulates chromatin remodeling and gene expression via the interaction with genomic nuclear matrix attachment regions. In the neocortex it is required for the development of callosal and subcortical projection neurons (Alcamo et al., 2008; Britanova et al., 2008; Leone et al., 2015; McKenna et al., 2015).

Ctip2 is a transcription factor, which controls the appropriate differentiation of subcortical projection neurons (SCPN). SCPN are normally located in layer V and show strong defects in axon outgrowth, fasciculation, and pathfinding in the absence of Ctip2 (Greig et al., 2013).

The two proteins have opposite effects since Satb2 prevents the activity of Ctip2 but still, they are sometimes co-expressed (Alcamo et al., 2008; Baranek et al., 2012; Britanova et al., 2008; Leone et al., 2015). The co-expressing cells are subpopulations, which either project to the brainstem or the contralateral cortex and have unique molecular, morphological and electrophysiological features (Harb et al., 2016).

1.2 Cajal-Retzius cells

Cajal-Retzius cells belong to the earliest born neurons during cortical development. This cell type was discovered by two scientists Santiago Ramón y Cajal and Gustav Retzius at two different times, in 1891 and 1893 in different species. They were described as fusiform, flat cells located close to the

outer surface with long dendritic processes that extend towards the pia mater (Cajal SR, 1891). In addition, Cajal-Retzius cells were also found in the developing hippocampus (Soriano et al., 1994). Cajal-Retzius cells are characterized by their mostly transient appearance in the uppermost layer of the developing cerebral cortex and their expression of the extracellular matrix protein Reelin. Based on location in the most superficial layer, their characteristic shape (Fig. 3), and their expression of Reelin, Cajal-Retzius cells can be found in many species, extending from amniotes to mammals (Aboitiz & Montiel, 2007). Cajal-Retzius cells derive from at least three cortical regions: the caudomedial cortical hem, the pallial-subpallial boundary, and the pallial septum.

Figure 3 Original drawing of Cajal-Retzius cells.
Slender horizontal bipolar cells were described in the developing marginal zone of lagomorphs by Santiago Ramón y Cajal in 1891. Gustav Retzius found a similar cell type in humans and other mammals two year later in 1893 (Retzius, 1893, 1894). Therefore these cells were then termed as Cajal-Retzius cells.

1.2.1 Reelin

Reelin is an extracellular matrix molecule that is synthesized and secreted by Cajal-Retzius cells into the extracellular matrix of the cortical marginal zone (D'Arcangelo et al., 1995, 1997). From E18.5 on also interneurons start to secrete Reelin (Alcántara et al., 1998; Drakew et al., 1997). The 460 kDa large molecule consists of eight epidermal growth factor (EGF)-like repeats (350-390 amino acids/repeat), a sequence homology to F-spondin near the N-terminus and a C-terminal region with positively charged amino acids (D'Arcangelo et al., 1997; De Bergeyck et al., 1997). Whereas the C-terminal region is important for the secretion of Reelin, the N-terminal region is needed for homodimerization and signaling induction (Kubo et al., 2002). There are two known isoforms (320 kDa and 180 kDa), produced by alternative splicing (D'Arcangelo et al., 1999; Lambert De Rouvroit et al., 1999). Reelin is crucial for the correct positioning of neurons during cerebral cortex development and therefore for the formation of cortical layers during development (Cooper, 2008; D'Arcangelo et al., 1999; Förster et al., 2006; Frotscher, 1998; Rakic & Caviness, 1995a; Soriano & Del Río, 2005; Tissir & Goffinet, 2003).

The mouse mutant "*reeler*" revealed the function of Reelin. The lack of Reelin in this mutant causes ataxia and neuronal migration defects in neocortex, hippocampus, and cerebellum (D'Arcangelo et al., 1995; Hirotsune et al., 1995; Rice & Curran, 2001). It could be shown that cortical layers are roughly inverted in this mouse mutant (Fig. 4) (Boyle et al., 2011; Caviness & Sidman, 1973;

D'Arcangelo et al., 1995; Mikoshiba et al., 1980; Ogawa & Miyata, 1995), suggesting that Reelin regulates the inside-out formation of the mammalian neocortex. In *reeler* mice neurons of the cortical plate fail to split the preplate, resulting in a superficial "superplate" (Caviness & Sidman, 1973; Caviness, 1982). Arriving neurons accumulate beneath the superplate and fail to find their right position. This leads to the result that the positions of the major classes of neurons are inverted in cerebral cortex (Caviness, 1982). More recent studies rather describe a more disorganized pattern with intermingled cortical neurons, which fail to place themselves and form patterns depending on cortical area (Boyle et al., 2011; Dekimoto et al., 2010; Pielecka-Fortuna et al., 2015; Wagener et al., 2010). This leads to the assumption that Reelin is controlling somal translocation via regulation of the actin cytoskeleton and cellular adhesion through two possible pathways: The LIMK1 activation leads to n-cofilin phosphorylation which then promotes anchoring of leading processes to marginal zone(Chai et al., 2009). The second pathway may influence the cell adhesion through neuronal cadherin, N-cadherin (Franco et al., 2011).

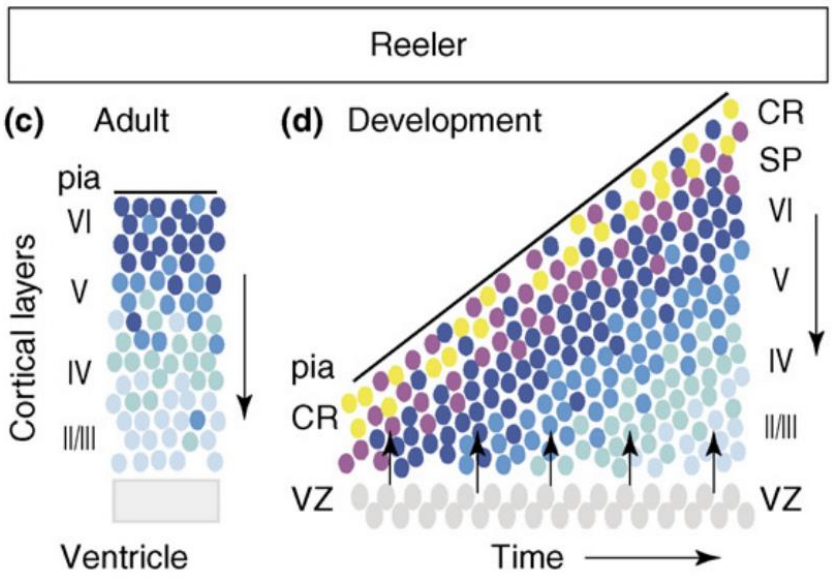

Figure 4 Formation of cortex layer in *reeler*-mutants.
(a) The cortical layer in *reeler*-mutants are inverted. (b) During development the preplate fails to split into MZ and SP and the CP cannot be formed. The migrating cells from the VZ are not able to migrate through the earlier born neurons and cannot stop at the uppermost layer. They build an inverted layer order (Figure from Cooper, 2008).

1.2.2 Reelin signaling pathway

Reelin can bind to two lipoprotein receptors, apolipoprotein E receptor 2 (ApoER2) and very-low-density lipoprotein receptor (VLDLR), expressed by radial glial cells and newborn neurons migrating to the cortical plate (D'Arcangelo et al., 1999; Rice et al., 1998; Rice & Curran, 2001; Tissir & Goffinet,

2003). Through the binding, the extracellular Reelin-signal leads to the phosphorylation of the adaptor protein disabled-1 (Dab1) by non-receptor tyrosine kinases (Fyn (Proto-oncogene tyrosine-protein kinase) or Src (Non-receptor tyrosine kinase protein that in humans is encoded by the SRC gene)). Several intracellular signaling cascades can so get activated (Arnaud et al., 2003; Bock & Herz, 2003; Howell et al., 1999). Double knock-out of ApoER2 and VLDLR or deficiency in Dab1 expression show *reeler*-like phenotypes (Kojima et al., 2000; Sheldon et al., 1997; Sweet et al., 1996; Trommsdorff et al., 1999; Ware et al., 1997; Yoneshima et al., 1997). If only one receptor is missing, the structural defects are less prominent assuming that both receptors have different effects after Reelin-binding (Bock & Herz, 2003; Hack et al., 2007).

The binding of Reelin to ApoER2 initiates a pathway where phosphatidylinositol-3-kinase (PI3K), protein kinase B (PKB/Akt), and LIM-kinase 1 (LIMK-1) activation, leading to phosphorylation of n-cofilin (Bock & Herz, 2003). Cell migration requires changes in cell shape and therefore a re-organization of the actin cytoskeleton, which involves assembly and disassembly of F-actin mediated by actin-associated proteins. Cofilin is an actin-depolymerizing protein that promotes the disassembly of F-actin and thereby controls the structural rearrangement at extending cell processes and directional cell movement (Jovceva et al., 2007; Kiuchi et al., 2007). Phosphorylation of cofilin at serine3 mediated through LIM-kinase 1 (LIMK1) (Arber et al., 1998; Yang et al., 1998) will end the actin-depolymerizing activity. Actin dynamics and process elongation are inhibited and as a result, the cytoskeleton becomes stabilized (Nagaoka et al., 1996; Zebda et al., 2000) and cell migration is terminated.

The activation of PKB/Akt inhibits Glykogensynthase-3β (GSK3β), decreases the phosphorylation of the Tau-protein and therefore stabilizes the microtubule. Interaction of CRK-like (CRKL) with tyrosine-phosphorylated dab1, induces the phosphorylation of C3G which mediates, as guanine nucleotide exchange factor, the transformation of Rap1-GDP to Rap1-GTP. This finally leads to changes within the actin cytoskeleton causing the splitting of the preplate (Voss et al., 2008) (Fig. 5).

Binding of Reelin to VLDLR, however leads to intracellular binding to the adaptor protein lissencephaly1 (Lis1) (Assadi et al., 2003), which is linked to the microtubule-cytoskeleton through the proteins NudE-like (Nudel), NudE, and dynein (McKenney et al., 2010). Mutations in the Lis1 coding gene Pafah 1b (Zhang et al., 2007) cause disordered radial migration and therefore lissencephaly.

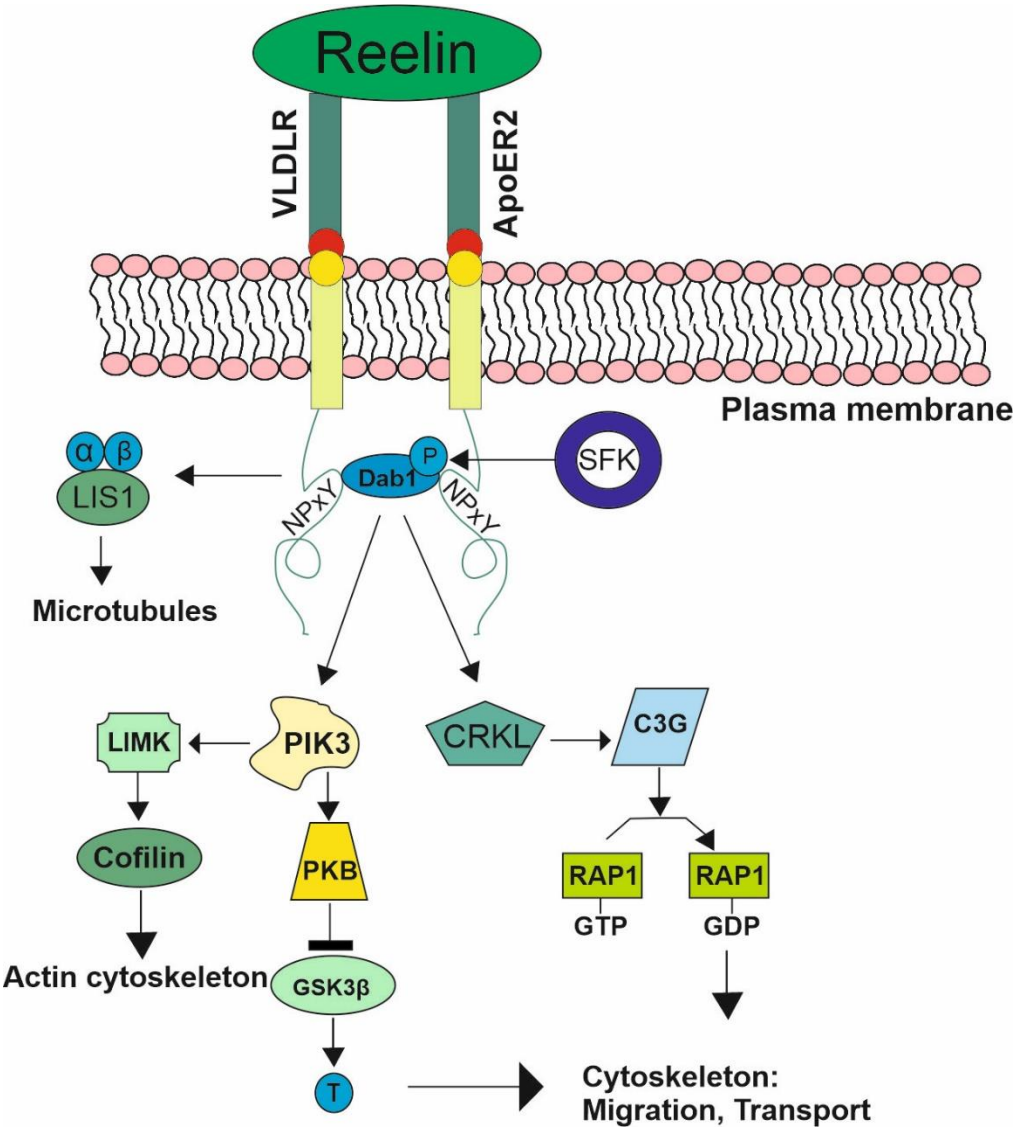

Figure 5 Scheme of the Reelin-signaling cascade.
Reelin interacts with the transmembrane receptors VLDLR and ApoER2 located on migrating neurons. By the binding of Reelin to its receptors, the kinase activity of receptor-associated SRC-family kinases (SFKs) is activated. This activation phosphorylates dab1, which then interacts with NPxY-motifs of both receptors leading to the possibility to activate many other signaling cascades. Through the activation of phosphatidylinositol-3-kinase (PIK3) and LIM-kinase, cofilin can be phosphorylated and therefore the cytoskeleton gets stabilized (Beffert et al., 2005; Bock & Herz, 2003). The activation of protein kinase B (PKB) inhibits Glykogensynthase-3β (GSK3β), which decreases the phosphorylation of the Tau-protein and therefore stabilizes the microtubule. Interaction of CRK-like (CRKL) with tyrosine-phosphorylated dab1, induces the phosphorylation of a guanine nucleotide exchange factor, C3G, which mediates the transformation of Rap1-GDP to Rap1-GTP. This finally leads to changes within the actin cytoskeleton causing the splitting of the preplate (Voss et al., 2008). Another dab1 binding partner is lissencephaly1 (LIS1), which influences microtubule dynamics (Assadi et al., 2003; Piomelli, 2003). (adapted from Herz and Chen (Herz & Chen, 2006)).

1.3 The endocannabinoid system (ECS)

1.3.1 History of cannabinoids

The origin of the plant *cannabis sativa* can be found 12,000 years ago in central Asia, where it was cultured by settlers as a source for fibers, food, medicine, and recreation (Merlin, 2003). 4000 years ago the movement of nomadic tribes spread the plant to the rest of the world. In the 17th century, it reached South America and from there, North America through Mexico in the 20th century.

Endocannabinoid research started in 1964 with the discovery of Δ^9-tetrahydrocannabinol (Δ^9-THC, Fig. 6), the main psychoactive compound in the cannabis sativa plant (Gaoni & Mechoulam, 1964). More than 500 molecules have been identified in *C.sativa*, from which 131 belong to the group of cannabinoids.

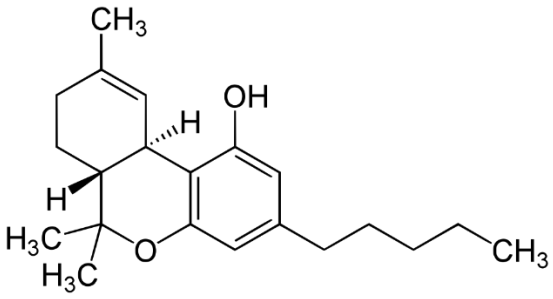

Figure 6 Molecular structure of Δ^9-THC.

The mechanism, how it acts on the brain, remained unknown until the identification of the cannabinoid type 1 receptor (CB1) 25 years later (Howlett et al., 1986; Matsuda et al., 1990). Three years later the cannabinoid type 2 receptor (CB2) was discovered (reviewed in Mechoulam & Parker, 2013). It became clear that CB1 is one of the most abundant G coupled receptors (GPCRs) in the central nervous system (CNS) and is expressed in the peripheral nervous system (PNS) and other peripheral tissues. The CB2 receptor, however, is mainly expressed in immune cells (Malfitano et al., 2014). With the discovery of the receptors, it became clear that endogenous substances, named endocannabinoids (eCB), exist. In 1992 and 1995 two lipophilic substances were isolated: arachidonoyl ethanolamide (anandamide (AEA)) (Devane et al., 1992) and 2-arachidonoyl glycerol (2-AG) (Mechoulam et al., 1995). The two eCBs are derivatives of the membrane lipid component arachidonic acid (Katona & Freund, 2012). To synthesize and degrade eCBs several different enzymes are involved in the system. N-acylphosphatatidyl-ethanolamine-specific phospholipase D (NAPE-PLD) synthesizes AEA and fatty acid amide hydrolase (FAAH) degrades it (Kano et al., 2009). 2-AG is synthesized by two isoforms of diacylglycerol lipase α and β (DAGLα, -β) and is degraded by monoacylglycerol lipase (MAGL)(Kano et al., 2009).

1.3.2 The CB1 receptor

The CB1 receptor is a G-coupled transmembrane domain receptor, which is primarily located in the central and peripheral nervous system. G-coupled receptors are cell surface receptors, which detect molecules outside the cell and can activate cellular responses there. In the brain, CB1 receptor is expressed mainly in the basal forebrain, cortex, hippocampus, striatum, amygdala, and some nuclei of the thalamus and hypothalamus. So the endogenous cannabinoid system is involved in the capacity of remembering, learning, cognition, pain reception, emotional states, motoric activity, protection against inflammation of neurons, and energy balance (Childers & Breivogel, 1998; Di Marzo et al., 1998; Howlett, 1995; Massa et al., 2004; Mechoulam et al., 1994; Pertwee, 1997; Richard et al., 2009). In the adult brain, CB1 is expressed in glutamatergic (Domenici et al., 2006; Kawamura et al., 2006; Monory et al., 2006; Takahashi & Castillo, 2006) as well as in a subpopulation of GABAergic neurons (Katona et al., 2001; Marsicano & Lutz, 1999).

1.3.3 The endocannabinoid system in development

Neurogenesis during embryonic brain development is orchestrated by many processes including the action of extracellular signaling systems. The signaling systems provide the necessary information for proliferation and differentiation of cells. An important factor during these developmental processes is the endocannabinoid-system, which controls embryonic neuronal development and maturation. CB1 regulates together with locally produced eCBs the neuronal progenitor (NP) proliferation, pyramidal specification and axonal navigation. Further, eCBs act as an axonal growth cone signal to regulate interneuron morphogenesis.

The CB1 receptor is expressed very early in embryonic development, beginning with its expression in the pre-implantation mouse embryo (Paria & Dey, 2000), where CB1 arrests the cannabinoid-induced embryonal growth (Paria & Dey, 2000; Schmid et al., 1997; Yang et al., 1996). In trophoblast stem cells, endocannabinoids are involved in cell proliferation and differentiation (Sun & Dey, 2008). The CB1 receptor is expressed along with CB2 receptor during blastocyst stage, and they are involved in embryonic stem-derived hematopoietic cell proliferation and lineage differentiation (Jiang et al., 2007). A remarkable thing about CB1 receptor expression during neuronal development in mammals is that it is expressed in white matter areas before birth and the expression levels in grey matter areas increase until adulthood (Berrendero et al., 1998). At the time of this atypical expression of CB1 receptor in brain development, active neurogenesis and axonal migration occur. The CB1 receptor signaling seems to be different to their regulatory role of neurotransmitter release and neuronal activity.

During development of the central nervous system, the endocannabinoids AEA, 2-AG and the psychoactive component of *cannabis sativa* THC, can target on neuronal progenitors (Arévalo-Martín et al., 2007; Molina-Holgado et al., 2007) , immature neurons (Berghuis et al., 2005, 2007; Mulder, Aguado, Keimpema, Baraba, et al., 2008) and glia (Aguado et al., 2006; Molina-Holgado et al., 2002). Endocannabinoids are involved in many processes throughout brain development including neural progenitor proliferation (Aguado, 2005)differentiation (Harkany et al., 2008), neuronal migration (Díaz-Alonso et al., 2017), and axonal growth cone directionality (Gaffuri et al., 2012; Oudin et al., 2011; Watson et al., 2008). Many processes involving eCB in brain development are not understood so far but divergent roles of eCB signaling in the developing brain can be suggested as its activity controls fundamental developmental processes. Endocannabinoids can induce cell migration by interacting with other signaling systems, including neurotrophins (Berghuis et al., 2005), growth factors (Preet et al., 2008) and inflammatory cytokines (Rajesh et al., 2007).

2-AG and AEA mediate the proliferation of neuronal progenitors in the VZ/SVZ and control the radial migration of these immature pyramidal cells to their destined regions in the cortex. CB1 receptor deletion leads to a significant reduction of neural progenitor proliferation rate in the VZ/SVZ and the migration of a neural progenitor population is arrested in deep cortical layers (Mulder, Aguado, Keimpema, Baraba, et al., 2008).

In the ganglionic eminence (GE), the endocannabinoid signal regulates tangential migration of cortical neuronal progenitors. They are guided to their positions in the neocortex and the hippocampus, where they differentiate into interneurons (Berghuis et al., 2005). All along their migratory route through the telencephalon, they may be influenced by Reelin and CB1 interaction (Morozov et al., 2009) as Reelin and CB1 share some signaling pathways. Just like Reelin, CB1 influences the PIK3/Akt signaling, which inhibits the activity of glycogen-synthase-kinase-3-beta (GSK3β) and therefore stabilizes microtubule (Bromberg et al., 2008; Hall & Lalli, 2010). At the same time, activation of PIK3/Akt stimulates the MAP-kinase (ERK1/2) signaling pathway, which influences the formation of the cytoskeleton by activating Raf (Derkinderen et al., 2003; Klemke et al., 1997). CB1 also stabilizes the cytoskeleton through the LIMK pathway and the phosphorylation of cofilin. Small GTPases, like Rap, Rac, and Rho, can influence the formation of the cytoskeleton and the control of cell adhesion (Hall & Lalli, 2010) (Fig. 7).

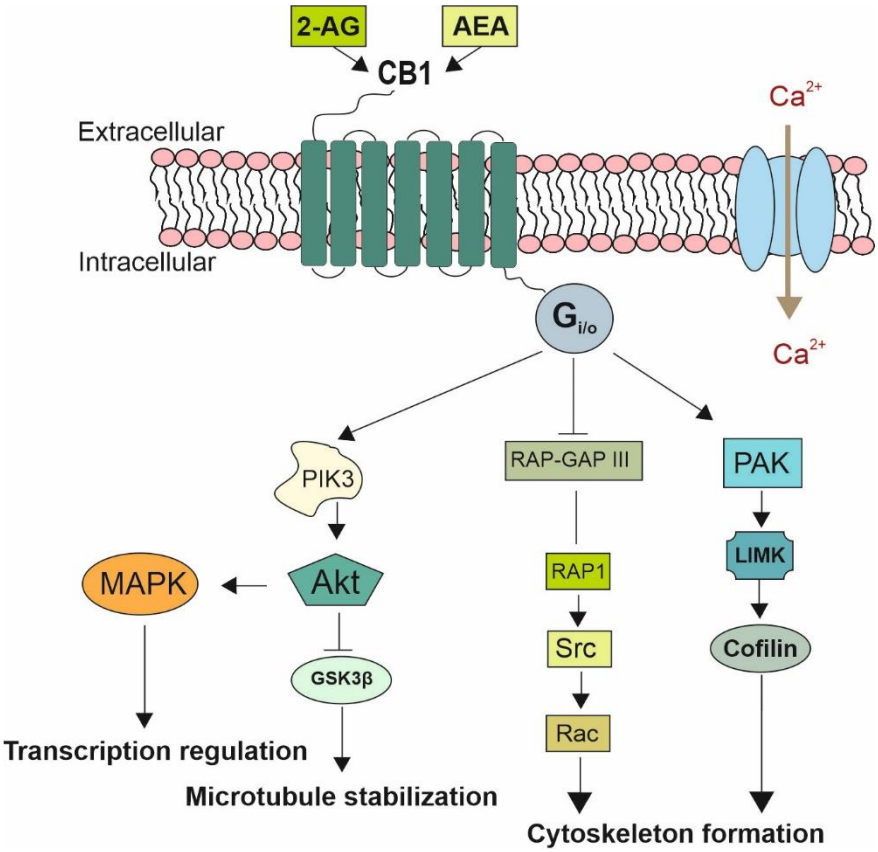

Figure 7 Overview of eCB signaling pathway during neuronal migration.
Binding of eCB to the $G_{i/o}$-coupled CB1-receptor triggers stimulation of pathways influencing neuronal migration. Activation of the CB1 receptor stimulates Phosphoinositid-3-kinase (PIK3)/AKT signaling, which then inhibits the activity of Glycogensynthase-3-beta (GSK3β) resulting in microtubule stabilization. PI3K/AKT can also stimulate mitogen-activated protein kinase (MAPK) signaling pathway which has direct effects on cytoskeletal remodeling and indirect effects via transcriptional regulation. Through $G_{i/o}$-mediated degradation of the Rap GTPase activated protein (GAP) Rap-Gap II, the Rap-Src-Rac signaling cascade is activated. Small GTPases (Rap1/Rac/Rho) are crucial molecular switches and their activation controls adhesion and promotes cytoskeleton remodeling. P21-activated kinase (PAK) dependent phosphorylation and activation of LIM kinases (LIMK) leads to phosphorylation of cofilin and consequently to F-actin stabilization and termination of neuronal migration. (figure according to Zhou et al., 2014).

During development, endocannabinoids regulate the fundamental processes, like the development of the central nervous system, cell proliferation, migration, differentiation, axon outgrowth, and the survival of progenitor cells (Galve-Roperh et al., 2009). They control fate decision (Aguado et al., 2006), interneuron migration (Berghuis et al., 2005) and axonal specification (Berghuis et al., 2007).

1.4 Genome editing

The function of a gene can be determined by inactivation through homologous recombination or by blocking targeted mRNA (messenger ribonucleic acid) molecules through RNA (ribonucleic acid) interference (Im et al., 2016). Since the 1970s genetic engineering (Rothstein, 1983), the manipulation of

DNA or RNA, developed at a rapid pace. Gene editing allows the conversion of a targeted DNA sequence into a new desired DNA sequence in the native context of a cell's genome (Scherer & Davis, 1979; Smithies et al., 1985; Thomas et al., 1986). The first important steps in gene editing were achieved when scientists demonstrated that a DNA sequence flanked with homology arms could be introduced into the cell, integrated into the host genome through homologous recombination and was able to cause intended changes in the cell (Capecchi, 1989). Homologous recombination alone in genetic modifications caused many problems such as inefficient integration and external DNA and random integration into undesired genomic locations. The development of highly specific and programmable nucleases helped to promote the output. By induction of a double-strand break a specific genomic target it was now possible to enable specific changes in regions of interest in the genome (Rouet et al., 1994). The DSB can later be repaired by repair mechanisms, including non-homologous end joining (NHEJ) or homology-directed repair (HDR). Error-prone NHEJ repair leads to indels (insertions, deletions or substitutions (Cox et al., 2015; Gaj et al., 2013; Sander & Joung, 2014) in the target area, which may interfere with the function of the targeted gene. Within the last years, there was the possibility to use several different nucleases, including meganucleases (Epinat et al., 2003), zinc-finger nucleases (Urnov et al., 2010), transcription activator-like effector nucleases (Miller et al., 2011) and the CRISPR/Cas9 [Clustered Regularly Interspaced Short Palindromic Repeats and nucleases associated to the CRISPR locus] (Jinek et al., 2012) system. (reviewed here (Khalil, 2020))

1.4.1 CRISPR/Cas9-an adaptive immune system of bacteria

In nature, the CRISPR/Cas-system is part of the adaptive immune system of certain bacteria and archaea, which is widely used as a powerful tool to edit genetic information and to study gene function and biological mechanisms.

CRISPR (clustered regularly interspaced short palindromic repeats) was first mentioned in 1987 as the group of Nakata initially described the CRISPR locus as a group of 29 nucleotide repeats downstream of the *iap* gene (alkaline phosphatase isozyme gene is responsible for alkaline phosphatase isozyme conversion in E.coli) interspaced with non-repetitive short sequences (spacer) in *Escherichia coli* (Ishino et al., 1987). Over the years, several interspaced repeat sequences were classified as a unique family of clustered repeat elements, which are present in approximately 50% of sequenced bacteria and 90% of archaea (Mojica et al., 2000). Besides these repetitive sequences, three types of associated genes (Cas) Type I-III (Haft et al., 2005; Makarova et al., 2011) were found to bind invariably adjacent to a CRISPR locus and so lead to the assumption that it shares a functional association (Jansen et al., 2002). In 2005, findings led to the hypothesis that the CRISPR system may be involved in the immune memory and defense mechanism against invading nucleic acids, and the sequence of the

individual spacers derive from invading phage and plasmid genomes (Bolotin et al., 2005; Mojica et al., 2005; Pourcel et al., 2005). After viral infection, a part of the viral DNA (protospacer) is integrated into the microbial genome and remains there as a spacer. The experimental proof that CRISPR serves as an adaptive immune system was made in 2007. It was demonstrated that, after a viral infection, a new spacer-sequence was integrated into the CRISPR/Cas locus of *Streptococcus thermophiles* and the bacteria become resistant against phages with the same protospacers (Barrangou et al., 2007). Besides, Barrangou et al. found in 2007 that after Cas inactivation, the immunity is not active anymore.

The final breakthrough was made in 2013, describing the use of the CRISPR/Cas9 system (using the type II effector system, which can be found in many bacteria and the engineered version of the Cas9 protein is used from the bacterium *Streptococcus pyogenes*) as a genome-editing tool in mammalian cells (Charpentier & Doudna, 2013). Since then, the method has been widely used by laboratories all over the world for genome editing in different model systems (Cong et al., 2013; Mali et al., 2013b; Sander & Joung, 2014).

The simplest and best characterized CRISPR/Cas system, and the most commonly used for genome editing, is type II of *Streptococcus pyogenes* and *Streptococcus thermophiles* (Dupuis & Moineau, 2013). *S. thermophiles*/ *S. pyogenes* use the Cas9 endonuclease in its immune defense system against bacteriophages and plasmids (reviewed here: (Jackson et al., 2017; Sternberg et al., 2016)).

The molecular mechanism of CRISPR-based adaptive immunity of procaryotes can be divided into two distinct proceses: i) immunization or acquisition, ii) immunity or defense.

In the first step, the **immunization** or **acquisition phase** (Fig. 8), DNA from invading viruses gets recognized and subsequently a new spacer sequence known as a protospacer is acquired and integrated between two adjacent repeats into the CRISPR locus (Yosef et al., 2012). To get acquired, the protospacer sequence needs to be located next to a protospacer-adjacent motif (PAM) to avoid the destruction of the host CRISPR array by its own CRISPR-Cas elements. Besides, the type II effector system comprises a long pre-crRNA, a Cas9 protein, and a trans-activating crRNA (tracrRNA).

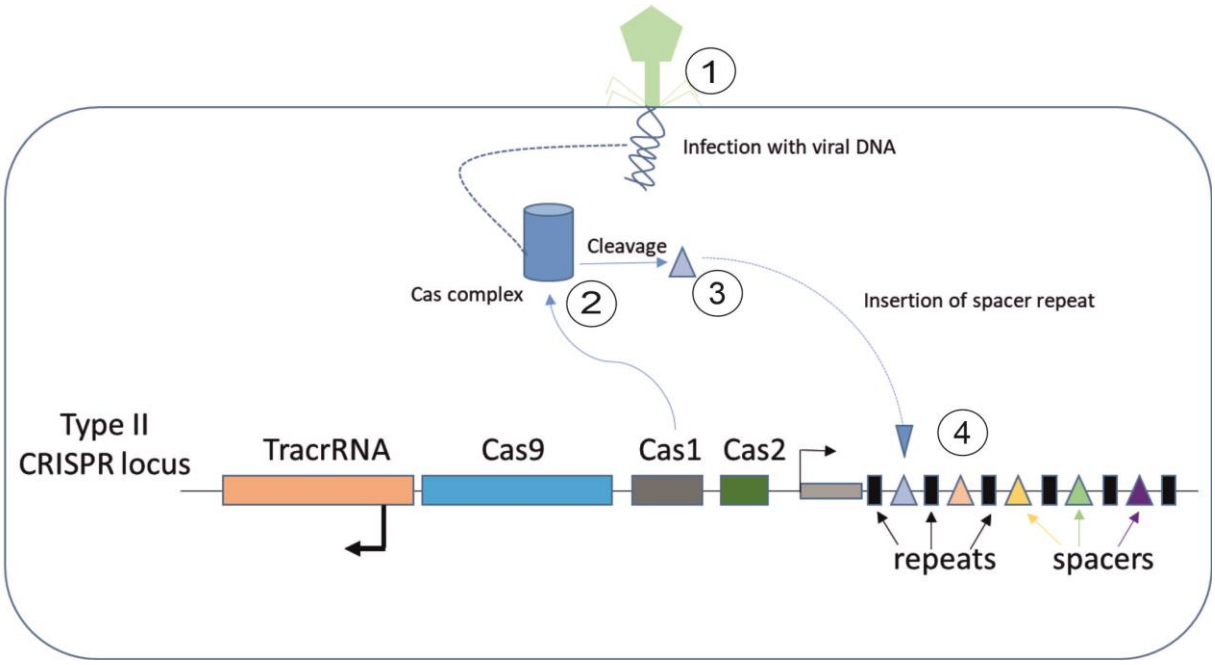

Figure 8 Immunization phase.
After infection by a virus with viral DNA (1), the Cas complex, consisting of Cas1 and Cas2 (2), recognizes the invading phage or plasmid DNA (3) and mediates the incorporation of short sequences into the bacterial CRISPR locus as “spacers” separated by “repeats” (4). (according to Mali, Esvelt, & Church, 2013a).

In the second step, the **immunity phase** (Fig. 9), a primary transcript or pre-CRISPR-RNA (pre-crRNA) is transcribed from the spacer repeat CRISPR locus. TracrRNA which is important for processing the pre cr-RNA and the formation of the Cas9 complex hybridizes to repeat regions of the pre-crRNA. In the next step, RNase III cleaves the hybridized crRNA-tracrRNAs and removes the 5’ end of each spacer to obtain mature crRNAs that remain associated with both the tracrRNA and the Cas9. Each mature complex can locate a target dsDNA sequence and cuts both strands when a complementary “protoscaper” sequence with a proximate PAM sequence at the 3’ end of the protospacer sequence are present. The PAM sequence is a short DNA sequence with 2-6 base pairs in length, which follows the targeted DNA region. It is essential for the Cas-mediated cut and is generally located 3-4 nucleotides downstream from the cut site. The PAM region is different among the bacterial species (e.g. *Steptococcus pyogenes* is NGG, where N is any nucleotide). It helps to distinguish between self and non-self to prevent the CRISPR locus itself from being targeted.

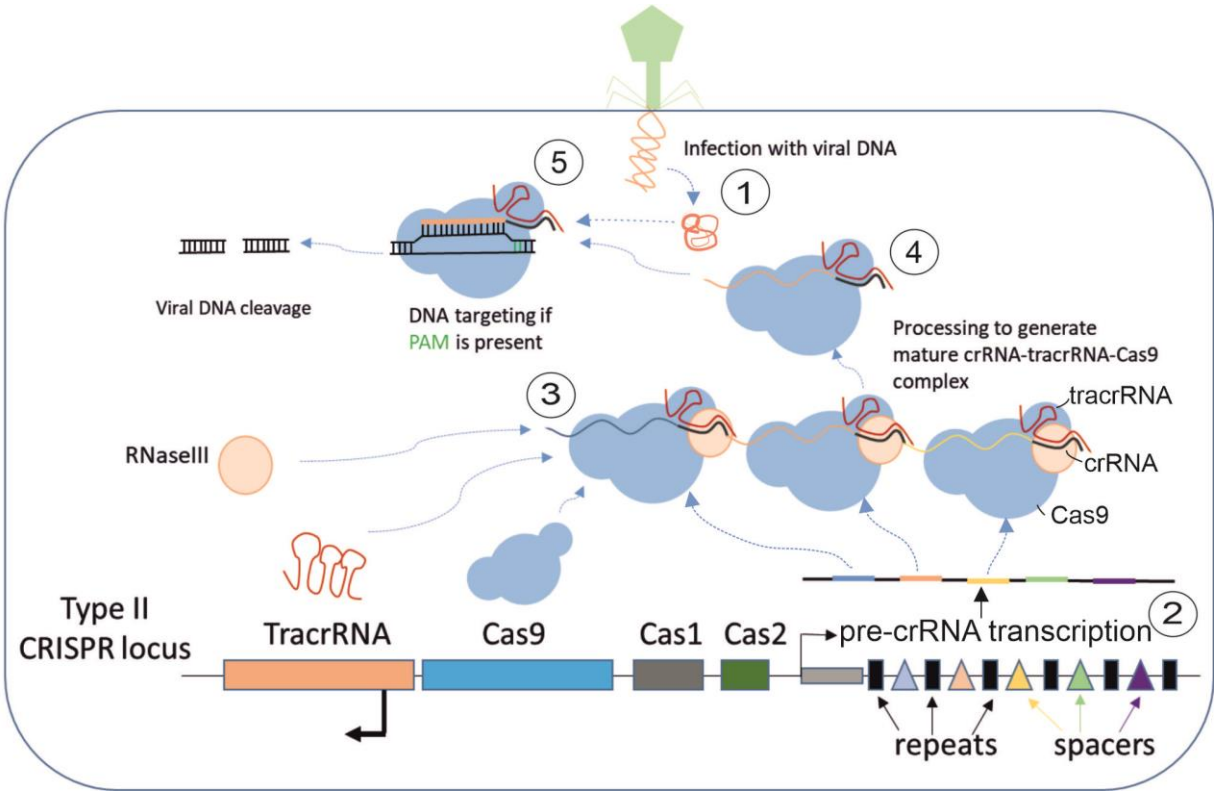

Figure 9 Immunity phase.
During the immunity phase, the bacterium uses stored information to defend against invading pathogens. The type II effector system includes the sequence information from former infections stored in spacer flanked by repeats, a Cas9 protein and a trans-activating crRNA (tracrRNA). At re-exposure of viral DNA (1) the immune system gets activated: (2) A long pre-crRNA is transcribed from the spacer repeat CRISPR locus. (3) TracrRNAs hybridize to repeat regions of the pre-crRNA. (4) Endogenous RNase III cleaves the hybridized crRNA-tracrRNAs and the 5' end of each spacer is removed to obtain mature crRNAs that remain associated with the tracrRNA and the Cas9 protein. (5) Each mature complex can locate a target dsDNA sequence and cleaves foreign DNA strands when it recognizes a complementary sequence between spacer and the target "protospacer" sequence which is followed by a PAM sequence at the 3' end of the protospacer sequence. (Figure according to Mali, Esvelt et al., 2013a).

1.4.2 CRISPR/Cas9 as genome editing tool

Until now, mostly embryonic stem cells (ESCs) and homologous recombination techniques (Limaye et al., 2009; Ukai et al., 2017) have been used to develop targeted genome editing-based mouse models. The role as "gold standard" of ESCs has recently been challenged by CRISPR/Cas9 technology because this technique overcomes most of the limitations found in the ESC based methodologies (Baumgart & Beyer, 2017; Lee et al., 2016; Skarnes, 2015; Skarnes et al., 2011).

The main advantages of the CRISPR/Cas9 method are the application to all mammalian cells, the commercial availability of the reagents, and the increased homologous recombination efficiency. The system relies on the introduction of double-strand breaks (DSB) at defined genomics locations, followed by DNA repair pathways activated by mutagenic events (Gaj et al., 2013). Alternatively, DSBs

can be repaired by homology-directed repair (HDR) events (reviewed in Wefers et al., 2017) (Fig. 10). The CRISPR/Cas 9 system comprises a ribonucleic protein complex composed of a Cas9 protein nuclease, tracrRNA that binds the Cas9 protein and a CRISPR RNA (crRNA) which defines the target specificity. The targeting is simplified by creating a crRNA-tracrRNA hybrid molecule (called gRNA), which can be transcribed *in vitro* as a single guide RNA molecule (sgRNA) out of a synthetic chimera of tracrRNA and crRNA (Jinek et al., 2012; Ran et al., 2013). The discovery of different Cas9 proteins optimized to suit mammalian expression. Each Cas9 protein has its own area of application: Wild-type Cas9 can cleave dsDNA causing DSBs, which can then be repaired by NHEJ or HDR when a template is offered (Hwang et al., 2013; Mali et al., 2013a). Cas9 nickase (Cas9n) introduces site-specific single-strand nicks for higher efficiency for large genomic deletions and multiplex editing (Cong et al., 2013; Ran et al., 2013). The dead, inactive Cas9 (dCas9) can be fused to various domains (e.g. transcriptional activators/repressors) with distinct regulatory functions and so can enable stable transcriptional repression or activation (Gilbert et al., 2013; Maeder et al., 2013).

By the interaction between the guide RNA and its complementary genomic sequence, Cas9 can introduce a DSB and therefore activates the repair mechanism of the cell (Hsu et al., 2013a). Through the cell-specific repair mechanisms, different mutations are introduced at the DSB site: the non-homologous end-joining (NHEJ) DNA repair mechanism will introduce small deletions or insertions whereas the homology-directed DNA repair mechanism (HDR) can use exogenous DNA sequences as templates to introduce specific mutations.

By introducing the CRISPR/Cas9 components into the pronucleus of zygotes, offspring with genetic modifications (knock-out or knock-ins) can be generated. The method can be processed in four steps:

1) Design of guide RNA to target a specific sequence
2) Assembling and cloning of HDR construct DNA components (homology arms, 2A-HA-NLS-Cre-recombinase) and processing into single-stranded DNA
3) Preparation of zygotes, microinjection of CRISPR/Cas components and transfer of injected embryos into foster mice
4) Genotyping and sequencing of offspring to identify mutations

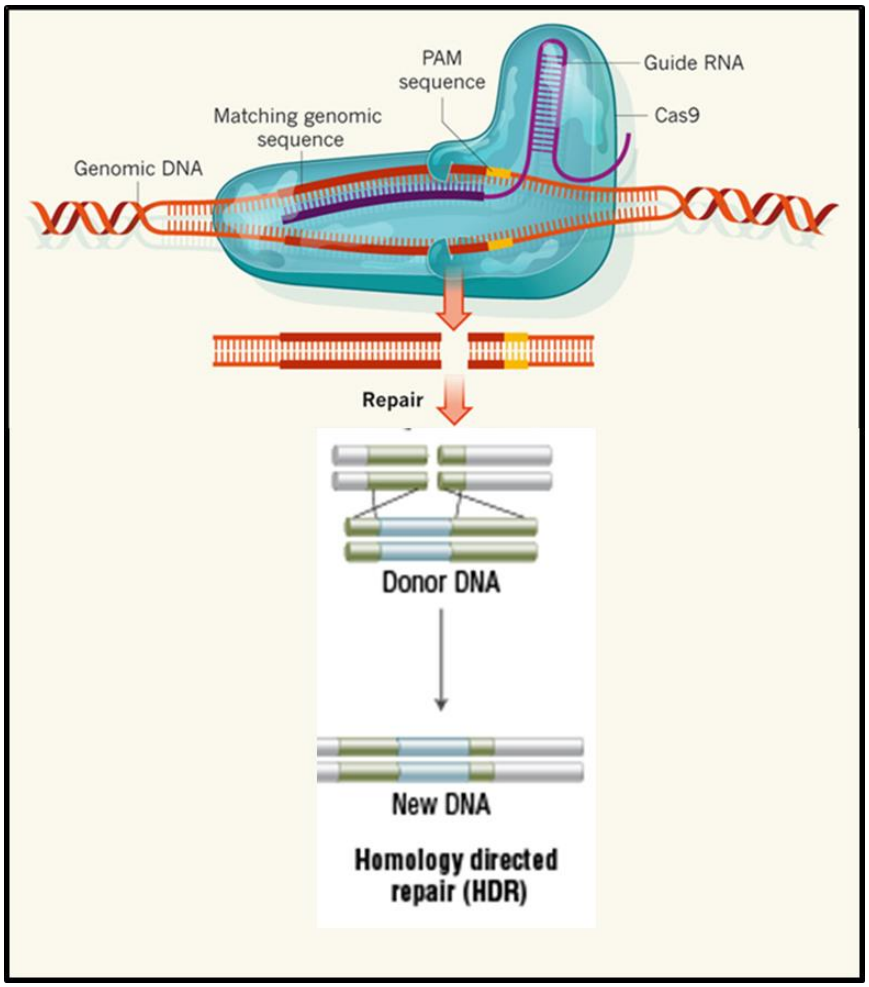

Figure 10 Targeted genome editing with RNA-guided Cas9.
The Cas9 complex consists of the guide RNA, a crRNA-tracrRNA hybrid (shown in purple), and the Cas9 effector nuclease. The guide RNA can be designed in a sequence-specific manner to target any part of the genome where a PAM sequence is available. The Cas9 complex will be guided to the targeted region, binds and cleaves there to cause a site-specific double-strand DNA break. This break either can be repaired by error-prone NHEJ (not shown) or by homology-directed repair (HDR) when offering a donor DNA with homology arms. This allows the insertion of new sequence information at the break site (adapted from (Charpentier & Doudna, 2013)).

1.5 Cre/loxP system

The Cre/loxP system is a recombination system that allows targeted gene modification restricted to certain cell types or developmental stages of the mouse (conditional gene targeting) depending on tissue-specific or time-dependent expression of Cre-recombinase. As a genetic tool, it allows controlling gene expression, can delete or insert DNA sequences, and can modify the architecture of the chromosome by translocations or inversions(Kühn & Torres, 2002). The Cre (causes recombination)-recombinase can recognize loxP (locus of crossover [x] in P1 bacteriophage) sites and mediates site-specific recombination between them. Cre recombinase and loxP sequences derive from the P1 bac-

teriophage, which uses the recombination system to maintain the phage genome as a unit copy plasmid in the lysogenic state during its life cycle (Austin et al., 1981; Hochman et al., 1983). For the use of this tool as Cre/loxP-mediated excision in mice, two different modified organisms are needed: One carrying the sequence for Cre-recombinase linked to the cell type-specific promotor and one carrying two loxP sites flanking the gene/exon of interest. Mating the two types of genetically modified mice will result in offspring that express carry a modification in the Cre-targeted cells. When loxP sites are in the same direction on the DNA sequence, Cre-recombinase mediates the excision of the loxP-flanked or "floxed" DNA sequence as a circular molecule and one loxP-site remains on each reaction product (Fig. 11).

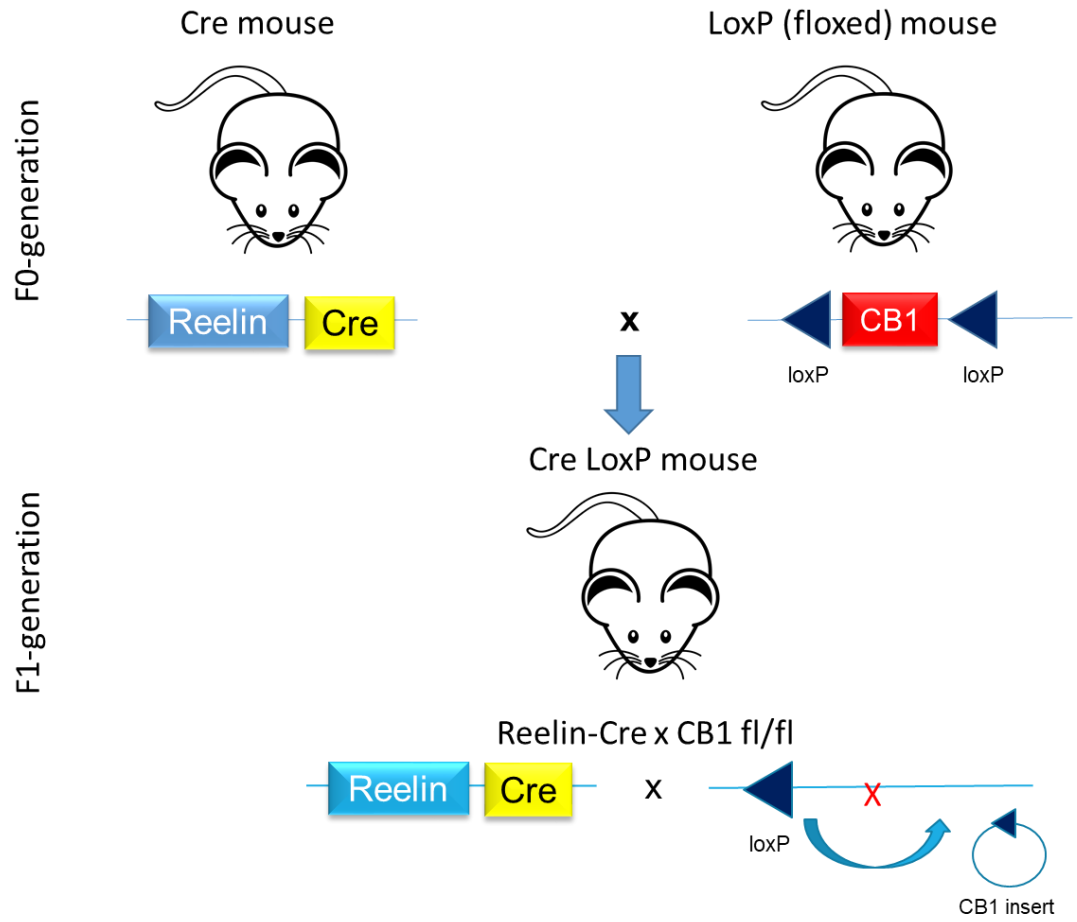

Figure 11 Scheme of Cre/loxP recombination system used as cell-type-specific gene knock-out.
In the F0 generation, one mouse is carrying a Cre-recombinase gene under the control of a cell-type-specific promotor (Reelin) and the other mouse has two loxP sites flanking the targeted gene (CB1). Crossing the Cre-mouse to a loxP mouse, the expression of Cre-recombinase induces a DNA excision between the loxP sites. The Cre-containing cells in the resulting progeny show no CB1-expression anymore as the targeted gene function has been disrupted.

1.6 Aim of the project

Reelin regulates the migration and the formation of the six-layered cortex structure. CB1 is known to play a key role in brain development. As CB1 is expressed together with Reelin in a subpopulation of Cajal-Retzius cells the question arises whether the Reelin activity is modulated by CB1. One way to answer this question is by conditional modulation of the CB1 expression within the Reelin-expressing cell population. Thus, the aim of this project was to create a Reelin-Cre mouse line to study the function of CB1 in Cajal-Retzius cells. To obtain the Reelin-Cre mouse line, a targeted DSB is caused in front of the translational stop of the Reelin gene with the help of CRISPR/Cas9. The editing of genomic DNA is achieved upon repair of the CRISPR-induced DNA double-strand break by homology-directed repair when offering a 2A-HA-NLS-Cre-recombinase construct containing homology arms. After the proper evaluation of the function of the Reelin-Cre mouse, by crossing it to a ROSA26-floxed-stop-YFP reporter mouse line, gain-of-function and loss-of-function studies of CB1 in Reelin-Cre cells are made. For the specific knock-out of CB1 in Reelin expressing cells, the Reelin-Cre mouse is crossed with a CB1 floxed mouse line. Reelin-Cre wild-type and mutant embryos with an age of E18.5 were then analyzed for cortex layer marker expression (Ctip2 and Satb2) to see possible migrational defects caused by CB1 inactivation in Reelin-expressing cells.

With this approach, we will be able to uncover the function of CB1 in the Reelin expressing Cajal-Retzius cells population.

2 Material and Methods

2.1 Molecular biological methods

2.1.1 Tissue preparation

Adult pregnant mice at gestational day E10.5–E18.5 were killed by cervical dislocation. Embryos were removed, washed in ice-cold 1x PBS (phosphate buffered saline containing: 136 mM NaCl (sodium chloride) 2.7 mM KCl; 10 mM Na_2HPO_4; 1.8 mM KH2PO4, pH 7.4) and then fixed overnight in 4% paraformaldehyde in PBS (PFA). Embryos from E16.5-E18.5 and pups from P0 to P2 were killed by decapitation, brains were removed and fixed overnight in 4% PFA/PBS. On the next day, embryos were washed several times in 1x PBS and then transferred into 20% sucrose (4661.1, Roth, Germany) in PBS until they set down to the bottom of the falcon.

Embryonic brains were mounted on Tissue Tek (14020108926, Leica, Germany), frozen at -20°C, and 14-µm-thick coronal sections were cut from the forebrain in coronal plane on a cryostat Microtome (CM3050 S, Leica, Germany). Sections were mounted onto frozen Menzel SuperFrost Plus slides (10149870, Thermo Scientific, USA), dried on a 38°C warming plate and stored at -20°C until usage.

2.1.2 Extraction of genomic DNA

2.1.2.1 Tail biopsies

To obtain genomic DNA from tail biopsies to determine the genotype of a mouse, a piece of less than 0.5 cm was cut from animals' tails. The tail was transferred into an Eppendorf reaction tube and incubated for at least 3 h at 56°C/1000 rpm in 500 µl lysis buffer (100 mM Tris-HCl (hydrogen chloride) pH 8.0, 5 mM EDTA, 200 mM NaCl, 0.2% SDS) and 25 µl of proteinase K (10 mg/ml, Proteinase K recombinant PCR Grade, 03115852001, Roche) on a thermomixer (Eppendorf). As soon as the tail was completely dissolved, it was centrifuged at 14,000 rpm for 10 min to separate DNA from tissue debris. 450 µl of the liquid was then transferred into a new tube containing 350 µl isopropanol. The tube had to be inverted several times until a DNA precipitate was visible and then centrifuged again at 14,000 rpm for 10 min. Afterwards the supernatant was discarded, and the pellet was washed with 300 µl 70% ethanol and centrifuged for 5 min at 14,000 rpm. The ethanol was removed thoroughly, and the DNA pellet was air-dried for 20-40 min until no ethanol was visible anymore. To dissolve the pellet 100 µl of 0.1x TE buffer (10 mM Tris pH 8.0, 0.1 mM EDTA pH 8.0) was used. To dissolve the pellet

completely the Eppendorf tube was mixed at 50°C for 30 min on a thermomix (Eppendorf). The dissolved DNA was stored at 4°C.

2.1.2.2 Blastocysts

To obtain single blastocysts, injected zygotes were incubated for 3-4 days in culture, then harvested and stored briefly in 5-10 µl PBS at -20°C prior to analysis. For isolation of genomic DNA from blastocysts, 10 µl of 1x lysis buffer (100 mM Tris-HCl pH 8.3, 100 mM KCl, 0.02% gelatin, 0.45% Tween-20, 60 µg/ml yeast tRNA, 125 µg/ml proteinase K) was added per blastocyst and incubated in a thermocycler for 10 min at 56°C followed by an 10 min incubation step at 95°C.

2.1.3 Polymerase chain reaction (PCR)

PCRs were used to amplify and analyze specific DNA parts by generating a large number of copies. The primers with a length of about 25 nucleotides (Tab. 1) were designed to bind to one part of the DNA and serve as a starting point for the polymerase.

The reaction was performed in a thermocycler (BiometraTrio, Analytikjena, Germany) in 3 steps:

1. DNA melting step to separate the two strands of the DNA double helix at a high temperature (95°C)
2. DNA annealing at a lower temperature which ensured the specific binding of the primers to their complementary sequences (Tab. 2)
3. Elongation where DNA strands become templates for DNA polymerase, which assemble a new DNA strand from free nucleotides.

These 3 steps were repeated for 25-35 cycles.

For reactions with Q5® High-Fidelity DNA Polymerase (M0491L, NEB, MA)

Reactions with a total volume of 25 µl were prepared as follows:

Constituent	**Volume (µl)**	**Final concentration**
5x Q5 buffer	5	
Forward Primer	1	10 µM
Reverse Primer	1	10 µM
dNTPs	1	10 mM
DNA (20-300 ng)	2	
Q5 Hifi DNA Polymerase	0.5	2 U/µl
H_2O	15.5	
Total volume	25	

Program for PCR reactions with Q5 High-Fidelity Polymerase

Step	**Temperature (°C)**	**Time (s)**	**Cycles**
Initial denaturation	95	300	
Denaturation	95	30	30
Annealing	66-68	30	
Elongation	72	120	
Final Elongation	72	600	
Storage	4	Hold	

For reactions with Go Taq G2 Flexi DNA Polymerase (M7808, Promega, WI)

Constituent	**Volume (µl)**	**Final concentration**
5x buffer (supplied with Taq polymerase)	5	
$MgCl_2$	2.5	25 mM
Forward Primer	1	10 µM
Reverse Primer	1	10 µM
dNTPs	1	10 mM
DNA (20-300 ng)	2	
GoTaq G2 DNA Polymerase	0.125	1.25 U/µl
H_2O	14.375	
Total volume	25	

Parameters used to program the thermocycler as follows:

Program for PCR reactions with Taq polymerase (*M7808, Promega, WI*)

Step	**Temperature (°C)**	**Time (s)**	**Cycles**
Initial denaturation	98	300	
Denaturation	98	45	27
Annealing	55	45	
Elongation	72	300	
Final Elongation	72	180	
Storage	4	Hold	

Table 1 List of primer sequences used for genotyping, e.g. analysis of correct founders

Primer #	Sequence (5'-3')	Location in the genome (chromosome, strand, start, end)
1.1 Fwd	AAA TCC AAT CCC AGT TGC CG	chr5 AC113028.15: 99851 to 99870 mouse (GRCm39/mm39, C57BL/6)
1.2 Rev	ATC ACA ATT TCC ACG GAC GC	chr5 AC113028.15: 99110 to 99129 mouse (GRCm39/mm39, C57BL/6)
2.1 Fwd	GAA AGT CCA GCT CAT TCC GC	chr5 AC113028.15: 99807 to 99826 mouse (GRCm39/mm39, C57BL/6)
2.2 Rev	CAA TTT CCA CGG ACG CAC TG	chr5 AC113028.15: 99114 to 99133 mouse (GRCm39/mm39, C57BL/6)
3.1 Fwd	TTA TGC TAG CCT CGA ATT CCC	HA-Tag
3.2 Rev	ACC CTG ATC CTG GCA ATT TC	Cre-recombinase Bakteriophage P1
5.1 Fwd	AGT CTG CAT GAC TTC TGA ATT CTG	chr5 AC113028.15: 99560 to 99583 mouse (GRCm39/mm39, C57BL/6)
5.2 Rev	TTT TCC TAT CCA CAA AAT GAT GC	chr5 AC113028.15: 98695 to 98717 mouse (GRCm39/mm39, C57BL/6)
6.1 Fwd	AAC ATG GGC TCA GGC ACT TC	chr5 AC113028.15: 99376 to 99395 mouse (GRCm39/mm39, C57BL/6)
6.2 Fwd	CGC TGG AGT TTC AAT ACC GG	Cre-recombinase Bakteriophage P1
6.3 Rev	GGT CAA AGT CCA GCA GCA AA	chr5 AC113028.15: 98821 to 98840 mouse (GRCm39/mm39, C57BL/6)
7.1 Fwd	CAC AGA CAG TGG AAT CTA GGA AAG	chr5 AC113028.15: 99822 to 99845 mouse (GRCm39/mm39, C57BL/6)
7.2 Rev	ATC GAC CGG TAA TGC AGG	Cre-recombinase Bakteriophage P1
G100	CGG CAT GGT GCA AGT TGA ATA	Cre-recombinase fwd Bateriophage P1
G101	GCG ATC GCA ATT TTC CAT GAG	Cre-Recombinase rev

		Bakteriophage P1
G50	GCT GTC TCT GGT CCT CTT AAA	chr4 BX005292.13: 120882 to 120902 mouse (GRCm39/mm39, C57BL/6)
G51	GGT GTC ACC TCT GAA AAC AGA	chr4 BX005292.13: 121274 to 121294 mouse (GRCm39/mm39, C57BL/6)
G53	CTC CTG TAT GCC ATA GCT CTT	chr4 BX005292.13: 123382 to 123402 mouse (GRCm39/mm39, C57BL/6)

Table 2 List of annealing temperatures and expected products for all primers used for genotyping.

Primer	**Annealing temperature (T_m) (°C)** **(optimized for polymerase)**	**Expected product**
1.1 + 1.2	67 (Q5 High-Fidelity Polymerase)	WT 761 bp MUT 1931 bp
2.1 + 2.2	67 (Q5 High-Fidelity Polymerase)	WT 713 bp MUT 1883 bp
3.1 + 3.2	68 (Q5 High-Fidelity Polymerase)	MUT 582 bp
7.1 + 7.2	66 (Q5 High-Fidelity Polymerase)	MUT 689 bp
5.1 + 5.2	62 (Q5 High-Fidelity Polymerase)	WT 889 bp MUT 2056 bp
6.1 + 6.3	67 (Q5 High-Fidelity Polymerase)	WT 575 bp MUT 1742 bp
6.2 + 6.3	67 (Q5 High-Fidelity Polymerase)	MUT 652 bp

G100 + G101	55 (Tag polymerase)	MUT 300 bp (Cre only)
G50 + G51 + G53	55 (Tag polymerase)	Deletion product for CB1 600 bp CB1 fl/fl 500 bp CB1 wt 400 bp

After establishing the Reelin-Cre mouse line, for routinely testing the line, primer 1.1 and 1.2 are used and the following protocol with Q5 Polymerase for adults as well as for genotyping of embryonic tissue.

Reactions with Q5® High-Fidelity DNA Polymerase (M0491L, NEB, MA)

Constituent	**Volume (µl)**	**Final concentration**
5x Q5 buffer	5	
Forward Primer	1	10 µM
Reverse Primer	1	10 µM
dNTPs	1	10 mM
DNA (20-300 ng)	2	
Q5 Hifi DNA Polymerase	0.5	2 U/µl
H_2O	15.5	
Total volume	25	

PCR program for reactions with Q5® High-Fidelity DNA Polymerase

Step	Temperature (°C)	Time (s)	Cycles
Initial denaturation	95	300	
Denaturation	95	30	30
Annealing	67	30	
Elongation	72	120	
Final Elongation	72	600	
Storage	4	Hold	

Blastocyst genotyping

For the genotyping of the blastocysts a nested PCR according to the protocol from Lars Schomacher, Institute of Molecular Biology, Mainz was performed. Because the amount of DNA in single blastocysts is generally low, a nested PCR was performed. For the nested PCR 2 separated PCRs with Q5 Polymerase were conducted: First PCR was with primer pair 1, and then the products from the first PCR were used for a second PCR with primer pair 2. The first PCR was performed with primer pair 1.1 and 1.2, which amplifies a 761 bp region before the left homology arm and within the right homology arm. The reaction was set with 5 µl 5x Q5 buffer, 10 µM forward primer 1.1, 10 µM reverse primer 1.2, 10 mM dNTP's (desoxy NukleosidTriPhosphat), 20-300 ng blastocysts DNA, 2 U/µl Q5 Hifi DNA polymerase (M0491L, NEB, MA) and adjusted to 25 µl with H_2O. The amplification was operated in a thermocycler under following conditions: 1x 95°C for 5 min, 30x (95°C for 30 sec; 67°C for 30 sec, 72°C for 2 min), 1x72°C for 10 min.

The second PCR used primers located within the first PCR product and creates a 713 bp product. For the nested PCR reaction, primer pair 2.1 and 2.2 and amplified DNA from the first reaction was used. The cycling conditions were the same as before.

2.1.4 Analytical and preparative agarose gel electrophoresis

To analyze and separate PCR products or digested DNA 1% agarose gel (agarose in TBE buffer (10x TBE: 0.89 M Tris, 0.89M boric acid, 2.5 mM EDTA in autoclaved H_2O) containing ethidium bromide 0.025% (0.2-0.5 µg/ml of 250 µg/ml solution) (HP47.1, Roth, Germany), to visualize the DNA, was used. The molecular marker (Massruler, SM0403, Thermo Fisher Scientific/former Fermentas) which

was run in one lane was used to determine the fragment sizes of the samples. For preparative gel electrophoresis the band was cut out of the gel under UV light and the DNA was subsequently purified using the PureLink™ PCR Quick Gel Extraction Kit (K2100-12, Invitrogen, USA) by following manufacturer's instructions.

2.1.5 Determination of DNA concentration

DNA concentrations were measured using a Spectrophotometer (Nanodrop 2000c, Thermo scientific, USA) which determines the concentration through the amount of absorbed light at 260 nm. To determine the sample purity, respectively the amount of protein that contaminates the sample, the 260nm: 280 nm ratio is used since proteins absorb at 280 nm. The ratio for pure DNA, $A_{260/280}$ is 1.8 and for RNA $A_{260/280}$ is 2.0.

2.1.6 Restriction analysis of DNA

DNA restriction was performed using NEB restriction enzymes in the recommended buffer as followed:

Component	**amount**
10x buffer	2 µl
DNA	10 µg
Restriction enzyme	2 µl
RNase/DNase free H_2O	X µl
Total volume	20 µl

The mixture was incubated for 2 h at 37°C in a thermomix.
The restriction digest was analyzed via agarose gel electrophoresis (see 2.1.4).

2.1.7 Cloning

2.1.7.1 Ligation of DNA

2.1.7.1.1 With T4-Ligase

Ligation was performed with T4-ligase (M0202S, NEB, USA) and the supplied buffer. Ligation with T4 ligase was used for restriction site cloning. In this case when cloning guide RNA into the BbsI site of the PX330 vector (see 2.5.1), cloning the 2A-HA-NLS-Cre construct into the NotI and HindIII site of the

pBSKS vector (see 2.5.5) and cloning the CB1 floxed stop construct for overexpression (see 2.6). Vector and insert ligation was performed in a ratio, which has to be determined beforehand. Standard ligation was performed either 1:5 or 1:10. The reaction was set up as followed and incubated overnight at 4°C.

Component	amount
10x buffer	2 µl
vector	200 ng
insert	$\text{Insert ng} = \text{ratio x } \frac{\text{Insert bp x Vector ng}}{\text{Vector bp}}$
ligase	1 µl
RNase/DNase free H_2O	x µl
Total amount	20 µl

2.1.7.1.2 With Gibson-cloning

"Ligation" with the Gibson System (E2611S, NEB, MA) was applied for cloning and assembly of the construct used for homology-directed repair for the CRISPR/Cas approach. The pBluescript vector (pBSKS+, Stratagene, CA) was used as vector backbone.

2.1.7.2 Transformation

For transformation, competent cells (Escherichia coli DH5α (C2989K, NEB, MA) or stbl3 (C3040I, NEB, MA) strain) were thawed on ice. Per transformation 10 µl ligation reaction was added to 100 µl competent cells and incubated for 30 min on ice. Cells were then heat shocked at 42°C for 45 s and immediately put back on ice. 250 µl LB (lysogeny broth)-medium was added and then incubated for 1 h at 37°C in a gently shaking incubator. After incubation, cells were plated on pre-warmed LB-Agarose plates containing 10 mg/ml Ampicillin (K029.2, Roth, Germany) and incubated overnight at 37°C in an incubator.

2.1.8 Small-scale plasmid preparation (miniprep)

Single bacterial colonies from overnight culture were picked with a pipette tip and added to a 15 ml falcon tube containing 4 ml LB-medium with 0.1% ampicillin (100 µg/ml). Falcon tubes were incu-

bated overnight (12-16 h) at 37°C and 200 rpm in an incubator (Schüttelinkubator Typ 3032, Gesellschaft für Labortechnik mbH, Germany or Schüttelinkubator Typ ZH80/ZK80, Infors AG, Germany). The next day, 2 ml of the bacterial suspension was transferred into an Eppendorf tube and then pelleted at 6000 x g for 2 min. The plasmid extraction was continued with the PureLink™ Quick Plasmid Miniprep Kit (K2100-11, Invitrogen, USA) according to the user manual. A following restriction digest could verify the correctness of the plasmids. Positive clones from the restriction digest were sequenced by Eurofins MWG (Luxembourg).

2.1.9 Large-scale plasmid preparation (maxiprep)

200 ml LB medium, containing 200 µl of miniprep culture and 100 µg/ml ampicillin, was incubated in an incubator (Schüttelinkubator Typ 3032, Gesellschaft für Labortechnik mbH, Germany or Schüttelinkubator Typ ZH80/ZK80, Infors AG, Germany) as an overnight culture at 37°C shaking at 200 rpm to amplify the bacteria. The plasmids were purified the next day with the PureLink™ Maxiprep Kit (K210012, Invitrogen, USA) following manufacturer's instructions.

2.1.10 TOPO-Cloning

TOPO Cloning was used for subcloning a PCR product for later sequencing. The TOPO TA Cloning Kit for subcloning (451641, Thermofisher Scientific, MA) was used for subcloning of mutated fragments e.g. corresponding DNA fragments of potential founders, which had to be sequenced. TOPO Cloning enables a highly efficient PCR product insertion into a specific vector without prior digestion of the PCR products. Instead, 3' A overhangs complementary to 3' T overhangs of the supplied pCR 2.1-TOPO vector were added by a Taq DNA polymerase (Fig. 12). The 3' phosphates of the pCR 2.1-TOPO vector are bound to topoisomerase I enzymes to catalyze the linearization of the vector. Only a brief ligation reaction without DNA ligase was needed to integrate the vector. Beforehand, PCR fragments were separated on a gel, cut out and purified. To facilitate the TA-cloning procedure, adenine-nucleotide overhangs were added at the 3' end of the inserts in order to integrate into the pCR 2.1 cloning plasmid as follows. 16.375 µl purified PCR product was mixed with 1 µl dATP (0.2 mM), 2.5 µl $MgCl_2$ (25 mM), 5 µl Go flexi buffer (not green) (M7808, Promega, WI) and 0.125 µl Tag Polymerase (M7808, Promega, WI). The reaction was performed in a thermocycler for 20 min at 72°C, adjusted to 100 µl and then purified with a PCR purification Kit (Nucleospin extraction Kit, 11992242, Macherey-Nagel™, Germany) according to the supplied manual. To ligate the PCR product with A-overhangs and the TOPO cloning vector, 4 µl of the fresh PCR product, 1 µl salt solution and 1 µl TOPO Vector were incubated at room temperature for 30 min.

This ligation was then used to transform competent cells (Stbl3), colonies were picked one day after transformation and a mini-prep was done. DNA from the single colonies was digested with EcoRI to screen for wild-type and mutated constructs and then sent to sequencing (Eurofins, Luxembourg).

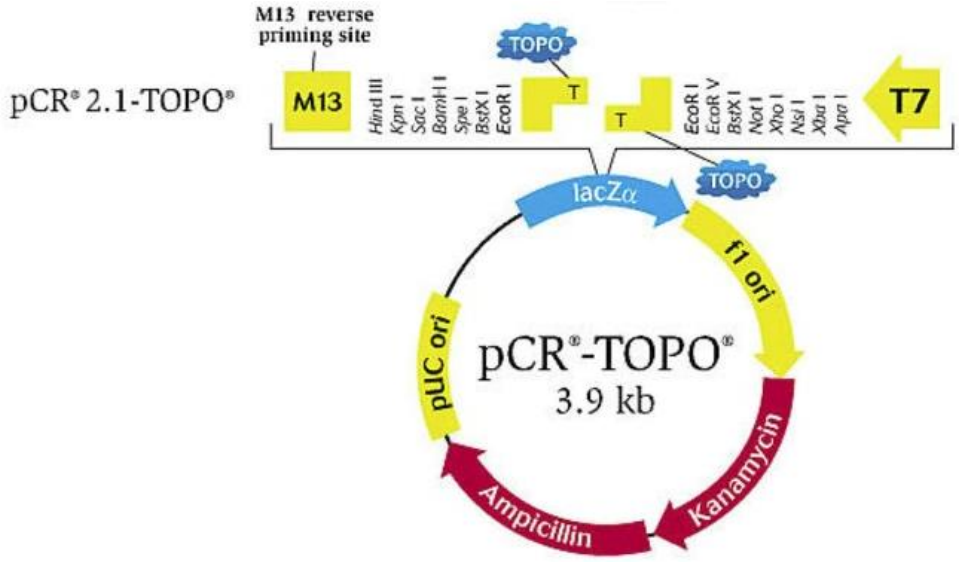

Figure 12 pCR 2.1-TOPO Vector used for TOPO-cloning.
The TOPO Cloning vector pCR 2.1 contains a resistance against ampicillin and kanamycin, two different origins of replication (pUC and f1) where replication is initiated and a lacZ gene for blue/white screening for recombinant bacteria clones. Within the lacZ site, the multiple cloning site and the TOPO cloning site for topoisomerase I cloning is located. With two promotor sites (M13 and T7) the inserts can be sequenced. (https://assets.thermofisher.com/TFS-Assets/LSG/figures/1994.jpg-650.jpg).

2.1.11 Immunohistochemistry

PFA-fixed frozen brain sections were put into Shandon chambers (Shandon coverplates, 72110017, Thermofisher; Shandon slide rack and lid, 73310017, Thermofisher) and rinsed in PBS with 0.3% Triton X-100 (3051.2, Roth, Germany) (PBS-T). To suppress unspecific immunoreactivity, sections were incubated for 15 min in 4% goat serum (G6767-100ml, Sigma, USA) in PBS-T at RT. Afterwards, sections were incubated overnight at 4°C with a primary antibody diluted with 4% goat serum PBS-T (see Tab. 3). On the next day, sections were washed 3 times with PBS-T and then incubated for 1 h with a secondary antibody (see Tab. 4). The secondary antibody was washed away with PBS-T, before the counterstaining for 5 min with the nuclear dye 4', 6-diamidino-2-phenylindole (Hoechst 33342 (DAPI, 4',6-diamidino-2-phenylindole), H1399, Invitrogen, CA). After the final wash step with PBS, slides were mounted in MOWIOL (475904, Merck, Germany) (containing 6 g Glycerol, 2.4 g Mowiol 4-88 (475904, Merck, Germany), 12 ml Tris 0.2 M pH 8.5, 6 ml autoclaved H_2O).

Table 3 List of primary antibodies used for immunohistochemical stainings.

primary antibody	host animal	company	catalog number	working con-centrantion
rat anti-Ctip2	rat	abcam	ab18465	1:100
mouse anti-Pax6	mouse	Biolegend	AB528427	1:200
rabbit anti-Satb2	rabbit	abcam	ab34735	1:200
rabbit anti-Tbr1	rabbit	abcam	ab31940	1:500
rabbit anti-Tbr2	rabbit	abcam	ab23345	1:500
mouse anti-Tuj1	mouse	Biolegend	MMS-435P	1:1000
mouse anti-Reelin	mouse	Millipore	MAB5364	1:500
rabbit anti-mouse CB1	rabbit	Frontier institute	CB1-Rb-Af380	1:500
mouse anti-mouse Reelin	mouse	Millipore	164-469,clone G10	1:1000
rabbit anti-GFP (Aequorea victoria)	rabbit	custom made (Ruth)		1:1000
rabbit anti-Cre (Bakteriophage 1)	rabbit	Biolegend	#PRB-106-P	1:500

Table 4 List of secondary antibodies used for immunohistochemical stainings.

secondary antibody	host animal	company	Catalog number	working con-centrantion
goat anti-rat alexa 488	goat	Invitrogen	A-11006	1:1000
goat anti-mouse alexa 488	goat	Invitrogen	A11001	1:1000
goat anti-rabbit alexa 488	goat	Invitrogen	A11008	1:1000
goat anti-chicken alexa 488	goat	Invitrogen	A-11039	1:1000
goat anti-rat alexa 546	goat	Invitrogen	A11081	1:1000

donkey anti-mouse alexa 546	donkey	Invitrogen	A10036	1:1000
goat anti-rabbit alexa 546	goat	Invitrogen	A11010	1:1000
donkey anti-mouse Cy3	donkey	Jackson Immuno-Research	715-165-151	1:1000
goat anti-rabbit Cy3	goat	Jackson Immuno-Research	111-165-003	1:500
donkey anti-rabbit Cy3	donkey	Jackson Immuno-Research	711-165-152	1:500
donkey anti-mouse F(ab)2 FP-547H	donkey	Interchim	FP-SB4120	1:125 1:250
donkey anti-rat F(ab)2 FP-547H	donkey	Interchim	FP-SB6120	1:250/ 1:500/ 1:1000
donkey anti-rabbit Cy3	donkey	Dianova	711-265-152	1:500
donkey anti- mouse Cy3	donkey	Dianova	115-165-166	1:250

2.2 *In situ* hybridization (ISH)

2.2.1 Synthesis of probes by *in vitro* transcription

The transcription produces single-stranded RNA-probes (riboprobes), which can later detect mRNA in tissue by complementary binding to it. In a first step, plasmid-DNA has to be linearized with appropriate restriction enzymes (see Tab. 5). For FITC (Fluorescein isothiocyanate)-/DIG (Digoxigenin)-labelled riboprobes, *in vitro* transcription was carried out for 3 h at 37°C in a total volume of 20 µL containing 1.5 µg of linearized DNA, 1x transcription buffer, 2 µL FITC-rUTP (Uridine-5'-triphosphate) (11685619910, Sigma, USA)/DIG-UTP (11277073910, Sigma, USA), 0.5 µL RNasin® RNase Inhibitor (N211, 2500u, Promega, USA), and 2 µL of SP6 (10810274001, Sigma, USA), T3 (11031163001, Sigma, USA) or T7 (10881767001, Sigma, USA) RNA Polymerase. Reactions were treated with 20 units of RNase-free DNaseI/ 1x DNase buffer (4716728001, Sigma, USA) and filled up to a total volume of 50 µL for 15 min at 37°C, and labelled probes were purified (74106, RNeasy kit, Qiagen).

Table 5 List of riboprobes used for *in situ* hybridization including host vector, polymerase, restriction enzyme and size.

Probe	Vector		Polymerase	Restriction enzyme	Size
CB1	pBSKS (-)	AS	T3	BamHI	1.5 kb
		S	T7	EcoRI	1.5 kb
Reelin	pBSKS (-)	AS	T7	XbaI	1.27 kb
		S	T3	KpnI	1.27 kb
GAD65	pBSKS (-)	AS	T3	BamHI	1 kb
		S	T7	EcoRI	1kb

DNA templates for CB1 and GAD65 were originally generated by RT-PCR from cDNA derived from total mouse brain (Marsicano and Lutz, 1999) GeneBank accession numbers are given here: CB1, accession number U22948, 1530 bp from 152 to 1682 (forward primer 5'-GTT GAG CCT GGC CTA ATC AAA, reverse primer 5'-GTT GAC CGA ACC TCT GTT TTC) and GAD 65, accession number D42051, 1041 bp, from 1055 to 2096 (forward primer 5'-GGC GAT GGA ATC TTT TCT CCT, reverse primer 5'-CGA GGC GTT CGA TTT CTT CAA). PCR products were cloned into pBluescript KS^- (Marsicano and Lutz, 1999) and used as templates for riboprobe synthesis as described above.

For Reelin riboprobe synthesis, a template (rlCR-50) was used, which contains a Reelin cDNA fragment, accession number NM 001310464.1, 1279 bp from 394 to 1672; it was cloned into pBS-SK^- vector and kindly provided by M. Frotscher, University Medical Center Hamburg.

2.2.2 Pre-hybridization

Slides were thawed for 30 min at RT, fixed in ice-cold 4% paraformaldehyde in phosphate-buffered saline (PBS, containing: 136 mM NaCl; 2.7 mM KCl; 10 mM Na_2HPO_4; 1.8 mM KH_2PO_4, pH 7.4) for 20 min, washed two times in PBS for 5 min, incubated for 15 min in methanol (8388.5, Roth, Germany) containing 1% H_2O_2 (CP26.1, Roth, Germany) washed in PBS 2 times for 2 min, incubated for 8 min in 0.2M HCl (T134.1, Roth, Germany), washed 2 min in PBS, incubated 10 min in 50 mM Tris (4855.2, Roth, Germany)-HCl pH 8.0/5 mM EDTA (8043.2, Roth, Germany) pH 8.0 which contains 0.4U/mL Proteinase K (Proteinase K recombinant PCR Grade, 03115852001, Roche), washed in PBS for 5 min and fixed again for 20 min in icecold 4% PFA in PBS. Afterward, the slides were directly incubated for

10 min in 0.1 M triethanolamine-HCl (6300.1, Roth, Germany) (pH 8.0) to which 0.60 mL of acetic anhydride (320102-100ML, Sigma, USA) was added dropwise, washed first for 5min in PBS and then 5 min in 0.9% NaCl followed by dehydration steps through successive baths of ethanol (EtOH): 20 sec 30% EtOH, 20 sec 50% EtOH, 1 min 70% EtOH, 20 sec 80% EtOH, 20 sec 95% EtOH, two times 20 sec 100% EtOH (32205-2.5 L, Honeywell, USA), and air-dried.

Hybridization was carried out overnight at 54°C in 100 µL of hybridization buffer containing DIG-labelled riboprobe (i.e. DIG-UTP labelled CB1 600 ng/mL) and/or FITC-labelled riboprobe (FITC-UTP labelled GAD65 1200 ng/mL, FITC-UTP labelled Reelin 600 ng/mL). A cover slide avoided dehydration. Hybridization buffer consisted of 50% formamide (6749.2, Roth, Germany), 20 mM Tris–HCl, pH 8.0, 0.3 M NaCl, 5 mM ethylenediaminetetraacetic acid (EDTA), pH8.0, 10% dextran sulphate (D8906, Sigma, USA), 0.02% Ficoll 400 (F2637, Sigma, USA), 0.02% polyvinylpyrrolidone (MW 40 000, PVP40, Sigma, USA), 0.02% bovine serum albumin (BSA, A6793, USA), 0.5 mg/mL tRNA (10109517001, Sigma, USA), 0.2 mg/mL fragmented herring sperm DNA (D6898-250mg, Sigma, USA) and 200 mM DTT (1114740005, Sigma, USA).

2.2.3 Post-hybridization

After incubation in a humid chamber, cover slips were washed away in 5x SSC (standard saline citrate)/ 0.05% Tween 20 (9127.1 , Roth, Germany) at 64°C and then the slides were incubated in decreasing concentrations of SSC for 30 min each (2x SSC/ 50% formamide (6749.2, Roth, Germany) /0.05% Tween 20, 1x SSC/ 50% formamide/0.05% Tween 20, 0.1x SSC/ 0.05% Tween 20) at 64°C and finally incubated for 1 h at 30°C in 4% heat inactivated sheep serum in TNT (Tris-NaCl-Tween buffer, i.e. 100mM Tris-HCl, pH 7.6, 150 mM NaCl, 0.05% Tween 20), sterile filtered.

Next steps were performed in shandon cassettes (Shandon coverplates, 72110017, Thermo Fisher, USA; Shandon slide rack and lid, 73310017, Thermo Fisher, USA) at 30°C for antibody administration. Slides were washed 3 times in 500 µl TNT each for 2 min. Afterwards slides were incubated for 30 min in Perkin Elmer (PE) blocking buffer (TSA Blocking Reagent, FP1020, Akoya, USA), followed by 1.5 h incubation with antiFITC (Fab)-POD (Peroxidase) antibody (11426346910, Sigma, USA) 1:1000 diluted in PE blocking buffer, followed by three washing steps in TNT buffer for 2 min each at 30°C. Immediately before use, fluorescent tyramine FITC (TSA™ Plus Fluorescein System, NEL741001KT, Akoya, USA) was prepared by diluting 1:50 into Amplification diluent, added to the slides and incubated for 15 min in the dark at 30°C. Slides were then washed in TNT, five times in 3% H_2O_2 in PBS, twice in TNT, each for 2 min, 30°C. For detection of DIG-labelled probe, slides were incubated in PE blocking buffer for 30 min at 30°C, then overnight at 4°C with anti-DIG(Fab)-POD-antibody

(11207733910, Sigma, USA) 1:1200 diluted in PE blocking buffer. Slides were washed again in TNT buffer three times at 30°C, 2 min each, fluorescent tyramine CY3 (TSA Plus Cyanine 3 System, NEL744001KT, Akoya) was diluted 1:75 in Amplification diluent, incubated 15 min in the dark, 30°C, followed by five PBS washes, one containing 1:5000 DAPI (Hoechst 33342 (DAPI), H1399, Invitrogen, CA) to stain nuclei. Afterward, slides were mounted in Mowiol mounting medium (see 2.1.11).

2.2.4 Image acquisition

Tissue samples (i.a for CB1-Reelin quantification) were analyzed and images were collected using a Zeiss LSM-710 laser scanning confocal microscope (Oberkochen, Germany) and the ZEN 2011 SP2 software (black edition, Zeiss). The microscope was equipped with Argon and HeNe (helium-neon laser) laser mounted on an Axio Observer ZI inverted microscope. The cell structures were specifically visualized by using the 488 nm excitation laser lines to detect FITC/Alexa 488, respectively 554 nm to detect Cy3/Alexa 546. DAPI was excited with 405 nm. All images were recorded using an EC Plan-Neofluar Plan-Apochromat 20x/0.80 dry objective and 40x/1.30 Oil DIC M27 Zeiss objective. To determine the intensity of the light for the individual color channel within a defined region of interest (ROI) the histogram function was used.

For cortex layer studies the confocal imaging was performed using a Visiscope 5-Elements spinning disk confocal system (Visitron Systems, Germany), built over Nikon TI equipped with Yokogawa CSU-W1 scan head and Prime BSI sCMOS camera (2048 × 2048 pixels, 6.5 µm pixel size, Photometrics). Laser lines of 488 and 561 nm were used for the fluorescence excitation and the fluorescence emission was acquired using filters 525/30 bandpass (Chroma) and 570 longpass (Chroma) for AF488-rabbit and AF546-rat, respectively. In addition, a DAPI channel was used with 405 nm excitation and emission filter 460/50 bandpass. The imaging was performed sequentially to minimize the spectral crosstalk. The sections were imaged in tile scan mode using a CFI Plan Apo Lambda S 25x / 1.05 NA (Nikon) Silicone immersion objective. Tile stitching was done using the microscope acquisition software VisiView. The images were prepared using Fiji distribution of ImageJ (Vers. 1.53c).

Confocal fluorescence images were obtained in a blinded manner and all were obtained from a minimum of 3 sections from 1 in 5 series per mouse. The immunofluorescence of cortical sections was performed along the rostral-to-caudal axis, and the quantifications were performed in the mediolateral and dorsolateral area of coronal sections that correspond to the motor/somatosensory cortex. Cortex layer specification was determined at embryonic day 18.5 (E18.5) in a 12.5 x 6.5 cm square column divided into 11 equally sized bins, from the ventricular surface to the marginal zone. Positive

cells for the corresponding marker were quantified and referred to the total cell number identified by Hoechst (DAPI).

2.3 Cell biological methods

2.3.1 Culture of cells

Cells (HT22, N2a, HEK 293) were thawed and diluted in Dulbecco's modified Eagle's medium (DMEM) (Gibco by life technologies, Carlsbad, USA), containing 10% FBS (fetal bovine serum, 12103C-100ML, Sigma, USA), 1% sodium-pyruvate (S8636-100ML, Sigma, USA), 1% Penicillin-streptomycin (P0781-100ML, Sigma Aldrich, USA), 1% non-essential amino acids (11350912, Gibco® Invitrogen, Carlsbad, USA). After centrifugation for 5 min on 1000 rpm, the supernatant was thrown away and the pellet was resuspended in 1 ml DMEM. The cell suspension was then added to a cell culture bottle containing 10 ml DMEM. Cells were split 1:10 every 4-5 days. For splitting, the cells were washed two times with warm phosphate-buffered saline (Dulbecco's PBS for cell culture) (D8537-500ML, Sigma-Aldrich, USA), and treated with trypsin-EDTA (Ethylenediaminetetraacetic acid) (T3924-100ML, Gibco by life technologies, Carlsbad, USA) solution for approximately 1 min until the cells detached visibly from the dish surface. The enzymatic reaction was then stopped by adding 10 ml warm plating medium and the suspension was centrifuged at 1000 x g at room temperature for 5 min. The cell pellet was re-suspended in plating medium and an appropriate amount was plated in a flask containing pre-warmed plating medium.

2.3.2 Lipofectamine 2000® transfection

One day before transfection 0.5-2x 10^5 cells/per well were split on 24-well plates in 1 ml DMEM medium so that cells will be 70% confluent at day of transfection. The old DMEM medium was replaced with fresh Opti-MEM medium without antibiotics (31085-070, Reduced Serum Medium, Gibco Life Technologies, USA). For each transfection sample, complexes were prepared as follows: 2 µl of Lipofectamine 2000 reagent (11668027, Invitrogen, USA) was diluted in 23 µl of Opti-MEM medium and then incubated for 5 min at room temperature. In parallel 500 ng of DNA was diluted in Opti-MEM medium to 25 µl per well and mixed gently. After 5 min incubation, the diluted DNA was added to diluted Lipofectamine 2000 reagent, gently mixed and 50 µl were added per well to the plated cells. After transfection, cells were incubated at 37°C in a CO_2 incubator for 48 h. The day after transfection, 500 µl Opti-MEM medium was added per well. Cells were harvested 48h after Lipofectamine treatment with trypsin (100-150 µl per well). Trypsin reaction was stopped with 1 ml medium and

cells were centrifuged at 200x g for 5 min. The pellet was treated with Quick extract (QE0905T, Lucigen, USA) according to manufactures protocol: add 50 µl QuickExtract DNA Extract solution vortex for 15 s, incubate at 65°C for 6 min, 15 s vortex, incubate at 98°C for 2 min. Concentration was measured with a Nanodrop and DNA was stored at -20°C.

2.3.3 Cell lines used

N2a and HT22 cells

Neuro2a (N2a) cells derived from a spontaneous neuroblastoma of an albino mouse (Olmsted et al., 1970). The cells grow as an adherent monolayer and form longitudinal extensions in culture (neurites).

HT22 cells (SCC129, Merck, Germany) are derived from a mouse hippocampal neuronal cell line. Both cell lines were used for transfection and later T7 Endonuclease assay (see 2.3.4).

With the transfection of designed sgRNAs it should be evaluated whether the guide RNA correctly guides the Cas9 for a DNA cut. The correct cut and the guiding efficiency can later be revealed with the T7 endonuclease assay. Five different plasmids were used: PX-330-sgRNA 1 and PX330-sgRNA 2 to test the guide efficiency; a GFP plasmid #174 as positive transfection control, (transfection can be monitored by detection of fluorescent GFP in the cells); PX330 Vector without sgRNA and no plasmid control as negative controls.

2.3.4 T7 Endonuclease assay

The T7 Endonuclease assay can determine the gene target efficiency of CRISPR/Cas9 modified genomes by digesting annealed PCR products. In the first step, products from genomic Cas9 modified DNA are amplified by PCR with specific primers against the targeted region. In this case a PCR with Q5 HotStart polymerase (M0493L, NEB, USA) was performed with primer pair 1.1 and 1.2 (1.1 fwd AAATCCAATCCCAGTTGCCG + 1.2 rev ATCACAATTTCCACGGACGC) covering the modified area. PCR amplicons from targeted genomic region were purified with the PureLink PCR purification kit (K310001, ThermoFisher Scientific, USA). PCR products were denatured so they can re-anneal to form heteroduplexes where modified and non-modified DNA strands form double-stranded PCR products again before T7 Endonuclease I (M0302S, NEB, USA) digestion. For the T7 Endonuclease digest, 2 µl of NEBuffer 2, 200 ng of purified PCR product and *dd*H_2O to 19 µl was added to a PCR tube. The hybridization reaction was run in a PCR cycler: 5 min 95°C, ramp down to 85°C at -2°C/s, ramp down to 25°C at -0.1°C/s, hold at 4°C. Then 1 µl T7 Endonuclease I was added and incubated at 37°C for 15

min. To stop the reaction, 2 µl of 0.25 M EDTA was added. The wild-type unmodified single strands will then pair with Cas9 modified single strands, which may not perfectly be repaired after a Cas9 double-strand break. The so-called indels result from non-homologous end joining (NHEJ) after a double-strand break. Because of the NHEJ the two strands will not match perfectly and this non-perfectly matched DNA can be recognized and cleaved by T7 Endonuclease I. The resulting fragments can then be analyzed on a 1.5% agarose gel to determine the efficiency of genome targeting by comparing the intensity of wild-type and cleaved strands (Fig. 13).

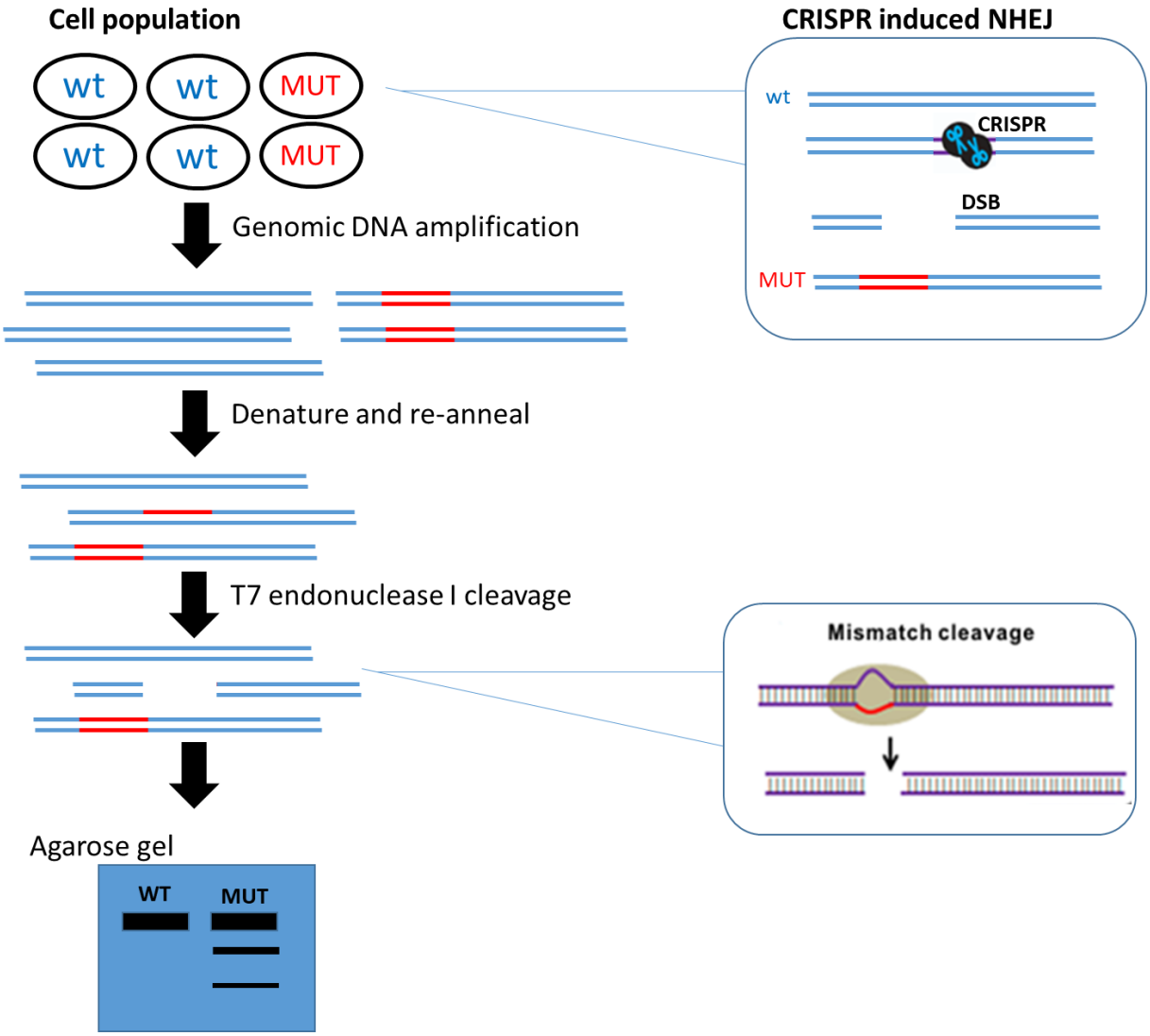

Figure 13 Model of T7 Endonuclease assay to detect indels caused by Cas9 mediated cuts.
After Cas9 mediated modification, genomic DNA is harvested and the modified region is amplified with specific primers. The amplified products are then re-annealed to form heteroduplexes of wild-type and modified DNA strands. These heteroduplex strands do not perfectly match, so this mismatch cleavage will be recognized and cleaved by T7 Endonuclease I. The resulting fragments can be visualized on an agarose gel and the gRNA modification efficiency can be estimated by comparing the intensity of the wild-type (WT) band compared to the additional mutation (MUT) bands.

2.3.5 Culture of embryonic stem cells

Embryonic stem (ES) cells were used to test the efficiency of sgRNA transfection again and as an option to produce a transgenic Reelin-Cre mouse line by electroporation of the CRISPR/Cas9 edited expression vector (carrying sgRNA, the sequence for Cas9 expression and a puromycin resistance gene, pX459, Addgene) and the HDR construct for Reelin-Cre sequences. The targeted ES cells would have to be injected into mouse blastocysts. Yet, we decided to create the CRISPR/Cas9 edited Reelin-Cre mouse via zygote injection. Nevertheless, test assays for gRNA efficiency were performed using the embryonic stem cell clone H4, provided by J. Leschik and T. Zimmermann in our institute, which originally was electroporated and positively selected for insertion with floxed-stop-floxed GFP (Zimmermann, PhD thesis, 2016).

2.3.6 Feeder cells

2.3.6.1 Thawing

Feeder cells were thawed in 37°C water bath and diluted into 10 ml of pre-warmed MEF (Mouse Embryonic Fibroblasts) feeder medium (Tab. 6) (1x stock solution contained: DMEM/F12 Glutamax (Dulbecco's Modified Eagle Medium/Nutrient mixture F-12 with GlutaMAX™, 10565-018, Invitrogen, USA), FBS (fetal bovine serum, 10270098, Gibco by life technologies, Carlsbad, USA), 10 mM non-essential amino acids, 100 mM sodium pyruvate, 10.000U/ml pen/strep) (must be diluted as soon as thawed) and put in 50 ml falcon tube with another 5 ml medium. Cells were pelleted by spinning for 4 min at 1000 rpm in a bench-top centrifuge. Afterwards, the medium was aspirated, and the cells were gently re-suspended in 5 ml of pre-warmed MEF feeder medium before the cells were counted. 5 ml of MEF feeder medium was prepared in 10 cm diameter plates und 5ml of cell suspension was added to the plate (best 3x 10^4 cells). Cells grow at 37°C in a humified 5% CO_2 incubator for 2-5 days.

Table 6 Mouse embryonic feeder medium

Reagent	**Stock concentration**	**Final concentration**	**Volume (total: 600ml)**
DMEM with Glutamax	1x	1x	500 ml
FBS	100%		60 ml
Non-essential Aminoacids	10 mM	0.1 mM	6 ml
Sodium Pyruvate	100 mM	1 mM	6 ml
Pen/Strep	10.000 U/ml	100 U/ml	6 ml

2.3.6.2 Splitting

Feeder dishes with confluent cells were washed twice with 10 ml PBS per wash. Cells were detached with 3 ml pre-warmed 0.05% trypsin (Trypsin/ EDTA 0.5/ 0.2 g/ PBS w/o Ca/Mg, T3924-100ML, Sigma Aldrich, USA) per dish at 37°C for 2 min. Afterward, the trypsin reaction was stopped with 5 ml feeder medium and all cell suspension were combined in a 50 ml falcon tube. The remaining dishes were rinsed with 10 ml feeder medium to collect remaining cells. The falcon tubes with the cell suspension were centrifuged for 4 min at 1000 rpm on room temperature. The medium was discarded and the pellet was re-suspended in 20 ml feeder medium. 8 ml feeder medium was pre-plated on 10 cm diameter dishes and 2 ml cell suspension was added. The cells were split 1:3 so that approximately 1.1 x 10^6 cells per 10 cm diameter dish were plated. Cells were incubated at 37°C and 5% CO_2. Possible further steps could be another split of cells, freezing or mitomycin (M4287, suitable for cell culture, Merck, Germany) treatment. Embryonic feeder cells can only be used until passage 6.

2.3.7 Embryonic stem cells

2.3.7.1 Thawing

Embryonic stem cells (ES) were thawed in a pre-warmed 37°C water bath and diluted into 10 ml of pre-warmed ES-cell medium (Tab. 7). Cells were pelleted by spinning for 4 min at 1000 rpm in a bench-top centrifuge. Then the medium was aspirated, and cells were gently re-suspended in 3 ml of pre-warmed ES-cell medium (final concentration should be ~ 2.5 x 10^6). 7 ml of ES-cell medium was prepared in 10 cm diameter plates and 3ml of cell suspension was added to the plate. Cells grow at 37°C in a humidified 5% CO_2 incubator for 2-5 days. Medium has to be changed every day.

Table 7 Mouse embryonic stem cell medium.

Reagent	Stock concentration	Final concentration	Volume (total: 600 ml)	Company	Catalog number
DMEM	1x	1x	500 ml	Sigma	D5671
ES-FBS	100%		90 ml	PAA	A15-101
L-Glutamine	200 mM	2 mM	6 ml	Sigma	G7513
Non-essential amino acids	10 mM	0.1 mM	6 ml	Invitrogen	11140035
Sodium Pyruvate	100 mM	1 mM	6 ml	Sigma	S8636
Pen/Strep	5000 U/ml	100 U/ml	12 ml	Sigma	P0781
LIF			600 µl	Recombinant LIF from supernatant of transfected HEK cells	Kind gift from Ari Weissmann
β- Mercaptoethanol	100 mM	0.1 mM	600 µl	Sigma	M7522

2.3.7.2 Splitting

When cells were confluent, they were washed 2 times with 10 ml PBS. After aspirating off the PBS, 3 ml of trypsin was added to the plate and incubated for 2-3 min at 37°C. In between, the plate had to be hit to loosen the cells. The trypsin reaction was stopped by adding 10 ml MEF medium per plate. Cell suspension was taken up and put in a 50 ml falcon tube. The plate was washed with another 10 ml of MEF feeder medium and added to the same falcon tube. Afterward, cells were pelleted by spinning for 3 min at 800 rpm. Prior to the re-suspension of the pellet in 5 ml medium, the cells were counted. Cells were plated with a density of 2 x 10^6 cells/ ml within 10-12 ml per 10 cm diameter plate and incubated at 37°C in a humidified 5% CO_2 incubator for 2-5 days.

ES cells are cultured on a layer of mitotically inactivated primary mouse embryonic fibroblasts. They must be plated 24 h prior to the addition of ES cells and allowed to adhere to the tissue culture plate. MED medium is removed and replaced with ES-DMEM before ES cells were added to the plate.

Mouse ESCs (H4 line) were cultured on mouse embryonic feeder cells (inactivated with mitomycin-C) in the presence of leukemia inhibitory factor (LIF) according to standard protocols (Hogan et al., 1994). After 4 days the ESCs were split and plated on gelatin (G1393, cell culture grade, Sigma-Aldrich, USA).

2.3.7.3 Transfection

Prior to Lipofectamine transfection (described 2.3.2), ES cells had to be plated on gelatin plates (see 2.3.7.4) to separate them from the feeders. For transfection 5 different plasmids were used: PX-459-sgRNA 1, PX459-sgRNA 2, GFP plasmid #174 (transfection can be monitored by detection of fluorescent GFP in the cells), PX459 Vector without sgRNA, no plasmid control. ES cells were also used for testing the transfection rate of sgRNA (in pX459 vector) and T7 Endonuclease assay (described 2.3.4).

2.3.7.4 Preparing gelatin plates

Gelatin was pre-warmed at 37°C in a water bath. Liquefied gelatin was diluted from 2% to 0.1% in 20x PBS (1 ml gelatin + 19 ml PBS). 10 cm diameter plates were filled with 6 ml gelatin (G1393, Sigma-Aldrich, USA) per plate and dried for 30 min. The remaining liquid was then aspirated before plating the cells.

2.3.8 HEK 293

HEK293 ("Human Embryonic Kidney") cells derived from embryonic kidney cells, which were transformed with Adenovirus 5 (Graham et al., 1977). The cells grow adherent as a monolayer. Culture conditions see 2.2.1.

For the evaluation of the overexpression of CB1, HEK 293 cells were transfected with four different plasmids: 1. Empty pCAGIG vector as negative control, 2. CB1 (constitutively) expressing vector as positive control and 3. CB1 stop floxed vector plus Cre-recombinase expressing vector.

2.4 Protein biochemical methods

2.4.1 Western Blot

Harvested HEK 293 cells were lysed using RIPA buffer (50 mM Tris-HCl pH 7.4, 150 mM NaCl, 0.1% SDS, 0.1% sodium deoxycholate, 1% NP-40). Lysates of transfected cells were taken and the protein content was measured by Bradford test (QuickStart Bradford 1x Dye reagent, #500-0205, Biorad) according to the manufacturer's protocol.

To prepare the proteins 3x Laemmli sample buffer (13.6 ml 20% SDS, 2.82 ml 2M Tris/HCl pH 6.8, 3 ml ß-Mercaptoethanol, 10.35 g 87% Glycerol, 60 mg Bromphenolblue) and 10% β-Mercaptoethanol was added to 50 ng protein lysate. The samples were heated up to 95°C for 5 min, spinned down and put on ice until loaded onto the gel. Samples were adjusted to 20 µl with 1x PBS. The samples were heated up to 95°C for 5 min, spinned down and put on ice until loaded onto the gel.

Protein samples were separated on a 10% Polyacrylamide gel in running buffer (SDS Running Buffer: 1.9 M Glycerin, 0.25 M Tris, 1% SDS) for 1.5 h with a voltage of 130 V. The SDS-PAGE (sodium dodecyl sulfate–polyacrylamide gel electrophoresis) gel was composed of a resolving gel and an overlaid stacking gel.

The resolving gel consists of 2.5 ml 40% acrylamide/bisacrylamide, 2.5 ml lower buffer (1.5 M Tris/HCl pH 8.8, 0.4% SDS), 5 ml H_2O, 5 µl TEMED, 80 µl 10% APS. After 20 min polymerization time, the stacking gel was pipetted on top of the resolving gel. The stacking gel consists of 11 ml 40% acrylamide/bisacrylamide, 2.5 ml upper buffer (0.5 M Tris/HCl pH 6.8, 0.4% SDS), 6.5 ml H_2O, 10 µl TEMED, 70 µl 10% APS.

Proteins were electroblotted to a nitrocellulose membrane by wet blotting in transfer buffer (0.15 M Glycin, 0.2 M Tris/HCl, 20% EtOH) for 90 min at 300 mA. Afterwards the membrane was stained with Ponceau (114275, Merck, Germany) for 5-10 min on a rocker to control the successful transfer of proteins on the membrane. Subsequently, the membrane was blocked with 5% nonfat dry milk (w/v) in TBS-T (Tris-buffered saline: 10 mM Tris/HCl pH 8.0, 140 mM NaCl, 0.1% Tween 20 (S5151584.843, Merck, Germany)) for 1 h at room temperature. Then the primary antibody (Tab. 8) diluted in 5% nonfat dry milk (w/v) was added and incubated overnight at 4°C. To remove the antibody, the membrane was washed 3x 10 min with TBS-T. The horseradish peroxidase coupled secondary antibody (Tab. 9) diluted in 5% nonfat dry milk (w/v) was added and incubated for 30 min at RT. Afterwards, the membrane was washed 2x 10 min with TBS-T and 10 min with PBS. To detect the bound antibodies a chemiluminescent substrate (Westar ηC 2.0, Cyanagen, Bologna, Italy) was used according to manufacturer's instructions and imaged with the Peqlab Fusion-SL system (Peqlab, Erlangen, Germany) using the fusion software by Vilber lourmat.

Table 8 List of primary antibodies used for Western Blot.

first antibody	host animal	company	catalog number	working concentration
CB1	rabbit	Immunogenes	IMG-pAb001	1:1000
HA	mouse	Covance	PRB-101C	1:1000
GAPDH	rabbit	Merck Millipore, Billerica,USA	ABS16	1:1000

Table 9 List of secondary antibodies used for Western Blot.

secondary antibodys	host animal	company	catalog number	working concentration
HRP-goat anti mouse	mouse	Dianova, Hamburg, Germany	115-035-146	1:5000
HRP- goat anti-rabbit	rabbit	Dianova, Hamburg, Germany	111-035-045	1:5000

2.5 CRISPR/Cas9

2.5.1 Selection of guide RNAs

The mouse Reelin gene is encodes a protein of 3461 amino acids and consists of 65 exons spanning a region of 460252 bp (Royaux et al., 1997). It is located on chromosome 5 (GRCm38.p4 C57BL/6), Locus NC_000071 Region: 21884454..22344705. The gRNA sequences were designed based on the target site sequence that needs to be flanked by a 3 bp NGG PAM (Protospacer adjacent motif) sequence at its 3' end. The PAM region is important for the binding of the RNA-protein complex with the DNA. For targeting the Reelin gene, sites for two possible guide RNAs were designated in front of and after the translational stop, respectively, in exon 64 with the CRISPR design tool of the Zhang lab (www.CRISPR.mit.edu). After entering the base sequence, this tool shows all possible guide RNAs taking in account its uniqueness in the genome. Uniqueness means that the guide RNA should have as many mismatches to potential off-target regions as possible. A newer design-tool called CRISPOR (http://crispor.tefor.net/) also considers the on-target efficiency (after Doench et al., 2016; Moreno-Mateos et al., 2015). Two guide RNAs were selected, one before and one after the stop codon, gRNA1 and gRNA2, respectively. DNA oligonucleotides with the putative gRNA sequences were ordered for subcloning them into the bicistronic expression plasmid pX330 (former name from Addgene (Cambridge, MA; plasmid ID 42230; now pSpCas9 (BB)) to eventually test the cutting efficiency of the chosen gRNAs in cell culture (see above). For subcloning into the BbsI digested pX330 vector, to the ordered oligos, BbsI restriction sites needed to be added (marked in yellow, Tab. 10). The "CACCG" and "AAAC" (marked in yellow in Tab. 10) overhangs for cloning were added, so the ending sequence of the actual oligo that should be ordered is: 5'-CACCGN…N-3' and 3'-CN…NCAAA-5', respectively.

Table 10 List of ordered oligo sequences for the cloning into the Cas9 expression vector.

gRNA 1 (5'-3')	fwd	CACCGACAGAAGACGAAGGTCGCTT
	rev	AAACAAGCGACCTTCGTCTTCTGTC
gRNA 2 (5'-3')	fwd	CACCGGGAAGGGACACATTGTACGC
	rev	AAACGCGTACAATGTGTCCCTTCCC

2.5.2 Subcloning of guide RNA in Cas9 expression vector

Bicistronic expression vectors pX330 (for expression in HT22 and N2a cells) and pX459 (for expression in embryonic stem cells) expressing Cas9 and sgRNA (Cong et al., 2013) were digested with BbsI, the enzyme was inactivated on 65°C for 20 min and the linearized vector was purified with the PureLink PCR purification kit (K310001, ThermoFisher Scientific, USA). A pair of oligos for each targeting site was annealed, phosphorylated and ligated to the linearized vector. Cloned vector was transformed into stbl3 E. coli bacteria; single colonies were picked the next day and multiplied via miniprep. The miniprep was purified with PureLink Quick Plasmid Miniprep Kit (K210011, Thermofisher, USA) and the DNA was sequenced to verify the successful ligation.

2.5.2.1 Oligo annealing and phosphorylation

sgRNA oligos were resuspended in H_2O to a final concentration of 100 µM

1 µl	sgRNA fwd
1 µl	sgRNA rev
1 µl	10x T4 ligation buffer
1 µl	T4 PNK
6 µl	ddH_2O
10 µl	total

Oligos were annealed in a thermocycler by using the following parameters: 37°C for 30 min, 95°C for 5 min, ramp down to 25°C at 5°C/ min. 1 µl annealed Oligo was diluted in 199 µl H_2O.

2.5.2.2 BbsI digestion of backbone vector and cloning

Ligation and BbsI digestion reaction was setup as below and incubated for 1 h under following conditions: 37°C for 5 min, 21°C for 5 min, 6 cycles.

100 ng	Plasmid PX-330 (pSpCas9(BB))
2 µl	Diluted oligo duplex
2 µl	10x buffer 2.1
1 µl	DTT (Dithiothreitol) (10 mM)
1 µl	ATP (Adenosin Triphosphate)(10 mM)
1 µl	FastDigest BbsI
0.5 µl	T4 DNA ligase
x µl	ddH_2O
20 µl	total

Ligation reaction was treated with PlasmidSafe exonuclease (Plasmid-Safe™ ATP-Dependent DNase, 161010 (E3101K), Biozym (Epicentre, Germany)) to digest any residual linearized DNA.

11.9 µl	Ligation reaction
1.5 µl	10 x PlasmidSafe buffer
0.6 µl	ATP (25 mM)
1 µl	PlasmidSafe exonuclease
15 µl	total

Reaction was incubated in a thermocycler at 37°C for 30 min, followed by a 70°C for 30 min step.

2.5.3 Prediction of potential off-targets

Potential off-targets were predicted by searching the mouse genome for matches to the 20 nt sgRNA sequence followed by NGG PAM sequence while allowing for up to three mismatches. Matches were ranked first by ascending number of mismatches, then by ascending distance from the PAM sequence. Cas9 enzyme can tolerate a few base mismatches and can still cleave at such sites; in particular, mismatches in the first seven nucleotides (of the 20) are more tolerated than those from the 8th position onwards (Cong et al. 2013).

2.5.4 Cloning of the homology directed repair (HDR) construct

For the insertion of the Cre-construct into the Reelin locus after the Cas9 mediated cut, a HDR construct had to be cloned. The HDR construct consists of a left (477 bp) and right (420 bp) homology arm, a peptide 2A linker, a sequence encoding Cre-recombinase fused to a HA (hemagglutinin)-Tag, and a nuclear localization signal (NLS). The peptide 2A linker has the function to ensure the expression of two separate proteins, Reelin and Cre. The construct is 2067 bp in total. To design the construct, Vector NTI software (Invitrogen, Carlsbad, CA, USA) was used.

As backbone vector the pBluescript (pBSII-KS(+)) targeting vector (Fig. 14) was used, which was linearized with NotI and HindIII and gel purified before cloning the 2A and the HA-NLS-Cre fragments between the NotI and the HindIII sites of the pBSKS+ vector.

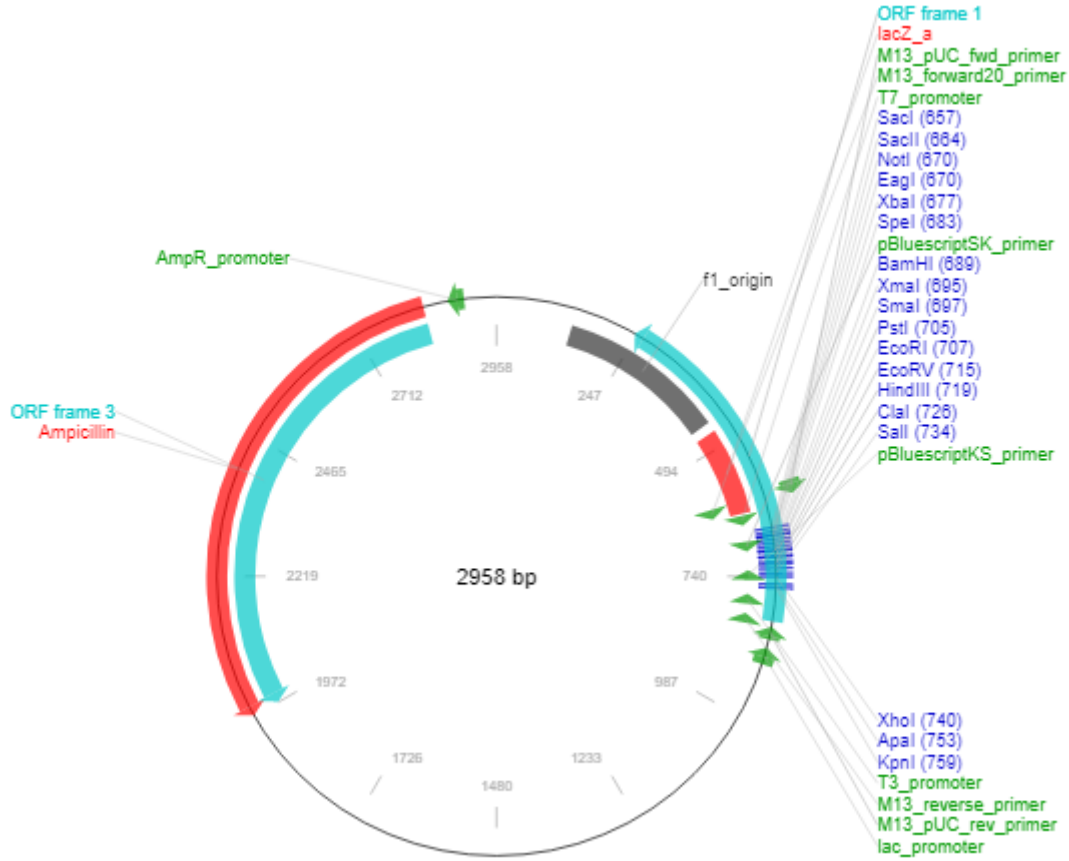

Figure 14 pBluesciptKS(+) vector.
Standard cloning vector (phagemid excised from lambda ZAP) with the 5' sequencing primer M13pUC-fwd and T7 and the 3' sequencing primer M13pUC-rev and T3. The vector carries a resistance against Ampicillin. https://www.addgene.org/vector-database/1949/ (20.05.2020).

2.5.5 Cloning strategy for 2A-Cre sequence

To create the 2A-Cre sequence, the sequences encoding 2A peptide and Cre-recombinase were obtained from two different vectors, which had been constructed in the lab before (S. Guggenhuber) using PCR (see below).

The 2A sequence (shown in green) was amplified out of vector #421 (pAAV-hSyn-HA-NLS-Cre-2A-hChR2-EYFP-WPRE) via PCR with primers Fwd AT GCGGCCGC GAGGGCAGAGGAAGTCTTCTAA and Rev AT GTTAAC GGATCCCGGTGCAGGGCCGGGATT. For correct insertion into the pBSII-KS(+) vector and to bind to the Cre-insert a 5' NotI, a 3' HpaI site and additional sites for restriction digest (AT or TA) were added (Tab. 11) shown in red).

Table 11 2A sequence with additional 5‘ NotI and 3‘ HpaI restriction sites and additional “AT” or “TA” sites for restriction digest

5’-AT GCGGCCGCGagggcagaggaagtcttctaacatgcggtgacgtggaggagaatcccggccctgcaccgggatccGTTAAC TA-3’

The HA-NLS-Cre sequence (Tab. 12, HA sequence shown in yellow; NLS sequence shown in green and Cre sequence in black) was extracted from vector #154 (HA-NLS-Cre) with PCR primers Fwd AT GTTAAC ATGTATCCGTATGATGTTCCTGA and Rev AT AAGCTT TCAATCGCCATCTTCCAGCA. A HpaI site at the 5’ end, a HindIII site at the 3’ end and additional sites for restriction digest (AT or TA) were added (shown in red). The HpaI site at the 5’ end is immediately in front of the start codon for the HA-NLS-Cre-sequence, the HindIII site is placed immediately after the stop codon (shown in bold red), which had to be present at the end of the Cre-recombinase, because the stop had to be re-moved from the Reelin left homology arm sequence to place the Cre-recombinase immediately in front of the Reelin stop-codon.

Table 12 HA-NLS-Cre sequence with additional 5‘ HpaI and 3‘ HindIII restriction sites and additional “AT” or “TA” sites for restriction digest

5’-ATGTTAAC
atgtatccgtatgatgttcctgattatgctagcctcgaattcccaagaagaagaggaaggtgtccaatttactgaccgtacaccaaaatttgcc
tgcattaccggtcgatgcaacgagtgatgaggttcgcaagaacctgatggacatgttcagggatcgccaggcgttttctgagcatacctggaa
aatgcttctgtccgtttgccggtcgtgggcggcatggtgcaagttgaataaccggaaatggtttcccgcagaacctgaagatgttcgcgattatc
ttctatatcttcaggcgcgcggtctggcagtaaaaactatccagcaacatttgggccagctaaacatgcttcatcgtcggtccgggctgccacg
accaagtgacagcaatgctgtttcactggttatgcggcggatccgaaaagaaaacgttgatgccggtgaacgtgcaaaacaggctctagcgtt
cgaacgcactgacttcgaccaggttcgttcactcatggaaaatagcgatcgctgccaggatatacgtaatctggcatttctggggattgcttgta
acaccctgttacgtatagccgaaattgccaggatcagggttaaagatatctcacgtactgacggtgggagaatgttaatccatattggcagaa
cgaaaacgctggttagcaccgcaggtgtagagaaggcacttagcctgggggtaactaaactggtcgagcgatggatttccgtctctggtgtag
ctgatgatccgaataactacctgttttgccgggtcagaaaaaatggtgttgccgcgccatctgccaccagccagctatcaactcgcgccctgga
agggatttttgaagcaactcatcgattgatttacggcgctaaggatgactctggtcagagatacctggcctggtctggacacagtgcccgtgtc
ggagccgcgcgagatatggcccgcgctggagtttcaataccggagatcatgcaagctggtggctggaccaatgtaaatattgtcatgaactat
atccgtaacctggatagtgaaacaggggcaatggtgcgcctgctggaagatggcgat**tga** AAGCTT AT-3’

Both PCR reactions were performed with Q5 Hifi Polymerase according to manufacturer's recommendations and afterwards PCR products were gel purified and digested with the appropriate enzymes (2A with NotI and HpaI, HA-NLS-Cre with HpaI and HindIII).

Q5 Hotstart PCR

25 µl	Q5 Hotstart 2x Mastermix
2.5 µl	Primer fwd (10 mM)
2.5 µl	Primer rev (10 mM)
2 µl	Vector (200 ng)
18 µl	H_2O
50 µl	Total volume

Vector pBSII-KS(+) (M#105) was linearized with two restriction enzymes NotI and HindIII and gel purified.

1 µl	Vector DNA (329 ng)
1 µl	HindIII
2 µl	CutSmart
16 µl	H_2O
20 µl	Total volume

Incubate 1 h at 37°C

Inactive enzyme at 80°C for 20 min

Add 1 µl NotI and incubate for another hour at 37°C. Inactivate the enzyme at 65°C.

Ligation

The NotI and HindIII digested pBSKS(+) backbone plasmid and the two PCR products were mixed in a volume of 20 µl containing 50 ng vector, 2A PCR product, Cre PCR product (in different ratios, see Tab. 13), 800 U T4 Ligase, 10 x Ligase buffer and *dd*H_2O and incubated for 2 h at room temperature.

Products were transformed into 100 µl of stbl3 competent cells as overnight culture and, on the following day, single transformed colonies were inoculated into LB medium containing ampicillin. On the next day the DNA products were isolated using a DNA miniprep kit. DNA could then be analyzed/verified via restriction digest with HindIII and NotI (2909 + 1170bp).

Table 13 Ligation reaction: 50 ng vector were combined with the two inserts, 2A and HA-NLS-Cre in different ratios.

	1:1:1	1:2:2	1:7:7	1:10:10
2A	1 ng	2 ng	7 ng	10 ng
HA-NLS-Cre	12 ng	24 ng	84 ng	120 ng

2.5.6 Cloning strategy for homology arms

Both homology arms of the Reelin sequence were obtained by PCR and used for construct cloning without adding restriction enzymes and previous subcloning.

First, the sequences for the homology arms were amplified out of a wild-type (C57BL/6J) mouse genome (Primers see in Tab. 14). Afterwards the PAM sequence and the guide RNA sequences had to be changed with silent mutations in a second PCR (Primers for modified sequences, see Tab. 15; modified bases shown in green, PAM sequence in yellow). The base pair change in each PAM sequence prevents the Cas9 from repetitive cutting, after the HDR construct is recombined into the locus (targeted at DSB site). Additionally, the modified sgRNA sequences in the homology arms inhibit /renders the sgRNA from proper binding after HDR binding.

All PCR steps were performed with Q5 Hifi Polymerase (NEB) under following conditions: 5 min 95°C, [30s 95°C, 30s 66°C, 2 min 72 °C] 30 cycles, 5 min 72 °C for right homology arm product and 5 min 95°C, [30s 95°C, 30s 70°C, 2 min 72°C] 30 cycles, 5 min 72°C for left homology arm product. The PCR mix contained 5x Q5 buffer, 10 µM forward primer, 10 µM reverse primer, 2 µl genomic DNA, 10 mM dNTPs, 1U Q5 Hifi DNA polymerase and was adjusted to a total volume of 25 µl with H_2O.

2.5.6.1 Cloning of homology arms from wild-type Reelin DNA with PCR

First of all, the homology arms were cloned out of a wild-type genome of a C57BL6J mouse. The PCR was performed according to the protocol mentioned in 2.5.6 with primers specified in Tab. 14, which shows primers for both left and right homology arms with their position in the mouse genome. Additionally, the PAM region is marked in yellow, and bases that will be changed in the second PCR step appear in red.

Table 14 List of primers used PCR step 1 for cloning the homology arms out of the mouse genome.

Left homology arm		Mouse genome position (GRCm39/mm39, C57BL/6)
lHarm fwd	CTCATTCCGCTAATGGAGCTTTT	chr5: AC113028.15: 99794 to 99816
lHarm rev	TGGGTATCGCCTAAGCGACCTT	chr5: AC113028.15: 99340 to 99361
Right homology arm		
rHarm fwd	AGAATCCAAGTTTATTTCCCTTTCC	chr5: AC113028.15: 99312 to 99336
rHarm rev	GGACAAACGACGAGAACTTATT	chr5: AC113028.15: 98904 to 98925

2.5.6.2 Change PAM sequence and 2 additional silent mutations within the guide sequence

The next step was to perform a second PCR with the products of step 1 (2.5.6.1) to change the bases of the PAM region (yellow) and add two (left homology arm) respectively three base pair changes (right homology arm) without changing the resulting amino acid (silent mutation). The changed bases were marked in red in Tab. 15, where the primers used in PCR step 2 are shown.

Table 15 List of primers for PCR step 2 used to change the PAM sequence and insert silent mutations within the guide RNA sequence.

Left homology arm	
lHarm oPAM fwd	CTCATTCCGCTAATGGAGCTTTT
lHarm oPAM rev	TGGGTATCGTCTAAGCGACCGC
Right homology arm	
rHarm oPAM fwd	AGAATCCAAGTTTATTTCCCTTTTCAACGGATAATGTGTC
rHarm oPAM rev	GAACTTATTCATATAAACAAGAGACAGAGC

To prevent a repeated cutting of the targeted site by Cas9, the PAM sequence had to be changed and at the same time, the guide RNA sequence had to be changed to hinder the binding of the Cas9 complex by using silent mutations. The primers for cutting the homology arms out of the mouse genome

are shown in red. The reverse primer for the left homology arm (Fig. 15) and the forward primer for the right homology arm (Fig. 16) contain the targeted guide RNA (underlined) and the PAM (marked in yellow) region. The intended changes within the PAM region and the two silent mutations in the guide RNA region are marked in green.

A) Left homology arm (wild-type sequence)

Ctcattccgctaatggagctttgttttcattttagcccttaaggttgaaatgaaaatgttaactagcat
aaccgaatcgcttttgctgtgtatgtgtgtaaataaggtaatgagtacagtgtgcatgtcctctggatgg
tgagatgtgttcaggttctgaaaagaaaaggactccggggcagaaggtagtgaggcaggtgcccgtc
taattattctgtccctaggcggtgaagtctgcatgacttctgaattctgaagtttttcagatatatagcag
gctaccttggggccttagaataaatcatacgttcattggtgggactcacatgctctctctcctttccctcc
ccacctgtaccttcttgtggtttttctaacagcactcgcaaacaaaattacatgatgaatttttcacgg
caacatgggctcaggcacttctaca acagaagacgaaggtcgcttagg cgataccca

B) Left homology arm (modified sequence)

Ctcattccgctaatggagctttgttttcattttagcccttaaggttgaaatgaaaatgttaactagc
ataaccgaatcgcttttgctgtgtatgtgtgtaaataaggtaatgagtacagtgtgcatgtcctctgg
atggtgagatgtgttcaggttctgaaaagaaaaggactccggggcagaaggtagtgaggcaggtg
cccgtctaattattctgtccctaggcggtgaagtctgcatgacttctgaattctgaagtttttcagatat
atagcaggctaccttggggccttagaataaatcatacgttcattggtgggactcacatgctctctctc
ctttccctccccacctgtaccttcttgtggtttttctaacagcactcgcaaacaaaattacatgatga
atttttcacggcaacatgggctcaggcacttctaca acagaagacggcggtcgcttaga
cgataccca

C) Summary for sgRNA1

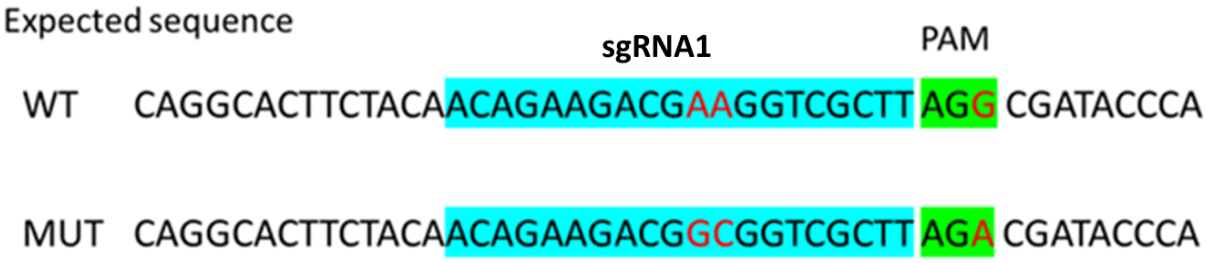

Figure 15 Insertion of silent mutations into the sgRNA1 sequence of the left homology arm
A) Wild-type sequence of the left homology arm including the used primers for cloning (red), the sgRNA1 sequence (underlined), the PAM region (yellow) and the bases which were planned to be changed (green). B) The putative sequence of the modified left homology arm after changing the intended bases (green) within the sgRNA1 sequence (underlined) and the PAM region (yellow)to silent mutations using specifically modified PCR primers (red). C) The summary shows the sgRNA1 containing section and compares the base changes within sgRNA1 of wild-type (WT) and the HDR sequence (MUT) directly. The section shows the guide RNA sequence (blue) and the PAM sequence (green) with the expected changes (red shaded). For the left homology arm, the

intention was to change the mutant PAM sequence from AGG to AGA and after inserting the silent mutations the mutant sequence was planned to be changed from CGA AGG to CGG CGG but for technical reasons the change of the sequence was not inserted.

Figure 16 Insertion of silent mutations into the sgRNA2 sequence of the left homology arm
A) Wild-type sequence of the right homology arm including the used primers for cloning (red), the sgRNA2 sequence (underlined), the PAM region (yellow) and the bases which were planned to be changed (green). B) The putative sequence of the modified right homology arm after changing the intended bases (green) within the sgRNA2 sequence (underlined) and the PAM region (yellow)to silent mutations using specifically modified PCR primers (red). C) The summary shows the sgRNA2 containing section and compares the base changes within sgRNA2 of wild-type (WT) and the HDR sequence (MUT) directly. The section shows the guide RNA sequence (blue) and the PAM sequence (green) with the expected changes (red shaded). For the right homology arm, the mutant PAM sequence was changed from CCA to TCA and after inserting the silent mutations the mutant sequence was successfully changed from GCG TAC to ACG GAT.

2.5.6.3 Assembling the fragments for the HDR construct

Cloning with the Gibson system (E2611S, NEB, USA) was used for cloning and assembly of all fragments to obtain the construct for homology directed repair for the CRISPR/Cas9 approach. The pBluescript vector (pBSKS+, Stratagene, USA) was used as vector backbone.

Gibson Assembly cloning allows the joining of multiple DNA fragments in a single, isothermal reaction. To assemble the inserts to the vector backbone each DNA fragment must contain a 20-40 bp overlap with adjacent DNA fragments (Tab. 16). These fragments need to be mixed with a cocktail of 3 enzymes: exonuclease, DNA polymerase and DNA ligase. The exonuclease chews back DNA from the 5' end, so the resulting single-stranded region is able to anneal with the fitting adjacent DNA strand. Afterwards, DNA polymerase incorporates nucleotides to fill in gaps and DNA ligase covalently joins the DNA segments and removes nicks in the DNA. The final construct contains a 2A sequence, which allows proteolytic cleavage of Reelin protein and HA-NLS-Cre-recombinase protein on the ribosome. The flanking homology arms ensure a targeted introduction of the insert into the Cas9-mediated double strand break (Fig. 17).

Table 16 List of primers used for Gibson cloning.

Primer name	5'-end	Primer sequence	3`-end
1F fwd	pBSKS	cgaattggagctccaccgcggtggcCTCATTCCGCTAATGGAG	Left homology arm
1R rev	2A-Cre	ttcctctgccctcTGGGTATCGTCTAAGCGAC	Left homology arm
2F fwd	Left homology arm	tagacgataccaGAGGGCAGAGGAAGTCTTC	2A-Cre
2R rev	Right homology arm	aaacttggattctAAGCTTTCAATCGCCATC	2A-Cre
3F fwd	2A-Cre	cgattgaaagcttAGAATCCAAGTTTATTTCCC	Right homology arm
3R rev	pBSKS	gggccccccctcgaggtcgacggtatcgataGAACTTATTCATATAAACAAGAGAC	Right homology arm

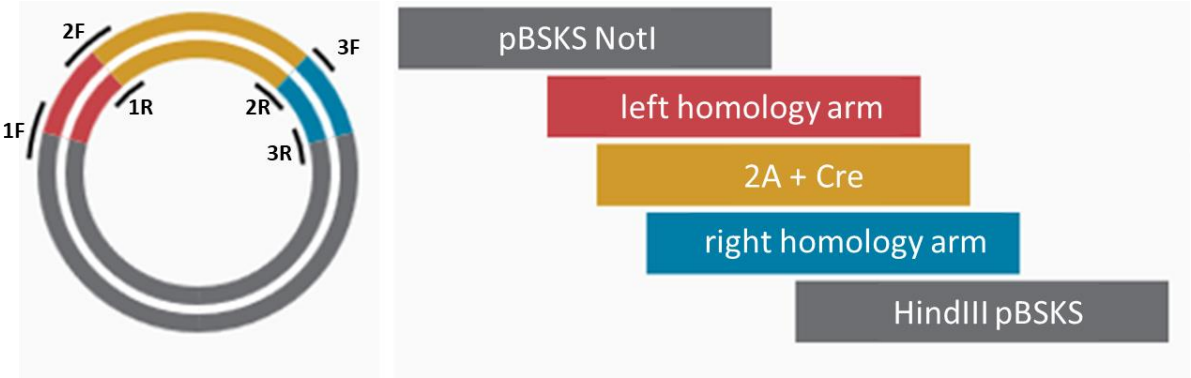

Figure 17 Schematic view of annealed insertion vector after Gibson cloning.
Three inserts were cloned between the NotI and HindIII restriction site within the multiple cloning site of the pBluescript vector (pBSKS NotI and HindIII pBSKS, grey). The inserts left homology arm (left homology arm, red), 2A + HA-NLS-Cre-recombinase (2A+Cre, yellow), right homology arm (right homology arm, blue) had a 3‘ and a 5‘ overlap to the adjacent component. With this homologous overlap, the constructs could be fused together in the right order. 2A was cloned out of vector #421 (pAAV-hSyn-HA-NLS-Cre-2A-hChR2-EYFP-WPRE) and HA-NLS-Cre was cloned out of vector #154 (HA-NLS-Cre) (vector described here: Guggenhuber et al., 2010) and contained a STOP-cassette. With the insertion of this construct into the Reelin gene, the original stop codon was removed and replaced with the new STOP codon from this vector. Small letters in the primer sequences always correspond to the previous fragments junction site, capital letters to the newly annealed junction.

To set up a total volume of 20 µl 2x Assembly master mix and 0.5 pmol of every PCR fragment was used and adjusted with *dd*H_2O.

2.5.7 Production of long single stranded DNA

For the production of long single-stranded DNA (ssDNA) oligo the Guide-it™ Long ssDNA Production System (632644, Takara, USA) was used. The ssDNA is produced by selective digest of either sense or antisense strand.

Preparation of the vector

In a first step the HDR construct has to be cut out of the 2A-HA-NLS-Cre-harm-pBSII-KS(+) Vector as follows:

2 µg	Plasmid
2.5 µl	SacII
2.5 µl	XhoI
6 µl	Cut Smart buffer
48.25 µl	RNAse-free H_2O
60 µl	Total volume

3 h at 37°C

Gel purification of the HDR construct followed.

2.5.7.1 Preparation of dsDNA substrate by PCR

In the second step the HDR construct has to be amplified in PCR reaction with specific primers lying within the HDR sequence. One of the primers must contain a 5' phosphorylation as recognition site for later strandase digestion. Antisense must use 5'phosphorylated forward primer paired with un-phosphorylated reverse primer, and sense strand needs an un-phosphorylated forward primer and a 5' phosphorylated reverse primer (Tab. 17).

Table 17 List of primers used to create recognition sites for strandase digestion to produce single stranded DNA.

Long ssDNA Primer		
longssDNA P 1	Fwd Primer	GCCCTTTAAGGTTGAAATGA
longssDNA P 2-P	5'-P rev Primer	5'P-CTGTGCTAAAATGCCACTTA
longssDNA P 3-P	5'-P fwd Primer	5'P-GCCCTTTAAGGTTGAAATGA
longssDNA P 4	Rev Primer	CTGTGCTAAAATGCCACTTA

Set up two 100-µl PCR reactions as shown below:

PCR Reaction A (rev-P):		PCR Reaction B (fwd-P):	
50 µl	PrimeSTAR® Max Premix (2X)	50 µl	PrimeSTAR Max Premix (2X)
20–40 ng (8 µl)	Template DNA	20–40 ng (8 µl)	Template DNA
2 µl	Primer 1 (40 µM)	2 µl	Primer 3 (40 µM)
2 µl	Primer 2 (40 µM)	2 µl	Primer 4 (40 µM)
38 µl	RNase free H_2O	38 µl	RNase free H_2O
100 µl	Total volume	100 µl	Total volume

Cycling conditions:

Step	Temperature (°C)	Time (sec)	Cycles
Denaturation	98	10	40
Annealing	55	5	
Elongation	72	10 (5sec/kb)	
Storage	4	hold	

Analyze 5 µl of each PCR reaction on an agarose gel

The PCR product was purified with the NucleoSpin Gel and PCR Clean-Up Kits (Cat. No. 740609.50 or 740609.250, Macherey-Nagel, Germany) provided with the kit according to manufacturer's recommendations.

2.5.7.2 Preparation of ssDNA

1. Set up Strandase A reaction as follows:

5-15 µg	dsDNA substrate
5 µl	Strandase A Buffer (10x)
5 µl	Strandase A Mix
x µl	RNase free H_2O
50 µl	total

2. Incubate reaction as follows
   37°C 5 min/kb (10min)
   80°C 5 min
   4°C until next step

3. Set up Strandase B reaction as follows:

50 µl	Strandase reaction mixture (entire reaction from step 1)
50 µl	Strandase B Buffer (2x)
1 µl	Strandase B Mix
101 µl	total

4. Incubate reaction as follows
   37°C 5 min/kb (10min)
   80°C 5 min
   4°C until next step

10 µl of each of the samples was run on a 1.5% agarose gel, including 100–200 ng of the dsDNA substrate, in a separate lane, as a control.

Column purify the ssDNA to remove free nucleotides with the NucleoSpin Gel and PCR Clean-Up Kits (Cat. No. 740609.50 or 740609.250, Macherey-Nagel, Germany) provided with the kit according to

manufacturer's recommendations. Afterward, the DNA concentration was measured by Nanodrop and the samples were kept at 4°C until usage.

2.5.8 Preparation of CRISPR injection mixes

CRISPR guide RNAs were used as annealed two part synthetic crRNA (Alt-R™ CRISPR guide RNAs, Integrated DNA technologies, Inc. (IDT), USA) and tracrRNA (#1072533, IDT, USA) molecules for all experiments. The Cas9 protein Alt-R™ S.p. Cas9 Nuclease 3NLS was purchased from Integrated DNA Technologies, Inc. (Cat 1074181 Lot 262883, IDT, USA) and Cas9 mRNA was purchased from Sigma, USA (Cat CAS9MRNA-1EA Lot 12081419MN).

To prepare the ctRNP mix, lyophilized crRNA and tracrRNA were resuspended in IDTE buffer (TrisHCl 10 mM, pH 7.5, EDTA 0.1 mM, pH 8.0). 5 µg of crRNA (5 µl of 1 µg/µl) and 10 µg of tracrRNA (10 µl of 1 µg/µl) were pipetted together and were annealed in a thermocycler as follows: 95°C for 5 min followed by ramp down to 25°C at 5°C/min. The produced guide RNA was then diluted in IDTE buffer to a final concentration of 20 ng/µl, mixed with Cas9 protein (work conc. 30 ng/ µL) and incubated for 10 min to obtain the ctRNP complex. The ctRNP (ribonucleoprotein containing guide RNA and Cas9 nuclease) complexes were mixed together with 500 ng ssDNA donors (50 ng/µl) and 45 ng Cas9 mRNA (work conc. 15 ng/ µL). The final injection mixes were spun at 13000 x g for 5 min at RT.

2.5.9 Zygote injections

Mouse embryo manipulation and microinjection into fertilized eggs were performed according to methods previously described (Behringer et al., 2014) by Dr.Eshkind from TARC, Mainz. For generation of mouse zygotes for injection C57BL/6J stud males were paired with FVB females (both strains from Charles River Laboratories, USA, and then from own breeding colonies). Donor FVB females (4-5 weeks old) were superovulated by intraperitoneal injection of 5IU pregnant mare serum gonadotropin (PMSG, G4877, Sigma-Aldrich, USA), followed by injection of 5 IU human chorionic gonadotropin (hCG, C1063, Sigma-Aldrich, USA) 48 hours later. Fertilized eggs could then be recovered from the oviducts of superovulated FVB/N females the morning after mating. For the isolation of zygotes three to four oviducts were placed in drops of M2 medium (MR-015-D, Merck Millipore, USA) with 10 mg/ml hyaluronidase (H3506, Sigma-Aldrich, USA) in a 60 mm culture dish. The swollen ampullae of oviducts were torn open under a stereomicroscope (SZ61, Olympus with top and bottom illumination) by using a 29-gauge needle to allow the cumulus mass to extrude into the media. Zygotes were collected and then sequentially transferred with an embryo transfer pipette into 3 drops of M2 medium to remove residual hyaluronidase and follicular cells. After washing the zygotes with 3 drops pf

M16 medium (MR-016-D, Merck Millipore, USA), the zygotes were stored in M16 medium coated with mineral embryo culture-tested light oil (M5310, Sigma-Aldrich, USA) in a 4-well culture dish (Z688754, Merck, Germany) in an incubator at 5% CO_2 and 37°C for several hours before and after injection until they were transferred into foster mothers.

Microinjections were performed with a mechanical micro-manipulator (Leica) using microinjection needles (glass capillaries with filament inside, 1B100F-6, World precision instruments, USA) and a micropipette puller (P-97, Sutter Instrument, USA) following standard protocols (Behringer et al. 2014). 2 µl of CRISPR-injection-mix was always injected into the larger pronucleus.

To collect injected zygotes, they were placed on a pre-siliconized slide covered with 100 µl M2 medium and mineral oil.

Injected zygotes were either used for genotyping of blastocysts or were transferred into foster mothers for the generation of embryos. For the single blastocyst test genotyping, microinjected zygotes were cultured in drops of HTF medium (EmbryoMax Human Tubal Fluid, Merck Millipore, MA, MR-070-D) under mineral oil in 4-well culture dishes at 37°C and 5% CO_2 in an incubator for 3-4 days until the blastocyst stage was reached.

Injected zygotes were transferred the same day (or some also as two-cell stage the next day) into the infundibulum of the oviducts of CD1 pseudo-pregnant foster mothers (anesthetized with ketamine/rampun mixture). We designated the FVBxC57BL/6J hybrid mice born of the foster mothers as F0 and the subsequent generations, crossed in with C57BL/6J wild-type mates as F1, F2 etc.

All animal experiments performed were approved by the respective institutional protocols and according with the European Community's Council Directive of 22 September 2010 (2010/63EU) and approved by the local animal care committee of the State Rhineland-Palatinate (Landesuntersuchungsamt Koblenz, permit number 23 177-07/G 17-1-085 E1).

2.6 Cloning of CB1 floxed- Stop-floxed construct for *in utero* electroporation

To achieve an overexpression in Reelin-Cre mice via *in utero* electroporation by injecting a floxed-stop-CB1-pCAGIG plasmid, the vector had to be cloned. The floxed-stop-floxed-CB1 cassette was taken from vector #291 (floxstop-HA-rCB1-pAM) (Guggenhuber et al., 2010) from AAV Lutz Lab. To subclone the floxed-stop-CB1 sequence into the targeting vector pCAGIG (#11159, Addgene, USA), the sequence had to be PCR amplified with Hot Start Q5 Polymerase. The used Primers (Fwd: ATCTCGAGATCATAACTTCGTATAGC, Rev: ATGCGGCCGCTTACAGAGCCTCGGCGGACGTGTCTGT) also

added restriction sites XhoI and NotI for easy subcloning into pCAGIG vector. Before ligation, the vector and the PCR construct were digested with XhoI and NotI (200 ng DNA, 2 µl Buffer, 1 µl XhoI, 1 µl NotI, H_2O to 20 µl; digestion for 2 h at 37°C). Prior to ligation, the digested products were gel purified to remove residual buffers and enzymes.

The T4 ligase reaction was set up in a 1:1 ratio.

14.43 ng	DNA
50 ng	Vector
1 µl	T4 Ligase
2 µl	T4 buffer
X µl to 20 µl	*dd*H_2O

The reaction was incubated for 2 h at room temperature. Transformation into competent cells and small scale preparation was set up as before. A restriction digest was made with BamHI and successful cloned vector were sent for sequencing.

3 Results

The main aim of this thesis was the generation of a novel mouse model, allowing the selective inactivation of CB1 in Reelin expressing cells. It was planned to achieve this by knock-in of an HA-NLS-Cre-recombinase construct into the Reelin gene of a wild-type mouse genome without compromising the endogenous expression of Reelin. To inactivate the CB1 gene in the targeted Reelin expressing cell type, a CB1 floxed STOP mouse line was planned to be crossed with this newly generated Reelin-Cre mouse.

3.1 Colocalization of Reelin and CB1 in embryonic mouse cortex

During cortical development, Cajal-Retzius cells, characterized by their expression of Reelin, populate the marginal zone of the dorsal neocortex. At the same developmental stages, CB1 shows high expression in pioneer neurons that populate the marginal zone. To a certain amount, CB1 and Reelin are co-expressed in the MZ, which was shown by Morozov, Vitalis (Morozov et al., 2009; Vitalis et al., 2008) and in preliminary data from C. Hofmann. The amount of co-expressing cells depends on the cortex area and the developmental stage. To determine the number of cells co-expressing Reelin and CB1 in the cortex, 2-4 pictures of the three main pallial regions were analyzed per cortex section (left and right hemisphere): dorsal pallium, DP; lateral pallium, LP and medial pallium, MP (Fig. 18). The expression of Reelin and the coexpression of Reelin with CB1 in 5 developmental stages (E10.5-E14.5) of the C57BL/6J mouse line were compared to each other. From each developmental stage, the cortices of 3 individual animals were analyzed along the dorsolateral axis. From each developmental stage we used the following amount of slides and sections: E10.5: 11 slides and 38 sections (average sections per animal 13 ± 4); E11.5: 10 slides and 39 sections (average sections per animal 13 ± 2); E12.5 12 slides and 31 sections (average sections per animal 10 ± 2); E13.5 18 slides and 58 sections (average sections per animal 20 ± 11); 14.5 11 slides and 50 sections (average sections per animal 17 ± 5). Due to the variability in quality of the sections and the staining, sometimes not all slides or regions within the sections could be considered for counting. Especially for medial pallium of E10.5 animals, there were difficulties in handling the tissue, so fewer pictures were analyzed. Further information can be found in supplementary material (6.1.4). For the staining, the double fluorescent *in situ* hybridization (FISH) method was used with two different mRNA probes, digoxigenin-UTP labeled CB1 and fluorescein-UTP-labeled Reelin and can subsequently be visualized with two different fluorophores (FITC and Cy3).

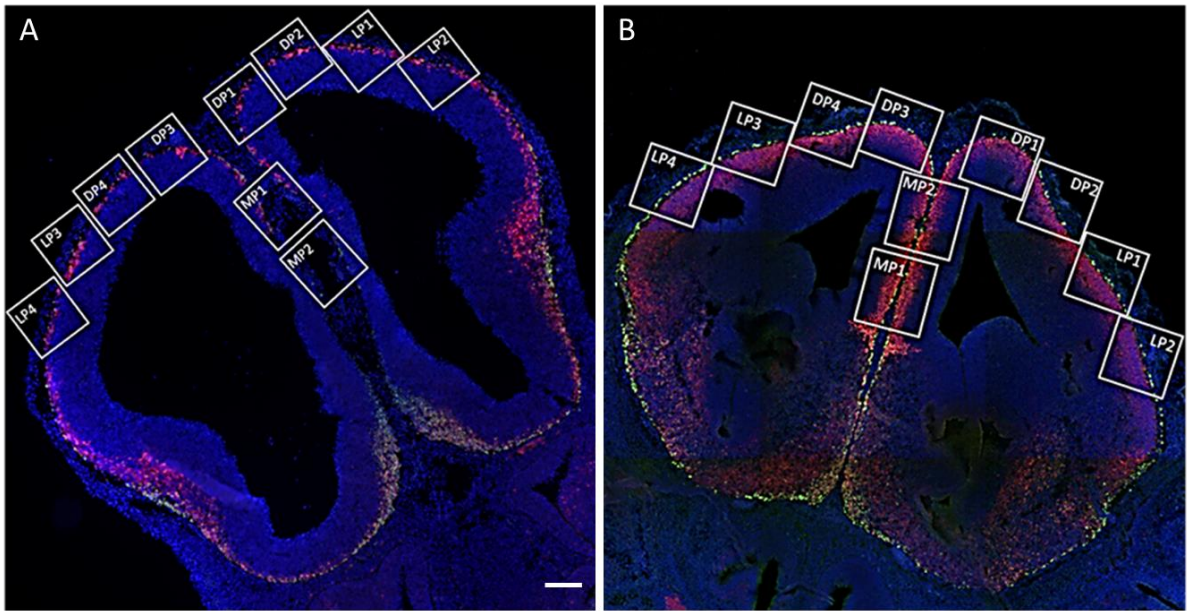

Figure 18 Overview picture of mouse embryonic cortex E11.5 (A) and E14.5 (B).
The picture is showing two different mouse cortical sections stained by fluorescent *in situ* hybridization against CB1 (red) and Reelin (green) at developmental stages E11.5 (left) and E14.5 (right). The overview is showing the area of the counted regions. Medial pallium: MP1, MP2 medial pallium, DP1-4: dorsal pallium, LP1-4: lateral pallium. Scale bar 100 µm.

The representative pictures show the three different pallial regions (medial/dorsal/lateral) at the five counted gestational days (Fig. 19). Reelin mRNA (stained in green) could be observed at the pial surface at all stages in the whole pallial area. From E10.5, CB1 mRNA (stained in red) expression is restricted to the preplate, then continuously increases by age and is strongly expressed in the entire cortical plate at E14.5. The amount of Reelin expressing cells increases slowly until it reaches its highest expression at E13.5. At E14.5, the Reelin expression slowly decreases in all areas but the amount of colocalization with CB1 cells stays the same. The amount of Reelin-expressing cells depends on age and pallial region and changes during brain development.

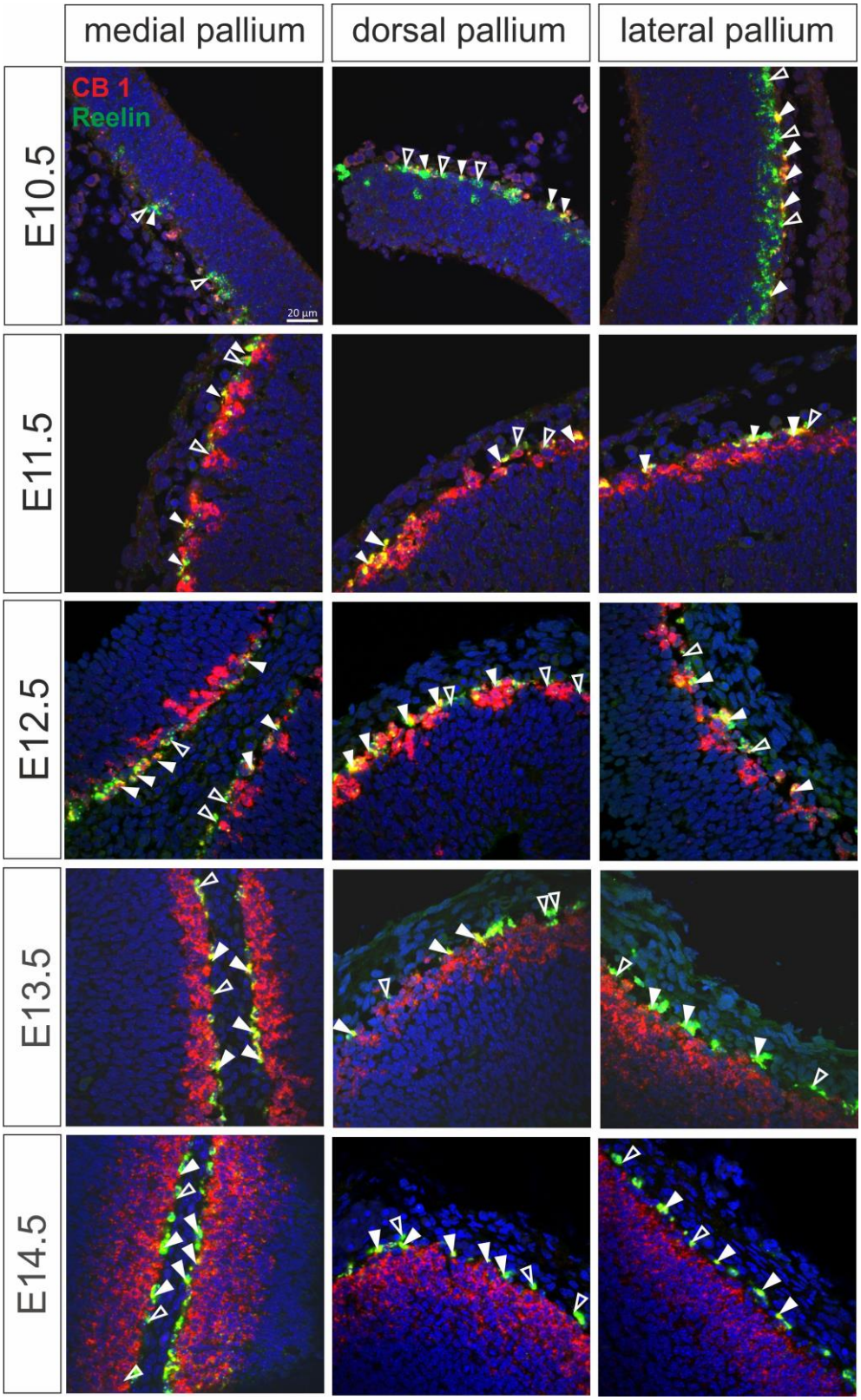

Figure 19 CB1 and Reelin mRNA colocalizes in cells located in the MZ of the pallium at embryonal stages. Representative pictures of *in situ* hybridization showing CB1 (CY3, red) and Reelin (FITC, green) mRNA expression at 5 different embryonal stages in three different regions of the cortex. Filled white arrows mark colocalizing cells with CB1 and Reelin and unfilled arrows show cells only expressing Reelin. The nucleus was stained with DAPI in blue. Scale bar 20 µm.

The medial pallium shows Reelin and CB1 mRNA expression from E10.5 on (Fig. 20). The amount of Reelin-expressing cells increases from 183 cells on average at E10.5 to 1399 cells on average at the age of E13.5 and slowly decreases at E14.5 where only 683 cells are visible on average. The amount of colocalizing cells follows the amount of Reelin-expressing cells. Whereas at E10.5 only 42.7% (± 9) of all cells express Reelin mRNA as well as CB1 mRNA, the number of colocalizing cells increases up to an average of 75.4% after that at age E11.5 and stays high at the later stages: E12.5 73.6%, E13.5 79% and E14.5 74.9% (Tab. 18). Due to difficulties in handling tissue at the age of E10.5, it must be considered that specifically tissue from the medial pallium was often damaged or contained few cells, so the amount of counted medial pallial regions was less.

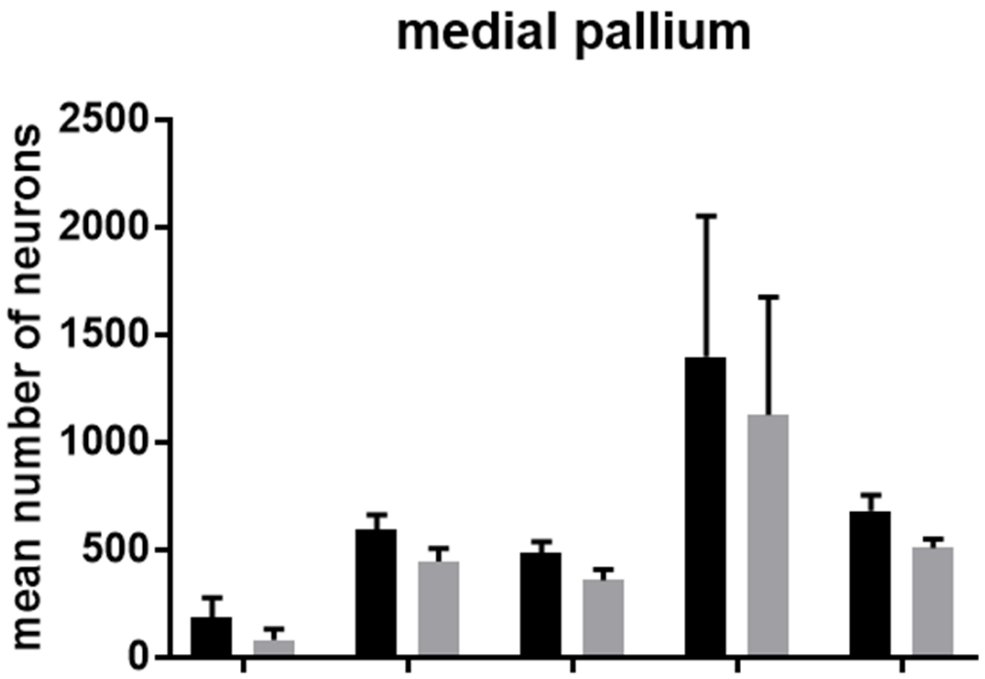

lateral pallium	E10.5	E11.5	E12.5	E13.5	E14.5
Reelin+	183.3	592.3	486.3	1399.0	683.0
CB1+/Reelin+	83.3	446.0	360.0	1127.3	509.3
Colocalization [%]	42.7	75.4	73.6	79.0	74.9

Figure 20 Number of cells expressing Reelin and Reelin/CB1 in the medial pallium.
The graph shows the total amount of counted Reelin positive cells along the different developmental stages (E10.5-E14.5) (black bar) compared to the total amount of Reelin- and CB1 co-expressing cells (grey bar). The amount of Reelin-expressing cells increases from 183.3 cells on average at E10.5 to its maximum at E13.5 with 1399 cells on average. After this at E14.5, the amount of Reelin-expressing cells visibly decreases to 683 cells on average. The amount of Reelin- and CB1 colocalizing cells follow this trend, but the ratio of cells expressing CB1 within the Reelin-expressing cell population stays high. Error bars show mean ± SEM.

Table 18 Amount of total Reelin-positive cells, Reelin- and CB1 co-expressing cells and the ratio in percent in the medial pallium. Standard deviation is shown in brackets.

medial pallium	Reelin+	CB1+/Reelin+	Colocalization [%]
E10.5	183.3 (± 163)	83.3 (± 83)	42.7 (± 9.0)
E11.5	592.3 (± 122)	446.0 (± 107)	75.4 (± 9.0)
E12.5	486.3 (± 92)	360.0 (± 86)	73.6 (± 6.4)
E13.5	1399 (± 1134)	1127.3 (± 949)	79.0 (± 3.3)
E14.5	683 (± 125)	509.3 (± 73)	74.9 (± 3.6)

In the dorsal pallium similar effects can be seen but much more cells express Reelin mRNA in this pallial area (Fig. 21). In embryos at age E10.5 on an average number of 573.3 cells express Reelin mRNA and the expression reaches a maximum at E13.5 with 1263.7 cells on average. At E14.5 on average only 733.7 cells were counted. At E10.5 31.4% (± 6.8) Reelin-positive cells also express CB1 at the age of E10.5. The amount of colocalizing cells increases after that to 72.5% at E11.5, 70.8% at E12.5, reaches its peak at E13.5 with 73% colocalization and at E14-5 with 72.7% colocalization. (Tab. 19).

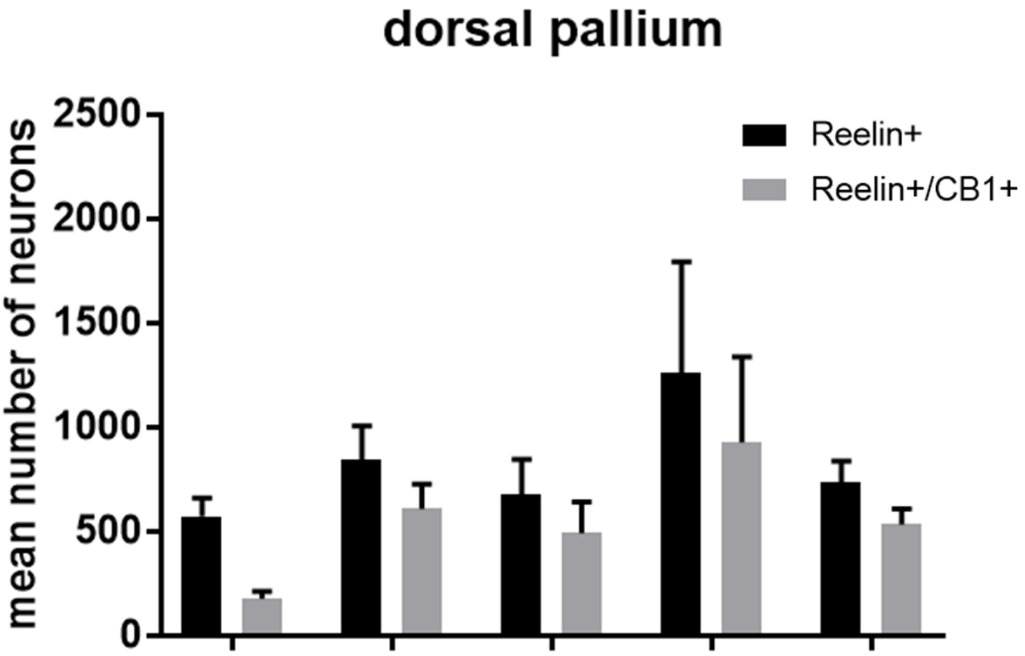

Dorsal pallium	E10.5	E11.5	E12.5	E13.5	E14.5
Reelin+	573.3	842.7	678.7	1263.7	733.7
CB1+/Reelin+	178.3	608.7	493.0	928.0	533.7
Colocalization [%]	31.4	72.5	70.8	73.0	72.7

Figure 21 Number of cells expressing Reelin and Reelin/CB1 in the dorsal pallium.
The graph shows the total amount of counted Reelin positive cells along the different developmental stages (E10.5-E14.5) (black bars) compared to the total amount of Reelin- and CB1 co-expressing cells (grey bars). The number of Reelin-expressing cells increases from 573.3 cells on average at E10.5 to its maximum at E13.5 with

1263.7 cells on average. After this at E14.5, the average amount of Reelin-expressing cells visibly decreases to 733.7 cells. The amount of Reelin- and CB1 colocalizing cells follow this trend. Error bars show mean ± SEM.

Table 19 Amount of total Reelin-positive cells, Reelin- and CB1 co-expressing cells and the ratio in percent in the dorsal pallium. Standard deviation is shown in brackets.

Dorsal pallium	Reelin+	CB1+/Reelin+	Colocalization [%]
E10.5	573.3 (± 154)	178.3 (± 61)	31.4 (± 6.8)
E11.5	842.7 (± 284)	608.7 (± 205)	72.5 (± 10.3)
E12.5	678.7 (± 291)	493.0 (± 259)	70.8 (± 6.4)
E13.5	1263.7 (± 920)	928.0 (± 710)	73.0 (± 4.8)
E14.5	733.7 (± 180)	533.7 (± 132)	72.7 (± 2.0)

Within the lateral pallium, 725 Reelin-expressing cells are counted on average at E10.5 (Fig. 22). This number increases to 1332.7 cells on average until the age of E13.5 and then again slowly decreases to a total amount of 736 cells on average at E14.5. This makes an average colocalization ratio of 33.3% (± 9.6) at E10.5. The average amount of colocalizing cells increases with the age; at E11.5 77% of Reelin-expressing cells, also express CB1. This amount slightly decreases at E12.5 (72.7%) and E13.5 (72.7%) and increases after that at E14.5 (76.8%). Remarkably, the ratio of colocalization of both genes seems to peak at E11.5 and E14.5, and not at E13.5 like in other areas examined (Tab. 20).

More detailed data from different animals can be found in the supplementary information (6.1.4).

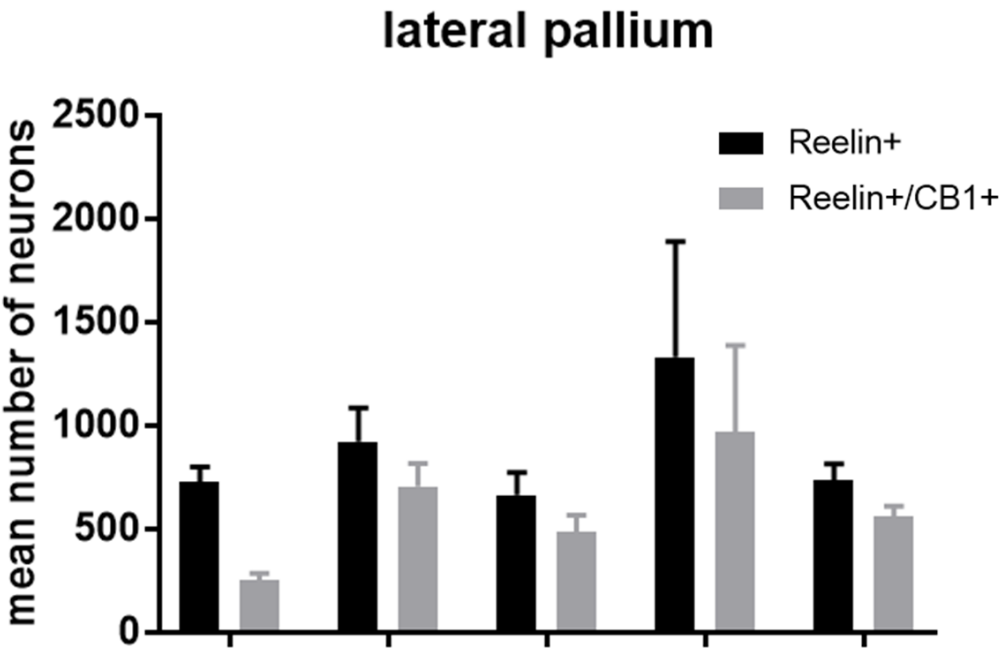

lateral pallium	E10.5	E11.5	E12.5	E13.5	E14.5
Reelin+	725.0	924.0	665.7	1332.7	736.0
CB1+/Reelin+	254.0	707.0	485.3	972.0	562.7
Colocalization [%]	33.3	77.0	72.7	72.7	76.8

Figure 22 Number of cells expressing Reelin and Reelin/CB1 in the lateral pallium.
The graph shows the total amount of counted Reelin positive cells along the different developmental stages (E10.5-E14.5) (black bars) compared to the total amount of Reelin- and CB1 co-expressing cells (grey bars). The number of Reelin-expressing cells increases from 725 cells on average at E10.5 to its maximum at E13.5 with 1332.7 cells. After this at E14.5, the average amount of Reelin-expressing cells visibly decreases to 736 cells. The amount of Reelin- and CB1 colocalizing cells follow this trend. Remarkably, the ratio of colocalization of both genes seems to peak at E11.5 and E14.5, and not at E13.5 like in other areas examined. Error bars show mean ± SEM.

Table 20 Amount of total Reelin-positive cells, Reelin- and CB1 co-expressing cells and the ratio in percent in the lateral pallium. Standard deviation is shown in brackets.

lateral pallium	Reelin+	CB1+/Reelin+	colocalization [%]
E10.5	725.0 (± 133)	254.0 (± 57)	33.3 (± 9.6)
E11.5	924.0 (± 282)	707.0 (± 193)	77.0 (± 7.1)
E12.5	665.7 (± 186)	485.3 (± 143)	72.7 (± 1.0)
E13.5	1332.7 (± 965)	972.0 (± 722)	72.7 (± 3.9)
E14.5	736.0 (± 136)	562.7 (± 83)	76.8 (± 2.8)

It could be shown that CB1 mRNA is expressed by a subpopulation of Reelin-expressing Cajal-Retzius pioneer neurons in the preplate.

CB1 is not only expressed by Reelin-expressing Cajal-Retzius cells and newly differentiated postmitotic glutamatergic neurons, but also by a subclass of γ-aminobutyric acid (GABA)ergic interneurons (Katona et al., 1999; Morozov & Freund, 2003).

Along distinct migratory pathways, which are similar to migrational pathways of Cajal-Retzius cells, GABAergic interneurons migrate to their destinations in the cerebral cortex at very early stages of development (Anderson et al., 1997; Lavdas et al., 1999). They originate in the GE during early gestation (11.5-E12.5), migrate in lateral-to-medial direction through the neocortical MZ (E12.5-E14.5) until they relocate in the hippocampal primordium (E13.5-E15.5) (Morozov et al., 2009). As a subclass of interneurons expresses CB1 and at later developmental stages also Reelin, we wanted to exclude that CB1/Reelin expressing cells within the MZ are interneurons. GAD65 was used as a marker for Interneurons. E13.5 mouse embryonic brain tissue was co-stained either with GAD65/Reelin or GAD65/CB1 via *in situ* hybridization. Our results showed that there is no GAD65 expression within the marginal zone neither at E13.5, in CB1-(Fig. 23) nor in Reelin-(Fig. 24) expressing cells. GAD65 expression was restricted to the GE. This leads to the conclusion that at E13.5 no GAD65-expressing interneurons populate the marginal zone and CB1 expression is unlikely to come from interneurons rather than from CR cells.

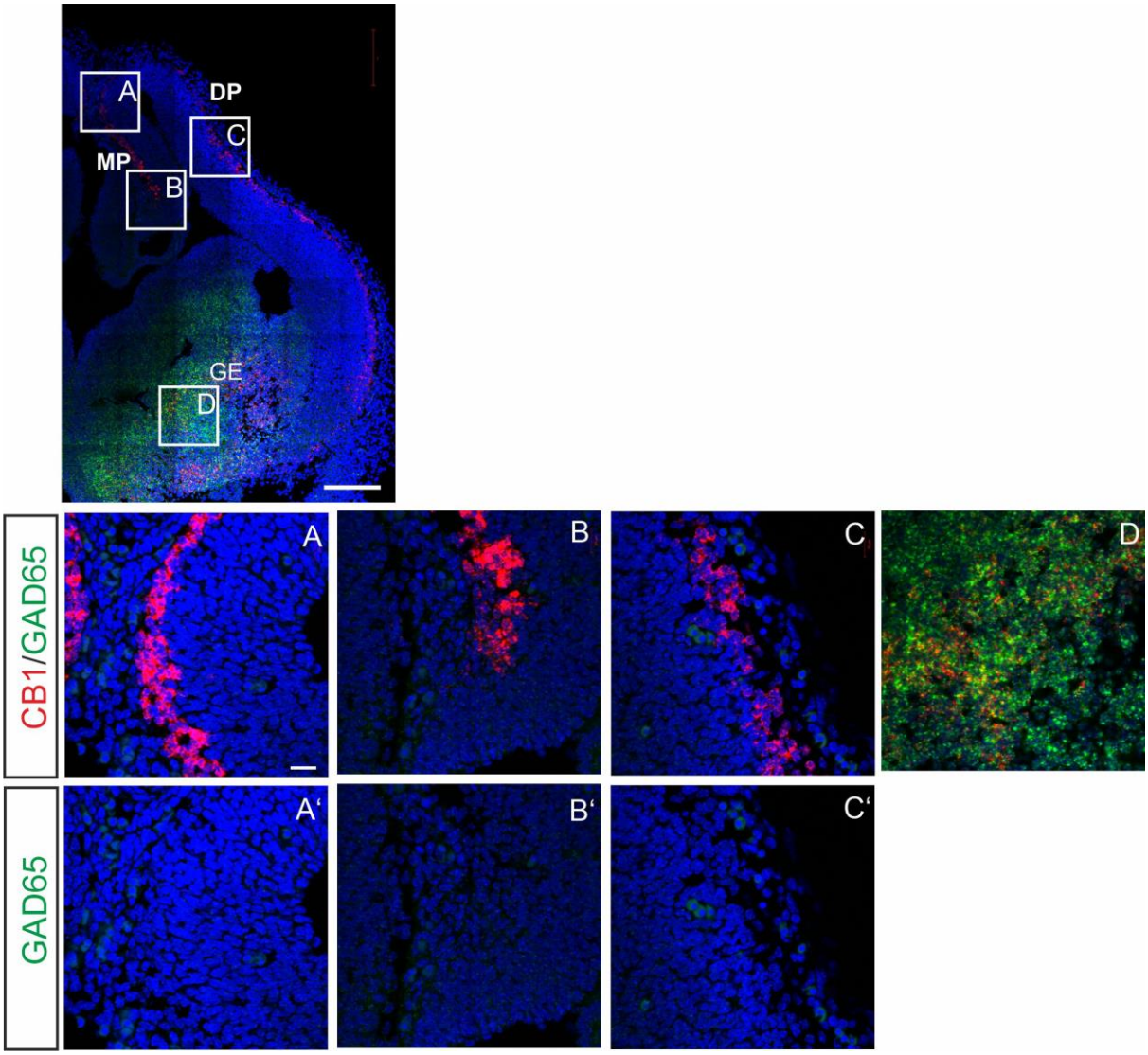

Figure 23 Representative pictures of in situ hybridization showing CB1 (CY3, red) and GAD65 (FITC, green) mRNA expression in three different regions of mouse E13.5 cortex (overview image at uppermost left corner).

(A-D) CB1 is expressed in the MZ of the cortex and in the ganglionic eminence (GE), the latter shown in (D). (A, C) Clearly visible CB1 expression within the dorsal pallium (DP) of the cortex but no Gad65 colocalization can be seen as GAD65 is not expressed in this area (A', C'). (B) The medial pallium (MP) is also expressing a high amount of CB1 but no GAD65, which is not expressed in the MP at all (B'). (D) GAD65 expression was restricted to the GE at this stage and some cells showed coexpression of CB1. Cell nuclei were counterstained with DAPI (blue). Scale bar 100 µm (Overview picture), 20 µm (magnifications).

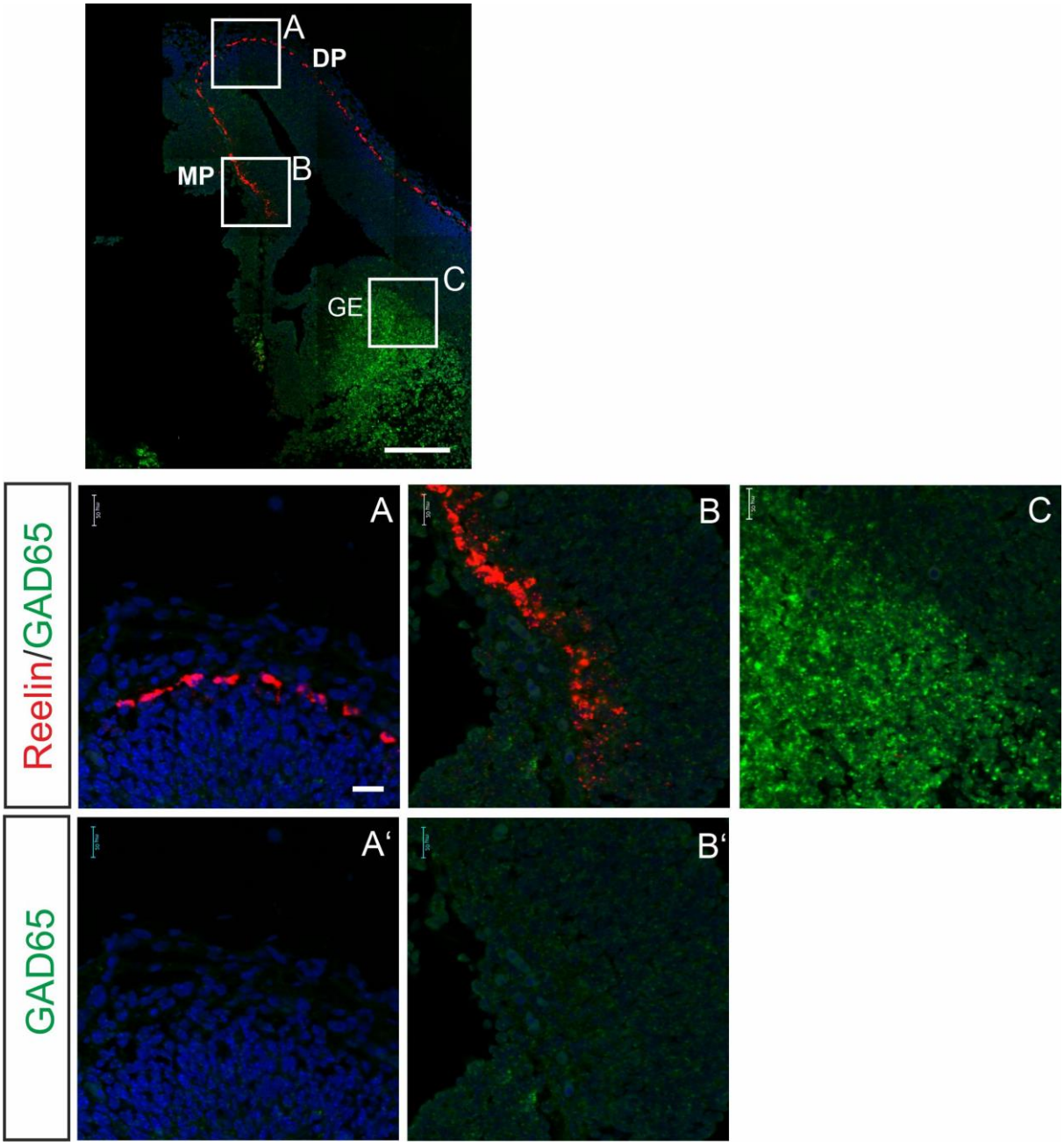

Figure 24 Representative pictures of in situ hybridization showing Reelin (CY3, red) and GAD65 (FITC, green) RNA expression in three different regions of mouse E13.5 cortex (overview image at uppermost left corner). (A-C) Reelin is expressed in the MZ of the cortex but not in the ganglionic eminence (GE), the latter shown in (C). (A) Clearly visible Reelin expression within the dorsal pallium (DP) of the cortex but no Gad65 colocalization can be seen as GAD65 is not expressed in this area (A'). (B) The medial pallium (MP) is also expressing a high amount of Reelin but no GAD65, which is not expressed in the MP at all (B'). (C) GAD65 expression was restricted to the GE at this stage, where no Reelin-expression could be seen. Cell nuclei were counterstained with DAPI (blue). Scale bar 100 µm (Overview picture), 20 µm (amplifications).

Thus, because there is no co-staining of GAD65 with CB1 nor with Reelin in the cortical pallium, the CB1 expression is unlikely to come from migrating interneurons to the cortical layers or marginal zone, but rather from Cajal-Retzius cells situated here. Further analysis of Reelin staining in Dlx expressing neuron-specific CB1 knock-out mice showed that in cortical sections CB1 and Reelin were still co-expressed in cortical upper layer cells (data not shown). But these stainings are not due to CB1 expression in Reelin-expressing cells in the marginal zone.

3.2 CRISPR/Cas9-generation of a Reelin-Cre mouse line

Reelin is expressed by Cajal-Retzius cells and is crucial for cortical layering. To do research on cell type-specific changes within Cajal-Retzius cells, a Reelin-Cre mouse line had to be generated. By crossing the Reelin-Cre mouse with a mouse line containing a floxed gene, the specific inactivation of the floxed gene within the Reelin-Cre expressing cell population is possible.

3.2.1 Mouse genome analysis

Reelin is a gene on Chromosome 5 in mice, consisting of 460252 bp, 3461 amino acids and 65 exons. Eight identical repeats make it difficult to target Reelin for genome editing (Royaux et al., 1997). As even small changes in the Reelin gene can cause defects in Reelin secretion or protein folding and will lead to severe defects in cortex lamination (D'Arcangelo et al., 1997), it was important to leave the Reelin gene intact when inserting the Cre-recombinase gene. The best region to insert a Cre construct was directly after the 8th repeat within exon 65 immediately in front of or after the translational stop codon of the Reelin-gene (3' untranslated region) (Fig. 25)

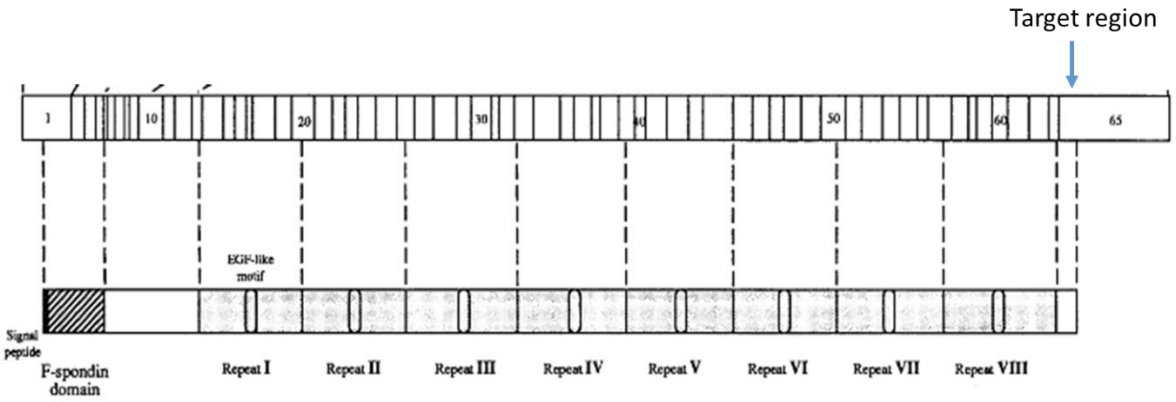

Figure 25 Schematic map of the Reelin gene.
The Reelin gene on chromosome 5 (GRCm38.p4 C57BL/6), Locus NC_000071 Region: 1884454..22344705 encodes for a protein of 3461 amino acids and consists of 65 exons spanning a region of 460 kbp (Royaux et al., 1997). 51 exons encode the 8 repeats with similar sequences to form the main part of the gene. In the beginning, a signal peptide is followed by an F-spondin domain. The targeted region was directly after the 8th repeat within exon 65 in front of and after the STOP-codon (blue arrow). (Figure from (Royaux et al., 1997).

To search for possible targets the MIT-CRISPR Design tool (http://crispr.mit.edu) (Fig. 26) and the tool http://crispor.org were used. The possible sgRNA sites are restricted to the presence of PAM sites, which serve as target recognition sites for the Cas9 complex. The tool lists possible targets for possible sgRNAs and scored them after their possible off-targets, whether those are within exons or may have more or fewer mismatches.

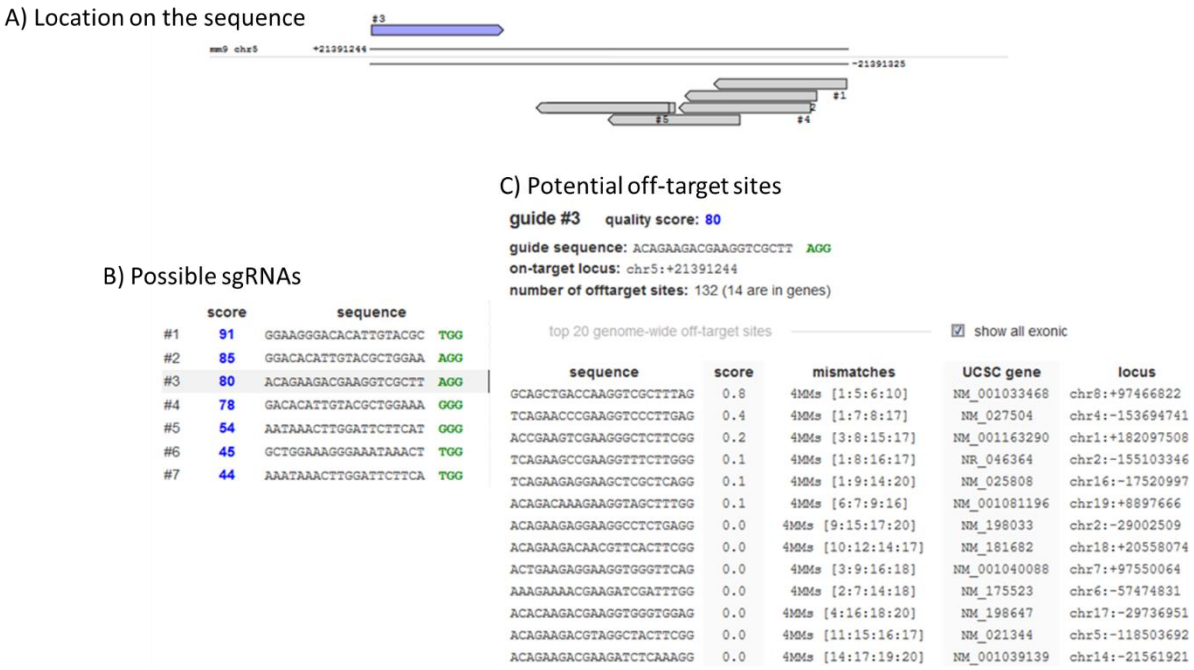

Figure 26 Overview of possible guide RNA sites analyzed with the crispr-mit.edu design tool.
A) Possible sgRNAs within the targeted Reelin region were shown along the inserted DNA sequence. B) Possible sgRNAs were scored after their possible off-targets, whether those are within exons or may have more or fewer mismatches. For this approach, the best (sgRNA2,#1 score 91) and the third-best (sgRNA1,#3 score 80) sgRNAs were used as they show a small number of off-targets. The sgRNAs were located directly in front of (sgRNA1) or immediately after (sgRNA2) the translational stop codon of Reelin. C) When selecting a possible sgRNAs the tool shows all potential off-targets scored after their amount of mismatches and their location in the mouse genomic DNA (example shows here sgRNA #3).

Table 21 Analysis of guide RNAs using the CRISPR design tool crispor.org.

	Guide sequence + PAM	MIT specificity score (1-100) (off-target)	CFD specificity score (1-100) (on-target)	Off-targets for 0-1-2-3-4 mis-matches
sgRNA 1	ACAGAAGACGAAGGTCGCTT AGG	86	89	0-0-1-5-95 101 off-targets
sgRNA 2	GGAAGGGACACATTGTACGC TGG	95	95	0-0-0-6-56 62 off-targets

The CRISPR design tool crispor.org includes the specificity score (MIT specificity score), which is a prediction of how much a guide RNA sequence for this target may lead to off-target cleavage at another sequence in the genome. The score ranges from 1-100 with 100 being the best and means that it was

not possible to find a single sequence in the genome that differs from the target at up to four positions (Hsu et al., 2013a). The CFD specificity score is a prediction of the on target efficiency and shows how well this target may be cut by the gRNA sequence (Doench et al., 2016). The predictive power is not well in general and needs further research. The tool also gives a prediction for possible off-targets with 0, 1, 2, 3 or 4 differences to the original sequence. 94 possible off-targets for 4 differences to the original sequence means that there are 94 similar sequences that have 4 different bases to the original sequence (Tab. 21). When ordering sgRNA sequence for subcloning, for analysis in cell culture or for zygote injection, there is no need to add the NGG PAM sequence, because the PAM region is used to select the genomic target. It is important that the NGG PAM sequence immediately follows the target on the genome but not on the oligo.

3.2.2 Cloning of sgRNA1 and sgRNA2 into an expression vector for *in vitro* test of sgRNAs

To implement the CRISPR/Cas system into mammalian cells, coexpression of the *Streptococcus pyogenes* Cas9 (SpCas9) nuclease along with a guide RNA is essential. Single-guide RNA derives from a synthetic fusion of CRISPR RNA (crRNA) and trans-activating crRNA (tracrRNA; (Hsu et al., 2013a)). The so-called pX330 vector includes a U6 promotor and two expression cassettes: one for human codon-optimized SpCas9 nuclease and one for the specific single-guide RNA.

Initially, the DNA sequence of the guide RNA (gRNA) had to be cloned between the BbsI restriction site of a pSpCas9(BB)-2A-Puro vector (protocol according to Ran et al 2013). To do so, restriction sites for BbsI were added to the gRNA construct for subcloning (Fig. 27). Two different gRNAs were cloned into the vector respectively (see 2.5.2). The correct insertion was tested and verified after amplification and following purification of the plasmid through stbl3 E. coli bacteria strains by restriction digest and sequencing.

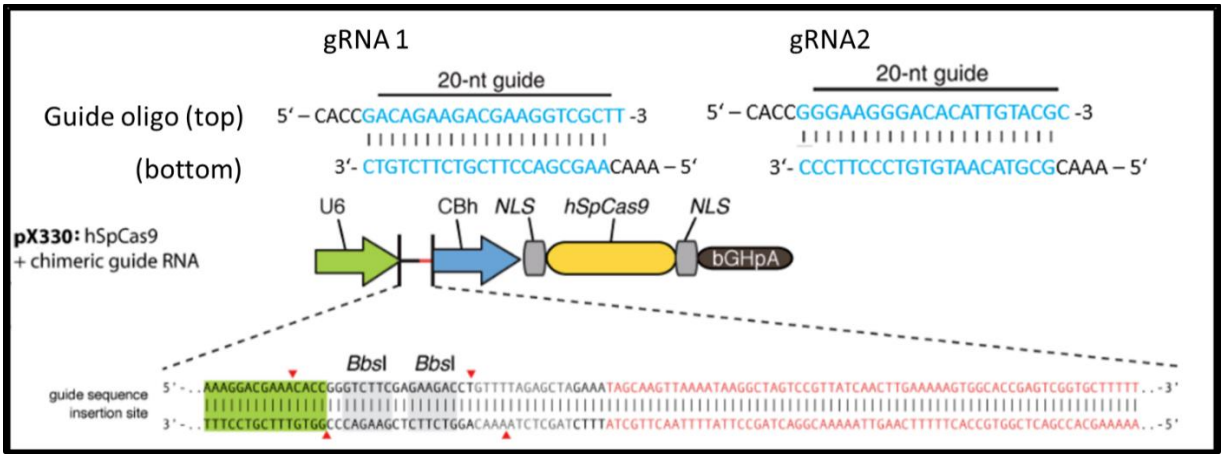

Figure 27 Schematic overview of the hSpCas9 vector (pX330) and the used gRNA sequences.
gRNA1 or gRNA2 were cloned individually into the pX330 vector between the BbsI restriction sites.

3.2.3 Functional testing in neuronal cell cultures to prove the validity of sgRNAs

The functionality of the cloned constructs was tested by transfection of the gRNA-pX330-vector into the neuronal cell lines HT22 (mouse hippocampal neuronal cell line) and N2a (neuroblastoma derived cell line). As a transfection control, a GFP expression vector was transfected. Around 40% of all cells showed GFP expression, so this verified that the transfection was working in general. After transfection, the DNA was harvested with QuickExtract according to the manufacturer's protocol (see chapter 2.3.2) for further analysis.

3.2.4 T7 endonuclease assay

3.2.4.1 T7 ENI Assay on cell DNA

The T7 Endonuclease assay detects heteroduplex DNA with mismatches that were caused by non-homologous end joining (NHEJ) repair events e.g. after a Cas9 mediated cut. In a denaturation and annealing reaction, wild-type DNA without modification is annealed to DNA with modification to form a fraction of heteroduplexes. T7 Endonuclease recognizes and cleaves DNA mismatches in those heteroduplexes. Running the cleaved products on an agarose gel will resolve full length and cleaved products and so gives a first estimation of whether the sgRNA/Cas9 targeting was successful. The cell DNA was amplified with primers (primers 1.1 and 1.2) covering the targeted region around the translational STOP codon of the Reelin gene and situated beyond or within the future homology arms. The estimated WT band size, without a cleavage by Cas9 and removal of indel loops by T7EN1, was 761 bp, whereas the Cas9 modification bands are supposed to show two additional bands caused by a double-strand break. The estimated sizes of annealed and T7EN1 treated DNA after PCR amplification with primer pair 1 for sgRNA1 was 518 bp and 243 bp and for sgRNA2 561 bp and 200 bp. The results showed that both sgRNAs worked as expected and are therefore functional (Fig. 28).

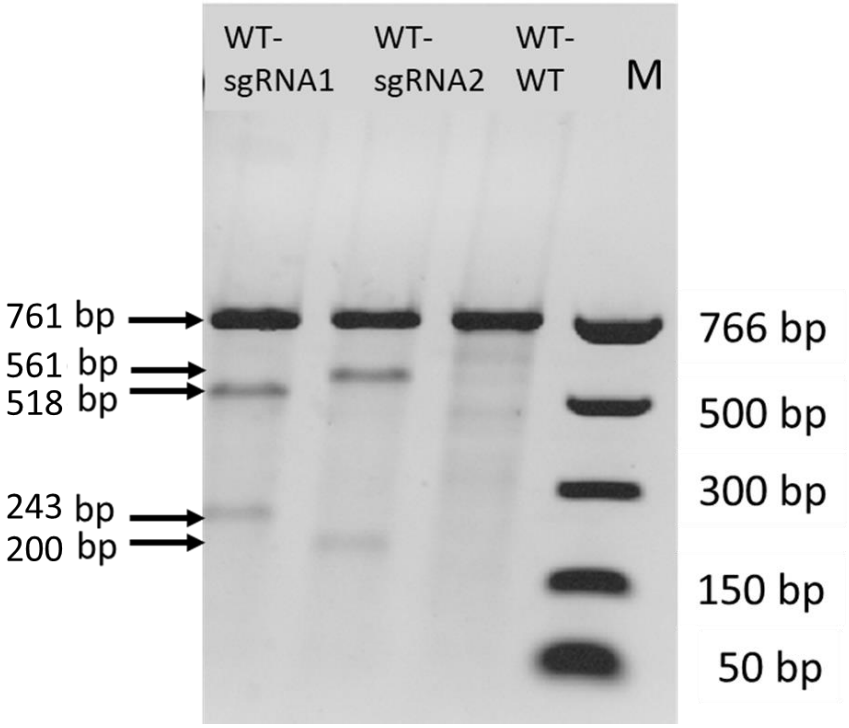

Figure 28 T7 endonuclease assay on HT22 cells.
Results for sgRNA1 modified DNA show a strong WT band with 761 bp and two additional bands sized 518 bp and 243 bp (lane 1 WT-sg1). SgRNA2 modified bands show a thick WT band at 761 bp and two additional bands at 561 bp and 200 bp (lane 2 WT-sg2). Non-modified DNA only shows a WT band at 761 bp (lane 3 WT-WT).

3.2.4.2 Analysis of off-targets

The CRISPR sgRNA design tool recognized 132 (crispr.mit.edu) and 101 (http://crispor.tefor.net/) off-targets, respectively, for sgRNA1. Only one off-target has 2 mismatches whereas the other off-targets have at least 3 mismatches. For sgRNA2 the tools were able to find 100 (crispr.mit.edu) or 62 (http://crispor.tefor.net/) off-targets. The selected gRNA will only bind to sequences which differ in more than 2 mismatches in rare cases. Cleavage of Cas9 to a given locus depends on the shared homology from the gRNA spacer sequence to the target DNA. When Cas9-gRNA complex binds a putative DNA target, the annealing begins with the seed sequence (8-10 bases at the 3' end of the gRNA targeting sequence). If the sequence of seed and target DNA match, the gRNA continues to anneal to the target DNA in a 3' to 5' direction. Therefore, mismatches within the PAM-proximal seed sequence can completely abolish Cas9 cleavage, whereas mismatches in more PAM-distal sequence towards the 5'end to the PAM still permit target cleavage (Kuscu et al., 2014; X. Wu et al., 2015).
One or two possible off-targets (see Tab. 22), according to the gRNA design tool, were analyzed by T7 Endonuclease assay. For this reason, primers for the targeted region were designed (see Tab. 22).
The first off-target (sgRNA1 Exon1) lies in the exon region of the G-protein-coupled receptor G5, which is a protein encoded by the ADGRG5 gene and is a member of the adhesion GPCR family

(Hamann et al., 2015).Adgrg5 mRNA is specifically expressed in mouse lymphocytes, monocytes, macrophage and dendritic cells (https://www.ncbi.nlm.nih.gov/gene/?term=NM_001033468).
The first off-target of sgRNA2 (sgRNA2 Exon1) is located in complement component 1r (C1r), which is a protein involved in the complement system of the innate immune system. The protein is highly expressed in liver and bladder (Muller-Eberhard, 1988).
The second off-target of sgRNA2 lies in an intron sequence on chromosome 17 between gene Gm20443 and Gm20442.

Table 22 List of tested off-targets including sequence, amount of mismatches, region within mouse genome, used primers and expected product length.

Off-target	Sequence	Mismatches	Region in genome	Primer	Product length
sgRNA1 Exon 1	GCAGCTGACCAAGGTCGCTTTAG	4MMs [1:5:6:10]	XM_017312886.1 Chr. 8: 2469 to 2491	Fwd aggcctctttctctttccct Rev ttgtcctcgctgtggatagg	712 bp
SgRNA2 Exon 1	GACAGGGACACATTGTTCAC-CAG	4MMs [2:3:17:19]	AC115911.14 chr6: 115988 to 116010	Fwd gctacttctgttcctgccat Rev ctccaccctaaccctctcac	730 bp
SgRNA2 Intron 3	CGCCGGGACACATT-GTGCGCGAG	4MMs [1:3:4:17]	AC112970.18 chr17: 132910 to 132932	Fwd tgcgattttaaccagggtgc Rev gatctcaagtcccaagcagc	760 bp

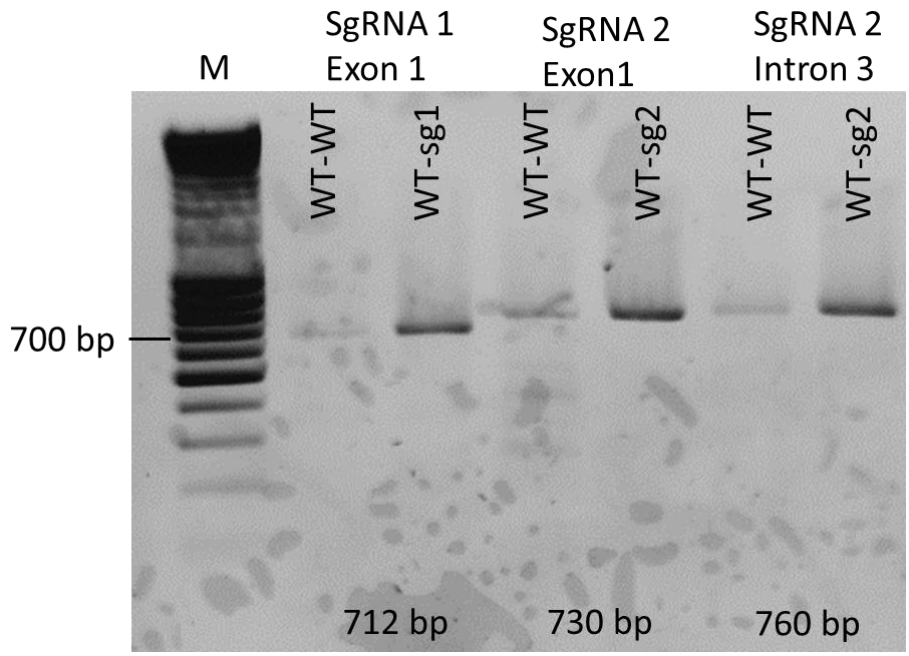

Figure 29 T7 Endonuclease assay of off-targets.
All results show a WT band at the expected size at 712 bp (sgRNA1 Exon1), 730 bp (sgRNA2 Exon1) and 760 bp (sgRNA2 Intron 3). If a DSB would have been initiated by unintended recognition and cleavage by Cas9 (off-target), the indel would have been recognized by T7 Endonuclease and the WT-sgRNA product would show two additional bands beside the WT band. As no additional bands are visible at WT-sgRNA1 Exon1, WT-sgRNA2 Exon1 or WT-sgRNA2 Intron1 no cleavage has occurred and the regions are no off-target regions. M: Marker MassRuler.

The results for the T7 Endonuclease assay for the off-targets (Fig. 29) indicate that the Cas9 nuclease with the specifically designed sgRNAs was not causing DSB's at the most likely off-target sites.

3.2.4.3 T7 EN1 Assay on sgRNA injected blastocysts

The blastocyst DNA was obtained by lysing each of the blastocysts derived from Cas9 and sgRNA injected zygotes. Afterward, the DNA was PCR amplified in two separate PCR steps. The first PCR reaction was performed with primer pair 1, followed by a PCR reaction with primer pair 2 as nested PCRs. This means that amplified DNA from primer pair 1 reaction was used for a second PCR with primer pair 2 resulting in a more specified band with more amplified DNA. The T7 EN1 Assay was performed in the same way it was performed before on cell DNA. 59 out of 62 (95%) of the samples showed a successfully amplified wild-type band with a size of 713 bp and sometimes other unexpected bands were produced. After the T7 EN1 assay, the guide RNA modified blastocysts show the estimated bands at 713 for the WT band and 474 bp and 239 bp (sgRNA 1) or 517 bp and 196 bp (sgRNA2). Additionally, the samples reveal some additional mutations by showing unexpected bands.

Therefore, in 24 out of 33 (72%) Cas9 sgRNA1 injected blastocysts a double-strand break had occurred and 9 of them (27%) showed the expected band. For sgRNA2 injected blastocysts, 19 out of 29 (65%) showed a double-strand break and 10 (34%) showed the expected bands.

SgRNA1 injected blastocysts

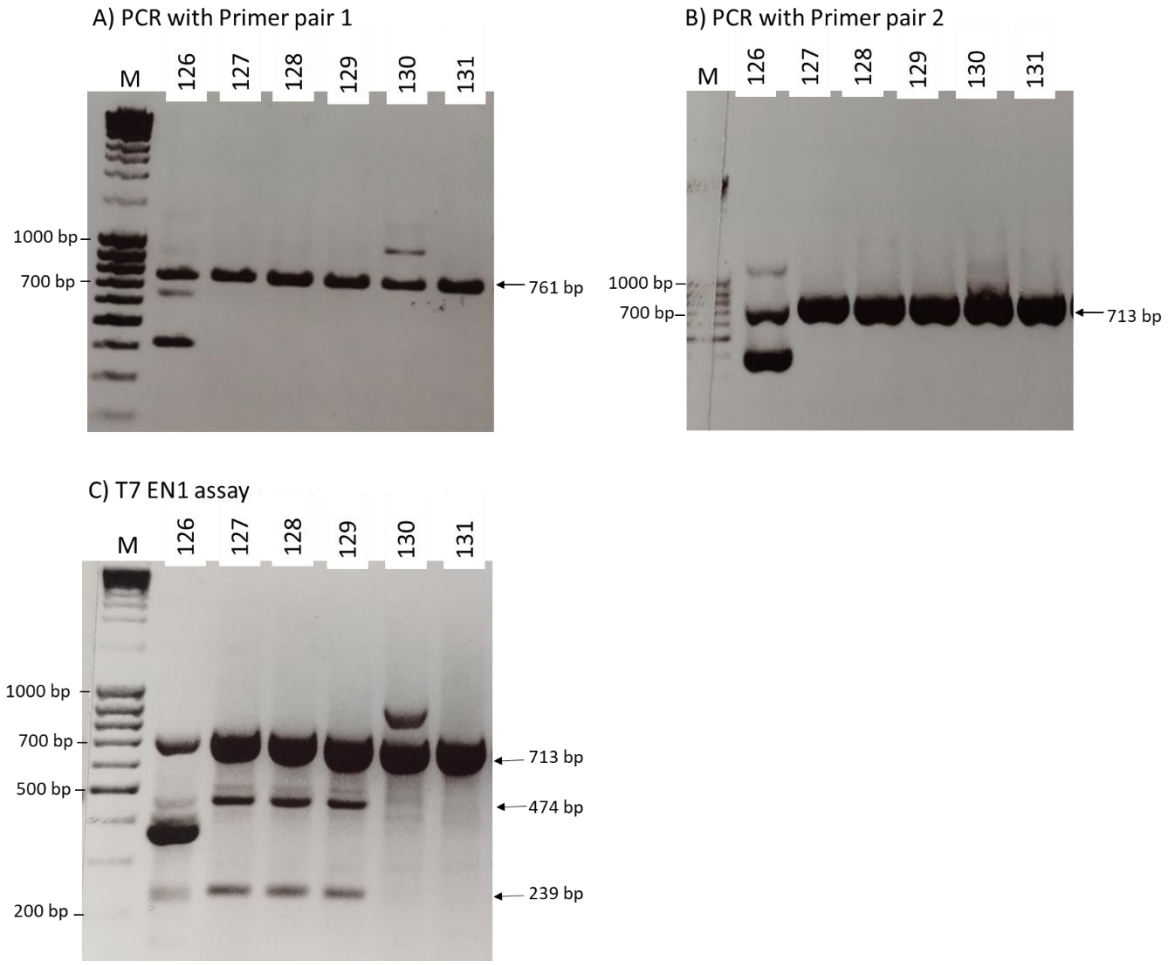

Figure 30 T7 endonuclease assay on sgRNA 1 injected blastocysts.
A) Results for sgRNA1 expect one band at 761 bp for all samples after the first PCR reaction with primer pair 1 (1.PCR). B) After the nested PCR with primer pair 2, one band at 713 bp was expected (2.PCR). C) For the T7 EN1 assay, a thick WT band with 713 bp and two additional bands sized 474 bp and 239 bp were expected for successfully modified blastocysts. Non-modified annealed DNA strands only show a WT band at 713 bp. M: Marker MassRuler.

After the first PCR reaction (Fig. 30A) 9 blastocysts out of a total number of 33 showed more bands than the expected band at 761 bp. The following additional bands were observed: 1x 430bp (e.g. #126, Fig. 30A, 1st lane), 1x 1030 bp (e.g # 130, Fig. 30A, 5th lane), 4 x 650 bp (e.g. #126, Fig. 30A, 1st lane), 3 x 500 bp, data not shown). After the second PCR reaction (Fig. 30B), 3 different patterns were visible: 1200 + 713 + 350 (4x, e.g. #126, Fig. 30B, 1st lane), 713 + 200 (1x, data not shown), 1300 + 713 + 600 (3x, data not shown). It could be possible that additional bands were masked by the thick band at 713 bp. The T7 Endonuclease assay (Fig. 30C) showed the expected bands in 9 cases (e.g. #127,

#128, #129). Additional bands always occurred when already additional bands could be seen in the nested PCR amplification reaction (e.g. #126).

For sgRNA1 33 blastocysts were analyzed in total. 8 Blastocysts show only a WT band (24%), 9 show the expected bands for Cas9 modified blastocysts (27%), 15 show additional or unexpected bands (46%) and one blastocyst didn't show any result due to poor DNA outcome.

SgRNA2 injected blastocysts

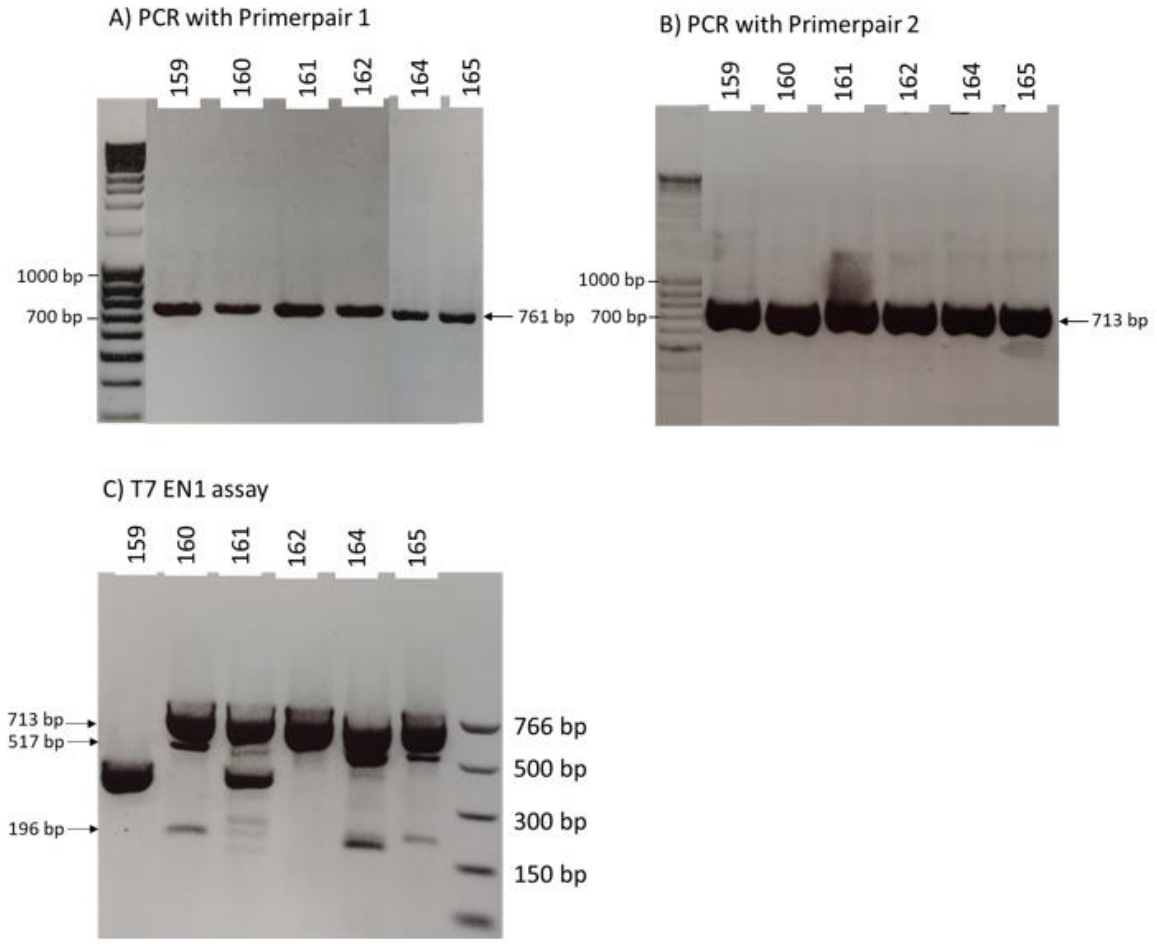

Figure 31 T7 endonuclease assay on sgRNA 2 injected blastocysts.
A) The results for sgRNA2 injected blastocysts expect one band at 761 bp for all samples after the first PCR reaction with primer pair 1 B) After the nested PCR reaction with primer pair 2, one band at 713 bp was expected C) For the T7 EN1 assay, a thick WT band with 713 bp and two additional bands sized 517 bp and 196 bp were expected for successfully modified blastocysts. Non-modified annealed DNA strands only show a WT band at 713 bp. M: Marker MassRuler.

29 sgRNA2 injected blastocysts were analyzed. After the first PCR reaction (Fig. 31A) 4 out of 29 blastocysts showed more bands than the expected band at 761 bp (3x 600 bp, 1x 600 + 500 bp, data not shown). After the second PCR reaction (Fig. 31B), all bands got stronger, but no additional bands appeared. The T7 EN1 assay (Fig. 31C) showed in 10 out of 29 blastocysts (35%) the expected additional bands (517 bp + 193 bp), resulting from the T7EN1 mediated cut (e.g. #160, #165). In 9 cases (31%)

the DNA was cut, but several additions or deletions occurred (e.g. #159, #161). 8 out of 29 blastocysts (28%) remained uncut (e.g. #162) and only the WT band (713 bp) was visible. For 2 blastocyst no result could be obtained due to poor DNA concentration.

It could be shown that Cas9 mediated sgRNA1 and 2 can cause DSBs at the expected site in the genome, therefore we could continue to inject the Cas9-sgRNA complex along with the cloned HDR construct into zygotes.

3.2.5 Cloning of knock-in insert

The gRNA guided Cas9 nuclease causes a double strand break within the targeted Reelin region in mouse genomic DNA. This DSB can then be repaired via homology-directed repair by providing a construct with complementary homology arms on both sides of the break. In between the homology arms, a construct was provided which consists of a 2A proteolytic cleavage site, an HA-tag, a nucleus localization signal (NLS) and the sequence for Cre-recombinase. To create the HDR construct, a left and a right homology arm were cloned out of genomic Reelin DNA with appropriate primers. To prevent the Cas9 from cutting after the HDR construct is inserted at the site of the DSB, the homology arms were modified with two silent mutations within the sgRNA sequence in a second PCR amplification step (Fig. 32).

The HDR construct was combined in two steps

The 2A-HA-NLS-Cre site was cloned out of existing vectors from the lab and subcloned into a pBSII-KS(+) backbone vector, transformed into stbl3 cells. Single colonies were picked and amplified in a miniprep. The miniprep was harvested, purified, and sent for sequencing.

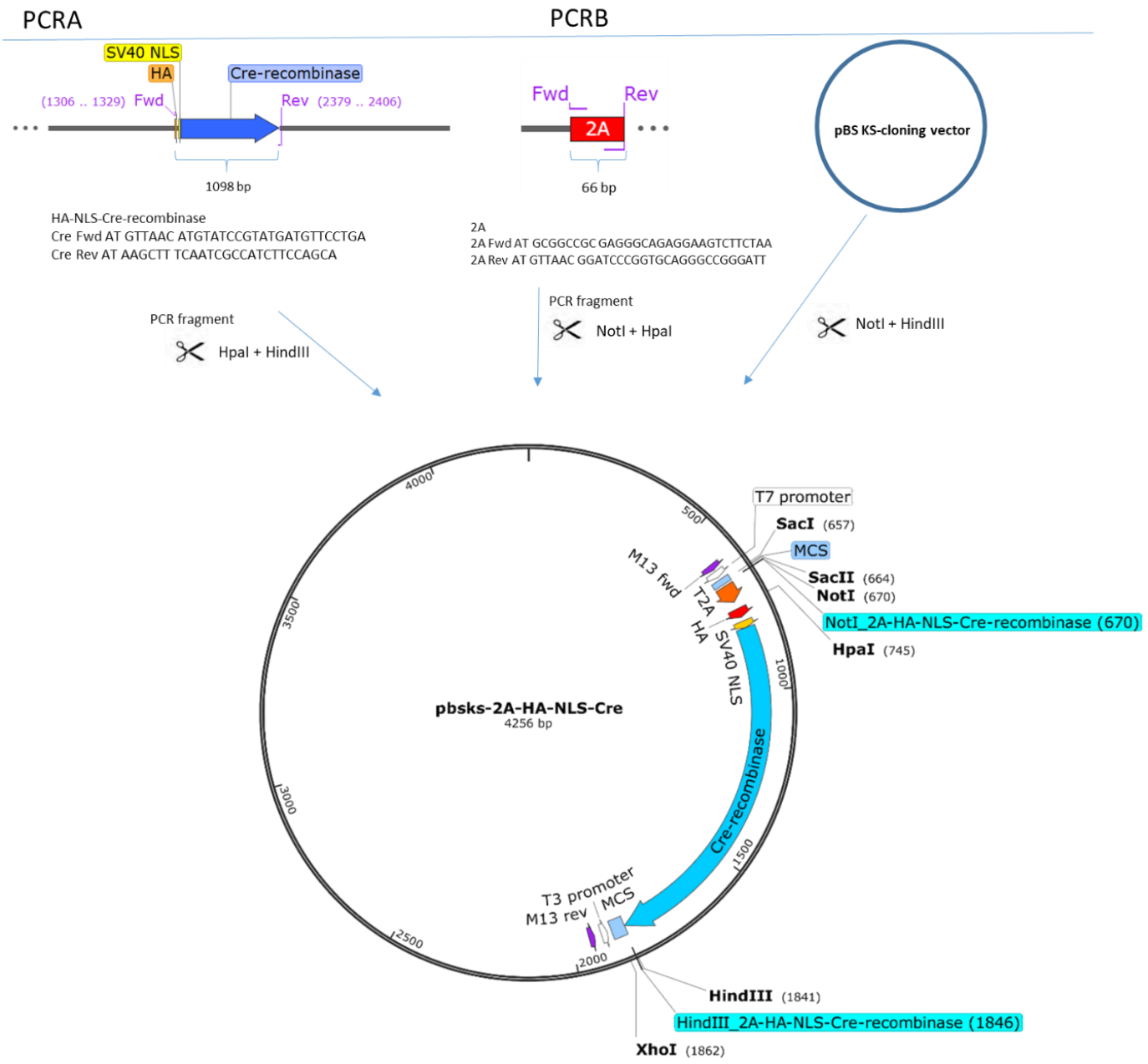

Figure 32 Schematic overview of performed steps to obtain 2A-HA-NLS-Cre-construct.
PCR A produces the HA-NLS-Cre-recombinase constructs adding a 5‘ HpaI and 3‘ HindIII restriction site with Cre Fwd AT GTTAAC ATGTATCCGTATGATGTTCCTGA, Cre Rev AT AAGCTT TCAATCGCCATCTTCCAGCA primers, PCR B produces the 2A construct with additionally 5‘ NotI and 3‘ HpaI restriction sites with 2A Fwd AT GCGGCCGC GAGGGCAGAGGAAGTCTTCTAA and 2A Rev AT GTTAAC GGATCCCGGTGCAGGGCCGGGATT primers. Both PCR fragments were digested with respective enzymes and cloned into a NotI and HindIII linearized pBSKS-vector. The final vector contains the 2A-HA-NLS-Cre-recombinase construct (see 2.5.5).

Sequencing of the resulting vector showed the expected base sequence without alterations (Fig. 33)

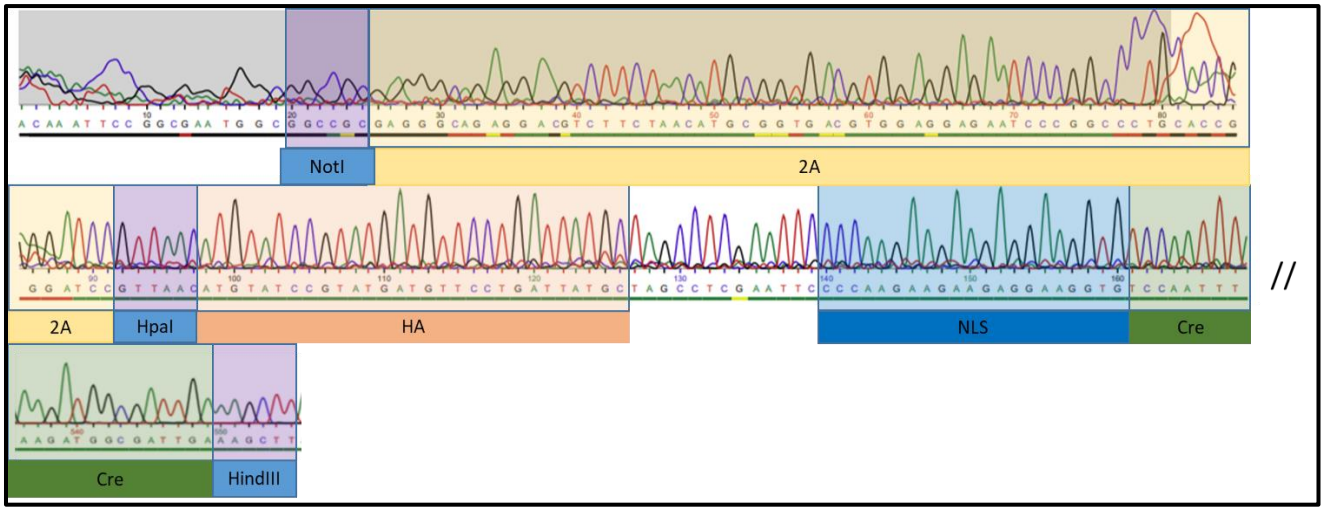

Figure 33 Sequencing results of 2A-HA-NLS-Cre construct without homology arms.
The 2A-HA-NLS-Cre construct was cloned into the multiple cloning site of the pBSKS vector via restriction site cloning. The sequence chromatograms showing correct targeted 5' to 3' junctions.

In the next step, homology arms had to be added on both sides of the 2A-HA-NLS-Cre-construct, which had to be cloned out of the mouse genome via PCR (see 2.5.6.1.). Prior to cloning, the PAM site, as well as the seed sequence of the sgRNA, had to be changed with silent mutations (see 2.5.6.2). Single base pairs were changed without changing the resulting amino acid to prevent repeatedly binding and cutting of Cas9 to the targeted sequence. To generate the complete HDR construct, I took advantage of the Gibson Assembly method (see 2.5.6.3). All products (left and right homology arm, 2A-HA-NLS-Cre-recombinase construct) could then be combined in a single, isothermal reaction with Gibson cloning to a complete HDR construct (Fig. 34 and Fig. 35).

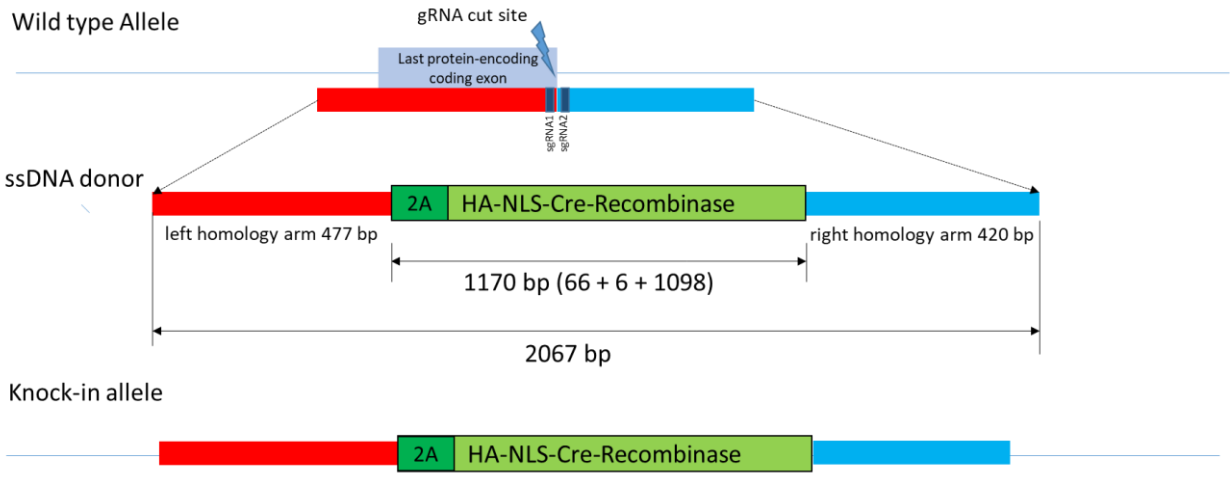

Figure 34 Scheme of whole HDR construct.
The final cloned construct for HDR contains 2A, HA-NLS-Cre-Sequence and two flanking homology arms. The 2A-HA-NLS-Cre-recombinase construct consists of the 66 bp 2A, the 1098 bp HA-NLS-Cre-recombinase and 6

additional base pairs as restriction sites after the 2A sequence. In the WT mouse Reelin allele, the Cas9 caused a DSB at the targeted guide RNA cut site immediately before the translational STOP by sgRNA1 or after the translational STOP pf the Reelin gene by sgRNA2. The editing of genomic DNA is achieved upon repair of the CRISPR-induced DNA double-strand break by homologous-directed repair when offering our ssDNA donor. Finally, the Reelin gene contains a 2A-HA-NLS-Cre-recombinase knock-in allele in front of the introduced translational stop codon (at the end of the Cre-recombinase) flanked by a left and right homology arm sequence.

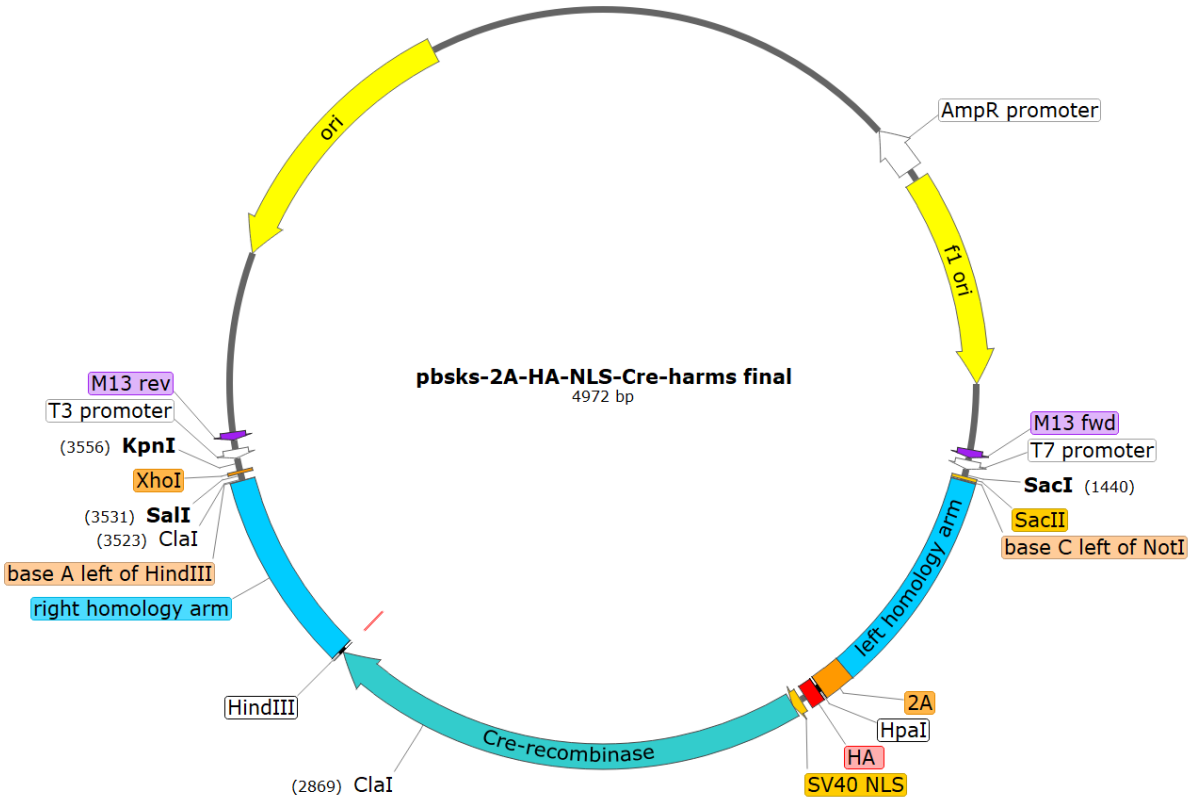

Figure 35 Final pBSKS vector with 2A-HA-NLS-Cre-recombinase construct and flanking homology arms resulting from Gibson cloning.
Restriction sites HpaI between 2A and HA; as well as HindIII in proximity to Cre-recombinase are residues from cloning. As the pBSKS vector was opened with restriction digest of HindIII and NotI but insertion was done with the help of Gibson cloning, both restriction sites were destroyed and only one base is left (light orange).

For sgRNA1 the PAM sequence could be modified to prevent further Cas9 targeting after integration (Fig. 36, green sequence: red letters). The intended silent mutations within the gRNA sequence could not be modified through a former PCR reaction (Fig. 36, blue sequence: red letters) and stayed the same as in the wild-type sequence.

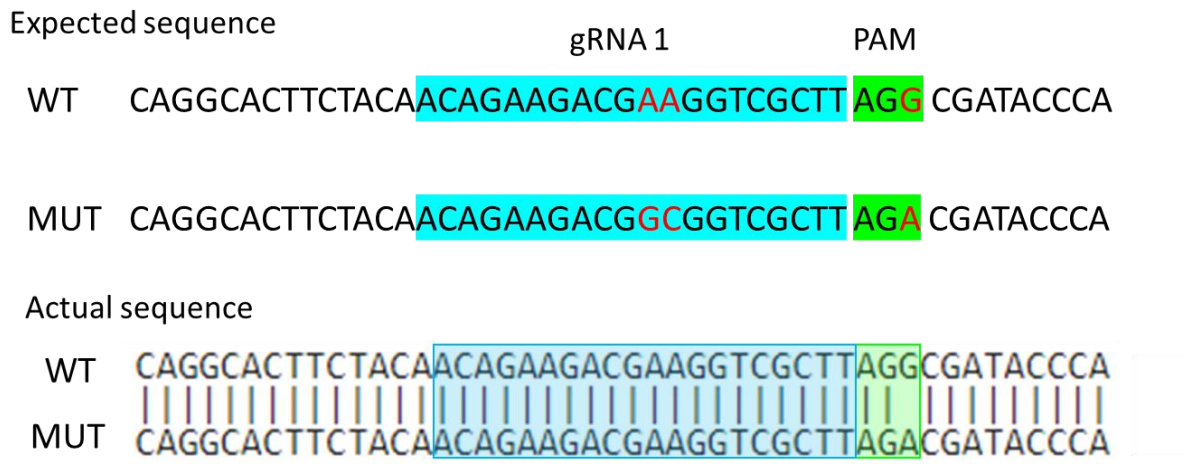

Figure 36 Comparison of base changes within the guideRNA1 sequence between expected and actual sequence of wild-type sequence (WT) and HDR sequence (MUT).
To prevent a repeated cutting of the targeted site by Cas9, the PAM sequence had to be changed and at the same time, it was tried to change the guide RNA sequence to hinder the binding of the Cas9 complex. The upper part (expected sequence) shows the guide RNA sequence (blue) and the PAM sequence (green) with the expected changes (red letters). In the mutant, the PAM sequence should have been changed from AGG to AGA whereas it was intended to insert two silent mutants to the mutant CGA AGG to CGG CGG. The blasted results of the sequencing of the final HDR vector after Gibson cloning in the lower part of the picture (actual bands) show that the PAM sequence change was successful, but the silent mutations could not be applied in the Gibson cloning aligned construct when compared to the wild-type mouse DNA.

For sgRNA2 a base within the PAM sequence change could successfully be integrated as well as three silent mutations within the sgRNA2 sequence (Fig. 37, red letters). The rest of the right homology arm sequence remained unchanged.

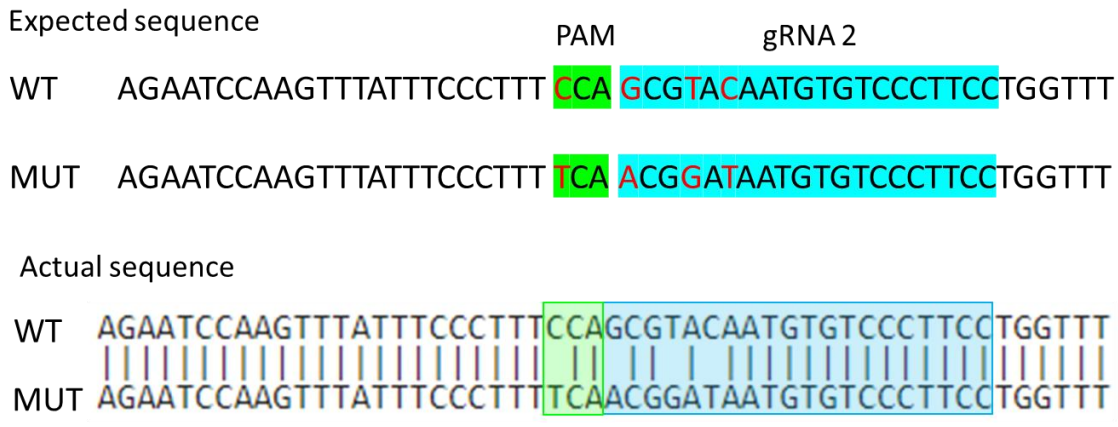

Figure 37 Comparison of base changes within the guideRNA2 sequence between expected and actual sequence of wild-type sequence (WT) and HDR sequence (MUT).
To prevent a repeated cutting of the targeted site by Cas9, the PAM sequence had to be changed and, at the same time, it was tried to change the guide RNA sequence to hinder the binding of the Cas9 complex. The upper part (expected sequence) shows the guide RNA sequence (blue) and the PAM sequence (green) with the expected changes (red letter). In the mutant, the PAM sequence should have been changed from CCA to TCA whereas it was intended to insert three silent mutations to the mutant GCG TAC to ACG GAT. The blasted re-

sults of the sequencing of the final HDR vector after Gibson cloning in the lower part of the picture (actual sequence) show that all intended changes could be applied successfully in the final HDR construct when compared to the wild-type mouse DNA.

The correct product was controlled via Sanger sequencing, by using the T7 and T3 promotor of the backbone vector. The blasted results of the HDR construct after Gibson cloning verify that the homology arms could successfully be added on both sides of the 2A-HA-NLS-Cre construct when compared to the wild-type mouse construct from NCBI-Blastn (Fig. 38).

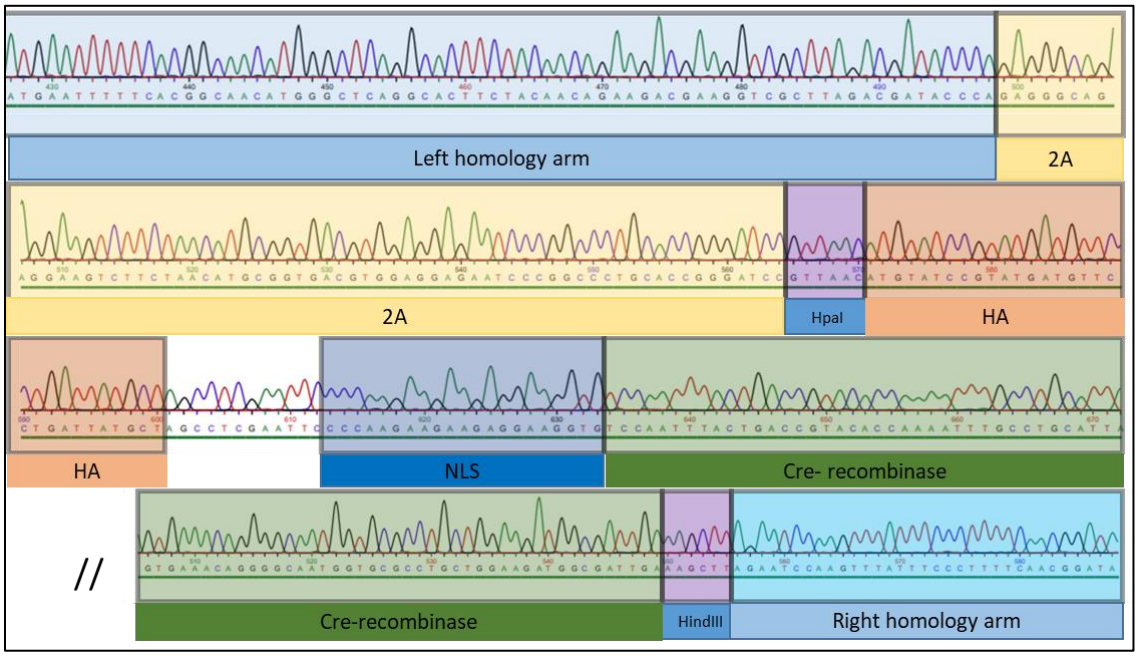

Figure 38 Sequencing results of 2A-HA-NLS-Cre final construct including left and right homology arms and sequence modifications.
The Reelin 2A-HA-NLS-Cre-recombinase construct with homology arms was assembled with Gibson cloning. The sequence chromatograms showing correct targeted 5' to 3' junctions. No base pair alterations could be found. The final sequence for genomic insertion contains the above-mentioned modifications within both PAM sequences and the sgRNA2.

3.3 EASI-CRISPR

Although all preliminary experiments worked fine with the method described by Ran (Ran et al., 2013), we decided to use the Easi-CRISPR method described by Quadros et al. in 2017 (Quadros et al., 2017). The new method promised to show better performance and higher knock-in efficiency using large inserts. With the Easi-CRISPR method, crRNA and tracrRNA (Alt-R™ CRISPR guide RNAs, Integrated DNA Technologies, Inc. (IDT), Coralville, IA, USA) were ordered separately and were used as annealed two part synthetic crRNA and tracrRNA molecules. Prior to zygote injection, the guide RNA was combined with recombinant Cas9 protein (Alt-R™ S.p. Cas9 Nuclease 3NLS (IDT)). The use of ssDNA instead of dsDNA has the advantage that it does not trigger cytotoxic responses in cells and is less likely to randomly integrate into the genome as dsDNA would do.

3.3.1 Preparation of long ssDNA

To inject the HDR construct into zygotes single-stranded DNA (ssDNA) instead of double-stranded DNA (dsDNA) was used. To produce ssDNA out of dsDNA the Guide-it™ Long ssDNA Production System (#632645, Takara, USA) was used. The correct function of the kit was shown with a comparison of dsDNA vs ssDNA product on an agarose gel (Fig. 39). The original HDR construct after PCR amplification prior to the strandase digest was 1955 bp. The ssDNA product is slightly smaller than the originally cloned product as the primers to amplify the ssDNA product are located with the left and right homology arm (35 bp downstream of the left homology arm and 78 bp upstream of the right homology arm). The single-stranded product has a smaller molecular weight than the corresponding dsDNA and can therefore run faster on the agarose gel which appears in a smaller product size. Sense and anti-sense strands are the same product, just as complementary strands, because either the 5'-3' strand (sense) or the 3'-5' strand (anti-sense) was formed when digesting the complementary strand, respectively.

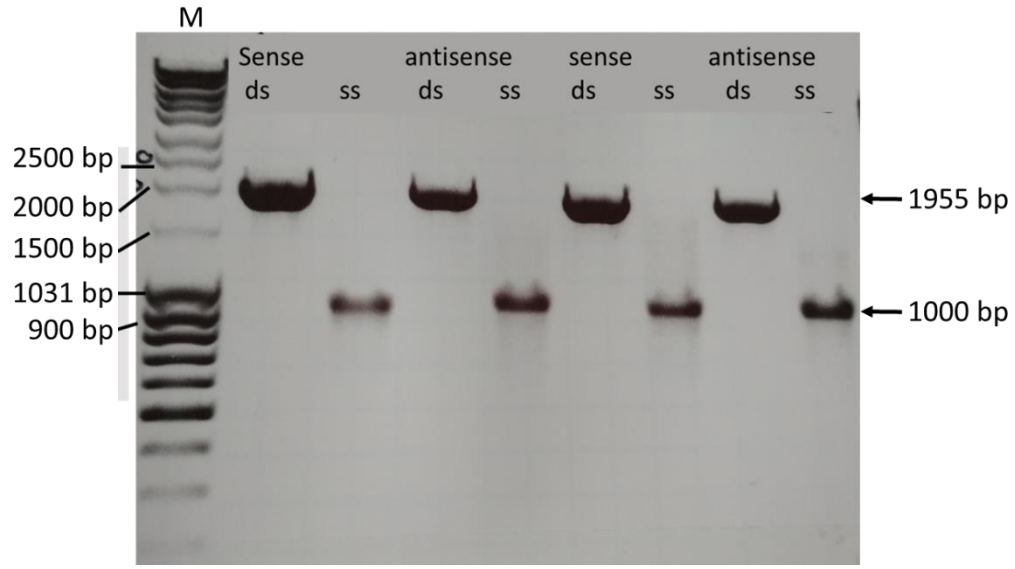

Figure 39 Agarose gel results for successful application of the ssDNA Kit.
10 µl of each of the samples was run on a 1.5% agarose gel, including 100–200 ng of the dsDNA substrate, in a separate lane, as a control. The original dsDNA product has a size of 1955 bp, the ssDNA product has a smaller molecular weight, can therefore run faster through the gel and appears as a smaller band with half of the corresponding dsDNA size (~1000 bp). Sense and antisense refer to the position of the phosphorylation site of the primer (5' or 3') as the phosphorylated primer will be digested and so the complementary strand is formed to ssDNA. M: Marker MassRuler.

3.3.2 Zygote injection

Prior to injection, ordered crRNA and tracrRNA were annealed to build a guide RNA and combined with Cas9 protein to a ctRNP complex. This complex was injected together with the ssDNA donor and

Cas9 mRNA into the pronucleus of a mouse zygote (Fig. 40). The zygotes were either cultured and developed into blastocysts for preliminary analysis or were later transferred into foster mothers to develop into pubs.

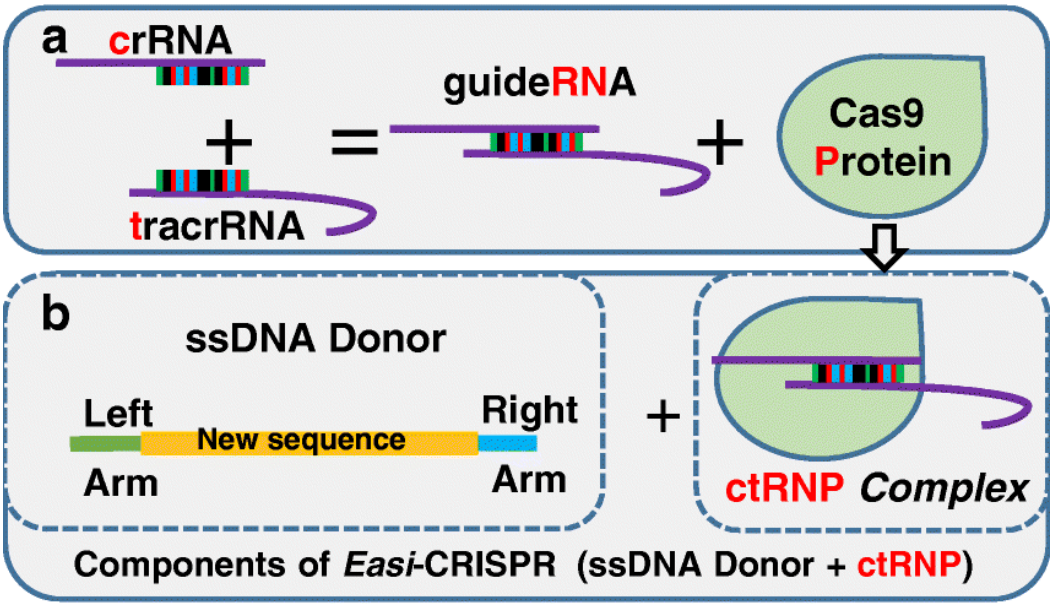

Figure 40 Scheme of preparation of the injection mix.
Prior to injection, either crRNA1 or crRNA2 and tracr RNA were annealed to a guide RNA and combined with the Cas9 complex to form the ctRNP complex. The ctRNP complex was then injected into mouse zygotes along with the ssDNA donor construct and Cas9 mRNA (Figure from Quadros et al., 2017).

3.3.3 Blastocyst analysis

Four different zygote injections were performed, either with sgRNA 1 or sgRNA 2 and either with “antisense” or “sense” ssDNA. For sgRNA1, 55 zygotes could develop into blastocysts and for sgRNA2 70 (Tab. 23). Zygotes could develop into blastocysts after injection. This means 60.7% of sgRNA 1-injected and 50% of sgRNA 2-injected zygotes survived and could develop into blastocysts. The DNA of the blastocysts was harvested and analyzed by PCR with a nested PCR reaction (primer pair 1 followed by primer pair 2) (Fig. 41).

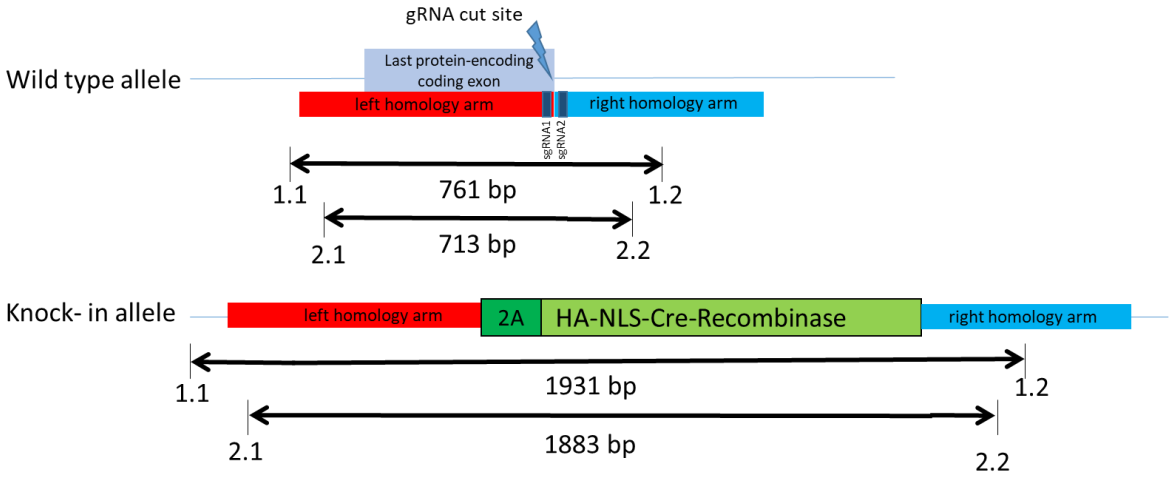

Figure 41 Scheme of nested PCR for blastocysts analysis.
The first PCR with primer pair 1 amplifies the region in front of the left homology arm until a region within the right homology arm (761 bp WT, 1931 bp MUT). The product of the first PCR is then taken to perform a second PCR reaction with primer pair 2. Primer 2 amplifies a region within the product of primer pair 1 (from the left homology arm to the right homology arm) and so further amplifies the DNA sequence (713 bp WT, 1883 bp MUT). This is important to verify the correct insertion of the HDR construct into the knock-in blastocysts even when only a small amount of start product is available.

As blastocysts have only a limited amount of DNA, a nested PCR was performed (1.PCR primer pair 1.1 + 1.2; 2.PCR primer pair 2.1 + 2.2) in order to amplify the product even more. Without nested PCR the results were hardly visible on an agarose gel (Fig. 42A). After the nested PCR thick WT bands were visible and some blastocysts showed a successful integration of the HDR construct (Fig. 42B). For example #5 (Fig. 42B) showed the expected bands, but also additional, unexpected bands were amplified.

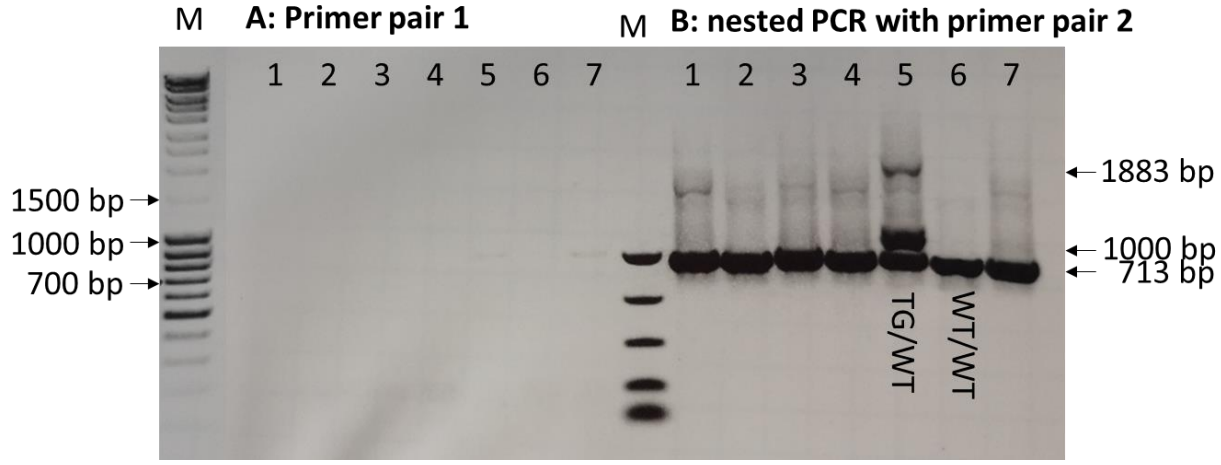

Figure 42 Agarose gel shows the comparison of sgRNA1 injected blastocyst PCR for a single and a nested PCR.
The first PCR with primer pair 1 (A) showed no results on the agarose gel. After performing the nested PCR with the product of the first PCR and primer pair 2 (B) TG/wt (#5, 1883 bp, 713 bp) and wt/wt (#6, 713 bp) blastocysts could be verified. M: Marker MassRuler (left), PCR Marker (NEB)(middle).

Although the survival rate of the injected blastocysts was good, only 3 out of 126 sgRNA1 injected blastocysts showed expected bands and no blastocyst injected with sgRNA2 showed a successful integration of the construct (Tab. 23).

Table 23 Number of injected zygotes, zygotes that successfully developed into blastocysts and correctly targeted blastocysts.

	zygotes injected	survived blastocysts	correctly targeted
sgRNA1	140	34+21= 55 (60.7%)	3
sgRNA2	140	55+15 = 70 (50%)	0

3.3.4 Embryo analysis

In total 1120 zygotes were injected with ctRNP1 complex containing guide sequence 1 and our single-stranded HDR construct in four separate experiments. 550 zygotes could be transferred into 25 foster mothers and we had a total outcome of 85 pups that could be analyzed by genotyping (Tab. 24). ctRNP2 complex containing guide sequence 2 and the single-stranded HDR construct was injected into 840 zygotes of which 389 were transferred into 17 foster mothers, so a total outcome of 60 pups was reached.

Table 24 Number of injected zygotes, number of transferred embryos and outcome of living pups.

Injected construct	# of injected zygotes	# of transferred embryos	# of pups
ctRNP 1 + ssDNA	1120	550	85
ctRNP 2 + ssDNA	840	389	60

The DNA of the pups was analyzed with 8 different primer pairs that cover all possible junction sites to show that our insert is inserted at the right position, in the right direction and without any deletions (Fig. 43).

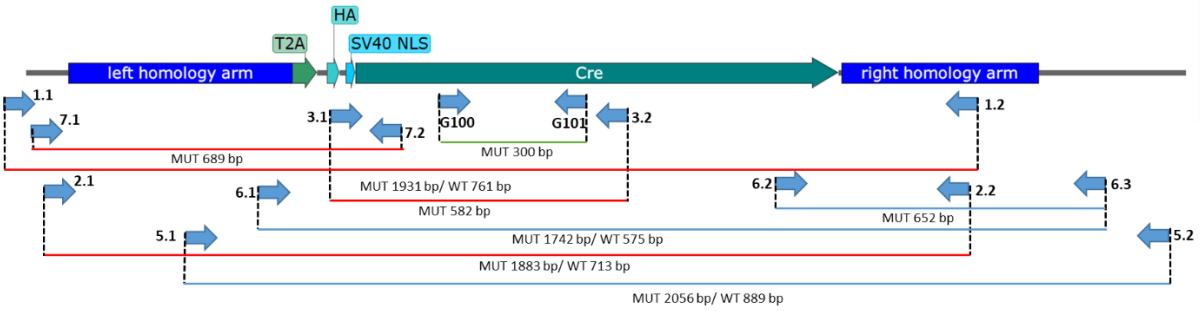

Figure 43 Scheme of the location with the Reelin gene of all primers used for genotyping.
All possible founders were genotyped with 8 different primer combinations located within the Reelin construct and beyond the homology arms. The primers were chosen to verify the insertion, the correct orientation the correct junctions between the homology arms and the 2A-HA-NLS-Cre construct.

3.3.4.1 SgRNA1 injected animals

Overall, 3 out of 85 analyzed pups showed all bands expected for successful insertion of our 2A-HA-NLS-Cre-construct (Fig. 44). To confirm the correct integration, all primer pairs from Fig. 43 were tested but only 5 primer pairs were shown. Primer 1.1 and 1.2 extended between the exogenous sequences and the left homology arm. The analysis verified the correct direction and the correct position within the Reelin locus as well as the junction sites in-between. With the size of the gel band, transgenic animals with successful integration of the construct could be distinguished from wild-type animals (WT 761 bp, TG/wt 761, 1931 bp; TG/TG 1931 bp). Primer pair 7.1 and 7.2 encompassed a sequence upstream of the left homology arm and a sequence within the Cre-recombinase. Only animals with successful integration of Cre-recombinase in the correct direction showed a gel band at 689 bp. Primer pair 6.1 and 6.3 verified the junction of the left homology arm to all downstream sequences 2A-HA-NLS-Cre, and to the right homology arm and exogenous sequences beyond that. Transgenic animals with successful integration of the HDR construct in the correct direction showed 575 bp and 1742 bp for TG/wt animals or 1742 bp for TG/TG animals. Primer pair 6.2 and 6.3 spans the sequence of Cre to the sequence downstream of the right homology arm and transgenic animals with Cre integration showed a band at 652 bp. The primers G100 and G101 verified the presence of Cre-recombinase with a band size of 300 bp.

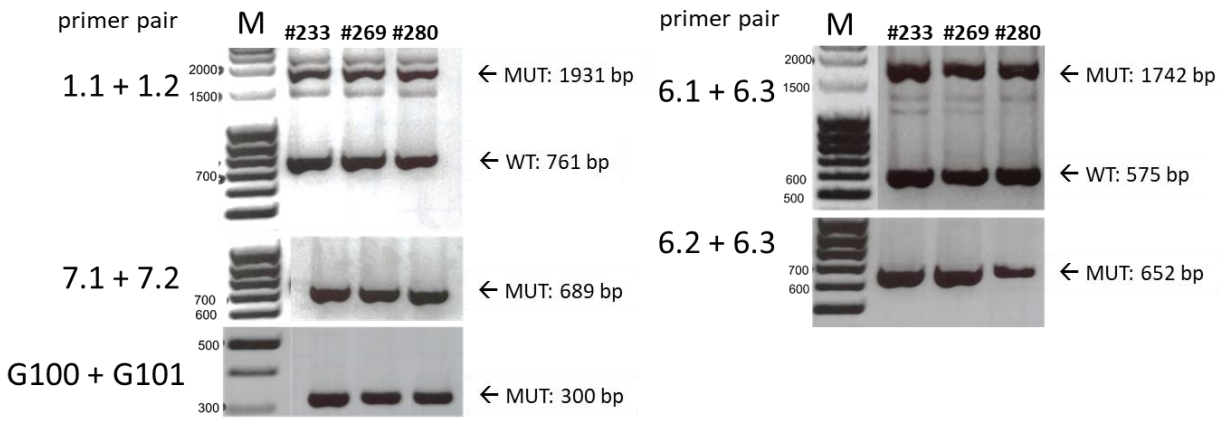

Figure 44 Genotyping results for three positive founders of sgRNA1 injected zygotes.
The genotyping results show 3 positive with sgRNA1 injected founders which carry the correct insertion of the HDR construct. Junction sites between left homology arm and neighboring endogenous sequences (Primer 1.1 + 1.2: WT 761 bp, MUT 1931 bp), sequence outside the homology arm and within Cre-recombinase construct (Primer 7.1+7.2: MUT 689 bp), sequence inside Cre-recombinase (Primer G100 + G101: MUT 300 bp), the junction between left and right homology arm including neighboring sequences (Primer 6.1 + 6.3: WT 575, MUT 1742 bp) and the sequence within Cre to sequences beyond the right homology arm (Primer 6.2 + 6.3: MUT 652 bp) were all tested for correct bands. M: Marker MassRuler.

After confirming the insert via genotyping, all three candidates were sent for Sanger sequencing to confirm that the insert shows no base pair alterations or indels.

3.3.5 Sanger sequencing

3.3.5.1 SgRNA1 RNA injected animals

When analyzing the sequencing results, it was important to check, if there were any deletions or wrong base pairs within our inserted construct. Before sequencing, a PCR reaction with primer 1.1 and 1.2 was performed, bands were separated on an agarose gel by electrophoresis (Fig. 45), all visible bands were cut out and purified. Four different bands were cloned into a TOPO cloning vector: A 2300 bp, B 1931 bp, C 1500 bp, D 761 bp.

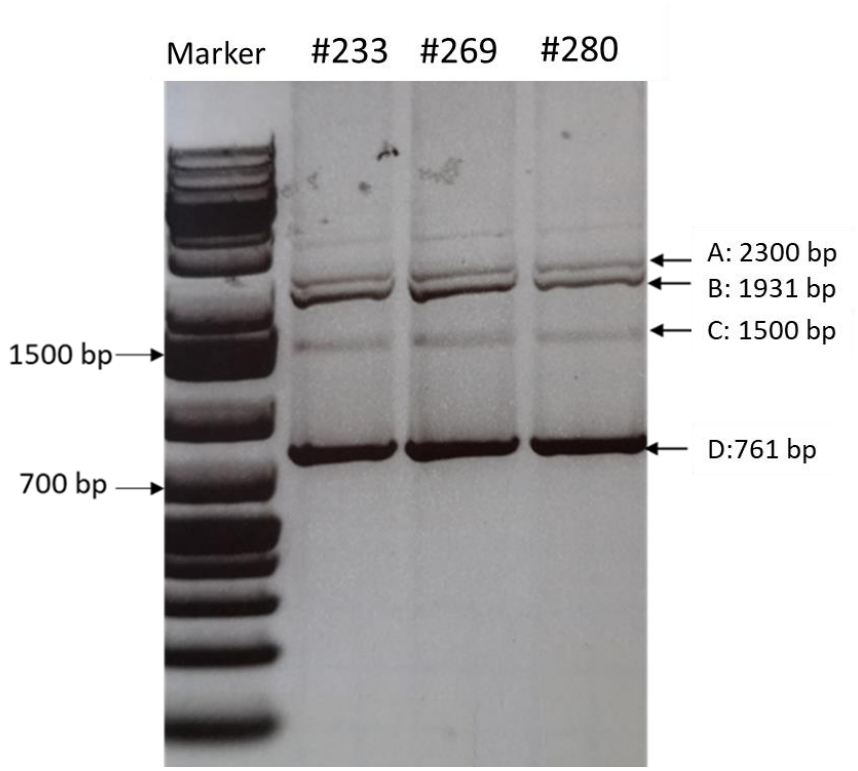

Figure 45 Agarose gel showing results of 3 sgRNA1 injected mice with a recombined targeting sequence (identified as putative founders).
All mice (Lane 1 #233, lane2 #269, lane 3 # 280) showing the expected bands for PCR amplification with primer pair 1.1 and 1.2 (B 1931 bp and D 761 bp), but also two additional bands (A 2300 bp and C 1500 bp). M: Marker MassRuler.

The sequencing results for band B amplified with primer pair 1.1 and 1.2 showed the correct insertion without base pair alterations at the intended part of the sequence for founder #233 (Fig. 46), #269, #280 (S2) and their offspring #233-10, #269-35, #280-40. Sequencing results for band A and C of founder 233 showed a mixed sequence beginning directly after the left homology arm. When analyzing the different peaks, the sequence of the 2A-HA-NLS-Cre insert and for the right homology arm interfere with each other. When cloning products from band A and C into a TOPO vector, as performed for animals #233-10 and #280, sequencing results for band A contains the correct sequence for the 2A-HA-NLS-Cre construct and band C contain an unaltered WT sequence. Surprisingly, the band size that could be seen on the gel could no longer be detected by sequencing as the WT size corresponds to 761 bp and the mutant band to 1931 bp. Sequencing results for three subfounders of #233 (#233-1, #233-3, #233-6) after several generations of backcrossing still showed the unaltered sequence of the 2A-HA-NLS-construct when sequencing the mutant band B (S3, S4 and S5).

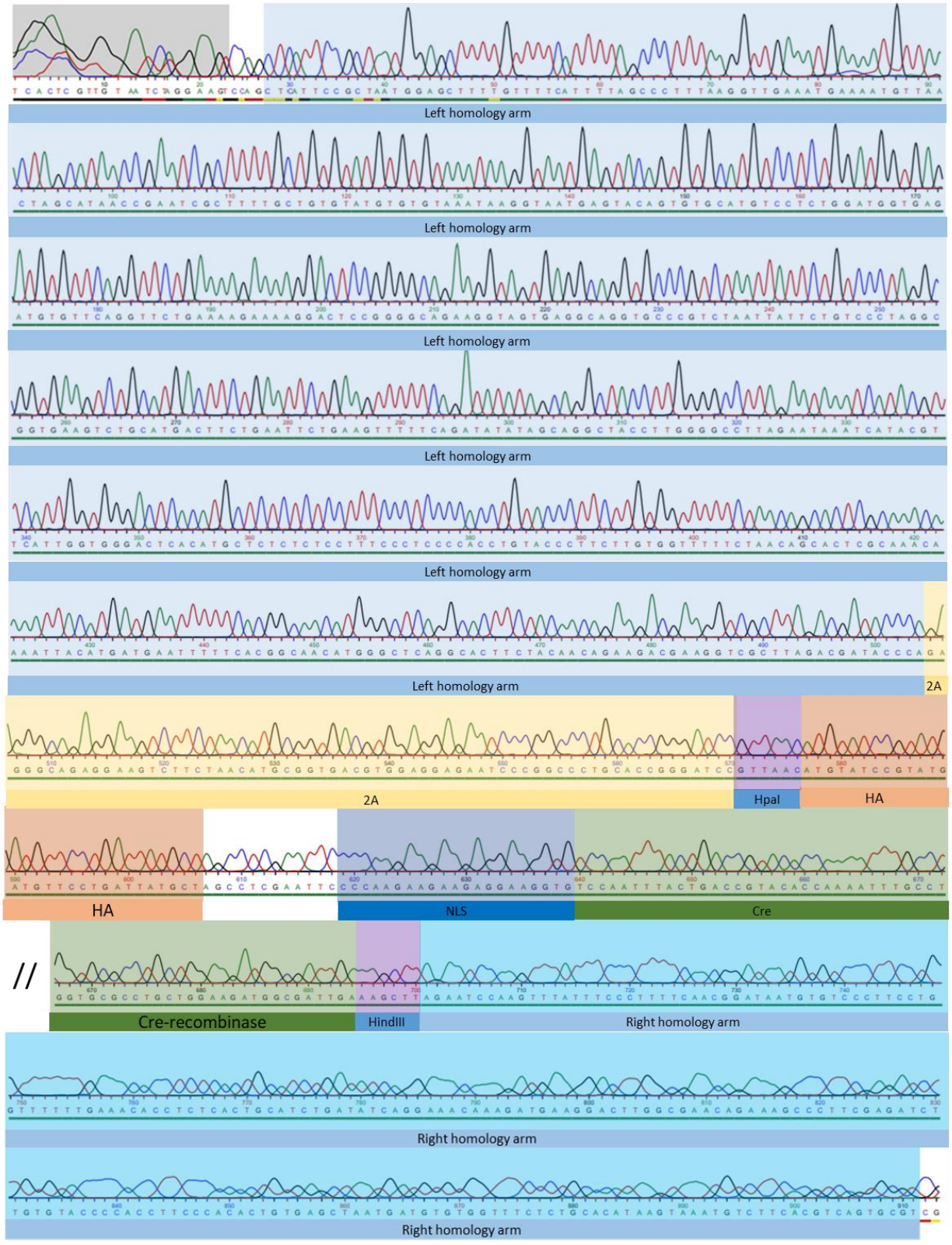

Figure 46 Sequencing results of 2A-HA-NLS-Cre inserted sequence into the genomic Reelin locus of founder animal #233.

The 2A-HA-NLS-Cre construct was successfully integrated via HDR into the Reelin gene. The sequencing results for band B from PCR reaction with primer pair 1.1 and 1.2 show a correct expected integration at the intended part of the sequence without alterations (sequence carries the expected silent mutations within both PAM sides and sgRNA2) in the sequence.

3.3.5.2 SgRNA2 RNA injected animals

PCR reactions with 6 different primers (Fig. 47A) of DNA from sg2 injected mice revealed three founders which show additional bands to the wild-type band of which some corresponded to the expected mutant band (Fig. 47B, Tab. 25).

Although the sgRNA2 injected animals seem to show a correct sized band for primer pair 1.1 + 1.2 (1931 bp) and 2.1 + 2.2 (1883 bp), many other stronger bands were visible (see Tab. 25). Although #360 showed the expected band for primer pair 6.2 + 6.3 (652 bp) and #355 showed the correct product for primer pair 7.1 + 7.2, the correct insertion could not be identified for all 3 animals as clear correct products were missing for primer pair 6.1 + 6.3 and G100 + G101 (#360 very weak band). The genotyping gave a first hint that the HDR was only partially integrated into the Reelin locus. To verify this, bands from the primer pair 1 product were separated by electrophoresis on a gel and all visible bands were cut out and cloned into a TOPO cloning vector. The cloned constructs of all three animals were sent for sequencing.

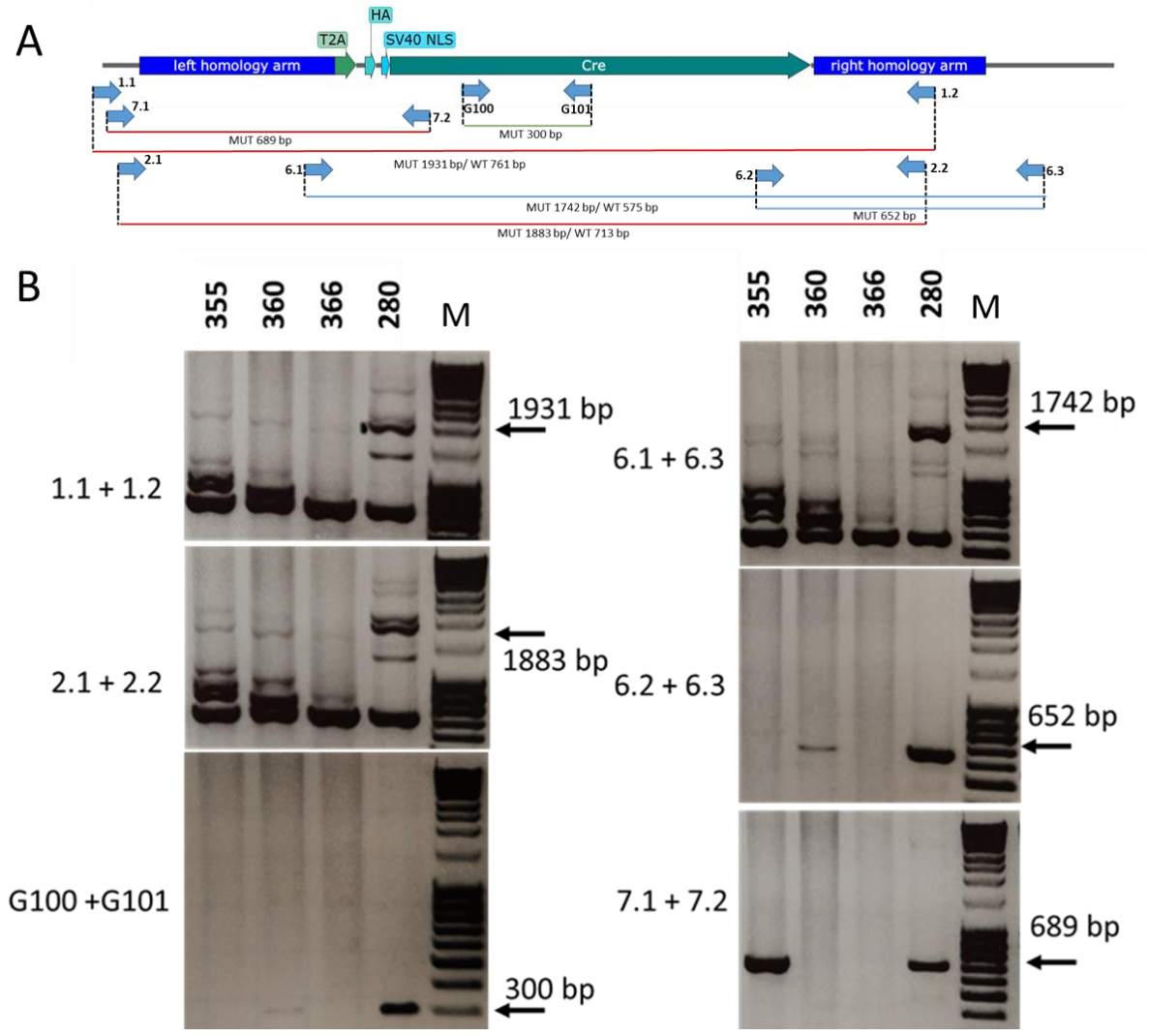

Figure 47 Representative genotyping results for sgRNA 2 injected mice.
A) Scheme shows the location of all 6 primers used across the HDR inserted construct. B) PCRs with 6 different primers, identified three animals with, sometimes faint, expected bands: #355, #360 and #366. Animal #280 was a sgRNA1 injected founder, who showed all expected bands and was therefore used as a positive control. All 3 sgRNA2 injected founders show a faint band for correct HDR construct insertion with Primer pair 1.2 + 1.2 as well as for Primer pair 2.1 + 2.2. Although #360 showed a faint MUT band with primer pair 6.2 + 6.3, the highest band for primer pair 6.1 + 6.3 runs a bit below the expected band. Animal #355 and #366 didn't show a correct band for all primer pair 6.1 + 6.3 or 6.2 + 6.3. #355 shows a clear band at 689 bp for primer pair 7.1 + 7.2, but all other animals did not and also for primer pair G100 + G101 it was not possible to detect the expected band. M: Marker MassRuler.

Table 25 All visible bands of 3 different sgRNA2 injected mice genotyped with different primers.

Primer	#355	#360	#366	expected
1.1 + 1.2	2000 bp 1200 bp 1000 bp 900 bp 761 bp	2000 bp 1931 bp 900 bp 800 bp 761 bp	1931 bp 761 bp	MUT 1931 bp WT 761 bp
2.1 + 2.2	2000 bp 1833 bp 1200 bp 1000 bp 900 bp 713 bp	2000 bp 1833 bp 900 bp 800 bp 713 bp	1833 bp 800 bp 713 bp	MUT 1833 bp WT 713 bp
6.1 + 6.3	1500 bp 900 bp 800 bp 700 bp 575 bp	1500 bp 1300 bp 800 bp 650 bp 575 bp	650 bp 575 bp	MUT 1742 bp WT 575 bp
6.2 + 6.3	-	652 bp	-	MUT 652 bp
7.1 + 7.2	689 bp			MUT 689 bp
G100 + G101	-	300 bp (very weak)	-	MUT 300 bp

The sequencing results could confirm the fragmented insertion of the HDR construct. All deletions start within the cutting region of sgRNA2 and end within the Cre-recombinase construct. These results show a partial integration of the HDR construct but it seems that when injecting gRNA2-containing ctRNP complex, further Cas9 cleavage was not prevented after HDR insertion.

Analysis of sgRNA2 injected animal #355

Genomic DNA from animal #355 was amplified with a PCR reaction using primer pair 1.1 and 1.2 expecting bands at 1931 bp as mutant band and 761 bp as WT band. The results showed bands at 2000

bp (Fig. 48A), 1300 bp (Fig. 48B), 1000 bp (Fig. 48C), 900 bp (Fig. 48D) and 761 bp (Fig. 48E). To analyze why there is no expected mutant band, the biggest bands were send for sequencing.

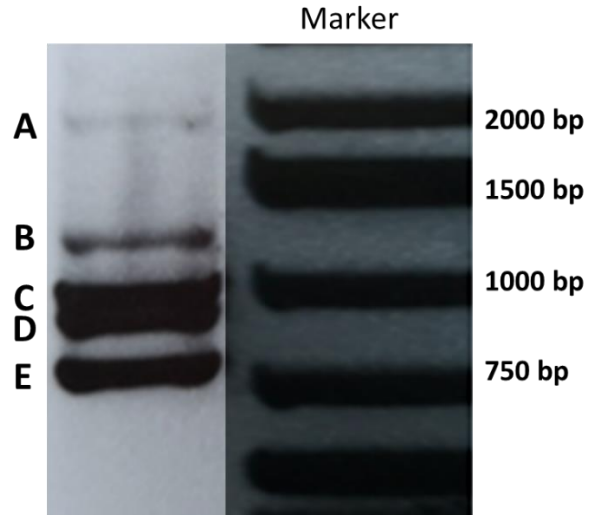

Figure 48 Founder 355:
PCR amplification of mouse genomic DNA from animal #355 with primer pair 1.1 and 1.2 revealed five different bands: A 2000 bp, B 1300 bp, C 1000 bp, D 900 bp, E 761 bp. All bands were unexpected, except for band E, which refers to the WT band, all other bands were unexpected as the correct mutant band should have a size of 1931 bp. M: Marker MassRuler.

For band A it was not possible to get an appropriate amount of DNA for further cloning and sequencing experiments. The sequencing results for band B showed a 41bp and a 892 bp deletion within the Cre construct, starting 235 bp after the beginning of the 2A-HA-NLS-Cre Sequence and ending at the cutting site of sg2 RNA directed Cas9. 35 bp within the Cre sequence after the first deletion could also be detected (Fig. 49). The same deletion pattern could be seen for bands C and D even if they appeared to be smaller on the agarose gel.

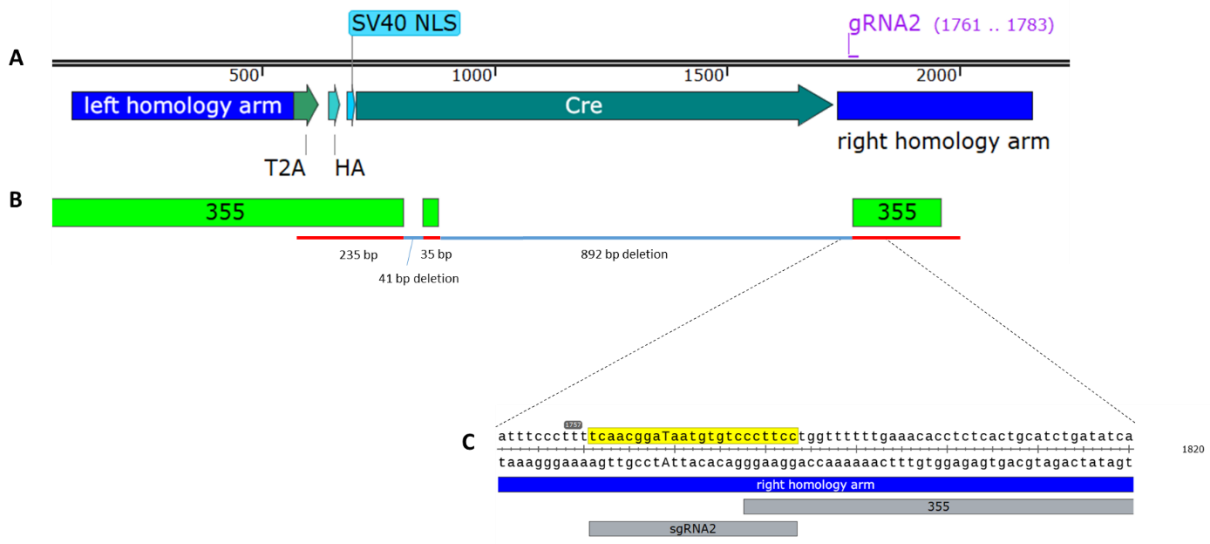

Figure 49 Results for band B (1300 bp) revealed a 41 bp and 892 bp deletion within the Cre-recombinase construct.
The originally expected sequence (A) was compared to the sequencing results of band B of sgRNA2 injected animal #355 (B). The results revealed that only the first 235 bp and 35 bp of downstream Cre-sequences of the 2A-HA-NLS-Cre-construct were integrated into the Reelin locus. The deletion starts at base 17 of the sgRNA2 sequence (C).

Analysis of sgRNA2 injected animal #360

Genomic DNA from animal #360 was amplified with a PCR reaction using primer pair 1.1 and 1.2 expecting the mutant band at 1931 bp after successful and complete integration of the HDR and a WT band at 761 bp. The results showed bands at 2500 bp (Fig. 50A), 2000 bp (Fig. 50B), 1300 bp (Fig. 50C), 965 bp (Fig. 50D) and 761 bp (Fig. 50E). To analyze why there is no expected mutant band the biggest bands were send for sequencing

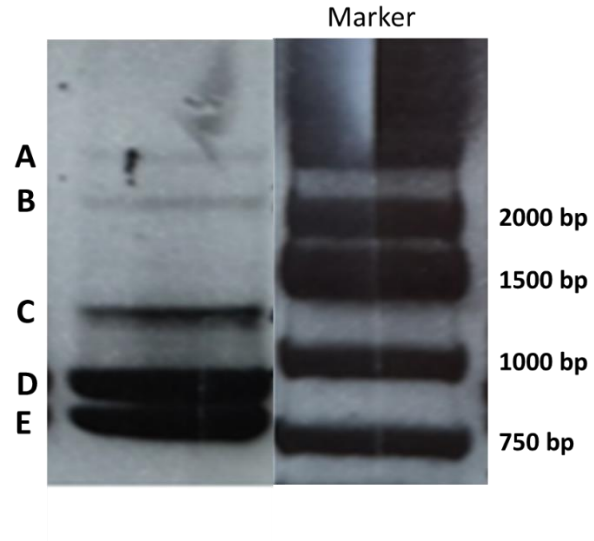

Figure 50 Founder 360:
Five different bands were detected by PCR amplification of mouse genomic DNA from animal #360 with primer pair 1.1 and 1.2: A 2500 bp, B 2000 bp, C 1300 bp, D 965 bp, E 761 bp. All bands were unexpected, except for

band E, which refers to the WT band, all other bands were unexpected as the correct mutant band should have a size of 1931 bp. M: Marker MassRuler.

The bands A, B and C did not give an appropriate amount of the DNA for subcloning. Band D showed a 1047 bp sized deletion within the Cre sequence, ranging from 155 bp after the beginning of the 2A-HA-NLS-Cre Sequence to the cutting site of sg2 guided Cas9 (Fig. 51).

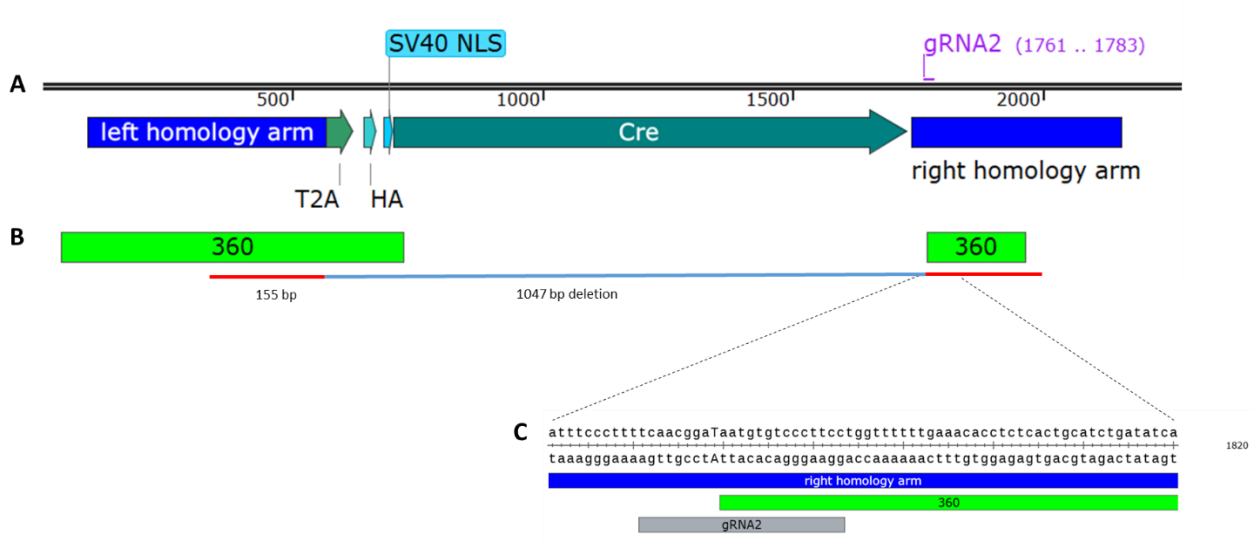

Figure 51 Results for band D (965 bp) revealed a 1047 bp deletion within the Cre-recombinase construct. The originally expected sequence (A) was compared to the sequencing results of band B of sgRNA2 injected animal #360 (B). The results revealed that only the first 155 bp of the 2A-HA-NLS-Cre-construct was integrated into the Reelin locus. The deletion starts at base 9 of the sgRNA2 sequence (C).

sgRNA2 injected animal # 366

Genomic DNA from animal #366 was amplified with a PCR reaction using primer pair 1.1 and 1.2 expecting the mutant band at 1931 bp after successful and complete integration of the HDR and a WT band at 761 bp. The results showed bands at 1900 bp (Fig. 52A), 1200 bp (Fig. 52B), 800 bp (Fig. 52C), and 761 bp (Fig. 52D). To analyze why there is no expected mutant band the biggest bands were send for sequencing

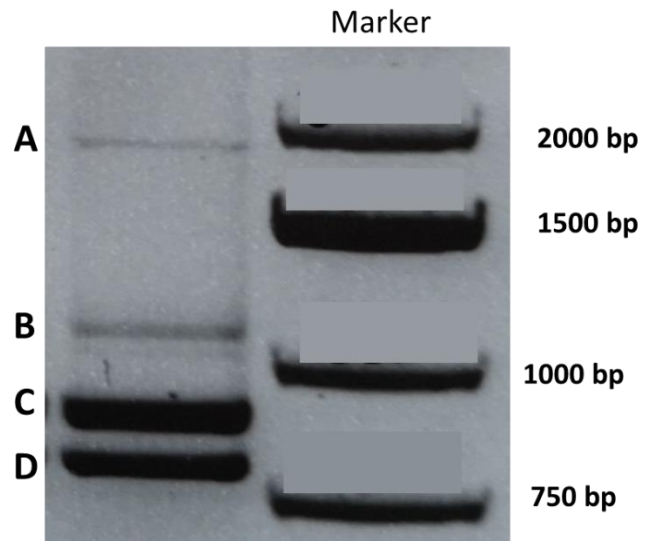

Figure 52 Founder 366:
Four different bands were detected by PCR amplification of mouse genomic DNA from animal #366 with primer pair 1.1 and 1.2: A 1900 bp, B 1200 bp, C 800 bp, D 761 bp. All bands were unexpected, except for band D, which refers to the WT band, all other bands were unexpected as the correct mutant band should have a size of 1931 bp. M: Marker MassRuler.

Only bands C and D could be used for subcloning as the band A and B did not give an appropriate DNA amount (Fig. 52). Whereas band D showed the same sequence as a wild-type sequence, band C had a 1047 bp deletion within the Cre-Sequence. The deletion starts 155 bp after the beginning of the 2A-HA-NLS-Cre and ends with the sg2 guided Cas9 cutting site (Fig. 53).

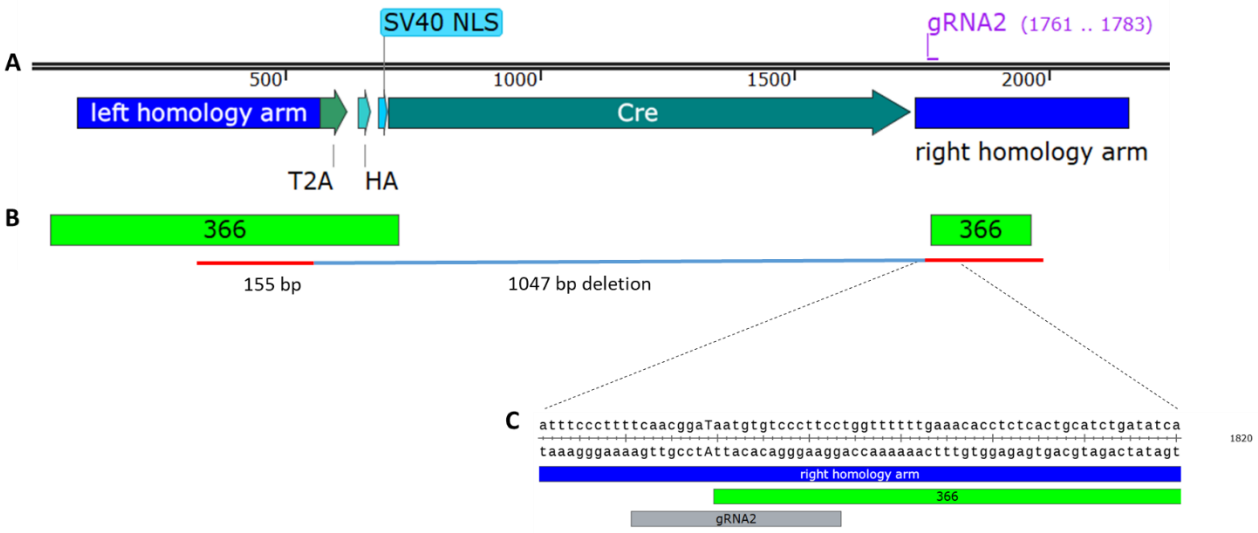

Figure 53 Results for band C (800 bp) revealed a 1047 bp deletion within the Cre-recombinase construct.
The originally expected sequence (A) was compared to the sequencing results of band B of sgRNA2 injected animal #366 (B). The results revealed that only the first 155 bp of the 2A-HA-NLS-Cre-construct was integrated into the Reelin locus. The deletion starts at base 9 of the sgRNA2 sequence (C).

3.3.6 Verification of Reelin-function

3.3.6.1 Crossing Reelin-Cre mouse with YFP reporter mouse line (Rosa26-floxed-stop-YFP)

We crossed F1 offspring animals of all three possible founder mice, which descended from sgRNA1 injections with an YFP reporter line. The Rosa26-floxed-stop-YFP line has a loxP-flanked STOP sequence followed by a yellow fluorescence protein gene inserted into the Rosa26 locus (Srinivas et al., 2001). Breeding this mouse line with mice expressing Cre-recombinase will lead to a deletion of the STOP sequence and to an expression of YFP in the Cre-expressing regions of the double mutant offspring. This double mutant then helps to monitor the Cre expression and will prove the functionality of the newly introduced Cre-recombinase.

Immunostainings with GFP antibody against YFP (therefore referred as GFP in figures) and Reelin antibody confirmed expression of Reelin and YFP in the same cells within the cortex (Fig. 54) and the hippocampus (Fig. 56) of P0 mouse pups. As also a strong Alexa 546 staining was seen at the pial surface the specificity of the staining was checked with a negative control (secondary antibody only). The negative control confirmed unspecific staining at the pial surface with Alexa 546 antibody (Fig. 55).

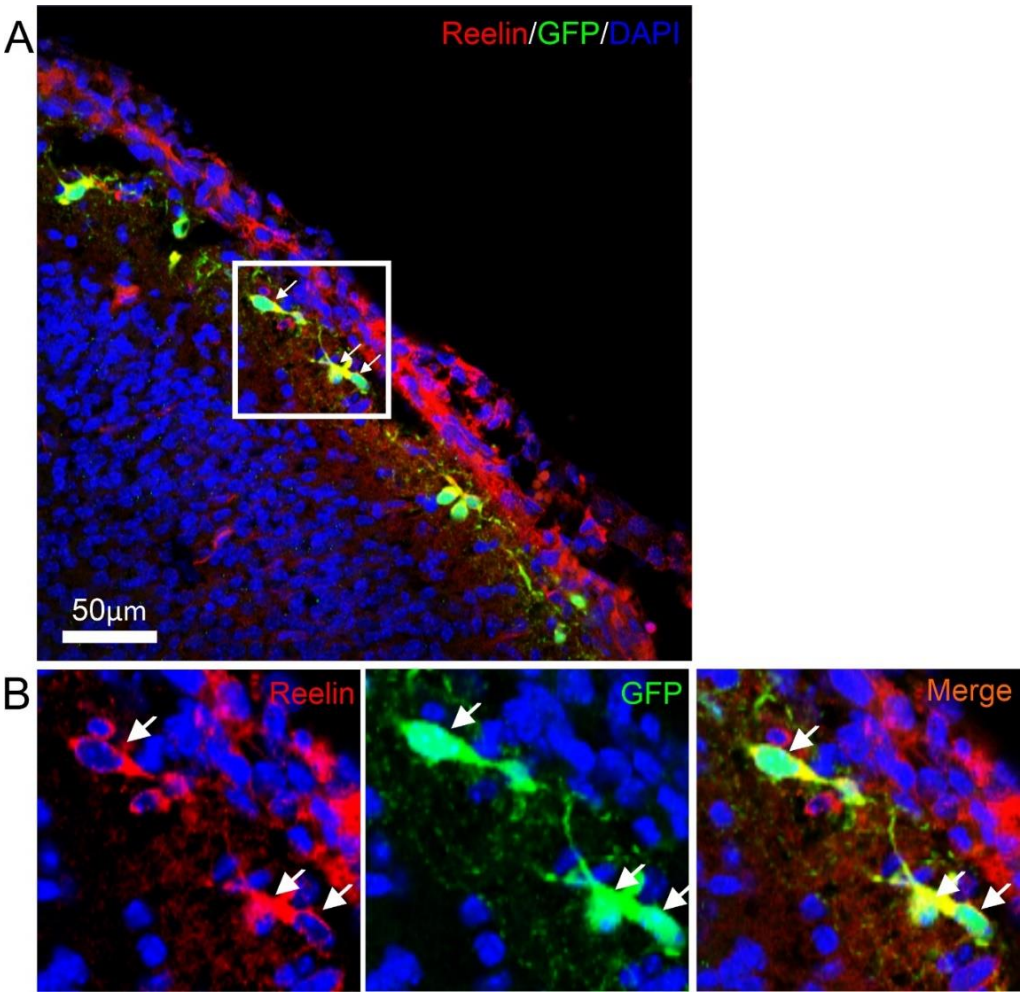

Figure 54 Cre recombinase-activated GFP expression of J-Reelin-Cre x ROSA26- floxed-stop-YFP mouse line (Rln-Cre TG/wt, ROSA26-floxed-stop M/M) confirms proper function of Cre insertion into Reelin locus. Representative section of a newborn cortical sections mouse brain (P0) after immunohistochemical staining for Reelin (red) and GFP (green). A) Stainings of the cortical plate confirmed normal Reelin expression in CR cells and Cre dependent GFP expression within targeted Reelin-expressing Cajal-Retzius cells (white arrow). The nucleus was stained with DAPI in blue. The cerebral membrane above the marginal zone appears in red due to unspecific binding of the secondary alexa 546 antibody (see negative control, Fig. 55). Scale bar: 50 µm. B) Enlarged pictures of the white squared region from A show Reelin (red), GFP (green) and merged- expression separately. Coexpression (filled arrows) can clearly be seen around the cell nucleus.

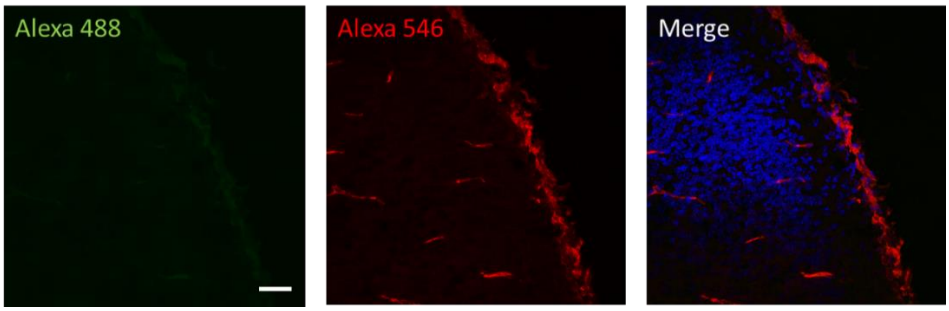

Figure 55 Negative control to test for unspecific binding of the secondary antibodies.
For negative control, sections from the same animal were stained with the same protocol but without primary antibody. Alexa 488 had no unspecific binding whereas alexa 546 showed a signal within blood vessels and the cerebral membrane. Scale bar: 20 µm.

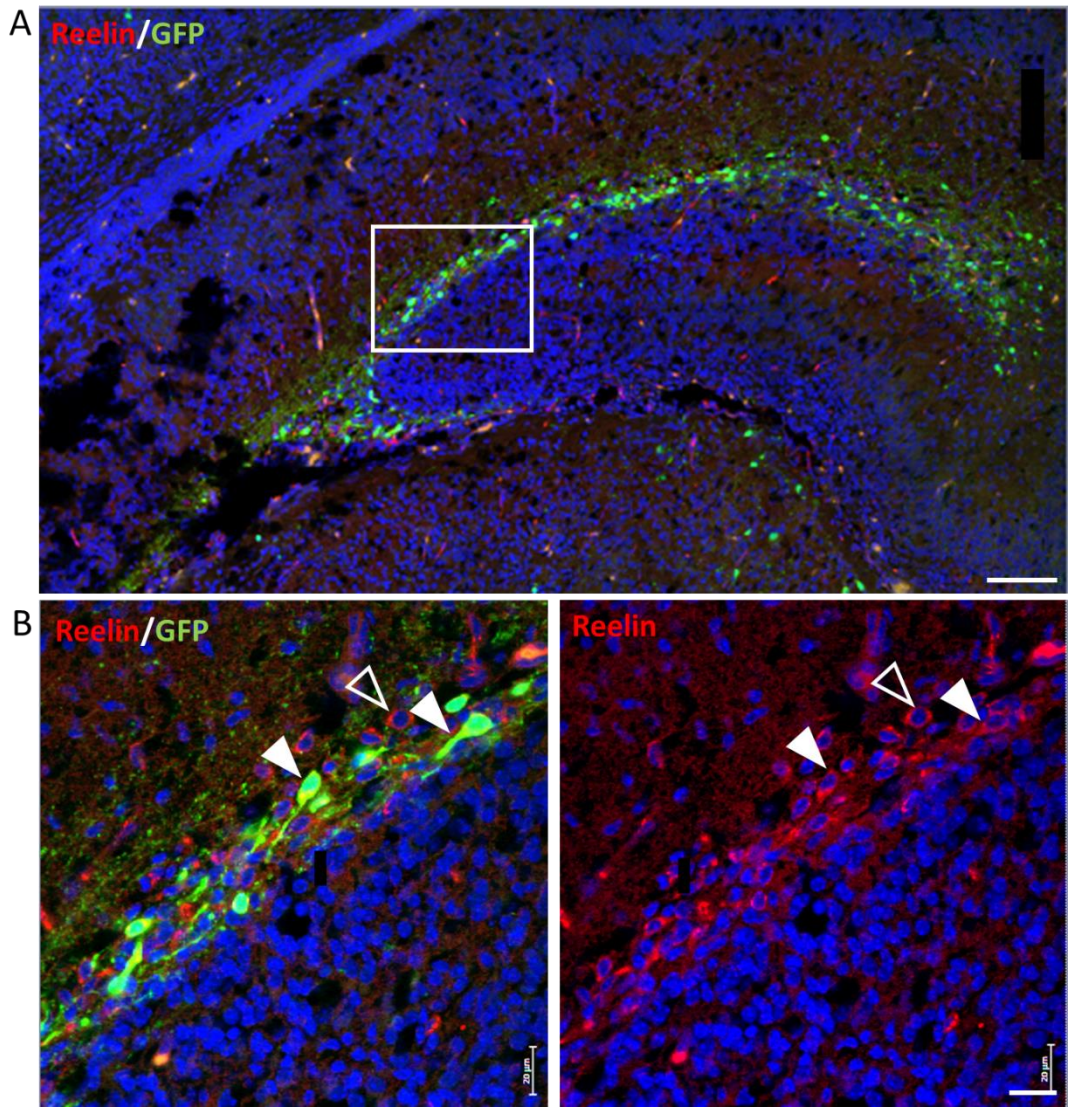

Figure 56 GFP labels Reelin-Cre expressing cells in P0 mouse hippocampus.
A) Immunohistochemically stained sections of P0 mouse show Reelin (red) and GFP (green) expression in hippocampus CA1, CA2 and CA3 regions. Scale bar 100 µm B) Enlarged pictures of the white squared region show coexpression of Reelin and GFP (white filled arrows) and cells expressing only Reelin (unfilled arrows). Counterstaining with DAPI. Scale bar 20 µm.

A different immunostaining for Reelin and Cre in P0 cortical brain slides detected Cre staining exclusively along with Reelin staining (Fig. 57) indicating that Cre was properly working and no leakiness could be observed.

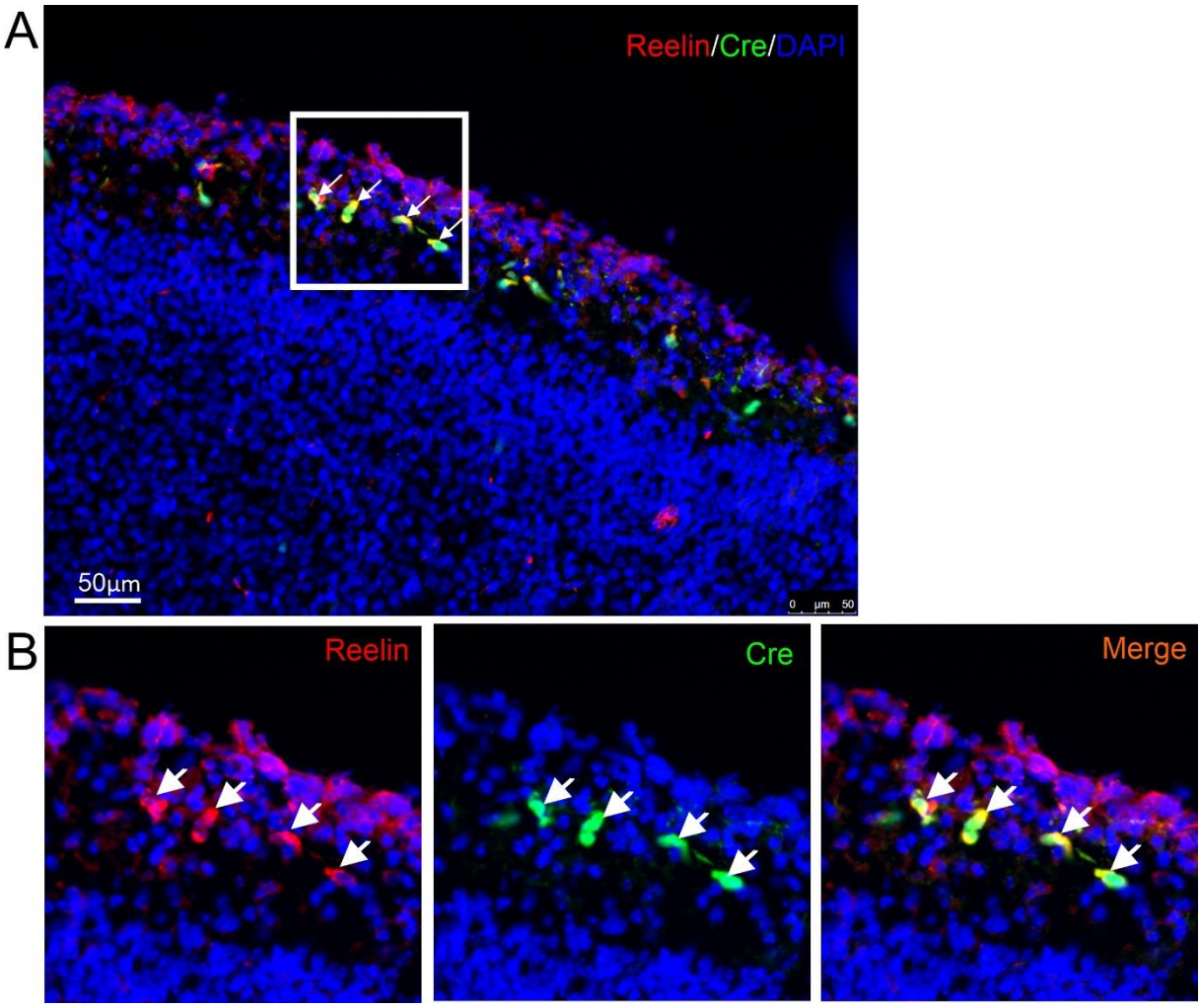

Figure 57 Analysis of Cre- and Reelin-expression in developing transgenic pallial mouse cortex at developmental stage P0 of J-Reelin-Cre x ROSA26- floxed-stop-YFP mouse line (Rln-Cre TG/wt, ROSA26-floxed-stop M/M).
A) Stainings of cortical brain tissue confirmed normal Reelin (red) expression in CR cells. Cre (green) positive cells colocalize with Reelin positive cells (white arrows). The nucleus was stained with DAPI in blue. The cerebral membrane above the marginal zone appears in red due to unspecific binding of the secondary alexa 546 antibody (see negative control). Scale bar: 50 µm. B) Enlarged pictures of white squared region from A show Reelin (red), Cre (green) and merged- expression separately. Coexpression (filled arrows) can be clearly seen around the cell nucleus.

Immunostainings for Reelin, Cre and GFP could confirm a proper functioning of the Reelin-Cre mouse.

3.4 Understanding the role of CB1 in Reelin-expressing cells

3.4.1 Loss-of-function

To understand the function of CB1 within Reelin-expressing Cajal-Retzius cells, we started to knock out CB1 expression within Reelin-expressing cells by crossing our Reelin-Cre mouse line with CB1 floxed mice (therefore referred as Reelin-Cre-CB1 mice), in which the CB1 gene is flanked by loxP sites (Marsicano et al., 2003). As a first step transgenic mice (Reelin-Cre $^{TG/wt}$ x CB1fl $^{fl/fl}$, therefore referred as Reelin-Cre-CB1 KO or MUT) were compared to wild-type siblings (Reelin-Cre $^{wt/wt}$ x CB1fl $^{fl/fl}$, therefore referred as Reelin-Cre-CB1 WT) to evaluate that CB1 expression is knocked out in Reelin-Cre expressing cells. To do so, *in situ* hybridization for Reelin and CB1 was performed on E13.5 and E14.5 embryonic mouse cortex. The results clearly show that CB1 expression within Cajal-Retzius cells was missing in transgenic Reelin-Cre-CB1 KO mice in both E13.5 and E14.5 (Fig. 58). CB1 expression apart from Reelin-expression in pyramidal neurons of the cortical plate of transgenic animals was the same when compared to Reelin-Cre-CB1 WT siblings. This confirmed the successful inactivation of CB1 in Reelin-Cre expressing cells.

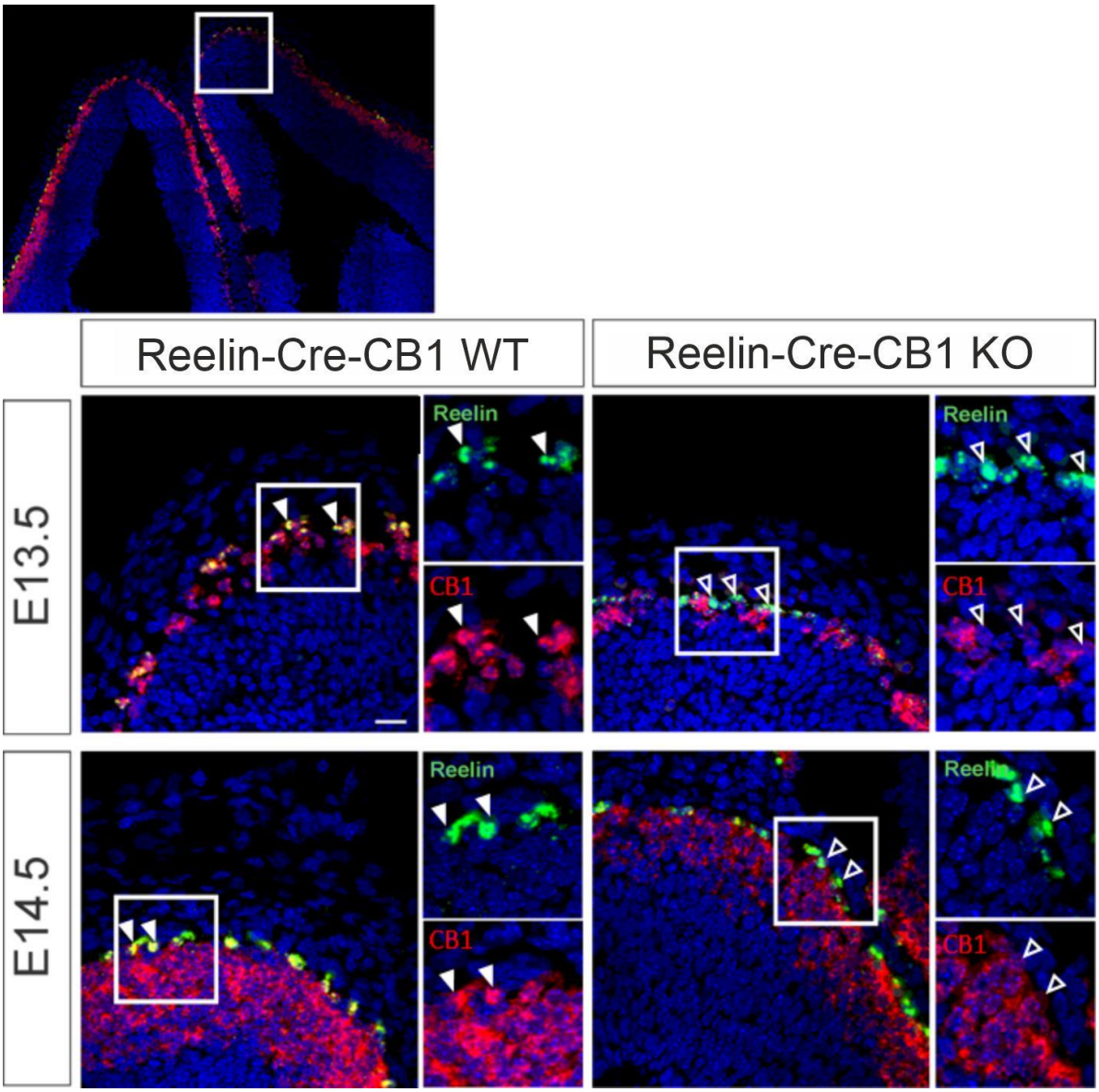

Figure 58 CB1 could be successfully knocked-out in Reelin-Cre expressing cells in Reelin-Cre-CB1 KO mice. *In situ* hybridization staining for Reelin (green) and CB1 (red) at developmental stages E13.5 and E14.5 in Reelin-Cre-CB1 WT (left) or Reelin-Cre-CB1 KO (right) mice. Representative confocal images of the dorsal pallium of the mouse embryonic cortex (see marked region in the overview image) confirmed normal Reelin expression in CR cells. Reelin and CB1 positive cells colocalized in Reelin-Cre-CB1 WT animals (filled arrow) whereas Reelin and CB1 expression was not colocalized in heterozygous Reelin-Cre-CB1 KO mice (unfilled arrows) in both E13.5 and E14.5. To highlight (missing) CB1-expression, pictures of the white squared regions were enlarged and separate channels of Reelin and CB1 are shown beside the merged pictures. This confirms the inactivation of CB1 expression within Reelin-positive cells in the Reelin-Cre-CB1 KO mouse line. Nucleus stained with DAPI in blue. Scale bar: 20 µm.

3.4.2 Analysis of cortex thickness

To determine the impact of specific inactivation of CB1 receptor in CR cells on cortical development, we analyzed Reelin-Cre-CB1 KO and Reelin-Cre-CB1 wt littermates. The cortex layer thickness was measured with the ruler tool of the Leica microscope software (Leica application suite X, vers.:

2.0.0.14332.2) by measuring the shortest distance from inner to outer cortex (VZ to CP) of every section per slide (Fig. 59). 1 to 3 sections were used to get 4 to 20 measurement points per animal. In total 7 animals per group at embryonal age E18.5 (Reelin-Cre-CB1 KO or Reelin-Cre-CB1 wt) from 5 different litters (XP39 2 WT/2 MUT) were analyzed. In every litter, it was possible to show that the cortical thickness of MUT littermates was reduced when compared to their WT siblings (Fig. 60, Tab. 26). Taken together all results, a reduction of cortical thickness was evident at E18.5 in Reelin-Cre-CB1 KO mice (total cortical thickness mean MUT: 640.3 ± 11, n=20; WT 778.3 ± 6.5, n=18; Fig. 61). An unpaired, two tailed t-test revealed a $p < 0.02$. These results support a significant role of the CB1 receptor in CR cells during cortical development and furthermore in controlling progenitor population size.

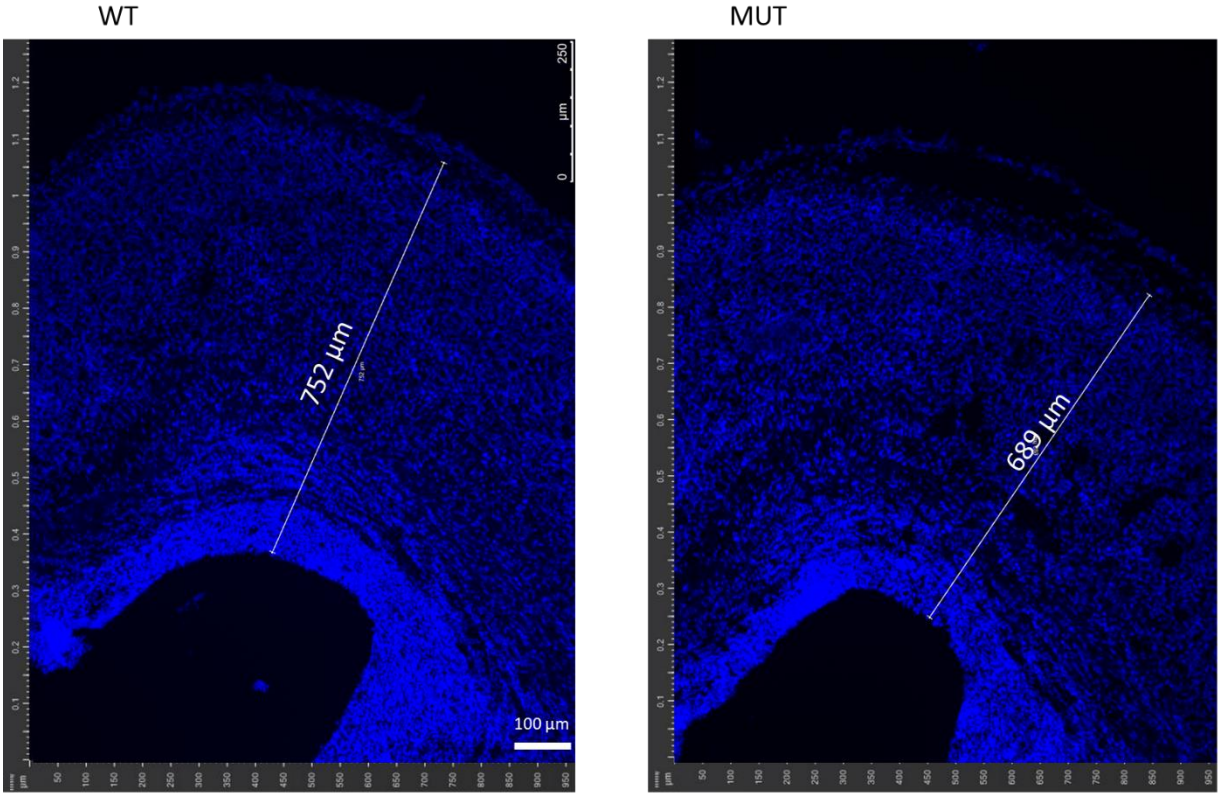

Figure 59 Comparison of cortical thickness between Reelin-Cre-CB1 WT (WT, left-hand panel) and Reelin-Cre-CB1 KO (MUT, right-hand panel) at E18.5.
The thickness of the dorsal cortex was measured with the ruler tool of the LasX imaging program from Leica on DAPI stained cortical sections. Scale bar: 100 µm.

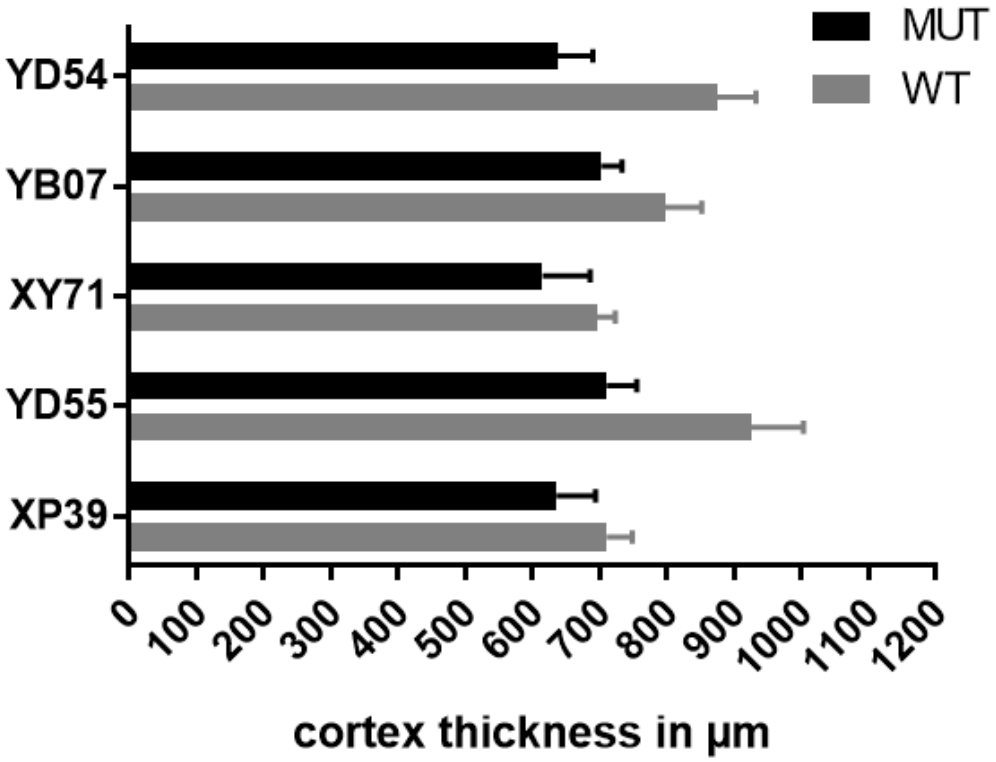

Figure 60 Comparison of cortical thickness between 5 different litters of E18.5 Reelin-Cre-CB1 WT (grey bars) and Reelin-Cre-CB1 KO (black bars) littermates confirmed increased cortical thickness in mutant mice.
* $p < 0.02$ Results are displayed as means ±SD.

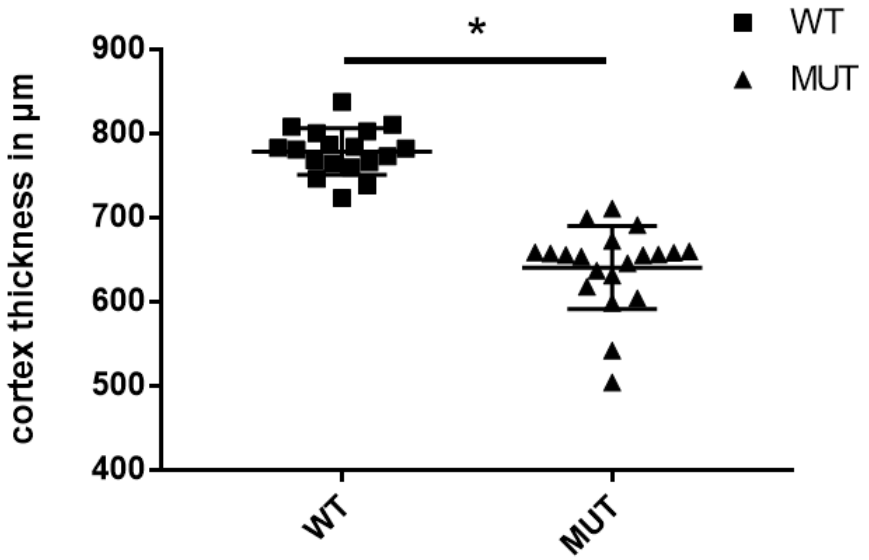

Figure 61 Comparison of all measured E18.5 Reelin-Cre-CB1 WT (left bar) and Reelin-Cre-CB1 KO (right bar) mice.
The cortical thickness of Reelin-Cre-CB1 KO mouse cortex was significantly reduced when compared to Reelin-Cre-CB1 WT. MUT: 640.3 ± 11, n=20; WT 778.3 ± 6.5, n=18; *$p < 0.02$. Results are displayed as means ±SD.

Table 26 Mean results for measurement of cortical thickness of E18.5 Reelin-Cre-CB1 KO mouse cortex compared to Reelin-Cre-CB1 wt littermates in in µm ± SD and the according number of samples as N.

	MUT (mean in µm ± SD)	Number of samples	WT (mean in µm ± SD)	Number of samples
YD54	638 (± 52)	N=16	874 (± 58)	N= 18
YB07	702 (± 30)	N=12	797 (± 55)	N= 15
XY71	615 (± 71)	N=20	697 (± 27)	N=14
YD55	711 (± 44)	N=11	925 (± 78)	N=6
XP39	636 (± 58)	N=20	711 (± 38)	N=22

3.4.3 Cortex layer analysis

As the cortical thickness in Reelin-Cre-CB1 KO mice is visibly affected, the next question to address was, if CB1 receptor signaling in Cajal-Retzius cells may have a selective function in the differentiation of neuronal populations of the different cortex layers. During cortical neurogenesis, neurons are produced by neural stem cells and then migrate long distances to their final destinations. To form the cerebral cortex, neurons born in the ventricular zone migrate radially to form the cortical plate (Rakic, 2009). For this reason, the cortical differentiation was evaluated at different sectional bins in the dorsal cortex. To characterize possible structural changes in migration behavior of developing cells in brains where CB1 is missing in Cajal-Retzius cells, Reelin-Cre-CB1 WT and Reelin-Cre-CB1 MUT E18.5 mouse cortex sections were immunostained for a panel of layer-specific markers (Fig. 62). Tbr1 is a transcription factor gene of the T box family that promotes deep-layer specification and cortico-thalamic neuron projections and is expressed after cortical progenitors begin to differentiate (Han et al., 2011; Hevner et al., 2001). Tbr1 is expressed in early-born neurons of the preplate (including CR cells) and layer VI (Bulfone et al., 1995). Satb2 is a cell marker for upper-layer neurons in layer IV-II (Britanova et al., 2008) whereas Ctip2 labels early born layer V and VI neurons (Molyneaux et al., 2007), which are predominantly corticospinal motor neurons.

Other markers for further investigations could be Tbr2 as basal progenitor marker in the subventricular zone, Pax6 as marker for radial glia progenitors within the ventricular zone.

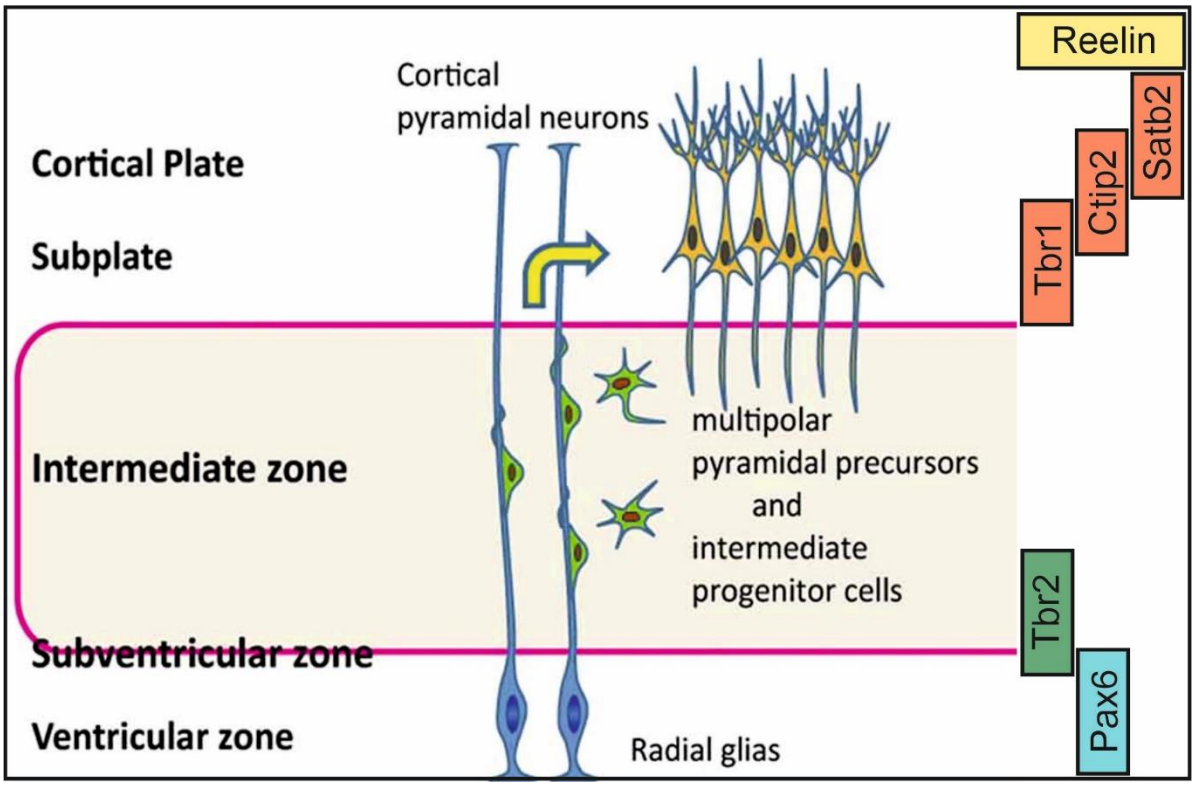

Figure 62 Cortex layer markers overview.
The figure gives an overview of the different layer zones (ventricular zone, subventricular zone, intermediate zone, subplate and cortical plate) and the cell types found in the particular zone. On the right the used markers for each zone was included: Reelin: CR cells in marginal zone, Satb2: upper-layer neurons, Ctip2: early born layer V and VI neurons, Tbr1: deep layer neurons, Tbr2: basal progenitors, Pax6: radial glia progenitors and proliferating cells in ventricular zone (Figure adapted from (Cánovas et al., 2015)

Quantification of the amount and the distribution of cells within a defined part of the dorsal cortex was performed by a custom developed workflow that utilizes multiple image analysis software "ilastik" (version 1.4.0b15)(Berg et al., 2019), Fiji (version 1.53c) (Schindelin et al., 2012) and Matlab™(version R2017b). The ilastik software uses supervised machine learning based random forest classifier and was used for cell segmentation and classification of Satb2 and Ctip2 positive cells. After user based training of the classifier for both segmentation and classification, the segmentation and classification tasks for all images were performed by running ilastik via a Fiji script.

The following analysis workflow was set up as follows:

1. The raw single tile images were first stitched using the Grid/Collection stitching tool (Plugin for Fiji) (Hörl et al., 2019).
2. Ctip2 and Satb2 stained cells from cortical sections were first segmented by using the ilastik "pixel classification" module to create a pixel prediction map between cells and background. The pixel classifier was trained by manually annotating "background" and "cell" class pixels. The trained classifier could then estimate the probability for each pixel to which semantic

classes it belongs. In the next step, the resulting pixel prediction map was subsequently segmented in Fiji with a threshold set to 50% probability, filtered with median filter (radius 2 px). Finally, any touching cells were split by applying watershed.

3. The segmented cells were then loaded back to ilastik for cell classification. The "object classification" module was used to classify "all cells"-blue (DAPI stained), "green" positive (Satb2 stained), "Red" positive (Ctip2 stained) and "Red and Green" positive (Satb2 and Ctip2 colocalizing) cells (Fig. 63 B, B'). The classifier was trained with 13 images and more than 30 cells per class were annotated manually. The position (x and y coordinates) of each classified cell was then extracted in the downstream analysis in Fiji.
4. To determine the spatial distribution of the cells in the dorsal cortex, the edge of the cortex needed to be detected accurately. This could be accomplished by segmenting the whole cortex using the nuclei channel. The segmentation could be automated by scripting the "magic wand" selection tool in Fiji, as the cortical edge was always on the left side of the image. With the "magic wand" tool the dark background area was selected and a binary mask (background vs. cell layer) was generated. Subsequently the Euclidean distance map (EDM) was generated for the brain area. This way it was possible to take the curving of the cortex into account and have defined curved layers. Due to variability of the shape and size of the background area, the automated script did not perform well for all the images. Thus all the generated masks were visually inspected and manually segmented if necessary.
5. The subsequent analysis was performed in custom developed Matlab script. The distance of a cell from the cortical edge was acquired from its coordinate in the EDM. The longest cell distances provide also information of the width of the brain section. To allow comparison of relative distances, the normalization was performed as follows: 0% = average of the shortest 10% distances. 100% = average of 10% of the longest distances (the other edge of the brain slice). With the data, we then could analyze the distribution of red and green cells within 11 equally distributed defined cortical bins and quantify the migration behavior of WT and MUT. To normalize for the unequal amount of cells per section, the number of cells per bin was converted into the percentage of cells per bin/ total amount of cells.

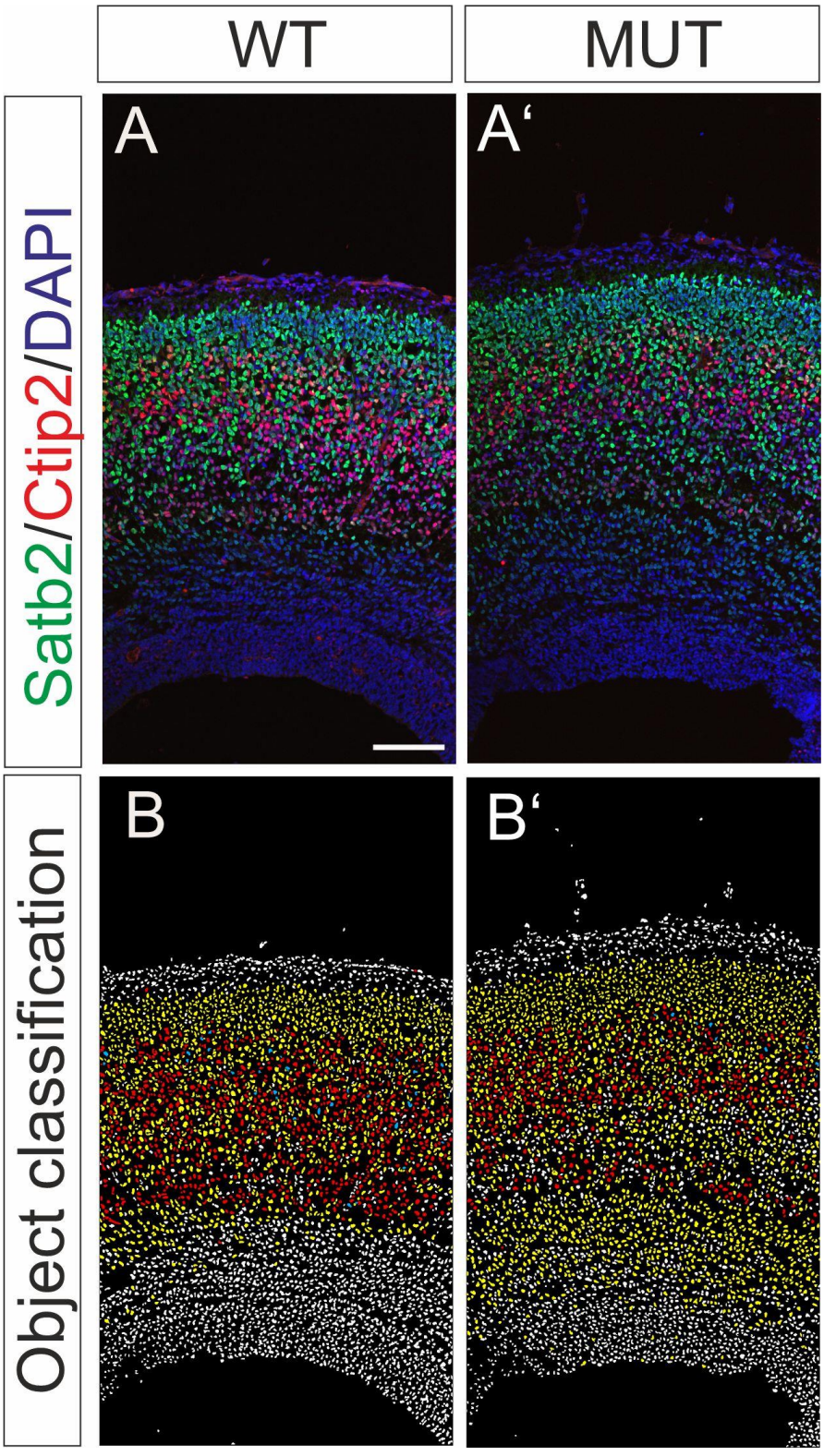

Figure 63 Visual object classification of E18.5 mouse pallium with classification into four semantic groups from Reelin-Cre-CB1 WT (left side) and Reelin-Cre-CB1 KO (right side) littermates.
A) Merged, unprocessed Spinning disc microscope pictures of Satb2 (green) and Ctip2 (red) immunostained cortical sections. Counterstaining was performed with DAPI (blue). B) Object classified pictures of A and A’ with division into 4 different groups: white: all cells, yellow: $Satb2^+$ cells, red: $Ctip2^+$ cells and blue: $Satb2^+$ and $Ctip2^+$ cells. Scale bar 100 µm.

The analysis was started with investigations on the impact of CB1 deletion in Cajal-Retzius cells in the development of $Satb2^+$ and $Ctip2^+$ neuronal cell populations. In total 5 different litters with 61 microscope pictures for wild-type and 26 microscope pictures for mutant mice were analyzed. In WT, most $Satb2^+$ cells are located from layer 2 to 4. A smaller number of $Satb2^+$ cells were present in layer 5 and layer 6, layers which are normally defined by an immune reactivity for Tbr1 and Ctip2. In zones with active proliferation, like the SVZ and the subjacent VZ, no $Satb2^+$-cells were detected (no expression by cortical neurons before migration) (Fig. 64, A and A'). Additionally, a little cexpression between Ctip2 and Satb2 could be observed (Fig. 63B). In mutant mice, this pattern did not change drastically but the distribution of neurons that express the upper-layer neuronal marker Satb2 was affected and in particular, significantly more Satb2 positive cells migrated into the uppermost layer in Reelin-Cre-CB1 KO ($P< 0.001$) (Fig. 64C).

Ctip2 is strongly expressed by developing layer 5 and 6 neurons in both WT and MUT (Fig. 64B and B'. Counting of 11 different bins of WT and MUT mice revealed significantly more Ctip2-positive cells in upper-layer bins in MUT mice in bin 0.2 ($P< 0.01$) (Fig. 64D). Deep layers in MUT tend to have fewer Ctip2 positive cells compared to WT, but this was not significant. For statistical analysis, a multiple t-test for each bin was performed and statistical significance was determined using the Bonferroni-Dunn method with alpha=0.05 as multiple comparison correction.

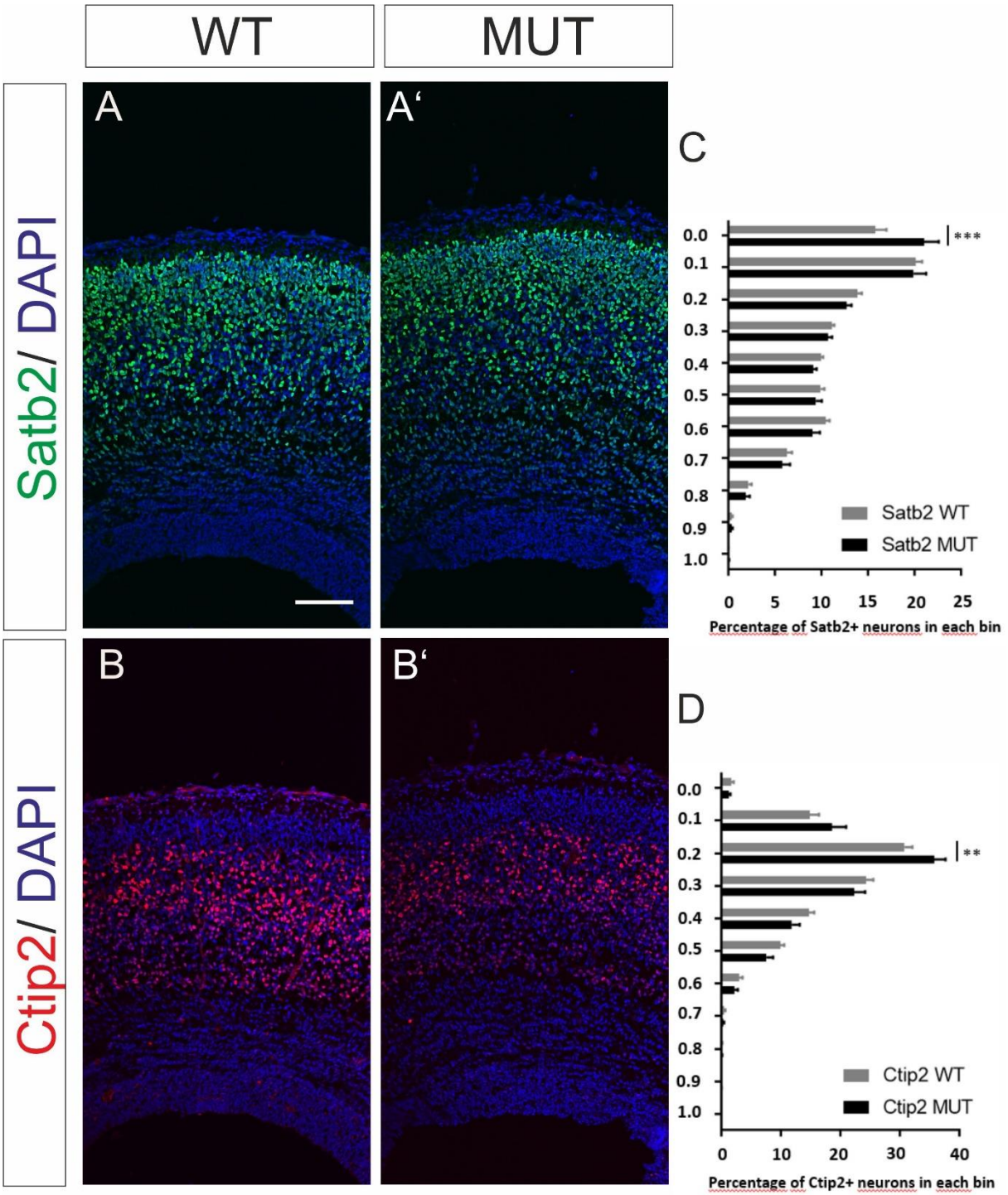

Figure 64 Deficiency of CB1 in Reelin-expressing neurons leads to alterations of cortical neuronal distribution in Reelin-Cre-CB1 KO mice.

Immunostaining was performed on coronal sections of E18.5 Reelin-Cre-CB1 wt or Reelin-Cre-CB1 KO mouse brains using anti-Satb2 (green) or anti-Ctip2 (red). Counterstaining was performed with DAPI (blue). Scale bar 100 µm. (A and A’) Coronal sections of E18.5 Reelin-Cre-CB1 wt (A) or KO (A’) cortex were stained with the neuronal layer-specific marker Satb2 (layers II to V) and with DAPI. (B and B’) Coronal sections of E18.5 Reelin-Cre-CB1 wt (B) or KO (B’) neocortex were stained with the neuronal layer-specific marker Ctip2 (layers V to VI) and with DAPI. (C) Scatter plot vertical graph represent percentages of Satb2-positive neurons per bin to total Satb2-positive cells. (D) Scatter plot vertical graph represent percentages of Ctip2-positive neurons per bin to total Ctip2-positive cells. Error bars show mean ± SEM * $P < 0.05$; **, $P < 0.01$; ***, $P < 0.001$.

3.4.4 Gain-of-function

Another possibility to uncover the function of a specific gene is to overexpress it. For overexpression, a possible method is to inject a CB1 floxed stop vector (Fig. 65) via *in utero* electroporation into the brain of mouse embryos.

The CB1 floxed stop vector was cloned starting from existing vectors in the lab, into an expression vector (see 2.6) and the correct sequence of the CB1 expression vector was confirmed via Sanger sequencing.

Figure 65 pCAGIG vector containing a CB1 expression cassette and a floxed Stop-site for ubiquitous CB1 expression during the presence of Cre-recombinase.

To test the vector function, the CB1 floxed stop vector was transfected with lipofectamine into HEK293 cells along with a Cre recombinase-expressing vector (#154 pAM-CAG-HA-NLS-Cre-WPRE-bGH). The pCAGIG vector will express CB1 in presence of a Cre recombinase on a bicistronic mRNA also encoding IRES (internal ribosomal entry site)-GFP. A CB1 expressing vector (#M186 pBS-CB1) was used as a positive control and the empty backbone of pCAGIG was used as a negative control. Afterward the protein lysate was harvested and used for Western blot. The Western blot confirmed the proper function of the CB1 floxed stop vector. A clear CB1 protein band was visible along with the HA Tag of the backbone vector. Whereas in the negative control only a HA Tag was visible confirming the successful transfection of the empty vector. The CB1 expression in double transfected cells proved the function of the CB1 floxed stop vector (Fig. 66).

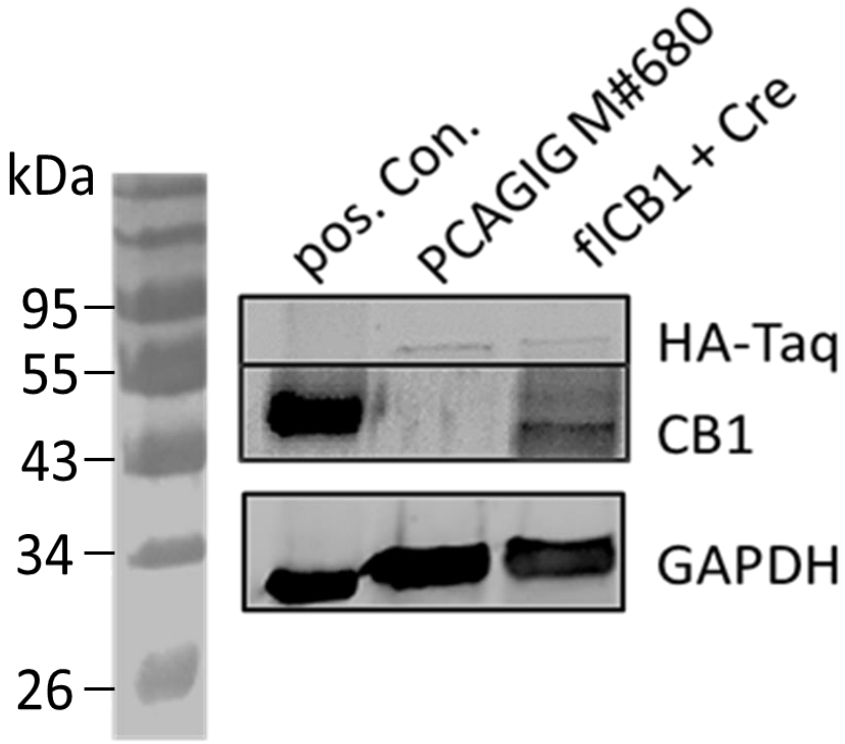

Figure 66 Western blot analysis of HEK293 samples after transfection with different CB1 expression vectors. The relative expression levels of CB1 were quantified by western blot analysis. A CB1-expressing vector was chosen as a positive control. The empty pCAGIG vector showed no CB1 expression but HA-Tag expression to verify a successful transfection. The cloned CB1 vector, which was transfected along with a Cre-expressing vector leads to CB1 expression in HEK293 cells.

4 Discussion

4.1 Establishing a Reelin-Cre mouse line

In this study, a Reelin-Cre mouse line could successfully be established to further unravel the possible impact of expressed proteins in the Reelin-expressing Cajal-Retzius cell population and on proper brain development. Through the successful application of the CRISPR/Cas9 method, we were able to integrate a Cre-recombinase expression cassette into the Reelin locus without disturbing proper Reelin function. With this mutant mouse, it is now possible to modulate protein expression within the Reelin-expressing cell population and further study specific protein function within this cell type and its impact on cortex development.

During the past decades, numerous studies have shown that prenatal Reelin controls neuronal radial migration and proper positioning in cortical layers in the developing cortex and hippocampus (Rakic & Caviness, 1995b). Although Reelin-expressing Cajal-Retzius cells disappear after birth, interneurons in the postnatal brain start to express Reelin (Pesold et al., 1998), which then promotes neuronal maturation, synaptic formation, and plasticity. Unraveling the mechanisms of neuronal migration has been of greatest interest because dysregulated migration has been linked to behavioral dysfunction similar to schizophrenia, modeled by animal studies involving heterozygous *reeler* mice (Costa et al., 2002). Furthermore, recent human genetic studies identify heterozygous Reelin mutations in lateral temporal epilepsy (Dazzo et al., 2015) or autism (De Rubeis et al., 2014). Thus, besides Reelin function itself, it is important to also study the function of putative Reelin influencing proteins.

For the establishment of a Reelin-Cre mouse line with the help of CRISPR/Cas9 and a HDR construct, all critical steps could be set up in the lab. As a first step, guide RNAs were designed and tested on functionality in neuronal cell lines. With this knowledge, we could continue to test the guide RNAs *in vivo* by injecting the ctRNP complex into mouse zygotes and analyze their function in blastocysts first with the T7 EN1 assay. Afterward, we continued with injections together with the HDR knock-in construct for creating progeny carrying the knock-in. The correct homologous recombination was verified by genotyping and sequencing. To test the proper function of the inserted Cre-recombinase, the mouse was crossed with a Rosa26-floxed-stop-YFP reporter mouse line and immunostainings against Reelin, Cre, and YFP were performed. Finally, the functioning Reelin-Cre mouse line could be crossed with a CB1 floxed line to specifically knock-out the CB1 function in Reelin-expressing cells to get insight on the possible interaction of both proteins during cortical development.

4.1.1 Coexpression of CB1 and Reelin mRNA indicates an interaction of both proteins during neuronal migration and positioning

In preliminary experiments, we saw that Reelin and CB1 mRNA coexpressed according to the analyzed cortical region and prenatal age. This was also observed in other studies (Vitalis et al., 2008), but was never quantified in detail. The results showed that the number of Reelin expressing cells increased by time until the age of E13.5 and so did the number of Reelin-/CB1-coexpressing cells. This is sound to literature as E12.5/E13.5 is the age where most structural processes happen in the developing mouse brain and most migrating post-mitotic neurons express CB1 in the preplate including tangentially migrating ones (Saez et al., 2014). At the age of E14.5, the Reelin-positive cell number decreases as the cortex expands very fast and so does the number of cells which then leads to a dilution of Reelin-positive cells. It was found that at E16.5 CB1 is expressed in the entire cortical plate and the hippocampus (Vitalis et al., 2008) which is mainly composed of the perikarya of glutamatergic projection neurons at this age (Rakic, 2006). After that age, the CB1 amount in the MZ slowly decreases until the development of the cortex is finished (Harkany et al., 2007). The high amount of Reelin and CB1 coexpressing cells with up to 79 %, lead to the proposition that Reelin and CB1 may share functions within Cajal-Retzius cells. So far, it is known that Reelin regulates neuronal migration and positioning during corticogenesis in the embryo and regulates maturation of neurons by promoting dendritic growth and spinogenesis in adult hippocampal neurons through the VLDLR/ ApoER2-Dab1 pathway (Niu et al., 2004, 2008), whereas CB1 in glutamatergic neurons is required for appropriate pyramidal neuron migration in the developing cortex (Díaz-Alonso et al., 2017) and is also expressed by a subpopulation of Reelin-secreting Cajal-Retzius cells (Vitalis et al., 2008, our results).

Strikingly, CB1 and Reelin are using the same proteins (e.g., cofilin) and enzymes (e.g., PI3K, GSK3beta) for similar mechanisms, such as cell adhesion and the formation of the cytoskeleton. The consideration of these similar signalling pathways already gives a greater indication of a possible shared function within cortex development. One example is the functional regulation of small GTP-binding proteins (e.g., Rho GTPase, Cdc42) through Reelin which is known to control neuronal cell morphology (Leemhuis et al., 2010) and induces activation of Rap1 and upregulation of N-cadherin in neuronal cell migration (Jossin and Cooper, 2011). CB1 activation can also modulate axonal morphology through multiple co-existing pathways (e.g. RhoGTPases,(Berghuis et al., 2007; Nithipatikom et al., 2012)). Furthermore, Reelin-dependent dendrite outgrowth requires transactivation of heterotrimeric $G_{i/o}$-protein, which is mediated by the non-receptor type tyrosine kinase Src in cultured hippocampal neurons (Cho et al., 2015). Another possibility of how CB1 can transmit signals during development could be an intrinsic “eCB tone” which is for example used by pyramidal cells to initiate their axonal polarization and neurochemical differentiation (Mulder et al., 2008). Newer studies also

found that CB1 promotes microtubule stabilization through degradation of Superior Cervical Ganglion 10 (SCG10)/stathmin2, a microtubule binding protein, in axons and so affects neuronal circuits during development (Tortoriello et al., 2014). But still, there are many open questions about the function of CB1 not only in cortical development in general but especially on its function on Reelin-signaling-sending cells.

Although a visual counting showed a high amount of colocalization of Reelin and CB1 mRNA, it was not possible to prove physical interaction between the two factors within one cell. Visual counting, but also statistical methods of pixel intensity correlation are prone to deliver false-positive results. By combining the pixel-intensity correlation with object recognition-based colocalization to calculate an object corrected Pearson coefficient, the colocalization analysis could be improved. But still, the ability to determine colocalization in a confocal microscope is limited by the resolution of the optical system and the wavelength of the light used to illuminate the section. Misalignment of the microscope, refractive index fluctuations and optical aberrations can drop the theoretical resolution of approximately 200 nm to a value between 400 and 600 nm.

To elucidate the function of CB1 in the Reelin-expressing cells, a new mouse model was needed to genetically target the whole population of this specific cell type. As Reelin is expressed in different subtypes of Cajal-Retzius cells with different origins and various expressions of different markers, researchers have not succeeded in targeting the whole Reelin-cell population (Hanashima et al., 2007) although, Cre mouse lines to study the molecular and cellular mechanisms of CR cells exist (Gu et al., 2008). Tracing of Reelin-expressing Cajal-Retzius cells is challenging as these cells begin to die due to apoptosis after birth and only a small percentage of CR neurons survive from P3 into adulthood (Chowdhury et al., 2010). To overcome these problems, recombinase-based genetic approach is an option for successfully generating cell-specific depletion and for labeling specific cell types (Loschko et al., 2016; Madisen et al., 2010, 2012, 2015).

4.1.2 Establishing a Reelin-Cre mouse line with the CRISPR/Cas9 system without disturbing Reelin protein function

In this study, we generated a Reelin-Cre mouse line for specific modifications of genes within the Reelin-expressing cell population when crossed with a loxP containing mouse line. As a first step, we used the CRISPR/Cas9 genome editing strategy to cause a double-strand break at a specific targeted part of Exon 65 in the Reelin gene. The double-strand break was subjected to a homology-directed repair process involving a HDR construct, containing a 2A cleavage site, the Cre-recombinase expres-

sion cassette along with a HA Tag and a nuclear localization signal. After the homologous recombination, the Cre-recombinase expression was under the control of the Reelin regulatory elements, and thus, is expressed in every Reelin-expressing cell.

The CRISPR/Cas9 system is a useful tool to facilitate the generation of DSB. Before the rise of the CRISPR/Cas9 technology, the generation of genetically modified organisms and especially the generation of targeted knock-in mice was laborious and time-consuming (zink-finger, TALEN, ES cells). In the present work, due to the missing experience in the application of the CRISPR/Cas9 methodology and the differing target efficiency among the single gRNA sequences, two possible crRNA molecules were chosen, both located in the region of the translational STOP codon of the Reelin gene. For the success of the experiment, it was crucial not to change the C-terminal region so the normal Reelin function will remain. The sgRNAs were chosen due to their high on-target efficiency and their low number of possible mismatching sites to the next similar sequences in the genome. Additionally, the existing similarities to other genomic sequences were mainly located in intron regions, were not next to the PAM and started with at least 3 mismatches to the guide sequence. Three or more total mismatches are expected to have a lower off-target probability than two of these mismatches in the seed region (Hsu et al., 2013b). For the selection of the sgRNAs and to test the approach in cell culture, we used the method paper published by Ran et al in 2013.

As the CRISPR/Cas9 method had to be established in our lab, we had many fields to optimize. We started with functional testing in neuronal cell lines to prove the function of the chosen sgRNAs.

4.1.3 T7 Endonuclease assay showed full function of both sgRNAs and a good on-target efficiency

The T7 endonuclease assay was chosen as a proof of principle of the chosen sgRNAs in cell culture in general and to detect induced in/del mutations or estimate the target efficiency. T7 endonuclease 1 is a structural-selective enzyme that can detect structural inconsistency in heteroduplex DNA (Mashal et al., 1995) and an assay with T7 endonuclease recognizes Watson-Crick base pair mismatches, which are caused by possible insertions or deletions through NHEJ and cuts the DNA at this mismatch site. Agarose-gel electrophoresis detects the cut DNA fragments. The T7EN1 assay revealed that both guide RNAs worked as expected and served as the first estimation of the efficiency of on target specificity in cell culture.

Nevertheless, the assay can not give an absolute score for efficiency as homoduplexes of modified strands can occur to a certain amount, which are then not recognized by T7EN1. The assay's performance can also be impacted by the length and identity of base pair mismatches, the flanking

sequence, secondary structures and relative abundance of mutant sequence (Mashal et al., 1995; Picksley et al., 1990; Vouillot et al., 2015). Furthermore, the ability of T7EN1 to cleave different structures differs, as deletions are preferred over single base substitutions (Judo et al., 1998; Mashal et al., 1995) and even homoduplex DNA can be cleaved to a certain extent if too much T7EN1 enzyme was used.

4.1.4 The 2A-HA-NLS-Cre-recombinase construct for HDR was successfully cloned

The 2A-HA-NLS-Cre recombinase construct was cloned with the help of already existing vectors from our lab. The final targeting construct contains two PCR amplified homology arms flanking the 2A-HA-NLS-Cre-recombinase sequence. To prevent a continued cutting of guided Cas9, the PAM sequence needed to be changed. To make it more difficult for the sgRNA to bind the targeted site after HDR, also silent mutations within the sequence for the guide RNA should have been added. The crucial changes in the PAM sequence worked fine for both gRNAs. The silent mutations in sgRNA2 could be inserted but for sgRNA1 the change was not present in the modified gene locus. The reason for this can be that two neighboring bases were used.

After the successful implementation of the protocol of Ran et al. on cell culture and the verification that the chosen gRNAs are working, we changed the protocol to EASI-CRISPR (Efficient additions with ssDNA inters-CRISPR) protocol published by the group of Quadros (Miura et al., 2018). Quadros et al. and Wang et al. were the first ones who successfully used ssDNA instead of dsDNA as a large knock-in allele of up to 2 kb (Quadros et al., 2017; Wang et al., 2013). The ssDNA can either be chemically synthesized or, as we did, generated via strandase reaction. The donor template was amplified using primers that include one phosphorylated oligodeoxynucleotide followed by selective digestion of the phosphorylated strand of the dsDNA by nucleases. The usage of ssDNA overcomes the disadvantage of the higher possibility of random integration of dsDNA (Sonoda et al., 2006) and results in higher recombination rates compared to dsDNA (Inui et al., 2014; Wang et al., 2013). The usage of ssDNA also allows more extended homology arms in the donor DNA. The transgenes could have been flanked by shorter homology arms (75-100 bp), which seemed to be sufficient for the target integration events (Miura et al., 2015, 2018; Quadros et al., 2017). Nevertheless, this approach was also successful with much longer arms (477 bp and 420 bp). Additionally, optimized Alt-R™ CRISPR RNAs from idtDNA (Integrated DNA Technologies, Coralville, Iowa) were used, because the shortening of the crRNA (from 42 nt to 36 nt) and the tracrRNA (from 89 nt to 67 nt) significantly increases the potency of the triggers for gene editing.

4.1.5 Blastocyst analysis for *in vivo* sgRNA tests

To verify that sgRNA guided Cas9 is working properly, the sgRNA-Cas9 complex was injected into mouse zygotes by Dr. Eshkind and his group from the mouse transgenic facility of the TARC, Mainz. The injected zygotes could develop into blastocysts and their DNA was harvested, to perform T7 Endonuclease assay again. When performing the T7EN1 assay on single blastocysts, the DNA content is very small, so only around 5 PCR reactions can be performed per blastocysts. This makes it difficult to examine different areas for possible off-target identification. Furthermore, the small content of DNA requires a nested PCR to amplify a sufficient amount of DNA to perform the assay. The T7EN1 assay on CRISPR/Cas9 microinjected blastocysts showed a high mutation efficiency of both sgRNAs. 24 out of 33 (72%) sgRNA1 injected blastocysts showed indels of which 9 blastocysts showed only the expected band (27%). For sgRNA2 injected blastocysts 19 out of 29 (65%) showed indels and 10 out of 29 (34%) showed the expected bands. Taken these results together, the overall performance of the Cas9 cleavage guided by the designed sgRNAs was good and comparable to other results (57–100%, Wang et al., 2013). This showed that the T7EN1 assay is also helpful to support animal welfare as it helps to reduce the numbers of mice used for this experiment as the efficiency of the sgRNAs can already be tested in 3 day old blastocysts.

The high variety of efficiency may depend on the cleavage efficiency of the sgRNA which influenced the amount of caused DSB. Also, the chromatin structure of the target can prevent the Cas9 complex from cutting at the targeted site. The high amount of additional bands, seen in blastocysts was unexpected but not unusual, as NHEJ can also cause greater in/del regions (Sakurai et al., 2014).

Targeted next-generation sequencing (NGS) could be an alternative to the T7EN1 assay and could serve as an optional tool for assaying edited pools and clones. NGS can estimate the indel size, the frequency and the sequence identity (Sentmanat et al., 2018), it enables relatively cheap high throughput analysis but needs expensive machines and knowledge to use (Cho et al., 2014; Hsu et al., 2013).

4.1.6 Offspring analysis showed successful integration of HDR construct

After verification that sgRNA guided Cas9 was working properly, we could perform the final experiment by injecting the sgRNA-Cas9 complex along with the HDR construct directly into zygotes. For the generation of the Reelin-Cre mouse, a knock-in strategy was used to place our 2A-HA-NLS-Cre construct under the control of the endogenous Reelin promotor. To prevent disturbance of the endogenous Reelin expression, the knock-in cassette was targeted directly in front of the translational stop codon in front of the 3’ UTR in exon 65 of the Reelin gene. During the translation of

the Reelin gene, the ribosome continues to translate the Cre-recombinase gene and so produces discrete proteins without disturbing the endogenous gene. The advantage of the 2A cleaving site compared to IRES is that the downstream ORF can be expressed at a level comparable to the upstream ORF. In our case, this is important to ensure a high level of Cre-recombinase expression as its amount must be sufficient to knock-out CB1 expression completely in Cre-expressing cells. The disadvantage of 2A is that possible undesired biological effects can occur due to additional peptide residues left behind on either the upstream or the downstream ORF.

The generation of Cre-driver mouse lines was always very laborious and time-consuming. The variety of approaches ranges from random transgenic insertion of Cre cDNA driven by a short promotor to gene-targeting-based knock-in into a defined locus (Deussing, 2013; Murray et al., 2012). The classic approach relies on homology-directed insertion of targeting cassettes into pre-defined endogenous loci of embryonic stem cells. This approach always showed very low targeting efficiency and was time-consuming and expensive (Gerlai, 1996). Even gene editing with engineered nucleases, such as zinc-finger nucleases (ZFNs) and transcription activator-like effector nucleases (TALENs), which can induce specific DSBs at specific loci, are difficult to use. They use protein motifs, which are difficult to engineer, for DNA sequence recognition. For this reason, the most recent editing tool CRISPR/Cas9 was the favored tool as it allows precisely targeted modifications in a short time (Heidenreich & Zhang, 2016). The CRISPR/Cas9 reagents, consisting of Cas9 nuclease/mRNA and a specifically designed guide RNA can directly be injected (along with an HDR-construct) into mouse zygotes. After injection, the DNA is cleaved precisely at the genomic locus of interest and the resulting DSB can be either repaired by NHEJ or via HDR. HDR enables the introduction of the insertions of DNA donor templates. The ongoing improvement of the efficiency and the specificity of the system makes CRISPR/Cas9 the method of choice for creating new mouse models and understanding complex neuronal networks.

For the final experiment, 1120 zygotes were injected with sgRNA1 of which 550 (49%) could be transferred into 25 foster mothers. For sgRNA2 we obtained 840 of which 389 (46%) were transferred into 17 foster mothers. In total, we obtained 85 sgRNA1 injected pups (15.45%) and 60 sgRNA2 injected pups (15.2%) for further analysis. When comparing the survival rates of zygotes after post-injection (75-95%) and the birth rate (30% on average) mentioned in Doe et al. (Doe et al., 2018), the rates in our experiment were a bit lower but still competing. One possibility for lower survival and birth rates could be that the CRISPR modification may cause developmental defects which will lead to the embryo's abortion.

For the analysis of the correct insertion to the Reelin locus, genotyping by PCR with specific primers was chosen. Insert-specific primers were combined with primers outside the modified region and the homology arm regions in an overlapping manner to cover the entire knock-in sequences as well as ensure the correct integration. For sgRNA1 injected mice, we obtained 3 positive founders in total. PCR products of all positive founders were sequenced to confirm that the insert does not contain mutations. It was also crucial to sequence the progeny of the founders, in order to verify the germline transmission of the Cre-insert. However, with this method, it was not possible to exclude off-target effects. To show off-targets or unintended Cre integration, a southern blot should have been performed with specific restriction sites in close proximity to the target regions and Cre as a probe. Unfortunately, this method was not established anymore in the lab. Alternatively, whole-genome sequencing of the founder genome could have been done before the mouse was backcrossed in the C57BL/6 background. One problem of the used genotyping approach was that multiple bands occur when using primers covering the whole insert length. In wild-type animals, a band with the size of 761 bp was amplified. Heterozygous animals with a successful insertion of the construct were supposed to show a 1931 bp and the 761 bp wt band, but also two unexpected additional bands with a size of 1500 bp and 2300 bp appeared. Sequencing of the additional bands gave no satisfactory result, as both unexpected bands showed inferring sequences of the WT and the MUT sequence. When cloning the unexpected bands into the TOPO-cloning vector the results showed a correct 2A-HA-NLS-Cre-sequence for the formerly 2300 bp sized product and for the 1500 bp sized gel band we only could amplify wild-type constructs. An easy ligation experiment with wild-type and homozygous Reelin-Cre mouse genome DNA was performed (see supplementary). While the two amplified genomic DNA constructs alone gave single bands on an agarose gel, they gave additional bands when reannealed in a religation reaction. This result can be explained by the unintended coupling of the WT (761 bp) product to a way bigger mutant (1931 bp) product, as they share the same sequence within the homology arm sequence. Therefore, the mutant product can anneal with one or two wild-type PCR products and form different isoforms differing in their size. The reason why TOPO cloning either just gave WT or MUT sequence could be that the products resulting from coupling of WT and MUT PCR product are not stable enough to be correctly cloned into the TOPO-vector.

When compared to other papers (e.g., Quadros et al., 2017) the knock-in efficiency via CRISPR/Cas9 mediated HDR in mammalian cells was relatively low (0.33%) and can be explained with two possible effects. First, the non-homologous end-joining pathway is always competing with HDR (Sargent et al., 1997). For targeted integration due to an HDR event, the donor DNA needs to be proximal to the DSB. Otherwise, the DNA ends can rejoin via NHEJ and may lead to insertion/deletions (indels) at the

break junctions. One advantage of our chosen method was that HDR-mediated knock-in is more effective in dividing cells, as they are still in late S/G2 phase (Liu et al., 2017; Pawelczak et al., 2018). Another explanation for the low efficiency could be because the full potential of ssDNA donors was not used since we did not change the homology arm length to shorter homology arms. The total length of 200 bp of one homology arm may have been sufficient according to Quadros et al. In our experiment 450 bp per homology arm was used to get the highest homology possible. But it's also known that knock-in efficiency and therefore HDR strongly depends on the targeted gene and varies widely from locus to locus (Ran et al., 2013; Saleh-Gohari & Helleday, 2004; Yang et al., 2016) as Quadros et al. reaches knock-in efficiencies ranging from 8.5 to 100%. A new genome-editing tool (CUNE, O'Brien et al., 2019) could have helped to enhance HDR efficiency as it calculates the expected efficiency in silico and recommends the best targeting sites.

4.1.7 sgRNA2 injected founders did not show complete integration of the HDR construct

PCR genotyping of sgRNA2 injected animals with 6 different primers revealed three animals with several unexpected strong bands and also some expected bands (see Fig. 45; e.g., #355, primer pair 7.1 and 7.2, 689 bp). To uncover the identity of these bands, the PCR product of each band was sequenced via Sanger-Sequencing. The sequencing results revealed a fragmented insertion of the HDR construct which always starts within the cutting region of sgRNA2 and ends within the middle of the Cre-recombinase sequence. One possible explanation for this phenomenon could be further cleavage of the targeted DNA strand by the sgRNA2-guided Cas9 nuclease as the sequencing results always showed a break at the cut site of sgRNA2. It seems that the introduction of silent mutations within the sgRNA2 sequence of the HDR construct was not sufficient to prevent a cleavage of sgRNA2-guided Cas9 nuclease. The second cut within the Cre-recombinase sequence is hard to explain as there is no homology for sgRNA2 sequence within the Cre-sequence. For some reason it could be that further cleavage of the sgRNA2 target site results in a big deletion of about 892 bp and 1047 bp respectively. To prevent further cleavage of Cas9 unwanted editing could have been suppressed with different methods that were just recently invented. For example the co-administration of catalytically inactivating truncated gRNAs which suppress unwanted CRISPR-Cas9 editing (Rose et al., 2020).

4.1.8 Crossing reelin-cre mouse line with a GFP reporter mouse line verifies proper function of Cre-expression under the control the reelin promotor

The aim of this study was the development of a Reelin-Cre mouse line with the expression of the Cre-recombinase restricted to a particular cell type as defined by the Reelin promotor. After identifying 3 positive founders via genotyping and sequencing, the proper function of Cre and Reelin had to be

evaluated. First, the protein expression pattern of Cre and Reelin was analyzed by immunostaining with specific antibodies. The Cre expression within the developing cortex corresponded with Reelin expression and was restricted to the marginal zone; within the developing hippocampus we only observed Cre expression in the dentate gyrus. As expected, there was no Cre expression apart from that in Reelin-expressing cells. When breeding homozygous Reelin-Cre mice, the Reelin expression was not impaired, assuming that Reelin function is properly working although no fuctional assays were done yet with homozygous animals. To check the proper function of the Cre-recombinase, the Reelin-Cre mouse line was crossed with a ROSA26-floxed-stop-YFP reporter mouse line. The YFP expression pattern appeared almost identical compared to the endogenous Reelin expression pattern. However, still, some Reelin-expressing cells did not show YFP expression. The reason for this may be the ROSA26 promoter. Even if ROSA26 is ubiquitously expressed in most cells, the transgene expression (even under the CAG promotor) can be lower when the transgene is adjacent to, and in the same orientation, as the endogenous promotor (Strathdee et al., 2006). This may cause a missing YFP expression in some Cre-expressing cells (see Fig. 56).

4.1.9 Loss of function studies of CB1 in Reelin-Cre mice to unravel the impact of CB1 and Reelin interaction on cortex development in embryonal mice

The CB1 receptor as a central component of eCB signaling (Heifets & Castillo, 2009) has a crucial role in embryonic neural development and maturation. During brain development CB1 is known to be involved in many different processes (refer to section in 4.1.1). During early brain development, CB1 allows the control of neural progenitor identity and pyramidal neuron generation through the activation of the mTORC1 (mammalian target of rapamycin complex1) pathway (Díaz-Alonso et al., 2015), regulates long-range axon projection (Argaw et al., 2011; Díaz-Alonso et al., 2012; Mulder et al., 2008) or is required for proper radial migration during cortical development (Díaz-Alonso et al., 2017). Cortex layer studies with CB1 depleted mice revealed that CB1 receptor inactivation leads to defective VZ/SVZ progenitor cell proliferation and axonal guidance alterations (Aguado, 2005.; Mulder et al., 2008), which will end in an impairment of long-range corticothalamic connectivity and disruption in cortex layer formation (Mulder et al., 2008; Wu et al., 2010). Furthermore, CB1 receptor is required for appropriate pyramidal neuron migration in the developing cortex (Díaz-Alonso et al., 2017). From embryonic day E10.5 on CB1 is present in Reelin-expressing Cajal-Retzius cells but its function within this cell type remains unknown.

To get insights into the developmental role of CB1 in Reelin cells, we used the Cre/loxP system to specifically target the Reelin expressing cell type. Therefore, we crossed the Reelin-Cre mouse line

with a CB1 floxed mouse line. The Reelin-dependent expression of Cre-recombinase leads to a removal of the CB1 coding sequence, which is flanked by loxP sites and therefore disrupts CB1 expression in Reelin-expressing cells. *In situ* hybridization stainings showed that no CB1 mRNA could be observed within Reelin-expressing cells in Reelin-Cre-CB1 KO animals. This proves that Reelin dependent Cre-recombinase expression was sufficient to knock-out CB1-expression in Reelin-secreting Cajal-Retzius cells.

As a first step, the general appearance of the cortex was examined, and it was found that cortical thickness was significantly affected in Reelin-Cre-CB1 KO mice. To see if this effect is based on impaired layer formation, different cortex layer-specific markers were tested on cortical brain tissue sections with immunohistochemical stainings. For cortex layer studies, we examined the expression of 7 proteins known as cortex layer markers (only data of Satb2 and Ctip2 stainings were shown). At first sight, we saw differences in the distribution of Satb2 and Ctip2 expressing cell population at E16.5 and E18.5. Thus, we focused on the analysis of Satb2 and Ctip2-expressing neurons and analyzed the distribution of these (migrating) neurons in the embryonic mouse cortex. It is known that CB1 receptor tunes the differentiation balance of deeper- and upper-layer cortical projection neurons and is coupled to the regulation of the Ctip2-Satb2 transcriptional regulatory code (Diaz-Alonso, 2012). Furthermore, CB1 deficient mice showed an altered neuronal differentiation as they show a delayed distribution of postmitotic Tbr1-positive neuroblasts (Díaz-Alonso et al., 2012). Therefore, the distribution of positive stained cells was counted along the vertical cortex axis and compared Reelin-Cre-CB1 WT animals to Reelin-Cre-CB1 KO animals. The results showed that in Reelin-Cre-CB1 KO mice, Satb2 as well as Ctip2 positive upcoming cells migrate further into the upper pallium when compared to Reelin-Cre-CB1 WT mice. Satb2 has an inhibitory effect on Ctip2 (Alcamo et al., 2008; Britanova et al., 2008) and the observed results show a tendency for more Satb2 positive neurons and fewer Ctip2 positive neurons in Reelin-Cre-CB1 KO mice, which was not significant but was already seen when knocking-out CB1 expression in glutamatergic pyramidal neurons (Diaz-Alonso et al., 2012). As CB1 was knocked-out in Cajal-Retzius cells, one can assume that there must be an influence of CB1 on Reelin-dependent pathways in order to cause an overmigration of cells within the cortical layers. In this case, loss of CB1 in Reelin-positive cells might influence the functionality of Reelin (e.g. its secretion) or other factors which regulate the stop of migration or influence the terminal somal translocation which takes place in the Reelin-rich MZ and requires detachment from radial glia followed by extension and stabilization of leading processes. Newest findings suggest that the recent models which explain Reelin function during cortical development might only partly explain the effects of Reelin on migrating neurons. As Reelin does not induce ectopic terminal somal translocation before neurons reach the top of the CP (Jossin et al., 2004; Magdaleno et al., 2002) the data

give cause for doubts that Reelin functions as an attractant cue (Gilmore & Herrup, 2000), a stop signal (Dulabon et al., 2000; Jossin, 2004) or as a signal that can induce a switch in migration type (Borrell et al., 2006; Cooper, 2008; Nadarajah et al., 2001; Olson et al., 2006; Sekine et al., 2011). Jossin suspects that the reasons for these results could be the cooperative acting of Reelin with another signal localized at the top pf the CP or that Reelin could be a permissive signal which allows neurons to respond to another signal localized near the MZ (Jossin, 2020). These findings may explain the change in the Reelin signal when CB1 is missing in Reelin-expressing neurons as CB1 or a cue that is activated by CB1 is necessary for enabling neurons to respond to Reelin. However, our results can only give an indication on the actual function of CB1 within the Reelin-expressing cell type, as many more experiments must be carried out to get a clearer insight.

As a next step, to get a better understanding on how CB1 signaling influences the Reelin pathway further investigations on cortical layering and migration should be performed. First, it would have to be determined whether the migration is generally affected or if just neurons in upper layers are impaired in their migration. Another possible impact could be impairment on terminal translocation and maturation, so it would also be interesting to investigate whether differences in migration occur already at earlier embryonic stages. To examine other layers, Tbr1 would be used as a preplate marker, wisteria floribunda agglutinin (WFA) as layer 4-specific marker, Rorb as layer 6 marker and Pax6 as deep-layer marker. As also cortical thickness is affected in Reelin-Cre-CB1 MUT mice, it would be interesting to investigate in the influence of CB1 in Cajal-Retzius cells on cell proliferation. Therefore, it would be interesting to have a closer look at impairments in proliferation by performing birth labeling experiments with BrdU (5-bromo-2'-deoxyuridine) injections into pregnant mice at E10.5 or immunostainings with Ki67. To see whether secretion of Reelin is affected it would be interesting to measure Reelin protein concentration within the cortex via western blot.

The machine learning-based image analysis tool Ilastik was used to segment the objects of interest from immunolabeled brain tissue images. The tool allowed the analysis of different levels (e.g., 3 types of cells: all cells, Satb2 and Ctip2) and gave the position of every single cell as an output. It was easy to use, and the workflow could be integrated into other tools like FIJI or Matlab. Once the workflow was set up and the Ilastik program was trained with the input data, the program could homogenously analyze a huge dataset automatically. Although the method facilitates cell counting a lot, even this method has some limitations that should be considered before data retrieval. The most important thing is that the staining of all immunolabeled sections must be comparably good, the images must always be taken with the same settings, the same objective, and the same size as Ilastik always uses the size of an image as reference. Unfortunately, some settings had to be made manually

as it was not properly recognized by the used plug-in (e.g., selection of the brain surface) but with further improvement of the code, the analysis could have been performed automatically.

Taken together these findings, the newly generated Reelin-Cre mouse line that expresses Cre-recombinase specifically in the Reelin-expressing Cajal-Retzius cell type represents a valuable tool to target almost the whole generation of Cajal-Retzius cells and now enables the possibility to get more insight into the interaction of Reelin with other proteins involved in migration. Furthermore, with the generated data even an influence of CB1 on Reelin-dependent neuronal migration can be suggested but needs further clarification.

5 References

Aboitiz, F., & Montiel, J. (2007). Origin and evolution of the vertebrate telencephalon, with special reference to the mammalian neocortex. In *Advances in anatomy, embryology, and cell biology*. https://doi.org/10.1007/978-3-540-49761-5

Aguado T, Monory K, Palazuelos J, Stella N, Cravatt B, Lutz B, Marsicano G, Kokaia Z, Guzmán M, G.-R. I. (2005). The endocannabinoid system drives neural progenitor proliferation. *FASEB Journal*, *1*(Oct;19(12)), 1704–1706. https://doi.org/10.1096/fj.05-3995fje

Aguado, T., Palazuelos, J., Monory, K., Stella, N., Cravatt, B., Lutz, B., Marsicano, G., Kokaia, Z., Guzmán, M., & Galve-Roperh, I. (2006). The endocannabinoid system promotes astroglial differentiation by acting on neural progenitor cells. *Journal of Neuroscience*. https://doi.org/10.1523/JNEUROSCI.3101-05.2006

Alcamo, E. A., Chirivella, L., Dautzenberg, M., Dobreva, G., Fariñas, I., Grosschedl, R., & McConnell, S. K. (2008). Satb2 Regulates Callosal Projection Neuron Identity in the Developing Cerebral Cortex. *Neuron*. https://doi.org/10.1016/j.neuron.2007.12.012

Alcántara, S., Ruiz, M., D'Arcangelo, G., Ezan, F., De Lecea, L., Curran, T., Sotelo, C., & Soriano, E. (1998). Regional and cellular patterns of reelin mRNA expression in the forebrain of the developing and adult mouse. *Journal of Neuroscience*, *18*(19), 7779–7799. https://doi.org/10.1523/jneurosci.18-19-07779.1998

Anderson, S. A. (2002). Distinct Origins of Neocortical Projection Neurons and Interneurons In Vivo. *Cerebral Cortex*, *12*(7), 702–709. https://doi.org/10.1093/cercor/12.7.702

Anderson, S. A., Eisenstat, D. D., Shi, L., & Rubenstein, J. L. R. (1997). Interneuron migration from basal forebrain to neocortex: Dependence on Dlx genes. *Science*. https://doi.org/10.1126/science.278.5337.474

Angevine, J. B., & Sidman, R. L. (1961). Autoradiographic study of cell migration during histogenesis of cerebral cortex in the mouse. *Nature*. https://doi.org/10.1038/192766b0

Arber, S., Barbayannis, F. A., Hanser, H., Schnelder, C., Stanyon, C. A., Bernards, O., & Caroni, P. (1998). Regulation of actin dynamics through phosphorylation of cofilin by LIM- kinase. *Nature*, *393*(6687), 805–809. https://doi.org/10.1038/31729

Arcangelo, G. D., Nakajima, K., Miyata, T., Ogawa, M., Mikoshiba, K., & Curran, T. (1997). *Reelin Is a Secreted Glycoprotein Recognized by the CR-50 Monoclonal Antibody*. *17*(1), 23–31.

Arévalo-Martín, Á., García-Ovejero, D., Rubio-Araiz, A., Gómez, O., Molina-Holgado, F., & Molina-Holgado, E. (2007). Cannabinoids modulate Olig2 and polysialylated neural cell adhesion molecule expression in the subventricular zone of post-natal rats through cannabinoid receptor 1 and cannabinoid receptor 2. *European Journal of Neuroscience*. https://doi.org/10.1111/j.1460-9568.2007.05782.x

Argaw, A., Duff, G., Zabouri, N., Cécyre, B., Chainé, N., Cherif, H., Tea, N., Lutz, B., Ptito, M., & Bouchard, J. F. (2011). Concerted action of CB1 cannabinoid receptor and deleted in colorectal cancer in axon guidance. *Journal of Neuroscience*, *31*(4), 1489–1499. https://doi.org/10.1523/JNEUROSCI.4134-09.2011

Arnaud, L., Ballif, B. A., & Cooper, J. A. (2003). Regulation of Protein Tyrosine Kinase Signaling by Substrate Degradation during Brain Development. *Molecular and Cellular Biology*. https://doi.org/10.1128/mcb.23.24.9293-9302.2003

Assadi, A. H., Zhang, G., Beffert, U., McNeil, R. S., Renfro, A. L., Niu, S., Quattrocchi, C. C., Antalffy, B. A., Sheldon, M., Armstrong, D. D., Wynshaw-Boris, A., Herz, J., D'Arcangelo, G., & Clark, G. D. (2003). Interaction of reelin signaling and Lis1 in brain development. *Nature Genetics*. https://doi.org/10.1038/ng1257

Austin, S., Ziese, M., & Sternberg, N. (1981). A novel role for site-specific recombination in maintenance of bacterial replicons. *Cell*, *25*(3), 729–736. https://doi.org/10.1016/0092-8674(81)90180-X

Baranek, C., Dittrich, M., Parthasarathy, S., Bonnon, C. G., Britanova, O., Lanshakov, D., Boukhtouche, F., Sommer, J. E., Colmenares, C., Tarabykin, V., & Atanasoski, S. (2012). Protooncogene Ski cooperates with the chromatin-remodeling factor Satb2 in specifying callosal neurons. *Proceedings of the National Academy of Sciences of the United States of America*. https://doi.org/10.1073/pnas.1108718109

Barrangou, R., Fremaux, C., Deveau, H., Richards, M., Boyaval, P., Moineau, S., Romero, D. A., & Horvath, P. (2007). CRISPR provides acquired resistance against viruses in prokaryotes. *Science*. https://doi.org/10.1126/science.1138140

Baumgart, A. K., & Beyer, M. (2017). Genetic engineering as a tool for the generation of mouse models to understand disease phenotypes and gene function. In *Current Opinion in Biotechnology*. https://doi.org/10.1016/j.copbio.2017.06.012

Beffert, U., Weeber, E. J., Durudas, A., Qiu, S., Masiulis, I., Sweatt, J. D., Li, W. P., Adelmann, G., Frotscher, M., Hammer, R. E., & Herz, J. (2005). Modulation of synaptic plasticity and memory by Reelin involves differential splicing of the lipoprotein receptor Apoer2. *Neuron*. https://doi.org/10.1016/j.neuron.2005.07.007

Behringer, Richard, A., Gertsenstein, Marina, A., Nagy, Kristina Vintersten, A., & Nagy, Andras, 1951-, A. (2014). Manipulating the mouse embryo : a laboratory manual / Richard Behringer, University of Texas, M.D. Anderson Cancer Center, Marina Gertsenstein, Toronto Centre for Phenogenomics, Transgenic Core, Kristina Vintersten Nagy, Samuel Lunenfeld Research Institut. *Cold Spring Harbor, New York : Cold Spring Harbor Laboratory Press*. https://doi.org/101622901 [Book]

Berg, S., Kutra, D., Kroeger, T., Straehle, C. N., Kausler, B. X., Haubold, C., Schiegg, M., Ales, J., Beier, T., Rudy, M., Eren, K., Cervantes, J. I., Xu, B., Beuttenmueller, F., Wolny, A., Zhang, C., Koethe, U., Hamprecht, F. A., & Kreshuk, A. (2019). Ilastik: Interactive Machine Learning for (Bio)Image Analysis. *Nature Methods*, *16*(12), 1226–1232. https://doi.org/10.1038/s41592-019-0582-9

Berghuis, P., Dobszay, M. B., Wang, X., Spano, S., Ledda, F., Sousa, K. M., Schulte, G., Ernfors, P., Mackie, K., Paratcha, G., Hurd, Y. L., & Harkany, T. (2005). Endocannabinoids regulate interneuron migration and morphogenesis by transactivating the TrkB receptor. *Proceedings of the National Academy of Sciences of the United States of America*. https://doi.org/10.1073/pnas.0509494102

Berghuis, P., Rajnicek, A. M., Morozov, Y. M., Ross, R. A., Mulder, J., Urbán, G. M., Monory, K., Marsicano, G., Matteoli, M., Canty, A., Irving, A. J., Katona, I., Yanagawa, Y., Rakic, P., Lutz, B., Mackie, K., & Harkany, T. (2007). Hardwiring the bain: Endocannabinoids shape neuronal connectivity. *Science*. https://doi.org/10.1126/science.1137406

Berrendero, F., García-Gil, L., Hernández, M. L., Romero, J., Cebeira, M., De Miguel, R., Ramos, J. A., & Fernández-Ruiz, J. J. (1998). Localization of mRNA expression and activation of signal transduction mechanisms for cannabinoid receptor in rat brain during fetal development. *Development*.

Bock, H. H., & Herz, J. (2003). Reelin activates Src family tyrosine kinases in neurons. *Current Biology*. https://doi.org/10.1016/S0960-9822(02)01403-3

Bolotin, A., Quinquis, B., Sorokin, A., & Dusko Ehrlich, S. (2005). Clustered regularly interspaced short palindrome repeats (CRISPRs) have spacers of extrachromosomal origin. *Microbiology*, *151*(8), 2551–2561. https://doi.org/10.1099/mic.0.28048-0

Borrell, V., Kaspar, B. K., Gage, F. H., & Callaway, E. M. (2006). In vivo evidence for radial migration of neurons by long-distance somal translocation in the developing ferret visual cortex. *Cerebral Cortex*, *16*(11), 1571–1583. https://doi.org/10.1093/cercor/bhj094

Boyle, M. P., Bernard, A., Thompson, C. L., Ng, L., Boe, A., Mortrud, M., Hawrylycz, M. J., Jones, A. R., Hevner, R. F., & Lein, E. S. (2011). Cell-type-specific consequences of reelin deficiency in the mouse neocortex, hippocampus, and amygdala. *Journal of Comparative Neurology*. https://doi.org/10.1002/cne.22655

Britanova, O., de Juan Romero, C., Cheung, A., Kwan, K. Y., Schwark, M., Gyorgy, A., Vogel, T., Akopov, S., Mitkovski, M., Agoston, D., Šestan, N., Molnár, Z., & Tarabykin, V. (2008). Satb2 Is a Postmitotic Determinant for Upper-Layer Neuron Specification in the Neocortex. *Neuron*. https://doi.org/10.1016/j.neuron.2007.12.028

Bromberg, K. D., Iyengar, R., & He, J. C. (2008). Regulation of neurite outgrowth by Gi/o signaling pathways. In *Frontiers in Bioscience*. https://doi.org/10.2741/3022

Bulfone, A., Smiga, S. M., Shimamura, K., Peterson, A., Puelles, L., & Rubenstein, J. L. R. (1995). T-Brain-1: A homolog of Brachyury whose expression defines molecularly distinct domains within the cerebral cortex. *Neuron*. https://doi.org/10.1016/0896-6273(95)90065-9

Bulfone, A., Wang, F., Hevner, R., Anderson, S., Cutforth, T., Chen, S., Meneses, J., Pederson, R., Axel, R., & Rubenstein, J. L. R. (1998). An olfactory sensory map develops in the absense of normal projection neurons or GABAergic interneurons. *Neuron*, *21*, 1273–1282.

Cajal, Ramon, S. F. (1891). Sur la structure de l'écorce cérébrale de quelques mammifères. *La Cellule*, *7*(c).

Cajal SR. (1891). No Title. *Oxford: Oxford University Press.*, *Sur la structure de l'ecorce cérébrale de quelques mammifères. La Cellule 7:123–176. English translation in DeFelipe J*, *Jones EG (1988) Cajal on the cerebral cortex*, 23–54.

Cánovas, J., Berndt, F. A., Sepúlveda, H., Aguilar, R., Veloso, F. A., Montecino, M., Oliva, C., Maass, J. C., Sierralta, J., & Kukuljan, M. (2015). The specification of cortical subcerebral projection neurons depends on the direct repression of TBR1 by CTIP1/BCL11a. *Journal of Neuroscience*, *35*(19), 7552–7564. https://doi.org/10.1523/JNEUROSCI.0169-15.2015

Capecchi, M. R. (1989). Altering the genome by homologous recombination. *Science*, *244*(4910), 1288–1292. https://doi.org/10.1126/science.2660260

Caviness, V. S., & Sidman, R. L. (1973). Time of origin of corresponding cell classes in the cerebral cortex of normal and reeler mutant mice: An autoradiographic analysis. *Journal of Comparative Neurology*. https://doi.org/10.1002/cne.901480202

Caviness, Verne S. (1982). Neocortical histogenesis in normal and reeler mice: A developmental study based upon [3H]thymidine autoradiography. *Developmental Brain Research*. https://doi.org/10.1016/0165-3806(82)90141-9

Chai, X., Förster, E., Zhao, S., Bock, H. H., & Frotscher, M. (2009). *Reelin acts as a stop signal for radially migrating neurons by inducing phosphorylation of n-cofilin at the leading edge*. *August*,

375–377.

Charpentier, E., & Doudna, J. A. (2013). Rewriting a genome. *Nature*, *495(7439)*, 50–51. https://doi.org/10.1038/495050a

Chenn, A., Braisted, J. E., McConnell, S. K., & O'Leary, D. D. M. (2009). Development of the cerebral cortex: Mechanisms controlling cell fate, laminar and areal patterning, and axonal connectivity. In *Molecular and Cellular Approaches to Neural Development*. https://doi.org/10.1093/acprof:oso/9780195111668.003.0012

Childers, S. R., & Breivogel, C. S. (1998). Cannabis and endogenous cannabinoid systems. *Drug and Alcohol Dependence*. https://doi.org/10.1016/S0376-8716(98)00075-1

Cho, S. K., Choi, J. M., Kim, J. M., Cho, J. Y., Kim, S. S., Hong, S., Suh-Kim, H., & Lee, Y. D. (2015). AKT-independent Reelin signaling requires interactions of heterotrimeric Go and Src. *Biochemical and Biophysical Research Communications*, *467*(4), 1063–1069. https://doi.org/10.1016/j.bbrc.2015.09.167

Cho, S. W., Kim, S., Kim, Y., Kweon, J., Kim, H. S., Bae, S., & Kim, J. S. (2014). Analysis of off-target effects of CRISPR/Cas-derived RNA-guided endonucleases and nickases. *Genome Research*, *24*(1), 132–141. https://doi.org/10.1101/gr.162339.113

Chowdhury, T. G., Jimenez, J. C., Bomar, J. M., Cruz-Martin, A., Cantle, J. P., & Portera-Cailliau, C. (2010). Fate of Cajal-Retzius neurons in the postnatal mouse neocortex. *Frontiers in Neuroanatomy*, *4*(MARCH), 1–8. https://doi.org/10.3389/neuro.05.010.2010

Cong, L., Ran, F. A., Cox, D., Lin, S., Barretto, R., Hsu, P. D., Wu, X., Jiang, W., & Marraffini, L. a. (2013). Multiplex Genome Engineering Using CRISPR/Cas Systems. *Science (New York, N.Y.)*, *Feb 15*(339(6121)), 819–823. https://doi.org/10.1126/science.1231143.Multiplex

Cooper, J. A. (2008). A mechanism for inside-out lamination in the neocortex. *Trends in Neurosciences*, *31*(3), 113–119. https://doi.org/10.1016/j.tins.2007.12.003

Costa, E., Chen, Y., Davis, J., Dong, E., Noh, J. S., Tremolizzo, L., Veldic, M., Grayson, D. R., & Guidotti, A. (2002). REELIN and schizophrenia: a disease at the interface of the genome and the epigenome. In *Molecular interventions*. https://doi.org/10.1124/mi.2.1.47

Cox, D. B. T., Platt, R. J., & Zhang, F. (2015). Therapeutic genome editing: Prospects and challenges. *Nature Medicine*, *21*(2), 121–131. https://doi.org/10.1038/nm.3793

D'Arcangelo, G., Homayouni, R., Keshvara, L., Rice, D. S., Sheldon, M., & Curran, T. (1999). Reelin is a ligand for lipoprotein receptors. *Neuron*, *24*(2), 471–479. https://doi.org/10.1016/S0896-6273(00)80860-0

D'Arcangelo, G., Miao, G. G., Chen, S. C., Scares, H. D., Morgan, J. I., & Curran, T. (1995). A protein related to extracellular matrix proteins deleted in the mouse mutant reeler. *Nature*, *374*(6524), 719–723. https://doi.org/10.1038/374719a0

D'Arcangelo, G., Nakajima, K., Miyata, T., Ogawa, M., Mikoshiba, K., & Curran, T. (1997). Reelin is a secreted glycoprotein recognized by the CR-50 monoclonal antibody. *Journal of Neuroscience*, *17*(1), 23–31. https://doi.org/10.1523/jneurosci.17-01-00023.1997

Dazzo, E., Fanciulli, M., Serioli, E., Minervini, G., Pulitano, P., Binelli, S., Di Bonaventura, C., Luisi, C., Pasini, E., Striano, S., Striano, P., Coppola, G., Chiavegato, A., Radovic, S., Spadotto, A., Uzzau, S., La Neve, A., Giallonardo, A. T., Mecarelli, O., … Nobile, C. (2015). Heterozygous Reelin Mutations Cause Autosomal-Dominant Lateral Temporal Epilepsy. *American Journal of Human Genetics*. https://doi.org/10.1016/j.ajhg.2015.04.020

De Bergeyck, V., Nakajima, K., Lambert de Rouvrait, C., Naerhuyzen, B., Goffinet, A. M., Miyata, T., Ogawa, M., & Mikoshiba, K. (1997). A truncated Reelin protein is produced but not secreted in the “Orleans” reeler mutation (Reln(rl-Orl)). *Molecular Brain Research*. https://doi.org/10.1016/S0169-328X(97)00166-6

De Rubeis, S., He, X., Goldberg, A. P., Poultney, C. S., Samocha, K., Cicek, A. E., Kou, Y., Liu, L., Fromer, M., Walker, S., Singh, T., Klei, L., Kosmicki, J., Fu, S. C., Aleksic, B., Biscaldi, M., Bolton, P. F., Brownfeld, J. M., Cai, J., … Buxbaum, J. D. (2014). Synaptic, transcriptional and chromatin genes disrupted in autism. *Nature*. https://doi.org/10.1038/nature13772

Dekimoto, H., Terashima, T., & Katsuyama, Y. (2010). Dispersion of the neurons expressing layer specific markers in the reeler brain. *Development Growth and Differentiation*. https://doi.org/10.1111/j.1440-169X.2009.01153.x

Derkinderen, P., Valjent, E., Toutant, M., Corvol, J. C., Enslen, H., Ledent, C., Trzaskos, J., Caboche, J., & Girault, J. A. (2003). Regulation of extracellular signal-regulated kinase by cannabinoids in hippocampus. *Journal of Neuroscience*. https://doi.org/10.1523/jneurosci.23-06-02371.2003

Deussing, J. M. (2013). Targeted mutagenesis tools for modelling psychiatric disorders. In *Cell and Tissue Research*. https://doi.org/10.1007/s00441-013-1708-5

Devane, W. A., Hanuš, L., Breuer, A., Pertwee, R. G., Stevenson, L. A., Griffin, G., Gibson, D., Mandelbaum, A., Etinger, A., & Mechoulam, R. (1992). Isolation and structure of a brain constituent that binds to the cannabinoid receptor. *Science*. https://doi.org/10.1126/science.1470919

Di Marzo, V., Melck, D., Bisogno, T., & De Petrocellis, L. (1998). Endocannabinoids: Endogenous cannabinoid receptor ligands with neuromodulatory action. In *Trends in Neurosciences*. https://doi.org/10.1016/S0166-2236(98)01283-1

Díaz-Alonso, J., Aguado, T., De Salas-Quiroga, A., Ortega, Z., Guzmán, M., & Galve-Roperh, I. (2015). CB1 Cannabinoid receptor-dependent activation of mTORC1/Pax6 signaling drives Tbr2 expression and basal progenitor expansion in the developing mouse cortex. *Cerebral Cortex*, *25*(9), 2395–2408. https://doi.org/10.1093/cercor/bhu039

Díaz-Alonso, J., Aguado, T., Wu, C. S., Palazuelos, J., Hofmann, C., Garcez, P., Guillemot, F., Lu, H. C., Lutz, B., Guzmán, M., & Galve-Roperh, I. (2012). The CB1 cannabinoid receptor drives corticospinal motor neuron differentiation through the Ctip2/Satb2 transcriptional regulation axis. *Journal of Neuroscience*, *32*(47), 16651–16665. https://doi.org/10.1523/JNEUROSCI.0681-12.2012

Díaz-Alonso, J., De Salas-Quiroga, A., Paraíso-Luna, J., García-Rincón, D., Garcez, P. P., Parsons, M., Andradas, C., Sánchez, C., Guillemot, F., Guzmán, M., & Galve-Roperh, I. (2017). Loss of Cannabinoid CB1 Receptors Induces Cortical Migration Malformations and Increases Seizure Susceptibility. *Cerebral Cortex*, *27*(11), 5303–5317. https://doi.org/10.1093/cercor/bhw309

Doe, B., Brown, E., & Boroviak, K. (2018). Generating crispr/cas9-derived mutant mice by zygote cytoplasmic injection using an automatic microinjector. *Methods and Protocols*, *1*(1), 1–5. https://doi.org/10.3390/mps1010005

Doench, J. G., Fusi, N., Sullender, M., Hegde, M., Vaimberg, E. W., Donovan, K. F., Smith, I., Tothova, Z., Wilen, C., Orchard, R., Virgin, H. W., Listgarten, J., & Root, D. E. (2016). Optimized sgRNA design to maximize activity and minimize off-target effects of CRISPR-Cas9. *Nature Biotechnology*. https://doi.org/10.1038/nbt.3437

Domenici, M. R., Azad, S. C., Marsicano, G., Schierloh, A., Wotjak, C. T., Dodt, H. U., Zieglgänsberger,

W., Lutz, B., & Rammes, G. (2006). Cannabinoid receptor type 1 located on presynaptic terminals of principal neurons in the forebrain controls glutamatergic synaptic transmission. *Journal of Neuroscience*. https://doi.org/10.1523/JNEUROSCI.0372-06.2006

Drakew, A., Frotscher, M., Deller, T., Ogawa, M., & Heimrich, B. (1997). Developmental distribution of a reeler gene-related antigen in the rat hippocampal formation visualized by CR-50 immunocytochemistry. *Neuroscience*. https://doi.org/10.1016/S0306-4522(97)00326-6

Dulabon, L., Olson, E. C., Taglienti, M. G., Eisenhuth, S., McGrath, B., Walsh, C. A., Kreidberg, J. A., & Anton, E. S. (2000). Reelin Binds α3β1 Integrin and Inhibits Neuronal Migration. *Neuron*, *27*(1), 33–44. https://doi.org/10.1016/S0896-6273(00)00007-6

Dupuis, M.-È., & Moineau, S. (2013). Type II: Streptococcus thermophilus. In R. Barrangou & J. van der Oost (Eds.), *CRISPR-Cas Systems* (pp. 171–200). Springer Berlin Heidelberg. https://doi.org/10.1007/978-3-642-34657-6_7

Epinat, J. C., Amould, S., Chames, P., Rochaix, P., Desfontaines, D., Puzin, C., Patin, A., Zanghellini, A., Pâques, F., & Lacroix, E. (2003). A novel engineered meganuclease induces homologous recombination in yeast and mammalian cells. *Nucleic Acids Research*, *31*(11), 2952–2962. https://doi.org/10.1093/nar/gkg375

Finlay, B. L., & Darlington, R. B. (1995). Linked regularities in the development and evolution of mammalian brains. *Science*, *268*(5217), 1578–1584. https://doi.org/10.1126/science.7777856

Förster, E., Zhao, S., & Frotscher, M. (2006). Laminating the hippocampus. *Nature Reviews Neuroscience*, *7*(4), 259–267. https://doi.org/10.1038/nrn1882

Franco, S. J., Martinez-Garay, I., Gil-Sanz, C., Harkins-Perry, S. R., & Müller, U. (2011). Reelin Regulates Cadherin Function via Dab1/Rap1 to Control Neuronal Migration and Lamination in the Neocortex. *Neuron*, *69(3)*, 482–497. https://doi.org/10.1016/j.neuron.2011.01.003

Frotscher, M. (1998). Cajal-Retzius cells, Reelin, and the formation of layers. *Current Opinion in Neurobiology*, *8*(5), 570–575. https://doi.org/10.1016/S0959-4388(98)80082-2

Gaffuri, A.-L., Ladarre, D., & Lenkei, Z. (2012). Type-1 Cannabinoid Receptor Signaling in Neuronal Development. *Pharmacology*, *90*(1–2), 19–39. https://doi.org/10.1159/000339075

Gaj, T., Gersbach, C. A., & Barbas, C. F. (2013). ZFN, TALEN, and CRISPR/Cas-based methods for genome engineering. *Trends in Biotechnology*, *31*(7), 397–405. https://doi.org/10.1016/j.tibtech.2013.04.004

Galve-Roperh, I., Palazuelos, J., Aguado, T., & Guzmán, M. (2009). The endocannabinoid system and the regulation of neural development: Potential implications in psychiatric disorders. In *European Archives of Psychiatry and Clinical Neuroscience*. https://doi.org/10.1007/s00406-009-0028-y

Gaoni, Y., & Mechoulam, R. (1964). Isolation, Structure, and Partial Synthesis of an Active Constituent of Hashish. *Journal of the American Chemical Society*, *86(8)*, 1646–1647. https://doi.org/10.1021/ja01062a046

Gelman, D. M., & Marín, O. (2010). Generation of interneuron diversity in the mouse cerebral cortex. In *European Journal of Neuroscience*. https://doi.org/10.1111/j.1460-9568.2010.07267.x

Gerlai, R. (1996). Gene-targeting studies of mammalian behavior: Is it the mutation or the background genotype? *Trends in Neurosciences*. https://doi.org/10.1016/S0166-2236(96)20020-7

Gilbert, L. A., Larson, M. H., Morsut, L., Liu, Z., Gloria, A., Torres, S. E., Stern-ginossar, N., Brandman, O., Whitehead, H., Doudna, J. A., Lim, W. A., & Jonathan, S. (2013). CRISPR-mediated modular RNA-guided regulation of transcription in eukaryotes. *Cell*, *Jul 18*(154(2)), 442–451. https://doi.org/10.1016/j.cell.2013.06.044.CRISPR-Mediated

Gilmore, E. C., & Herrup, K. (2000). Cortical development: Receiving Reelin. *Current Biology*, *10*(4), 162–166. https://doi.org/10.1016/S0960-9822(00)00332-8

Gorski, J. A., Talley, T., Qiu, M., Puelles, L., Rubenstein, J. L. R., & Jones, K. R. (2002). Cortical excitatory neurons and glia, but not GABAergic neurons, are produced in the Emx1-expressing lineage. *Journal of Neuroscience*, *22*(15), 6309–6314. https://doi.org/10.1523/jneurosci.22-15-06309.2002

Graham, F. L., Smiley, J., Russell, W. C., & Nairn, R. (1977). Characteristics of a human cell line transformed by DNA from human adenovirus type 5. *Journal of General Virology*, *Jul*(36(1)), 59–74. https://doi.org/10.1099/0022-1317-36-1-59

Greig, L. C., Woodworth, M. B., Galazo, M. J., Padmanabhan, H., & Macklis, J. D. (2013). Molecular logic of neocortical projection neuron specification, development and diversity. In *Nature Reviews Neuroscience* (pp. 14, 755–769). https://doi.org/10.1038/nrn3586

Guggenhuber, S., Monory, K., Lutz, B., & Klugmann, M. (2010). AAV vector-mediated overexpression of CB1 cannabinoid receptor in pyramidal neurons of the hippocampus protects against seizure-induced excitoxicity. *PLoS ONE*, *5*(12), 1–8. https://doi.org/10.1371/journal.pone.0015707

Hack, I., Hellwig, S., Junghans, D., Brunne, B., Bock, H. H., Zhao, S., & Frotscher, M. (2007). Divergent roles of ApoER2 and Vldlr in the migration of cortical neurons. *Development*, *Nov;134(21)*, 3883–3891. https://doi.org/10.1242/dev.005447

Haft, D. H., Selengut, J., Mongodin, E. F., & Nelson, K. E. (2005). A guild of 45 CRISPR-associated (Cas) protein families and multiple CRISPR/cas subtypes exist in prokaryotic genomes. *PLoS Computational Biology*, *1(6)*, e60. https://doi.org/10.1371 /journal.pcbi.0010060

Hall, A., & Lalli, G. (2010). Rho and Ras GTPases in axon growth, guidance, and branching. In *Cold Spring Harbor perspectives in biology* (p. Feb;2(2):a001818). https://doi.org/10.1101/cshperspect.a001818

Hamann, J., Aust, G., Araç, D., Engel, F. B., Formstone, C., Fredriksson, R., Hall, R. A., Harty, B. L., Kirchhoff, C., Knapp, B., Krishnan, A., Liebscher, I., Lin, H. H., Martinelli, D. C., Monk, K. R., Peeters, M. C., Piao, X., Prömel, S., Schöneberg, T., … Schiöth, H. B. (2015). International union of basic and clinical pharmacology. XCIV. adhesion G protein-coupled receptors. *Pharmacological Reviews*, *67(2)*, 338–367. https://doi.org/10.1124/pr.114.009647

Han, W., Kwan, K. Y., Shim, S., Lam, M. M. S., Shin, Y., Xu, M., Zhu, Y., Li, M., & Šestan, N. (2011). TBR1 directly represses Fezf2 to control the laminar origin and development of the corticospinal tract. *Proceedings of the National Academy of Sciences of the United States of America*, *108*(7), 3041–3046. https://doi.org/10.1073/pnas.1016723108

Hanashima, C., Fernandes, M., Hebert, J. M., & Fishell, G. (2007). The role of Foxg1 and dorsal midline signaling in the generation of Cajal-Retzius subtypes. *Journal of Neuroscience*, *27*(41), 11103–11111. https://doi.org/10.1523/JNEUROSCI.1066-07.2007

Harb, K., Magrinelli, E., Nicolas, C. S., Lukianets, N., Frangeul, L., Pietri, M., Sun, T., Sandoz, G., Grammont, F., Jabaudon, D., Studer, M., & Alfano, C. (2016). Area-specific development of distinct projection neuron subclasses is regulated by postnatal epigenetic modifications. *ELife*, *Jan*(27;5:e09531). https://doi.org/10.7554/eLife.09531

Harkany, T., Guzmán, M., Galve-Roperh, I., Berghuis, P., Devi, L. A., & Mackie, K. (2007). The emerging functions of endocannabinoid signaling during CNS development. In *Trends in Pharmacological Sciences* (p. Feb;28(2):83-92). https://doi.org/10.1016/j.tips.2006.12.004

Harkany, T., Keimpema, E., Barabás, K., & Mulder, J. (2008). Endocannabinoid functions controlling neuronal specification during brain development. *Molecular and Cellular Endocrinology*, *286*(1-2 SUPPL. 1), 84–90. https://doi.org/10.1016/j.mce.2008.02.011

Hatanaka, Y., Zhu, Y., Torigoe, M., Kita, Y., & Murakami, F. (2016). From migration to settlement: The pathways, migration modes and dynamics of neurons in the developing brai. In *Proceedings of the Japan Academy Series B: Physical and Biological Sciences* (pp. 92(1): 1-19). https://doi.org/10.2183/pjab.92.1

Hatten, M. E. (1999). Central nervous system neuronal migration. *Annual Review of Neuroscience*, *22*, 511–539. https://doi.org/10.1146/annurev.neuro.22.1.511

Heidenreich, M., & Zhang, F. (2016). Applications of CRISPR-Cas systems in neuroscience. In *Nature Reviews Neuroscience* (p. Jan; 17(1): 36–44.). https://doi.org/10.1038/nrn.2015.2

Heifets, B. D., & Castillo, P. E. (2009). Endocannabinoid signaling and long-term synaptic plasticity. *Annual Review of Physiology*, *71*, 283–306. https://doi.org/10.1146/annurev.physiol.010908.163149

Herz, J., & Chen, Y. (2006). Reelin, lipoprotein receptors and synaptic plasticity. *Nature Reviews Neuroscience*, *17(1)*, 36–44. https://doi.org/10.1038/nrn2009

Hevner, R. F., Shi, L., Justice, N., Hsueh, Y. P., Sheng, M., Smiga, S., Bulfone, A., Goffinet, A. M., Campagnoni, A. T., & Rubenstein, J. L. R. (2001). Tbr1 regulates differentiation of the preplate and layer 6. *Neuron*, *29*(2), 353–366. https://doi.org/10.1016/S0896-6273(01)00211-2

Hirotsune, S., Takahara, T., Sasaki, N., Hirose, K., Yoshiki, A., Ohashi, T., Kusakabe, M., Murakami, Y., Muramatsu, M., Watanabe, S., Nakao, K., Katsuki, M., & Hayashizaki, Y. (1995). The reeler gene encodes a protein with an EGF–like motif expressed by pioneer neurons. *Nature Genetics*, *10*, 77–83. https://doi.org/10.1038/ng0595-77

Hochman, L., Segev, N., Sternberg, N., & Cohen, G. (1983). Site-specific recombinational circularization of bacteriophage P1 DNA. *Virology*, *131*(1), 11–17. https://doi.org/10.1016/0042-6822(83)90528-7

Hörl, D., Rojas Rusak, F., Preusser, F., Tillberg, P., Randel, N., Chhetri, R. K., Cardona, A., Keller, P. J., Harz, H., Leonhardt, H., Treier, M., & Preibisch, S. (2019). BigStitcher: reconstructing high-resolution image datasets of cleared and expanded samples. *Nature Methods*, *16*(9), 870–874. https://doi.org/10.1038/s41592-019-0501-0

Howell, B. W., Herrick, T. M., & Cooper, J. A. (1999). Reelin-induced tryosine phosphorylation of Disabled 1 during neuronal positioning. *Genes and Development*, *Mar*(13(6)), 643–648. https://doi.org/10.1101/gad.13.6.643

Howlett, A. C., Qualy, J. M., & Khachatrian, L. L. (1986). Involvement of G(i) in the inhibition of adenylate cyclase by cannabimimetic drugs. *Molecular Pharmacology*.

Howlett, Allyn C. (1995). Pharmacology of cannabinoid receptors. *Annual Review of Pharmacology and Toxicology*, *35*, 607–634. https://doi.org/10.1146/annurev.pa.35.040195.003135

Hsu, P. D., Scott, D. A., Weinstein, J. A., Ran, F. A., Konermann, S., Agarwala, V., Li, Y., Fine, E. J., Wu, X., Shalem, O., Cradick, T. J., Marraffini, L. A., Bao, G., & Zhang, F. (2013a). DNA targeting specificity of RNA-guided Cas9 nucleases. *Nature Biotechnology*.

https://doi.org/10.1038/nbt.2647

Hsu, P. D., Scott, D. A., Weinstein, J. A., Ran, F. A., Konermann, S., Agarwala, V., Li, Y., Fine, E. J., Wu, X., Shalem, O., Cradick, T. J., Marraffini, L. A., Bao, G., & Zhang, F. (2013b). DNA targeting specificity of RNA-guided Cas9 nucleases. *Nature Biotechnology*, *31*, 827–832. https://doi.org/10.1038/nbt.2647

Hwang, W. Y., Fu, Y., Reyon, D., Maeder, M. L., Kaini, P., Sander, J. D., Joung, J. K., Peterson, R. T., & Yeh, J. R. J. (2013). Heritable and Precise Zebrafish Genome Editing Using a CRISPR-Cas System. *PLoS ONE*, *8(7): e687*(e68780). https://doi.org/10.1371/journal.pone.0068708

Im, W., Moon, J., & Kim, M. (2016). Applications of CRISPR/Cas9 for Gene Editing in Hereditary Movement Disorders. *Journal of Movement Disorders*, *9*(3), 136–143. https://doi.org/10.14802/jmd.16029

Inui, M., Miyado, M., Igarashi, M., Tamano, M., Kubo, A., Yamashita, S., Asahara, H., Fukami, M., & Takada, S. (2014). Rapid generation of mouse models with defined point mutations by the CRISPR/Cas9 system. *Scientific Reports*, *23*(4:5396). https://doi.org/10.1038/srep05396

Ishino, Y., Shinagawa, H., Makino, K., Amemura, M., & Nakatura, A. (1987). Nucleotide sequence of the iap gene, responsible for alkaline phosphatase isoenzyme conversion in Escherichia coli, and identification of the gene product. *Journal of Bacteriology*, *169*(12), 5429–5433. https://doi.org/10.1128/jb.169.12.5429-5433.1987

Jackson, S. A., McKenzie, R. E., Fagerlund, R. D., Kieper, S. N., Fineran, P. C., & Brouns, S. J. J. (2017). CRISPR-Cas: Adapting to change. *Science*, *356*(6333). https://doi.org/10.1126/science.aal5056

Jansen, R., Van Embden, J. D. A., Gaastra, W., & Schouls, L. M. (2002). Identification of genes that are associated with DNA repeats in prokaryotes. *Molecular Microbiology*, *Mar*(43(6)), 1565–1575. https://doi.org/10.1046/j.1365-2958.2002.02839.x

Jiang, S., Fu, Y., Williams, J., Wood, J. A., Pandarinathan, L., Avraham, S., Makriyannis, A., Avraham, S., & Avraham, H. K. (2007). Expression and function of cannabinoid receptors CB1 and CB2 and their cognate cannabinoid ligands in murine embryonic stem cells. *PLoS ONE*, *2(7)*, e641. https://doi.org/10.1371/journal.pone.0000641

Jinek, M., Chylinski, K., Fonfara, I., Hauer, M., Doudna, J. A., & Charpentier, E. (2012). A Programmable Dual-RNA – Guided. *Science*, *337*(August), 816–822. https://doi.org/10.1126/science.1225829

Jossin & Cooper. (2011). Reelin, Rap1 and N-cadherin orient the migration of multipolar neurons in the developing neocortex. *Nat Neurosci. 2011 June ; 14(6): 697–703. Doi:10.1038/Nn.2816*, *176*(3), 697–703. https://doi.org/10.1038/nn.2816.Reelin

Jossin, Y. (2004). Neuronal Migration and the Role of Reelin During Early Development of the Cerebral Cortex. *Molecular Neurobiology*, *30*(3), 225–251. https://doi.org/10.1385/MN:30:3:225

Jossin, Y. (2020). Reelin functions, mechanisms of action and signaling pathways during brain development and maturation. *Biomolecules*, *10*(6), 1–31. https://doi.org/10.3390/BIOM10060964

Jossin, Y., Ignatova, N., Hiesberger, T., Herz, J., Lambert De Rouvroit, C., & Goffinet, A. M. (2004). The Central Fragment of Reelin, Generated by Proteolytic Processing in Vivo, Is Critical to Its Function during Cortical Plate Development. *Journal of Neuroscience*, *24*(2), 514–521. https://doi.org/10.1523/JNEUROSCI.3408-03.2004

Jovceva, E., Larsen, M. R., Waterfield, M. D., Baum, B., & Timms, J. F. (2007). Dynamic cofilin phosphorylation in the control of lamellipodial actin homeostasis. *Journal of Cell Science*, *120*(11), 1888–1897. https://doi.org/10.1242/jcs.004366

Judo, M. S. B., Wedel, A. B., & Wilson, C. (1998). Stimulation and suppression of PCR-mediated recombination. *Nucleic Acids Research*, *26*(7), 1–7. https://doi.org/10.1093/nar/26.7.1819

Kano, M., Ohno-Shosaku, T., Hashimotodani, Y., Uchigashima, M., & Watanabe, M. (2009). Endocannabinoid-mediated control of synaptic transmission. *Physiological Reviews*, *Jan*(89(1)), 309–380. https://doi.org/10.1152/physrev.00019.2008

Katona, I., Rancz, E. A., Acsády, L., Ledent, C., Mackie, K., Hájos, N., & Freund, T. F. (2001). Distribution of CB1 cannabinoid receptors in the amygdala and their role in the control of GABAergic transmission. *Journal of Neuroscience*, *Dec 1*(21(23)), 9506–9518. https://doi.org/10.1523/jneurosci.21-23-09506.2001

Katona, István, & Freund, T. F. (2012). Multiple Functions of Endocannabinoid Signaling in the Brain. *Annual Review of Neuroscience*, *35*, 529–558. https://doi.org/10.1146/annurev-neuro-062111-150420

Katona, István, Sperlágh, B., Sík, A., Käfalvi, A., Vizi, E. S., Mackie, K., & Freund, T. F. (1999). Presynaptically located CB1 cannabinoid receptors regulate GABA release from axon terminals of specific hippocampal interneurons. *Journal of Neuroscience*, *19*(11), 4544–4558. https://doi.org/10.1523/jneurosci.19-11-04544.1999

Kawamura, Y., Fukaya, M., Maejima, T., Yoshida, T., Miura, E., Watanabe, M., Ohno-Shosaku, T., & Kano, M. (2006). The CB1 cannabinoid receptor is the major cannabinoid receptor at excitatory presynaptic sites in the hippocampus and cerebellum. *Journal of Neuroscience*, *Mar 15*(26(11)), 2991–3001. https://doi.org/10.1523/JNEUROSCI.4872-05.2006

Khalil, A. M. (2020). The genome editing revolution: review. *Journal of Genetic Engineering and Biotechnology*, *18*(1), 68. https://doi.org/10.1186/s43141-020-00078-y

Kiuchi, T., Ohashi, K., Kurita, S., & Mizuno, K. (2007). Cofilin promotes stimulus-induced lamellipodium formation by generating an abundant supply of actin monomers. *Journal of Cell Biology*, *177*(3), 465–476. https://doi.org/10.1083/jcb.200610005

Klemke, R. L., Cai, S., Giannini, A. L., Gallagher, P. J., De Lanerolle, P., & Cheresh, D. A. (1997). Regulation of cell motility by mitogen-activated protein kinase. *Journal of Cell Biology*, *Apr 21*(137(2)), 481–492. https://doi.org/10.1083/jcb.137.2.481

Kojima, T., Nakajima, K., & Mikoshiba, K. (2000). The disabled 1 gene is disrupted by a replacement with L1 fragment in yotari mice. *Molecular Brain Research*, *Jan 10*(75(1)), 121–127. https://doi.org/10.1016/S0169-328X(99)00313-7

Kubo, K. I., Mikoshiba, K., & Nakajima, K. (2002). Secreted Reelin molecules form homodimers. *Neuroscience Research*. https://doi.org/10.1016/S0168-0102(02)00068-8

Kühn, R., & Torres, R. M. (2002). Cre/loxP recombination system and gene targeting. *Methods in Molecular Biology (Clifton, N.J.)*, *180*, 175–204. https://doi.org/10.1385/1-59259-178-7:175

Kuscu, C., Arslan, S., Singh, R., Thorpe, J., & Adli, M. (2014). Genome-wide analysis reveals characteristics of off-target sites bound by the Cas9 endonuclease. *Nature Biotechnology*, *32*(7), 677–683. https://doi.org/10.1038/nbt.2916

Lambert De Rouvroit, C., De Bergeyck, V., Cortvrindt, C., Bar, I., Eeckhout, Y., & Goffinet, A. M. (1999). Reelin, the extracellular matrix protein deficient in reeler mutant mice, is processed by a

metalloproteinase. *Experimental Neurology*, *Mar*(156(1)), 214–217. https://doi.org/10.1006/exnr.1998.7007

Lavdas, a a, Grigoriou, M., Pachnis, V., & Parnavelas, J. G. (1999). The medial ganglionic eminence gives rise to a population of early neurons in the developing cerebral cortex. *The Journal of Neuroscience : The Official Journal of the Society for Neuroscience*, *19*(18), 7881–7888.

Lee, J., Rho, J. il, Devkota, S., Sung, Y. H., & Lee, H. W. (2016). Developing genetically engineered mouse models using engineered nucleases: Current status, challenges, and the way forward. *Drug Discovery Today: Disease Models*, *20*, 13–20. https://doi.org/10.1016/j.ddmod.2017.07.003

Leemhuis, J., Bouché, E., Frotscher, M., Henle, F., Hein, L., Herz, J., Meyer, D. K., Pichler, M., Roth, G., Schwan, C., & Bock, H. H. (2010). Reelin signals through apolipoprotein E receptor 2 and Cdc42 to increase growth cone motility and filopodia formation. *Journal of Neuroscience*, *30*(44), 14759–14772. https://doi.org/10.1523/JNEUROSCI.4036-10.2010

Leone, D. P., Heavner, W. E., Ferenczi, E. A., Dobreva, G., Huguenard, J. R., Grosschedl, R., & McConnell, S. K. (2015). Satb2 regulates the differentiation of both callosal and subcerebral projection neurons in the developing cerebral cortex. *Cerebral Cortex*, *Oct*(25(10)), 3406–3419. https://doi.org/10.1093/cercor/bhu156

Limaye, A., Hall, B., & Kulkarnil, A. B. (2009). Manipulation of mouse embryonic stem cells for knockout mouse production. *Current Protocols in Cell Biology*, *Chapter 19*, Unit-19.13.24. https://doi.org/10.1002/0471143030.cb1913s44

Liu, Y., Yang, Y., Kang, X., Lin, B., Yu, Q., Song, B., Gao, G., Chen, Y., Sun, X., Li, X., Bu, L., & Fan, Y. (2017). One-Step Biallelic and Scarless Correction of a β-Thalassemia Mutation in Patient-Specific iPSCs without Drug Selection. *Molecular Therapy - Nucleic Acids*, *Mar 17*(6), 57–67. https://doi.org/10.1016/j.omtn.2016.11.010

Loschko, J., Rieke, G. J., Schreiber, H. A., Meredith, M. M., Yao, K. H., Guermonprez, P., & Nussenzweig, M. C. (2016). Inducible targeting of cDCs and their subsets in vivo. *Journal of Immunological Methods*, *Jul*(434), 32–38. https://doi.org/10.1016/j.jim.2016.04.004

Madisen, L., Garner, A. R., Shimaoka, D., Chuong, A. S., Klapoetke, N. C., Li, L., van der Bourg, A., Niino, Y., Egolf, L., Monetti, C., Gu, H., Mills, M., Cheng, A., Tasic, B., Nguyen, T. N., Sunkin, S. M., Benucci, A., Nagy, A., Miyawaki, A., … Zeng, H. (2015). Transgenic mice for intersectional targeting of neural sensors and effectors with high specificity and performance. *Neuron*, *85*(5), 942–958. https://doi.org/10.1016/j.neuron.2015.02.022

Madisen, L., Mao, T., Koch, H., Zhuo, J. M., Berenyi, A., Fujisawa, S., Hsu, Y. W. A., Garcia, A. J., Gu, X., Zanella, S., Kidney, J., Gu, H., Mao, Y., Hooks, B. M., Boyden, E. S., Buzsáki, G., Ramirez, J. M., Jones, A. R., Svoboda, K., … Zeng, H. (2012). A toolbox of Cre-dependent optogenetic transgenic mice for light-induced activation and silencing. *Nature Neuroscience*, *15*, 793–802. https://doi.org/10.1038/nn.3078

Madisen, L., Zwingman, T. A., Sunkin, S. M., Oh, S. W., Zariwala, H. A., Gu, H., Ng, L. L., Palmiter, R. D., Hawrylycz, M. J., Jones, A. R., Lein, E. S., & Zeng, H. (2010). A robust and high-throughput Cre reporting and characterization system for the whole mouse brain. *Nature Neuroscience*, *13*, 133–140. https://doi.org/10.1038/nn.2467

Maeder, ML; Linder, S; Cascio, V; Fu, Y;Ho, Q; Joung, J. (2013). CRISPR RNA-guided activation of endogenous human genes. *Nat Methods*, *10*(10), 977–979. https://doi.org/10.1038/nmeth.2598

Magdaleno, S., Keshvara, L., & Curran, T. (2002). Rescue of ataxia and preplate splitting by ectopic expression of Reelin in reeler mice. *Neuron*, *33*(4), 573–586. https://doi.org/10.1016/S0896-6273(02)00582-2

Makarova, K. S., Haft, D. H., Barrangou, R., Brouns, S. J. J., Charpentier, E., Horvath, P., Moineau, S., Mojica, F. J. M., Wolf, Y. I., Yakunin, A. F., Van Der Oost, J., & Koonin, E. V. (2011). Evolution and classification of the CRISPR-Cas systems. *Nature Reviews Microbiology*, *9*(6), 467–477. https://doi.org/10.1038/nrmicro2577

Malfitano, A. M., Basu, S., Maresz, K., Bifulco, M., & Dittel, B. N. (2014). What we know and do not know about the cannabinoid receptor 2 (CB2). *Seminars in Immunology*, *Oct*(26(5)), 369–379. https://doi.org/10.1016/j.smim.2014.04.002

Mali, P., Esvelt, K. M., & Church, G. M. (2013). Cas9 as a versatile tool for engineering biology. *Nature Methods*, *10*, 957–963. https://doi.org/10.1038/nmeth.2649

Mali, P., Yang, L., Esvelt, K. M., Aach, J., Guell, M., DiCarlo, J. E., Norville, J. E., & Church, G. M. (2013). RNA-guided human genome engineering via Cas9. *Science*, *Feb 15*(339(6121)), 823–826. https://doi.org/10.1126/science.1232033

Marsicano, G., Goodenough, S., Monory, K., Hermann, H., Eder, M., Cannich, A., Azad, S. C., Cascio, M. G., Stelt, M. Van Der, & Lo, M. L. (2003). Protective Endocannabinoids. *Science Signaling*, *2003*(203), tw391–tw391. https://doi.org/10.1126/stke.2003.203.tw391

Marsicano, G., & Lutz, B. (1999). Expression of the cannabinoid receptor CB1 in distinct neuronal subpopulations in the adult mouse forebrain. *European Journal of Neuroscience*, *Dec*(11(12)), 4213–4225. https://doi.org/10.1046/j.1460-9568.1999.00847.x

Mashal, R. D., Koontz, J., & Sklar, J. (1995). Detection of mutations by cleavage of DNA heteroduplexes with bacteriophage resolvases. *Nature Genetics*, *9*(2), 177–183. https://doi.org/10.1038/ng0295-177

Massa, F., Marsicano, G., Hermana, H., Cannich, A., Monory, K., Cravatt, B. F., Ferri, G. L., Sibaev, A., Storr, M., & Lutz, B. (2004). The endogenous cannabinoid system protects against colonic inflammation. *Journal of Clinical Investigation*, *Apr 15*(113(8)), 1202–1209. https://doi.org/10.1172/JCI200419465

Matsuda, L. A., Lolait, S. J., Brownstein, M. J., Young, A. C., & Bonner, T. I. (1990). Structure of a cannabinoid receptor and functional expression of the cloned cDNA. *Nature*, *346*, 561–564. https://doi.org/10.1038/346561a0

McKenna, W. L., Ortiz-Londono, C. F., Mathew, T. K., Hoang, K., Katzman, S., & Chen, B. (2015). Mutual regulation between Satb2 and Fezf2 promotes subcerebral projection neuron identity in the developing cerebral cortex. *Proceedings of the National Academy of Sciences of the United States of America*, *112 (37)*, 11702–11707. https://doi.org/10.1073/pnas.1504144112

McKenney, R. J., Vershinin, M., Kunwar, A., Vallee, R. B., & Gross, S. P. (2010). LIS1 and NudE induce a persistent dynein force-producing state. *Cell*, *Apr 16*(141(2)), 304–314. https://doi.org/10.1016/j.cell.2010.02.035

Mechoulam, R., Ben-Shabat, S., Hanus, L., Ligumsky, M., Kaminski, N. E., Schatz, A. R., Gopher, A., Almog, S., Martin, B. R., Compton, D. R., Pertwee, R. G., Griffin, G., Bayewitch, M., Barg, J., & Vogel, Z. (1995). Identification of an endogenous 2-monoglyceride, present in canine gut, that binds to cannabinoid receptors. *Biochemical Pharmacology*, *Jun 29*(50(1)), 83–90. https://doi.org/10.1016/0006-2952(95)00109-D

Mechoulam, R., Hanuš, L., & Martin, B. R. (1994). Search for endogenous ligands of the cannabinoid receptor. *Biochemical Pharmacology*, *Oct 18*(48(8)), 1537–1544. https://doi.org/10.1016/0006-2952(94)90197-X

Mechoulam, R., & Parker, L. A. (2013). The Endocannabinoid System and the Brain. *Annual Review of Psychology*, *64*, 21–47. https://doi.org/10.1146/annurev-psych-113011-143739

Merlin, M. D. (2003). Archaeological Evidence for the Tradition of Psychoactive Plant Use in the Old World. *Economic Botany*, *57*(5), 295–323. https://doi.org/10.1663/0013-0001(2003)057[0295:AEFTTO]2.0.CO;2

Mikoshiba, K., Nagaike, K., Kohsaka, S., Takamatsu, K., Aoki, E., & Tsukada, Y. (1980). Developmental studies on the cerebellum from reeler mutant mouse in vivo and in vitro. *Developmental Biology*, *Sep*(79(1)), 64–80. https://doi.org/10.1016/0012-1606(80)90073-1

Miller, J. C., Tan, S., Qiao, G., Barlow, K. A., Wang, J., Xia, D. F., Meng, X., Paschon, D. E., Leung, E., Hinkley, S. J., Dulay, G. P., Hua, K. L., Ankoudinova, I., Cost, G. J., Urnov, F. D., Zhang, H. S., Holmes, M. C., Zhang, L., Gregory, P. D., & Rebar, E. J. (2011). A TALE nuclease architecture for efficient genome editing. *Nature Biotechnology*, *29*, 143–148. https://doi.org/10.1038/nbt.1755

Miura, H., Gurumurthy, C. B., Sato, T., Sato, M., & Ohtsuka, M. (2015). CRISPR/Cas9-based generation of knockdown mice by intronic insertion of artificial microRNA using longer single-stranded DNA. *Scientific Reports*, *5*, 12799. https://doi.org/10.1038/srep12799

Miura, H., Quadros, R. M., Gurumurthy, C. B., & Ohtsuka, M. (2018). Easi-CRISPR for creating knock-in and conditional knockout mouse models using long ssDNA donors. *Nature Protocols*. https://doi.org/10.1038/nprot.2017.153

Mojica, F. J. M., Díez-Villaseñor, C., García-Martínez, J., & Soria, E. (2005). Intervening sequences of regularly spaced prokaryotic repeats derive from foreign genetic elements. *Journal of Molecular Evolution*, *60*(2), 174–182. https://doi.org/10.1007/s00239-004-0046-3

Mojica, F. J. M., Díez-Villaseñor, C., Soria, E., & Juez, G. (2000). Biological significance of a family of regularly spaced repeats in the genomes of Archaea, Bacteria and mitochondria. *Molecular Microbiology*, *Apr*(36(1)), 244–246. https://doi.org/10.1046/j.1365-2958.2000.01838.x

Molina-Holgado, E., Vela, J. M., Arévalo-Martín, A., Almazán, G., Molina-Holgado, F., Borrell, J., & Guaza, C. (2002). Cannabinoids promote oligodendrocyte progenitor survival: Involvement of cannabinoid receptors and phosphatidylinositol-3 kinase/Akt signaling. *Journal of Neuroscience*, *Nov 15*(22(22)), 9742–9753. https://doi.org/10.1523/jneurosci.22-22-09742.2002

Molina-Holgado, F., Rubio-Araiz, A., García-Ovejero, D., Williams, R. J., Moore, J. D., Arévalo-Martín, Á., Gómez-Torres, O., & Molina-Holgado, E. (2007). CB2 cannabinoid receptors promote mouse neural stem cell proliferation. *European Journal of Neuroscience*, *Feb*(25(3)), 629–634. https://doi.org/10.1111/j.1460-9568.2007.05322.x

Molyneaux, B. J., Arlotta, P., Menezes, J. R. L., & Macklis, J. D. (2007). Neuronal subtype specification in the cerebral cortex. *Nature Reviews. Neuroscience*, *8*(6), 427–437. https://doi.org/10.1038/nrn2151

Monory, K., Massa, F., Egertová, M., Eder, M., Blaudzun, H., Westenbroek, R., Kelsch, W., Jacob, W., Marsch, R., Ekker, M., Long, J., Rubenstein, J. L., Goebbels, S., Nave, K. A., During, M., Klugmann, M., Wölfel, B., Dodt, H. U., Zieglgänsberger, W., … Lutz, B. (2006). The Endocannabinoid System Controls Key Epileptogenic Circuits in the Hippocampus. *Neuron*, *Aug 17*(51(4)), 455–466. https://doi.org/10.1016/j.neuron.2006.07.006

Moreno-Mateos, M. A., Vejnar, C. E., Beaudoin, J. D., Fernandez, J. P., Mis, E. K., Khokha, M. K., & Giraldez, A. J. (2015). CRISPRscan: Designing highly efficient sgRNAs for CRISPR-Cas9 targeting in vivo. *Nature Methods*, *12*, 982–988. https://doi.org/10.1038/nmeth.3543

Morozov, Y. M., & Freund, T. F. (2003). Post-natal development of type 1 cannabinoid receptor immunoreactivity in the rat hippocampus. *European Journal of Neuroscience*, *Sep*(18(5)), 1213–1222. https://doi.org/10.1046/j.1460-9568.2003.02852.x

Morozov, Y. M., Torii, M., & Rakic, P. (2009). Origin, early commitment, migratory routes, and destination of cannabinoid type 1 receptor-containing interneurons. *Cerebral Cortex*, *Jul*(19), i78-89. https://doi.org/10.1093/cercor/bhp028

Mulder, J., Aguado, T., Keimpema, E., Baraba, K., Ballester, C. J., Nguyen, L., Monory, K., Marsicano, G., Di, V., Hurd, Y. L., Guillemot, F., Mackie, K., Lutz, B., Guzma, M., Lu, H., Galve-roperh, I., & Harkany, T. (2008). *Endocannabinoid signaling controls pyramidal cell specification and long-range axon patterning*. *105 (25)*, 8760–8765. https://doi.org/https://doi.org/10.1073/pnas.0803545105

Mulder, J., Aguado, T., Keimpema, E., Barabás, K., Rosado, C. J. B., Nguyen, L., Menory, K., Marsicano, G., Di Marzo, V., Hurd, Y. L., Guillemot, F., Mackie, K., Lutz, B., Guzmán, M., Lu, H. C., Galve-Roperh, I., & Harkany, T. (2008). Endocannabinoid signaling controls pyramidal cell specification and long-range axon patterning. *Proceedings of the National Academy of Sciences of the United States of America*. https://doi.org/10.1073/pnas.0803545105

Muller-Eberhard, H. J. (1988). Molecular organization and function of the complement system. *Annual Review of Biochemistry*, *57*, 321–347. https://doi.org/10.1146/annurev.bi.57.070188.001541

Murray, S. A., Eppig, J. T., Smedley, D., Simpson, E. M., & Rosenthal, N. (2012). Beyond knockouts: Cre resources for conditional mutagenesis. *Mammalian Genome*, *23*, 587–599. https://doi.org/10.1007/s00335-012-9430-2

Nadarajah, B., Brunstrom, J. E., Grutzendler, J., Wong, R. O. L., & Pearlman, A. L. (2001). Two modes of radial migration in early development of the cerebral cortex. *Nature Neuroscience*, *4*(2), 143–150. https://doi.org/10.1038/83967

Nadarajah, B., & Parnavelas, J. G. (2002). Modes of neuronal migration in the developing cerebral cortex. *Nature Reviews. Neuroscience*, *3*(6), 423–432. https://doi.org/10.1038/nrn845

Nagaoka, R., Abe, H., & Obinata, T. (1996). Site-directed mutagenesis of the phosphorylation site of cofilin: Its role in cofilin-actin interaction and cytoplasmic localization. *Cell Motility and the Cytoskeleton*, *35*(3), 200–209. https://doi.org/10.1002/(SICI)1097-0169(1996)35:3<200::AID-CM3>3.0.CO;2-C

Nithipatikom, K., Gomez-Granados, A. D., Tang, A. T., Pfeiffer, A. W., Williams, C. L., & Campbell, W. B. (2012). Cannabinoid receptor type 1 (CB1) activation inhibits small GTPase RhoA activity and regulates motility of prostate carcinoma cells. *Endocrinology*, *153*(1), 29–41. https://doi.org/10.1210/en.2011-1144

Niu, S., Renfro, A., Quattrocchi, C. C., Sheldon, M., & D'Arcangelo, G. (2004). Reelin Promotes Hippocampal Dendrite Development through the VLDLR/ApoER2-Dab1 Pathway. *Neuron*, *41*(1), 71–84. https://doi.org/10.1016/S0896-6273(03)00819-5

Niu, S., Yabut, O., & D'Arcangelo, G. (2008). The reelin signaling pathway promotes dendritic spine development in hippocampal neurons. *Journal of Neuroscience*, *28*(41), 10339–10348. https://doi.org/10.1523/JNEUROSCI.1917-08.2008

O'Brien, A. R., Wilson, L. O. W., Burgio, G., & Bauer, D. C. (2019). Unlocking HDR-mediated nucleotide editing by identifying high-efficiency target sites using machine learning. *Scientific Reports*, *9*(1), 1–10. https://doi.org/10.1038/s41598-019-39142-0

Ogawa, M., Miyata, T., Nakajimat, K., Yagyu, K., Seike, M., Ikenaka, K., Yamamoto, H., & Mikoshibat, K. (1995). The reeler gene-associated antigen on cajal-retzius neurons is a crucial molecule for laminar organization of cortical neurons. *Neuron*, *14*(5), 899–912. https://doi.org/10.1016/0896-6273(95)90329-1

Olmsted, J. B., Carlson, K., Klebe, R., Ruddle, F., & Rosenbaum, J. (1970). Isolation of microtubule protein from cultured mouse neuroblastoma cells. *Proceedings of the National Academy of Sciences of the United States of America*, *Jan*(65(1)), 129–136. https://doi.org/10.1073/pnas.65.1.129

Olson, E. C., Kim, S., & Walsh, C. A. (2006). Impaired neuronal positioning and dendritogenesis in the neocortex after cell-autonomous Dab1 suppression. *Journal of Neuroscience*, *26*(6), 1767–1775. https://doi.org/10.1523/JNEUROSCI.3000-05.2006

Oudin, M. J., Hobbs, C., & Doherty, P. (2011). DAGL-dependent endocannabinoid signalling: Roles in axonal pathfinding, synaptic plasticity and adult neurogenesis. *European Journal of Neuroscience*, *34*(10), 1634–1646. https://doi.org/10.1111/j.1460-9568.2011.07831.x

Paria, B. C., & Dey, S. K. (2000). Ligand-receptor signaling with endocannabinoids in preimplantation embryo development and implantation. *Chemistry and Physics of Lipids*, *Nov*(108(1-2)), 211–220. https://doi.org/10.1016/S0009-3084(00)00197-3

Pawelczak, K. S., Gavande, N. S., VanderVere-Carozza, P. S., & Turchi, J. J. (2018). Modulating DNA Repair Pathways to Improve Precision Genome Engineering. *ACS Chemical Biology*, *Feb 16*(13(2)), 389–396. https://doi.org/10.1021/acschembio.7b00777

Pertwee, R. G. (1997). Pharmacology of cannabinoid CB1 and CB2 receptors. *Pharmacology and Therapeutics*, *74(2)*, 129–180. https://doi.org/10.1016/S0163-7258(97)82001-3

Pesold, C., Impagnatiello, F., Pisu, M., Uzunov, D., Costa, E., Guidotti, A., & Caruncho, H. (1998). Reelin is preferentially expressed in neurons synthesizing γ-aminobutyric acid in cortex and hippocampus of adult rats. *Proceedings of the National Academy of Sciences*, *95*(6), 3221–3226. https://doi.org/10.1073/pnas.95.6.3221

Picksley, S. M., Parsons, C. A., Kemper, B., & West, S. C. (1990). Cleavage specificity of bacteriophage T4 endonuclease VII and bacteriophage T7 endonuclease I on synthetic branch migratable holliday junctions. *Journal of Molecular Biology*, *Apr 20*(212(4)), 723–735. https://doi.org/10.1016/0022-2836(90)90233-C

Pielecka-Fortuna, J., Wagener, R. J., Martens, A. K., Goetze, B., Schmidt, K. F., Staiger, J. F., & Löwel, S. (2015). The disorganized visual cortex in reelin-deficient mice is functional and allows for enhanced plasticity. *Brain Structure and Function*, *220(6)*, 3449–3467. https://doi.org/10.1007/s00429-014-0866-x

Piomelli, D. (2003). The molecular logic of endocannabinoid signalling. *Nature Reviews. Neuroscience*, *4*(11), 873–884. https://doi.org/10.1038/nrn1247

Pourcel, C., Salvignol, G., & Vergnaud, G. (2005). CRISPR elements in Yersinia pestis acquire new repeats by preferential uptake of bacteriophage DNA, and provide additional tools for evolutionary studies. *Microbiology*, *151*(3), 653–663. https://doi.org/10.1099/mic.0.27437-0

Preet, A., Ganju, R. K., & Groopman, J. E. (2008). Δ9-Tetrahydrocannabinol inhibits epithelial growth

factor-induced lung cancer cell migration in vitro as well as its growth and metastasis in vivo. *Oncogene*, *Jan 10*(27(3)), 339–346. https://doi.org/10.1038/sj.onc.1210641

Quadros, R. M., Miura, H., Harms, D. W., Akatsuka, H., Sato, T., Aida, T., Redder, R., Richardson, G. P., Inagaki, Y., Sakai, D., Buckley, S. M., Seshacharyulu, P., Batra, S. K., Behlke, M. A., Zeiner, S. A., Jacobi, A. M., Izu, Y., Thoreson, W. B., Urness, L. D., … Gurumurthy, C. B. (2017). Easi-CRISPR: A robust method for one-step generation of mice carrying conditional and insertion alleles using long ssDNA donors and CRISPR ribonucleoproteins. *Genome Biology*, *18*(92). https://doi.org/10.1186/s13059-017-1220-4

Rajesh, M., Mukhopadhyay, P., Bátkai, S., Haskó, G., Liaudet, L., Huffman, J. W., Csiszar, A., Ungvari, Z., Mackie, K., Chatterjee, S., & Pacher, P. (2007). CB2-receptor stimulation attenuates TNF-α-induced human endothelial cell activation, transendothelial migration of monocytes, and monocyte-endothelial adhesion. *American Journal of Physiology - Heart and Circulatory Physiology*, *293(4)*, H2210–H2218. https://doi.org/10.1152/ajpheart.00688.2007

Rakic, P. (1972). Mode of cell migration to the superficial layers of fetal monkey neocortex. *Journal of Comparative Neurology*, *145*(1), 61–83. https://doi.org/10.1002/cne.901450105

Rakic, P. (1974). Neurons in Rhesus Monkey Visual Cortex: Systematic Relation between Time of Origin and Eventual Disposition. *Science*, *183*(4123), 425–427. https://doi.org/DOI: 10.1126/science.183.4123.425

Rakic, P. (2006). A century of progress in corticoneurogenesis: From silver impregnation to genetic engineering. *Cerebral Cortex*, *16*(i3--i17). https://doi.org/10.1093/cercor/bhk036

Rakic, P. (2009). Evolution of the neocortex: A perspective from developmental biology. *Nature Reviews Neuroscience*, *10*(10), 724–735. https://doi.org/10.1038/nrn2719

Rakic, P., & Caviness, V. S. (1995a). Cortical development: View from neurological mutants two decades later. *Neuron*, *14*(6), 1101–1104. https://doi.org/10.1016/0896-6273(95)90258-9

Rakic, P., & Caviness, V. S. (1995b). Cortical development: View from neurological mutants two decades later. In *Neuron* (Vol. 14, Issue 6, pp. 1101–1104). https://doi.org/10.1016/0896-6273(95)90258-9

Ran, F. A., Hsu, P. D., Wright, J., Agarwala, V., Scott, D. A., & Zhang, F. (2013). Genome engineering using the CRISPR-Cas9 system. *Nature Protocols*, *8*, 2281–2308. https://doi.org/10.1038/nprot.2013.143

Retzius, G. (1893). Die Cajal'schen Zellen der Grosshirnrinde beim Menschen und bei Säugethieren. *Biol Unters Neue Folge*, *5*, 1–8.

Retzius, G. (1894). Weitere Beiträge zur Kenntniss der Cajal'schen Zellen der Grosshirnrinde des Menschen. Biologische Untersuchungen. *Neue Folge*, *6*, 29–36.

Rice, D. S., & Curran, T. (2001). Role of the Reelin Signaling Pathway in Central Nervous System Development. *Annual Review of Neuroscience*, *24*, 1005–1039. https://doi.org/10.1146/annurev.neuro.24.1.1005

Rice, D. S., Sheldon, M., D'Arcangelo, G., Nakajima, K., Goldowitz, D., & Curran, T. (1998). Disabled-1 acts downstream of Reelin in a signaling pathway that controls laminar organization in the mammalian brain. *Development*, *Sep 125*(18), 3719–3729.

Richard, D., Guesdon, B., & Timofeeva, E. (2009). The brain endocannabinoid system in the regulation of energy balance. *Best Practice and Research: Clinical Endocrinology and Metabolism*, *Feb 23*(1), 17–32. https://doi.org/10.1016/j.beem.2008.10.007

Rose, J. C., Popp, N. A., Richardson, C. D., Stephany, J. J., Mathieu, J., Wei, C. T., Corn, J. E., Maly, D. J., & Fowler, D. M. (2020). Suppression of unwanted CRISPR-Cas9 editing by co-administration of catalytically inactivating truncated guide RNAs. *Nature Communications*, *11*(1), 1–11. https://doi.org/10.1038/s41467-020-16542-9

Rothstein, R. J. (1983). [12] One-step gene disruption in yeast. *Methods in Enzymology*, *101*(C), 202–211. https://doi.org/10.1016/0076-6879(83)01015-0

Rouet, P., Smih, F., & Jasin, M. (1994). Introduction of double-strand breaks into the genome of mouse cells by expression of a rare-cutting endonuclease. *Molecular and Cellular Biology*, *14*(12), 8096–8106. https://doi.org/10.1128/mcb.14.12.8096-8106.1994

Royaux, I., De Rouvroit, C. L., D'Arcangelo, G., Demirov, D., & Goffinet, A. M. (1997). Genomic organization of the mouse reelin gene. *Genomics*, *Dec 1;46*(2), 240–250. https://doi.org/10.1006/geno.1997.4983

Rubenstein, J. L. R., Anderson, S., Shi, L., Miyashita-Lin, E., Bulfone, A., & Hevner, R. (1999). Genetic control of cortical regionalization and connectivity. *Cerebral Cortex*, *Sep 9*(6), 524–532. https://doi.org/10.1093/cercor/9.6.524

Saez, T. M. M., Aronne, M. P., Caltana, L., & Brusco, A. H. (2014). Prenatal exposure to the CB1 and CB2 cannabinoid receptor agonist WIN 55,212-2 alters migration of early-born glutamatergic neurons and GABAergic interneurons in the rat cerebral cortex. *Journal of Neurochemistry*, *May 129*(4), 637–648. https://doi.org/10.1111/jnc.12636

Sakurai, T., Watanabe, S., Kamiyoshi, A., Sato, M., & Shindo, T. (2014). A single blastocyst assay optimized for detecting CRISPR/Cas9 system-induced indel mutations in mice. *BMC Biotechnology*, *14*, 1–11. https://doi.org/10.1186/1472-6750-14-69

Saleh-Gohari, N., & Helleday, T. (2004). Conservative homologous recombination preferentially repairs DNA double-strand breaks in the S phase of the cell cycle un human cells. *Nucleic Acids Research*, *32*(12), 3683–3688. https://doi.org/10.1093/nar/gkh703

Sander, J. D., & Joung, J. K. (2014). CRISPR-Cas systems for editing, regulating and targeting genomes. *Nature Biotechnology*, *32*(4), 347–350. https://doi.org/10.1038/nbt.2842

Sargent, R. G., Brenneman, M. A., & Wilson, J. H. (1997). Repair of site-specific double-strand breaks in a mammalian chromosome by homologous and illegitimate recombination. *Molecular and Cellular Biology*, *17*(1), 267–277. https://doi.org/10.1128/mcb.17.1.267

Scherer, S., & Davis, R. W. (1979). Replacement of chromosome segments with altered DNA sequences constructed in vitro. *Proceedings of the National Academy of Sciences of the United States of America*, *76*(10), 4951–4955. https://doi.org/10.1073/pnas.76.10.4951

Schindelin, J., Arganda-Carreras, I., Frise, E., Kaynig, V., Longair, M., Pietzsch, T., Preibisch, S., Rueden, C., Saalfeld, S., Schmid, B., Tinevez, J. Y., White, D. J., Hartenstein, V., Eliceiri, K., Tomancak, P., & Cardona, A. (2012). Fiji: An open-source platform for biological-image analysis. *Nature Methods*, *9*(7), 676–682. https://doi.org/10.1038/nmeth.2019

Schmid, P. C., Paria, B. C., Krebsbach, R. J., Schmid, H. H. O., & Dey, S. K. (1997). Changes in anandamide levels in mouse uterus are associated with uterine receptivity for embryo implantation. *Proceedings of the National Academy of Sciences of the United States of America*, *Apr 15;94*(8), 4188–4192. https://doi.org/10.1073/pnas.94.8.4188

Sekine, K., Honda, T., Kawauchi, T., Kubo, K. ichiro, & Nakajima, K. (2011). The outermost region of the developing cortical plate is crucial for both the switch of the radial migration mode and the

dab1-dependent “inside-out” lamination in the neocortex. *Journal of Neuroscience*, *31*(25), 9426–9439. https://doi.org/10.1523/JNEUROSCI.0650-11.2011

Sekine, K., Kawauchi, T., Kubo, K.-I., Honda, T., Herz, J., Hattori, M., Kinashi, T., & Nakajima, K. (2012). Reelin controls neuronal positioning by promoting cell-matrix adhesion via inside-out activation of integrin α5β1. *Neuron*, *76*(2), 353–369. https://doi.org/10.1016/j.neuron.2012.07.020

Sentmanat, M. F., Peters, S. T., Florian, C. P., Connelly, J. P., & Pruett-Miller, S. M. (2018). A Survey of Validation Strategies for CRISPR-Cas9 Editing. *Scientific Reports*, *8*(1). https://doi.org/10.1038/s41598-018-19441-8

Sheldon, M., Rice, D. S., D’Arcangelo, G., Yoneshima, H., Nakajima, K., Mikoshiba, K., Howell, B. W., Cooper, J. A., Goldowitz, D., & Curran, T. (1997). Scrambler and yotari disrupt the disabled gene and produce a reeler- like phenotype in mice. *Nature*, *389*(6652), 730–733. https://doi.org/10.1038/39601

Simon, A., Roland, A., Leterrier, C., Lenkei, Z., Vitalis, T., & Laine, J. (2008). *The type 1 cannabinoid receptor is highly expressed in embryonic cortical projection neurons and negatively regulates neurite growth in vitro*. *28*, 1705–1718. https://doi.org/10.1111/j.1460-9568.2008.06484.x

Skarnes, W. C. (2015). Is mouse embryonic stem cell technology obsolete? *Genome Biology*, *16*(1), 109. https://doi.org/10.1186/s13059-015-0673-6

Skarnes, W. C., Rosen, B., West, A. P., Koutsourakis, M., Bushell, W., Iyer, V., Mujica, A. O., Thomas, M., Harrow, J., Cox, T., Jackson, D., Severin, J., Biggs, P., Fu, J., Nefedov, M., De Jong, P. J., Stewart, A. F., & Bradley, A. (2011). A conditional knockout resource for the genome-wide study of mouse gene function. *Nature*, *474*, 337–342. https://doi.org/10.1038/nature10163

Smithies, O., Gregg, R. G., Boggst, S. S., Koralewski, M. A., & Kucherlapati, R. S. (1985). Insertion of DNA sequences into the locus by homologous recombination. *Nature*, *317*, 230–236.

Sonoda, E., Hochegger, H., Saberi, A., Taniguchi, Y., & Takeda, S. (2006). Differential usage of non-homologous end-joining and homologous recombination in double strand break repair. *DNA Repair*, *5*(9–10), 1021–1029. https://doi.org/10.1016/j.dnarep.2006.05.022

Soriano, E., & Del Río, J. A. (2005). The cells of cajal-retzius: still a mystery one century after. *Neuron*, *46*(3), 389–394. https://doi.org/10.1016/j.neuron.2005.04.019

Soriano, E., Del Río, J. A., Martínez, A., & Supèr, H. (1994). Organization of the embryonic and early postnatal murine hippocampus. I. Immunocytochemical characterization of neuronal populations in the subplate and marginal zone. *Journal of Comparative Neurology*, *342*(4), 571–595. https://doi.org/10.1002/cne.903420406

Srinivas, S., Watanabe, T., Lin, C. S., William, C. M., Tanabe, Y., Jessell, T. M., & Costantini, F. (2001). Cre reporter strains produced by targeted insertion of EYFP and ECFP into the ROSA26 locus. *BMC Developmental Biology*, *1*, 1–8. https://doi.org/10.1186/1471-213X-1-4

Sternberg, S. H., Richter, H., Charpentier, E., & Qimron, U. (2016). Adaptation in CRISPR-Cas Systems. *Molecular Cell*, *61*(6), 797–808. https://doi.org/10.1016/j.molcel.2016.01.030

Strathdee, D., Ibbotson, H., & Grant, S. G. N. (2006). Expression of transgenes targeted to the Gt(ROSA)26Sor locus is orientation dependent. *PLoS ONE*, *1*(1). https://doi.org/10.1371/journal.pone.0000004

Sun, X., & Dey, S. K. (2008). Aspects of endocannabinoid signaling in periimplantation biology. *Molecular and Cellular Endocrinology*, *286*(1–2), S3–S11. https://doi.org/10.1016/j.mce.2008.01.002

Sweet, H. O., Bronson, R. T., Johnson, K. R., Cook, S. A., & Davisson, M. T. (1996). Scrambler, a new neurological mutation of the mouse with abnormalities of neuronal migration. *Mammalian Genome*, *7*(11), 798–802. https://doi.org/10.1007/s003359900240

Takahashi, K. A., & Castillo, P. E. (2006). The CB1 cannabinoid receptor mediates glutamatergic synaptic suppression in the hippocampus. *Neuroscience*, *139*(3), 795–802. https://doi.org/10.1016/j.neuroscience.2006.01.024

Tan, S. S., Kalloniatis, M., Sturm, K., Tam, P. P. L., Reese, B. E., & Faulkner-Jones, B. (1998). Separate progenitors for radial and tangential cell dispersion during development of the cerebral neocortex. *Neuron*, *21*(2), 295–304. https://doi.org/10.1016/S0896-6273(00)80539-5

Thomas, K. R., Folger, K. R., & Capecchi, M. R. (1986). High frequency targeting of genes to specific sites in the mammalian genome. *Cell*, *44*(3), 419–428. https://doi.org/10.1016/0092-8674(86)90463-0

Tissir, F., & Goffinet, A. M. (2003). Reelin and brain development. *Nature Reviews Neuroscience*, *4*(6), 496–505. https://doi.org/10.1038/nrn1113

Tortoriello G, Morris CV, Alpar A, Fuzik J, Shirran SL, Calvigioni D, Keimpema E, Botting CH, Reinecke K, Herdegen T, Courtney M, Hurd YL, H. T. (2014). Miswiring the brain: Δ9-tetrahydrocannabinol disrupts cortical development by inducing an SCG10/stathmin-2 degradation pathway. *EMBO Journal*, *33*(7), 668–685. https://doi.org/10.1002/embj.201386035

Trommsdorff, M., Gotthardt, M., Hiesberger, T., Shelton, J., Stockinger, W., Nimpf, J., Hammer, R. E., Richardson, J. A., & Herz, J. (1999). Reeler/disabled-like disruption of neuronal migration in knockout mice lacking the VLDL receptor and ApoE receptor 2. *Cell*, *97*(6), 689–701. https://doi.org/10.1016/S0092-8674(00)80782-5

Ukai, H., Kiyonari, H., & Ueda, H. R. (2017). Production of knock-in mice in a single generation from embryonic stem cells. *Nature Protocols*, *12*(12), 2513–2530. https://doi.org/10.1038/nprot.2017.110

Urnov, F. D., Rebar, E. J., Holmes, M. C., Zhang, H. S., & Gregory, P. D. (2010). Genome editing with engineered zinc finger nucleases. *Nature Reviews Genetics*, *11*, 636–646. https://doi.org/10.1038/nrg2842

Vitalis, T., Lainé, J., Simon, A., Roland, A., Leterrier, C., & Lenkei, Z. (2008). The type 1 cannabinoid receptor is highly expressed in embryonic cortical projection neurons and negatively regulates neurite growth in vitro. *European Journal of Neuroscience*, *28*(9), 1705–1718. https://doi.org/10.1111/j.1460-9568.2008.06484.x

Voss, A. K., Britto, J. M., Dixon, M. P., Sheikh, B. N., Collin, C., Tan, S. S., & Thomas, T. (2008). C3G regulates cortical neuron migration, preplate splitting and radial glial cell attachment. *Development*, *135*(12), 2139–2149. https://doi.org/10.1242/dev.016725

Vouillot, L., Thélie, A., & Pollet, N. (2015). Comparison of T7E1 and surveyor mismatch cleavage assays to detect mutations triggered by engineered nucleases. *G3: Genes, Genomes, Genetics*, *5*(3), 407–415. https://doi.org/10.1534/g3.114.015834

Wagener, R. J., Dávid, C., Zhao, S., Haas, C. A., & Staiger, J. F. (2010). The somatosensory cortex of reeler mutant mice shows absent layering but intact formation and behavioral activation of columnar somatotopic maps. *Journal of Neuroscience*, *30*(46), 15700–15709. https://doi.org/10.1523/JNEUROSCI.3707-10.2010

Ware, M. L., Fox, J. W., González, J. L., Davis, N. M., Lambert De Rouvroit, C., Russo, C. J., Chua, S. C.,

Goffinet, A. M., & Walsh, C. A. (1997). Aberrant splicing of a mouse disabled homolog, mdab1, in the scrambler mouse. *Neuron*, *19*(2), 239–249. https://doi.org/10.1016/S0896-6273(00)80936-8

Ware, M. L., Tavazoie, S. F., Reid, C. B., & Walsh, C. A. (1999). Coexistence of widespread clones and large radial clones in early embryonic ferret cortex. *Cerebral Cortex*, *9*(6), 636–645. https://doi.org/10.1093/cercor/9.6.636

Watson, S., Chambers, D., Hobbs, C., Doherty, P., & Graham, A. (2008). The endocannabinoid receptor, CB1, is required for normal axonal growth and fasciculation. *Molecular and Cellular Neuroscience*, *38*(1), 89–97. https://doi.org/10.1016/j.mcn.2008.02.001

Wefers, B., Bashir, S., Rossius, J., Wurst, W., & Kühn, R. (2017). Gene editing in mouse zygotes using the CRISPR/Cas9 system. *Methods*, *121–122*, 55–67. https://doi.org/10.1016/j.ymeth.2017.02.008

Wonders, C. P., & Anderson, S. A. (2006). The origin and specification of cortical interneurons. *Nature Reviews Neuroscience*, *7*(9), 687–696. https://doi.org/10.1038/nrn1954

Wu, C. S., Zhu, J., Wager-Miller, J., Wang, S., O'Leary, D., Monory, K., Lutz, B., MacKie, K., & Lu, H. C. (2010). Requirement of cannabinoid CB1 receptors in cortical pyramidal neurons for appropriate development of corticothalamic and thalamocortical projections. *European Journal of Neuroscience*, *32*(5), 693–706. https://doi.org/10.1111/j.1460-9568.2010.07337.x

Wu, X., Scott, D. A., Kriz, A. J., Chiu, A. C., Hsu, P. D., Dadon, D. B., Cheng, A. W., Trevino, A. E., Konermann, S., Chen, S., Jaenisch, R., Zhang, F., & Sharp, P. A. (2015). Genome-wide binding of the CRISPR endonuclease Cas9 in mammalian cells Xuebing. *Nat Biotechnol*, *32*(7), 670–676. https://doi.org/10.1038/nbt.2889.Genome-wide

Xiaochun Gu, Yan Yan, Hanlin Li, Dongyang He, Samuel J. Pleasure, A., & Zhao, C. (2008). Characterization of the Frizzled10-CreER^{TM} Transgenic Mouse: An Inducible Cre Line for the Study of Cajal-Retzius Cell Development. *Bone*, *23*(1), 1–7. https://doi.org/10.1002/dvg.20472.Characterization

Yang, D., Scavuzzo, M. A., Chmielowiec, J., Sharp, R., Bajic, A., & Borowiak, M. (2016). Enrichment of G2/M cell cycle phase in human pluripotent stem cells enhances HDR-mediated gene repair with customizable endonucleases. *Scientific Reports*, *6*(January), 1–15. https://doi.org/10.1038/srep21264

Yang, H., Wang, H., Shivalila, C. S., Cheng, A. W., Shi, L., & Jaenisch, R. (2013). XOne-step generation of mice carrying reporter and conditional alleles by CRISPR/cas-mediated genome engineering. *Cell*, *154*(6), 1370. https://doi.org/10.1016/j.cell.2013.08.022

Yang, N., Higuchi, O., Ohashi, K., Nagata, K., Wada, A., Kangawa, K., Nishida, E., & Mizuno, K. (1998). Cofflin phosphorylation by LIM-kinase 1 and its role in Rac-mediated actin reorganization. *Nature*, *393*(6687), 809–812. https://doi.org/10.1038/31735

Yang, Z.-M., Paria, B. C., & Dey, S. K. (1996). Activation of Brain-Type Cannabinoid Receptors Interferes with Preimplantation Mouse Embryo Development1. *Biology of Reproduction*, *55*(4), 756–761. https://doi.org/10.1095/biolreprod55.4.756

Yoneshima, H., Nagata, E., Matsumoto, M., Yamada, M., Nakajima, K., Miyata, T., Ogawa, M., & Mikoshiba, K. (1997). A novel neurological mutant mouse, yotari, which exhibits reeler-like phenotype but expresses CR-50 antigen/Reelin. *Neuroscience Research*, *29*(3), 217–223. https://doi.org/10.1016/S0168-0102(97)00088-6

Yosef, I., Goren, M. G., & Qimron, U. (2012). Proteins and DNA elements essential for the CRISPR adaptation process in Escherichia coli. *Nucleic Acids Research*, *40*(12), 5569–5576. https://doi.org/10.1093/nar/gks216

Zebda, N., Bernard, O., Bailly, M., Welti, S., Lawrence, D. S., & Condeelis, J. S. (2000). Phosphorylation of Adf/Cofilin Abolishes Egf-Induced Actin Nucleation at the Leading Edge and Subsequent Lamellipod Extension. *Cell*, *151*(5), 1119–1128. https://doi.org/10.1083/jcb.151.5.1119

Zhang, G., Assadi, A. H., McNeil, R. S., Beffert, U., Wynshaw-Boris, A., Herz, J., Clark, G. D., & D'Arcangelo, G. (2007). The Pafah1b complex interacts with the reelin receptor VLDLR. *PLoS ONE*, *2*(2), e252. https://doi.org/10.1371/journal.pone.0000252

Zhou, Y., Falenta, K., & Lalli, G. (2014). Endocannabinoid signalling in neuronal migration. *International Journal of Biochemistry and Cell Biology*, *47*(1), 104–108. https://doi.org/10.1016/j.biocel.2013.12.007

6 Appendix

6.1 Supplementary information

6.1.1 PCR artefact using primer pair 1

The PCR products with primer pair 1 always showed multiple bands when amplifying DNA from heterozygous Reelin-Cre animals but not when amplifying DNA from homozygous Reelin-Cre animals. To find out whether unspecific binding or PCR artefacts causing the unspecific bands, another experiment with homozygous and wild-type PCR products was performed. PCR amplifications of two different samples, homozygous (-/-) (S1A, lane1) and wild-type (+/+) animals (S1A, lane2), were performed with primer pair 1. Additionally, DNA from both samples (+/+ and -/-) was mixed and a PCR with primer pair 1 was performed (S1A, lane 3). After the PCR, PCR products of WT (+/+, S1A lane 2) and homozygous mutants (-/-, S1A lane 1) were mixed and heated up to let them reanneal (heated up to 95°C for 5 min and ramped down to 25°C, then cooled down to 10°C) (S1A, lane 4).

The results on an agarose gel showed one clear expected band for homozygous mutant (1931bp, S1A lane 1) and wild-type (761 bp, S1A lane 2). When a PCR with DNA from both animals (WT and homozygous mutant) were mixed prior to PCR amplification, the unexpected bands (2300 bp and 1500 bp) appear beside the expected bands (761 bp and 1931 bp) (S1A lane 3). The same result can be seen when re-annealing the two clear PCR products from WT and homozygous mutants (S1A lane 4).

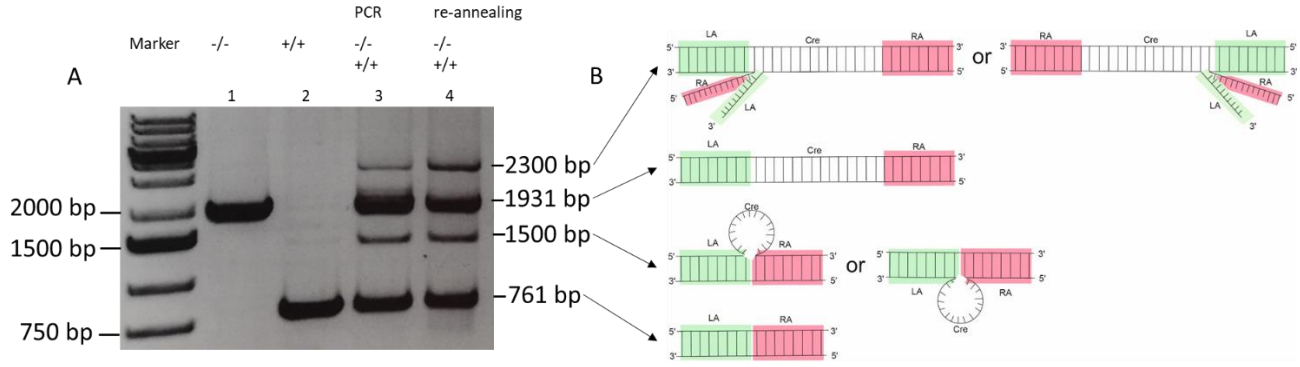

S 1 Analysis of PCR artefact.
A) Results for PCR with primer pair 1 from three different Reelin-Cre genotypes. Lane 1: homozygous mutant DNA with one clear band at 1931 bp. Lane 2: wild-type DNA (761 bp). Lane 3: Products after a PCR reaction with primer pair 1 and products from -/- and +/+. The result showed multiple expected (761 bp WT, 1931 bp MUT) and unexpected (2300 bp, 1500 bp) bands. Lane 4: Reannealed products of WT and homozygous DNA showed the same bands as seen in the PCR reaction of -/- and +/+. B) Possible reasons for multiple bands when combining WT and MUT product in one reaction could be different annealing conformations of WT and MUT products. For the 2300 bp band, two additional conformations are possible but not shown explicitly, whereby

the incomplete complementarities are present on the upper strand, and, thus, the lower strand contains the entire mutant sequence.

These results may hint to the possibility that the additional bands do not represent unintended coupling of the PCR primers to the genomic DNA but an unintended reannealing of WT and mutant PCR products due to the large homology they share in their homology arm sequence. At first glance, this possibility is not intuitively comprehensible, but is not impossible. A possible hypothesis can be that one WT product and one mutant product anneal for the 1500 bp band and the Cre-recombinase insert forms a loop. The 2300 bp product may result from annealing of two mutant products with one WT product (S1B).

To test the hypothesis, PCR products with primer pair 1 from heterozygous animals were separated on an agarose gel and single bands were cut out (Fig. 45). It was possible to separate 4 different bands: 2300 bp (A), 1931 bp (B), 1500 bp (C) and 761 bp (D). Important are the bands 2300 bp (A) and 1500 bp (C) because these bands were unexpected whereas the 1931 bp band corresponds to the mutant band and 761 bp to the wild-type band. Purified DNA was then either sent directly for sequencing or was subcloned into a TOPO vector. The TOPO vector was then transfected into bacteria, single colonies were picked and analyzed via restriction digest with EcoRI. The expected band size for the EcoRI digested wild-type sequence was 457 bp+ 334 bp and for the mutant sequence 1288 bp+ 370 bp+ 330 bp, respectively. The results revealed that clones with a subcloned band A contain a product whose expected EcoRI digested band size corresponds to that expected for mutant sequence (S2 A1, A2). The same results can be seen for band B (S2 B1, B2, B3) whereas the subcloned band C only shows the expected band size of a EcoRI digested wild-type sequence (S2 C1, C2, C3). Surprisingly, the digested bands for A (2300 bp) and C (1500 bp) never showed the size which could be seen on the gel. To verify these results, the purified clones were sent for sequencing.

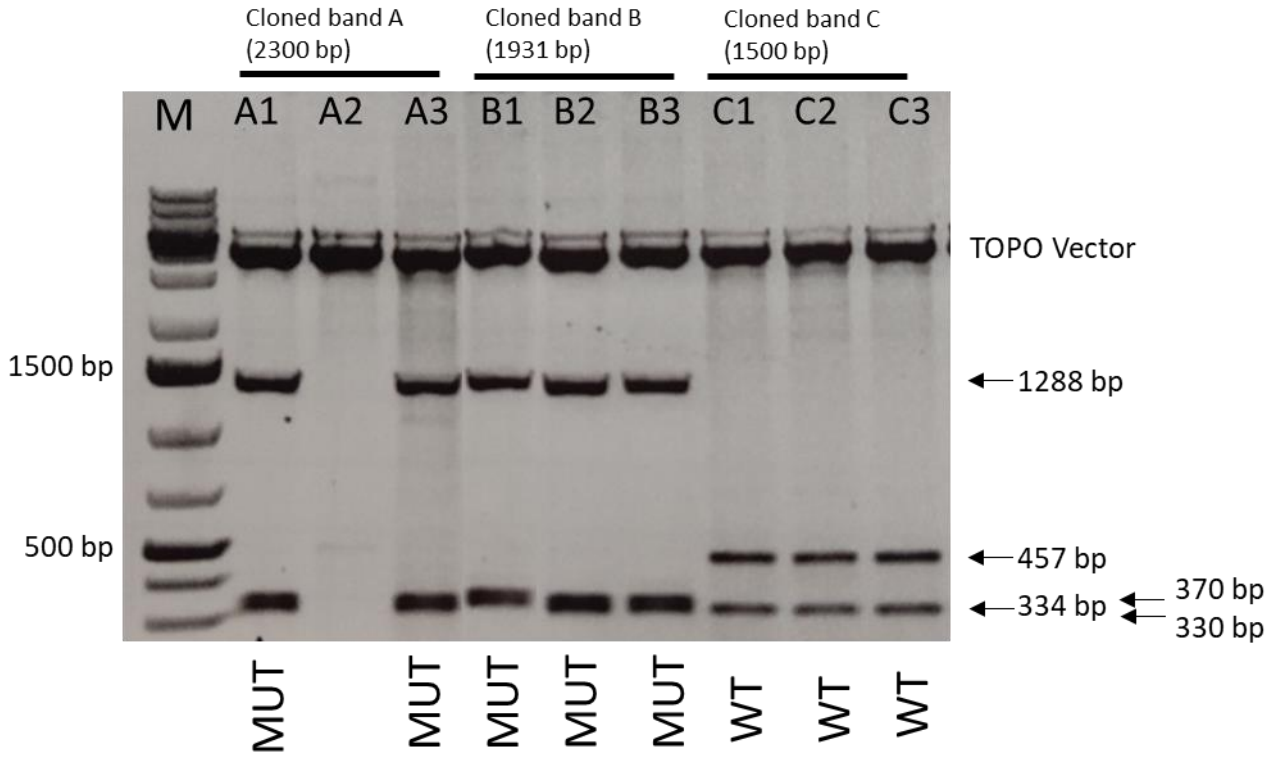

S 2 Representative agarose gel of EcoRI digested bacterial DNA. Bacteria were transfected with TOPO cloned vectors containing either PCR products of band A (2300 bp), B (1931 bp) or C (1500 bp) of founder 280.
The expected band size for the EcoRI digested wild-type sequence was 457 bp+ 334 bp and for the mutant sequence 1288 bp+ 370 bp+ 330 bp, respectively. Clones from band A (A1-3) and B (B1-3) transfected bacteria show the expected size for the mutant sequence and clones transfected with band C (C1-3) show the band sized which corresponds to the wild-type digested product.

Sequencing results of TOPO cloned PCR products confirmed the results from EcoRI digestion band A and B and showed a seamless mutant sequence without alterations (data not shown). The results for band C confirmed the wild-type sequence.

Importantly, PCR bands of the single bands, however, which were cut out from the gel and directly sent for sequencing, revealed a different result. Both bands, 2300 bp (band A, S3A) and 1500 bp (band C, S3B) showed united sequences, and did not show a sequence with the band size shown on the agarose gel (A 2300 bp, C 1500 bp) but a clear chromatogram signal for the complete mutant sequence with a mixed sequence beginning after the left homology arm sequence. Immediately when left homology arm sequence finishes, the quality of chromatogram signal deteriorates and shows a mixed signal. After 232 bp the quality of the chromatogram signal gets better and shows the Cre-sequence followed by the right homology arm sequence. When comparing the chromatogram for both, the following 2A-HA-NLS sequence as we would expect it for a mutant sequence and the chromato-

gram of the right homology arm which we would expect for a wild-type sequence, to the chromatogram we get, we can see that both sequences (for 2A-HA-NLS-Cre and the right homology arm) interfere with each other (S3).

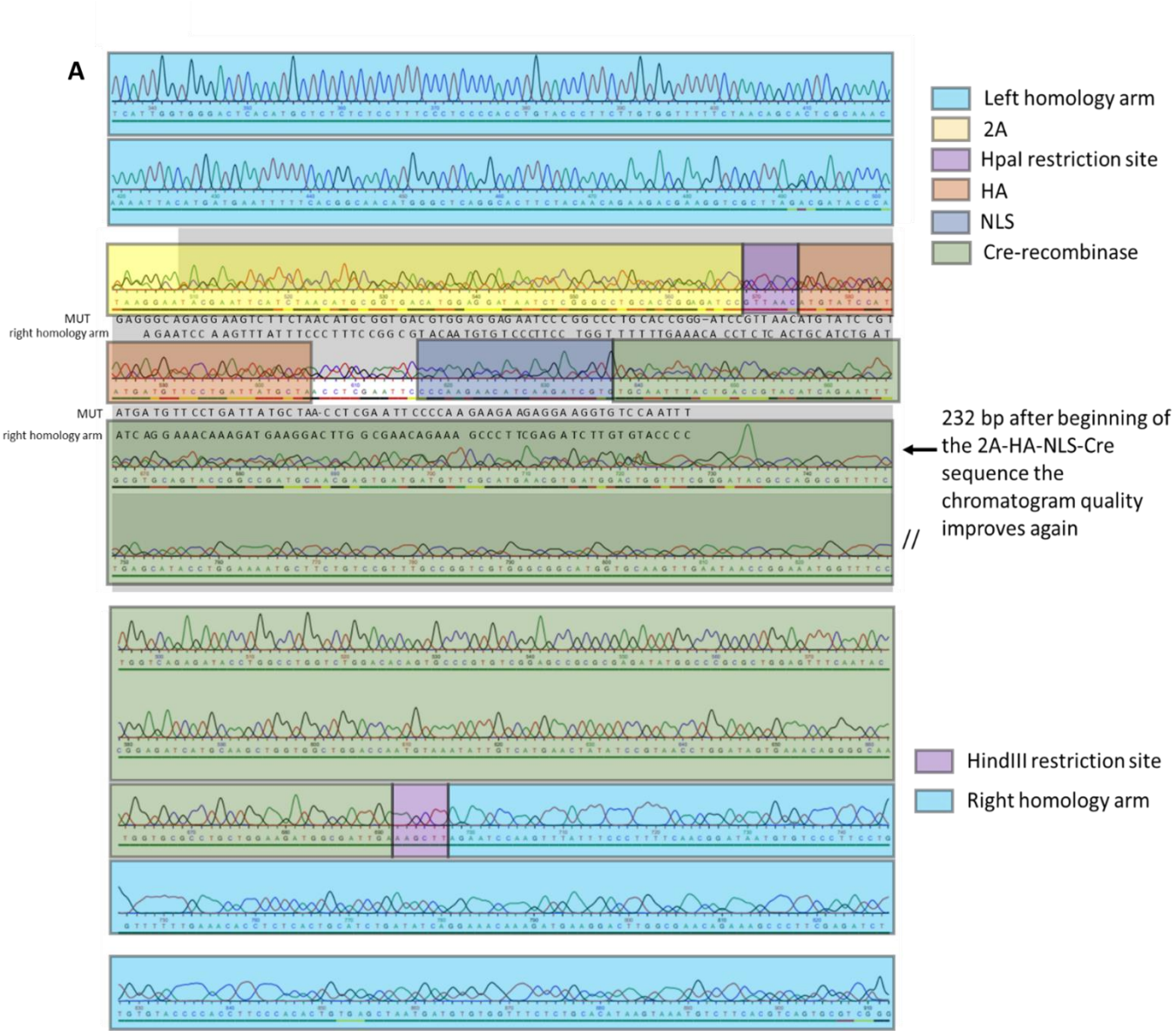

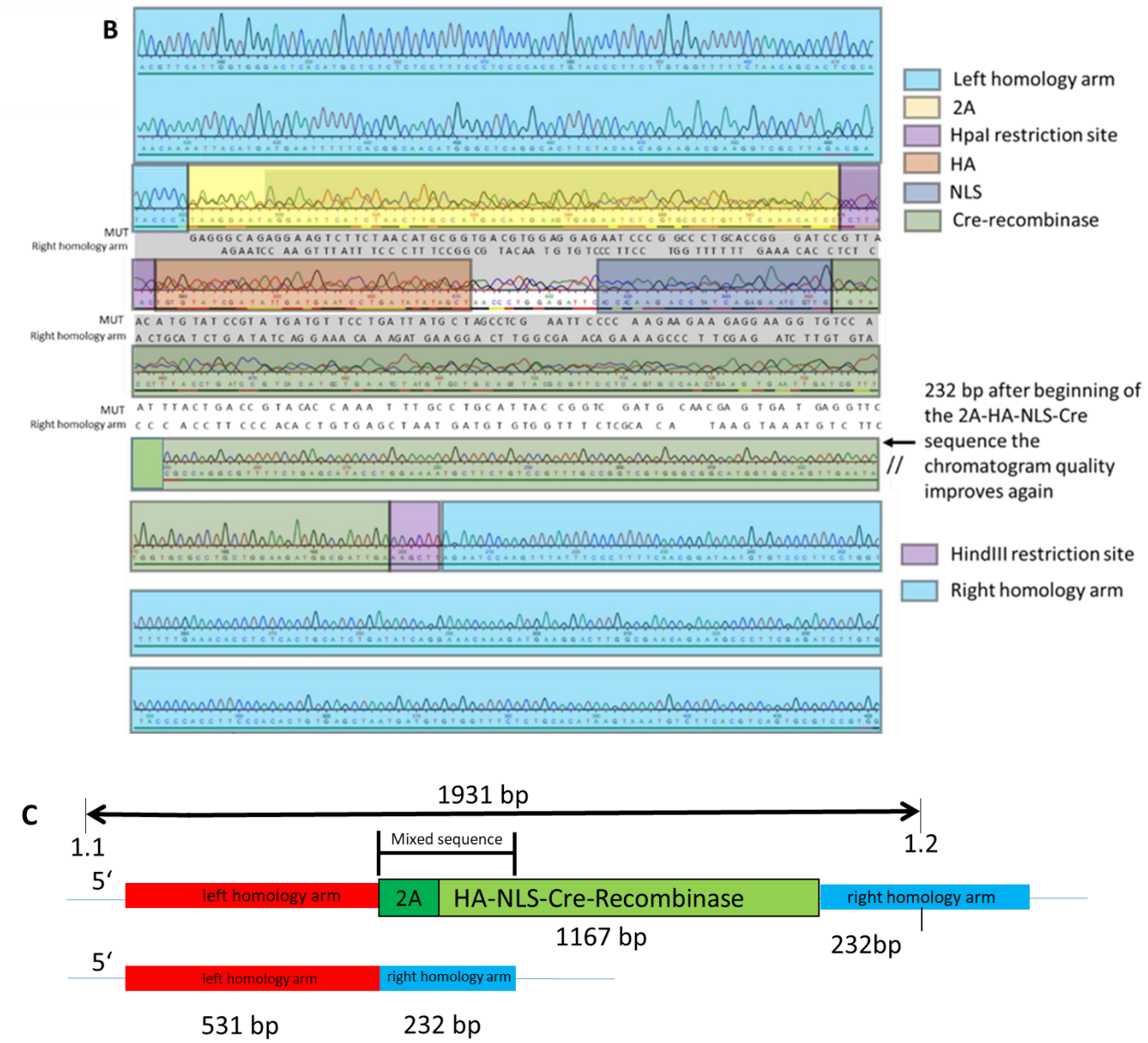

S 3 Representative sequence from band A from founder animal 233.
A, B) The results for both, band A (A) and C (B), show a mixed sequence when the sequence for the left homology arm ends. When comparing the peaks of the chromatogram to the expected WT and the expected MUT sequence, both sequences can be detected interfering with each other. 232 bp after the beginning of the mixed sequence it stops and the Cre-/right homology arm sequence without alterations can be detected.
C) An explanation for this finding could be that the PCR product of band A and band C contains both WT and MUT sequence. The difference between the two is that in the WT sequence the left homology arm sequence follows directly after the right homology arm whereas in the MUT sequence, the Cre-recombinase sequence is between the homology arm sequences. This is why there is a mixed sequence for 232 bp which is the size of the, by primer pair 1 amplified, right homology arm.

Another approach to test the hypothesis, is the digest of the heterozygous PCR products with T7EN1.

After PCR amplification of two heterozygous (S4 #1831 P1 and #1883 P1) and wild-type (S4 # 1832

P1) Reelin-Cre DNA with primer pair 1.1 and 1.2, all usual bands were visible (761 bp WT, 1931 bp MUT, unexpected bands: 1500 bp, 2300 bp). After T7 endonuclease digest the additional unexpected bands almost completely vanished and WT and MUT bands remained as well as some faint smaller bands (S4 # 1831 T7; #1833 T7; even more visible in the purified product # 1833 T7 aufg.). The WT product of the wild-type Reelin-Cre mouse did not change (S4 #1832 T7). As the 1500 bp and the 2300 bp bands faded after T7EN1 digest, these products must have been non-perfectly fitting PCR products/ single stranded DNA which could be cleaved by T7 endonuclease and now appear as smaller bands around 1200 bp and 500 bp. As the size of the Cre-insert is 1170 bp and one of the homology arms has a size of 477 bp one could assume that the faint bands of the cut products could belong to them. T7 is a structure-dependent enzyme and its activity on different DNA substrates cannot be precisely defined. T7 can recognizes for example hairpin structures, where the first nick occurs at the beginning of the loop but it is not clear where the nick is located on the opposite strand which will also eventually differ from molecule to molecule. For sure, it is known that T7 endonuclease has no activity against linear single-stranded DNA in general, but if double-stranded structures and loops are formed within the single-stranded construct, these can also be recognized. So, unfortunately, these results can not completely prove that the digested products are partially single-stranded DNA, as the expected bands can’t be determined exactly.

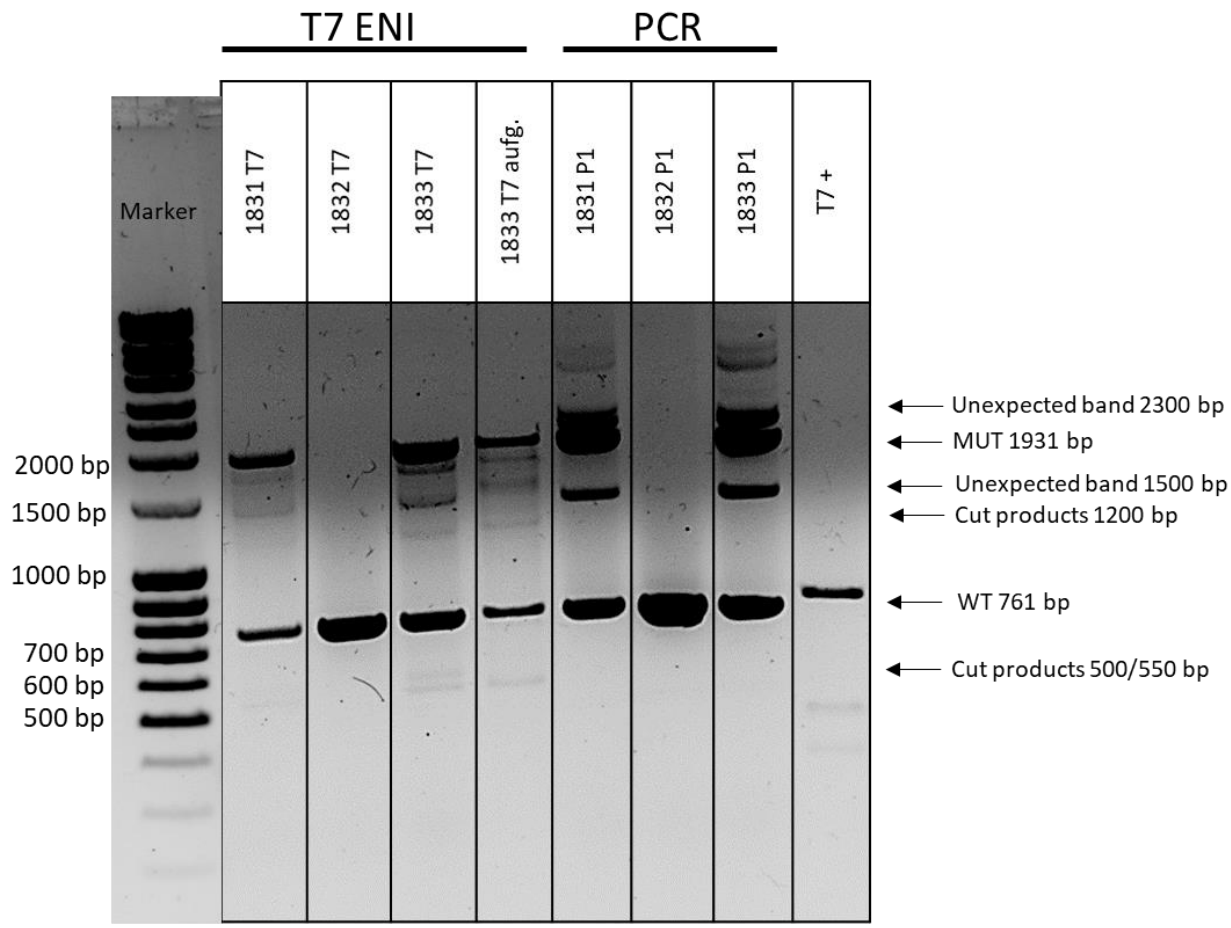

S 4 T7 Endonuclease assay on PCR amplified Reelin-Cre heterozygous and wild-type DNA with primer pair 1.1 and 1.2.

T7ENI: Results after T7EN1 digest showed faint multiple smaller bands when compared to undigested products, PCR: Results after PCR amplification prior to T7EN1 digest showed WT and Mutant band and besides unexpected bands with 2300 bp and 1500 bp. The rightmost lane shows the positive control, which was successfully digested by T7EN1 and confirmed proper functioning of the T7 Endonuclease.

Taken together all the results, the hypothesis regarding the structure of the additional and unexpected bands was tested using direct PCR fragment sequencing, cloning of the fragments into TOPO cloning vector and T7ENI digestion of the fragments. The results obtained did not disprove the hypothesis, but lack the direct prove of the existence of the proposed structure of the bands. One has to take into consideration that the formation of the structures as proposed in S1 are not well favorable from the thermodynamic point of view due to the long stretches with ssDNA.

6.1.2 Final HDR-Sequence

Sequence of final insertion

left homology arm (sgRNA1 + PAM)

cctcattccgctaatggagcttttgttttcattttagccctttaaggttgaaatgaaaatgttaactagcataaccgaatcgcttttgctgtgtatgtgt
gtaaataaggtaatgagtacagtgtgcatgtcctctggatggtgagatgtgttcaggttctgaaaagaaaaggactccggggcagaaggtagtg
aggcaggtgcccgtctaattattctgtccctaggcggtgaagtctgcatgacttctgaattctgaagtttttcagatatatagcaggctaccttgggg
ccttagaataaatcatacgttcattggtgggactcacatgctctctctcctttccctccccacctgtaccttcttgtggtttttctaacagcactcgca
aacaaaattacatgatgaatttttcacggcaacatgggctcaggcacttctacaacagaagacgaaggtcgcttagacgataccca

2A-HA-NLS-Cre

Gagggcagaggaagtcttctaacatgcggtgacgtggaggagaatcccggccctgcaccgggatccgttaacatgtatccgtatgatgttcctga
ttatgctagcctcgaattcccaagaagaagaggaaggtgtccaatttactgaccgtacaccaaaatttgcctgcattaccggtcgatgcaacga
gtgatgaggttcgcaagaacctgatggacatgttcagggatcgccaggcgttttctgagcatacctggaaaatgcttctgtccgtttgccggtcgtg
ggcggcatggtgcaagttgaataaccggaaatggtttcccgcagaacctgaagatgttcgcgattatcttctatatcttcaggcgcgcggtctggc
agtaaaaactatccagcaacatttgggccagctaaacatgcttcatcgtcggtccgggctgccacgaccaagtgacagcaatgctgtttcactggt
tatgcggcggatccgaaaagaaaacgttgatgccggtgaacgtgcaaaacaggctctagcgttcgaacgcactgacttcgaccaggttcgttcac
tcatggaaaatagcgatcgctgccaggatatacgtaatctggcatttctggggattgcttgtaacaccctgttacgtatagccgaaattgccagga
tcagggttaaagatatctcacgtactgacggtgggagaatgttaatccatattggcagaacgaaaacgctggttagcaccgcaggtgtagagaa
ggcacttagcctgggggtaactaaactggtcgagcgatggatttccgtctctggtgtagctgatgatccgaataactacctgttttgccgggtcaga
aaaaatggtgttgccgcgccatctgccaccagccagctatcaactcgcgccctggaagggatttttgaagcaactcatcgattgatttacggcgct
aaggatgactctggtcagagatacctggcctggtctggacacagtgcccgtgtcggagccgcgcgagatatggcccgcgctggagtttcaatacc
ggagatcatgcaagctggtggctggaccaatgtaaatattgtcatgaactatatccgtaacctggatagtgaaacaggggcaatggtgcgcctgc
tggaagatggcgattgaaagctt

Right homology arm (sgRNA2 + PAM)

Agaatccaagtttatttccctttcaacggataatgtgtcccttcctggttttttgaaacacctctcactgcatctgatatcaggaaacaaagatgaa
ggacttggcgaacagaaagcccttcgagatcttgtgtaccccaccttcccacactgtgagctaatgatgtgtggtttctctgcacataagtaaatgt
cttcacgtcagtgcgtccgtggaaattgtgatctgttgtaatatcagttacagtggcagtattgagaataagaaatagtttaacaggaaaaaacgt
ttaagcacaaacatttttaagatcttatgttttaagtggcattttagcacagtatttaacattgttggtcaccgagctatttaagtagactgtatttca
gctctgtctcttgtttatatgaataagttct

6.1.3 Sequencing data

Founder 280

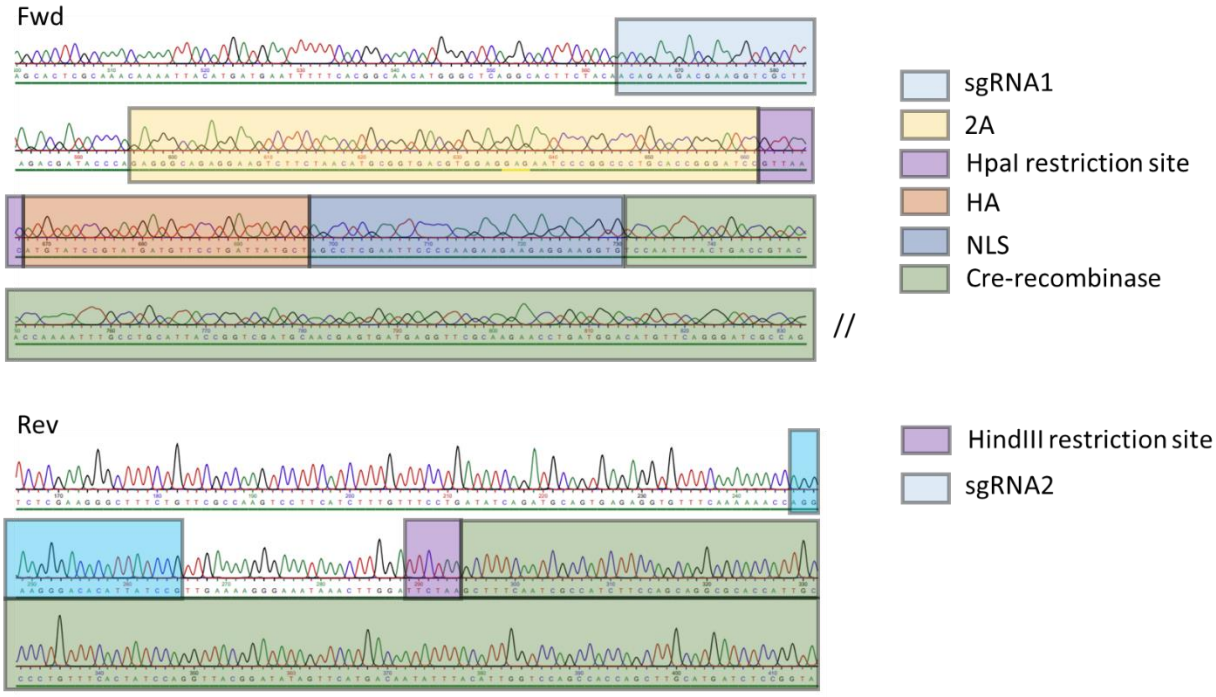

S 5 Sequencing data from Founder #280

Offspring of founder 233-1

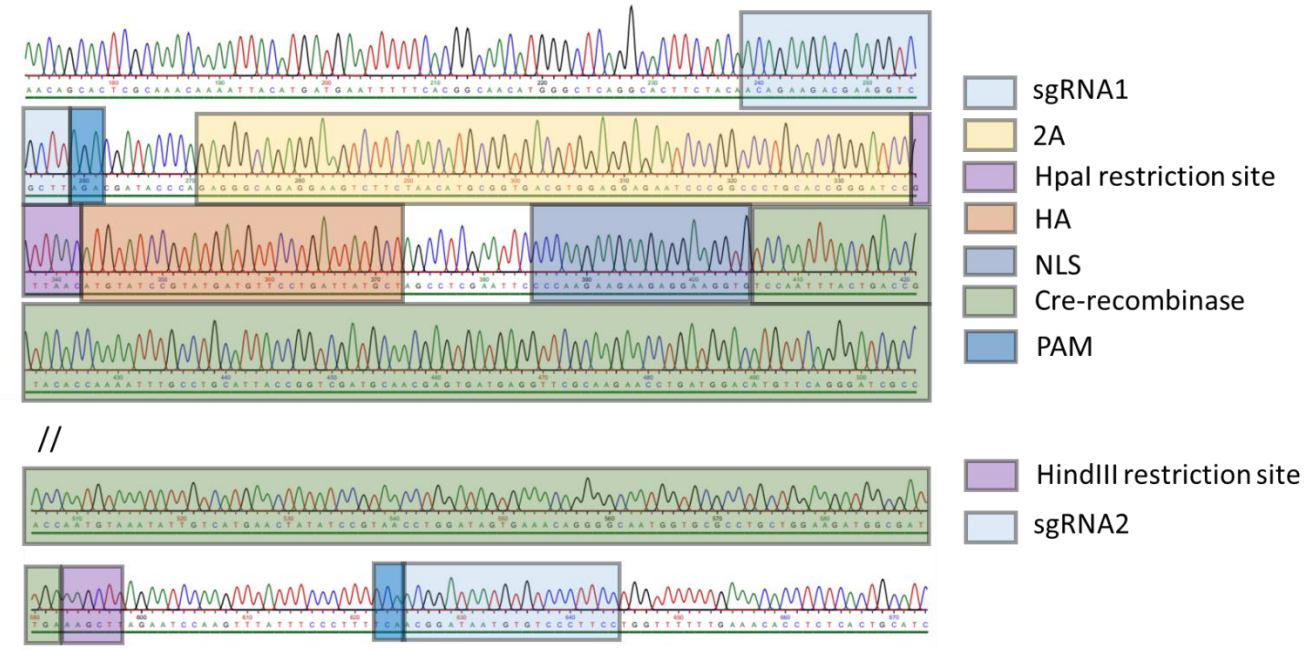

S 6 Sequencing data from successor of founder #233-1

Offspring of founder 233-3

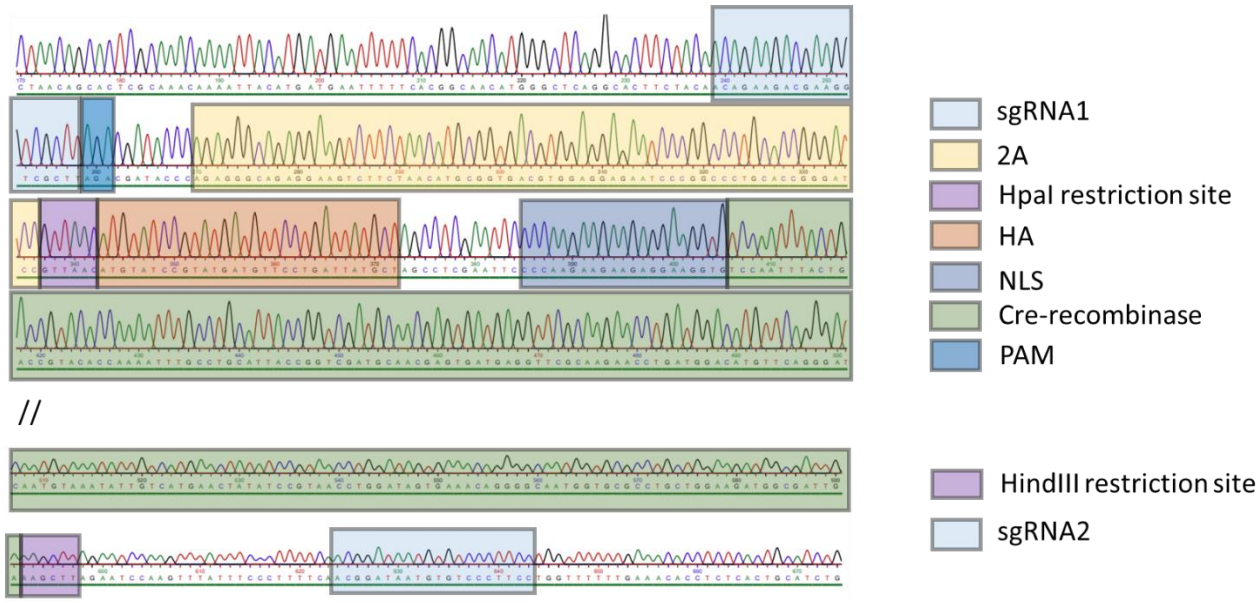

S 7 Sequencing data from successor of founder #233-3

Offspring of founder 233-6

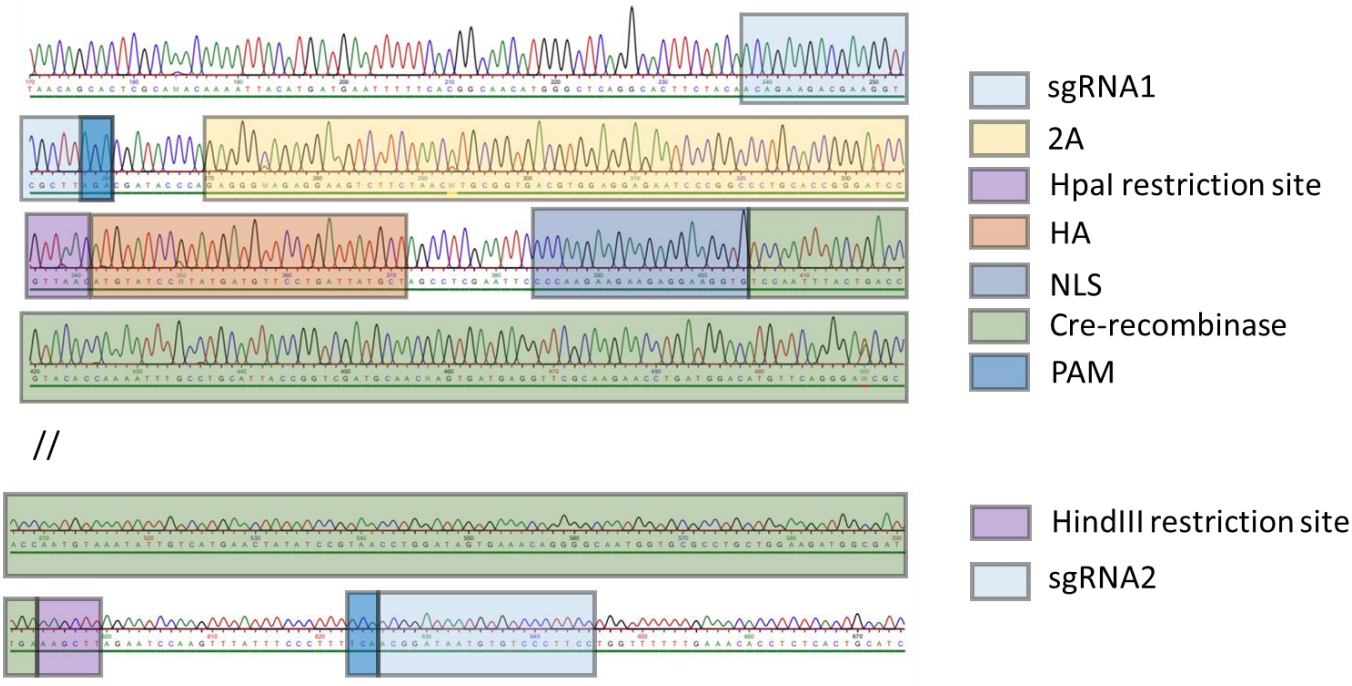

S 8 Sequencing data from successor of founder #233-6.

6.1.4 Colocalisation data list

	E10.5									
	BOQ8-3	9 sections		BOQ8-8	16 sections		BOQ8-9	13 sections		
	counted sections	total Reelin+ cells	total Reelin+/CB1+ cells	counted sections	total Reelin+ cells	total Reelin+/CB1+ cells		counted sections	total Reelin+ cells	total Reelin+/CB1+ cells
DP1	9	155	39	14	98	38	DP1+DP2	13	359	126
DP2	9	157	33	13	91	35				
DP3	9	163	46	15	118	41	DP3+DP4	11	317	122
DP4	8	173	36	9	89	19				
LP1	9	207	42	16	205	78	LP1+LP2	12	301	132
LP2	7	197	57	16	186	81				
LP3	8	207	33	16	183	72	LP3+LP4	12	284	137
LP4	6	238	59	16	167	71				
MP1	5	41	15	6	83	26	MP	11	372	179
MP2	2	47	27	1	7	3				

	E11.5									
	BZR5-3	12 sections		BZR5-6	15 sections		BTC3-7	12 sections		
	counted sections	total Reelin+ cells	total Reelin+/CB1+ cells	counted sections	total Reelin+ cells	total Reelin+/CB1+ cells		counted sections	total Reelin+ cells	total Reelin+/CB1+ cells
DP1	12	236	197	15	249	138	DP1+DP2	11	329	234
DP2	9	191	161	15	313	213				
DP3	12	262	220	15	247	146	DP3+DP4	11	209	139
DP4	9	201	170	15	291	208				
LP1	11	263	230	15	320	225	LP1+LP2	10	386	299
LP2	7	147	129	15	248	179				
LP3	11	296	241	15	353	259	LP3+LP4	11	292	203
LP4	7	157	135	15	310	221				
MP1	11	372	304	15	277	183	MP	8	481	395
MP2	9	350	265	15	297	191				

	E12.5								
	BTC4-1	10 sections		BTC4-3	9 sections		BTC4-4	12 sections	
	counted sections	total Reelin+ cells	total Reelin+/CB1+ cells	counted sections	total Reelin+ cells	total Reelin+/CB1+ cells	counted sections	total Reelin+ cells	total Reelin+/CB1+ cells
DP1	10	139	89	9	146	93	12	241	188
DP2	8	128	89	7	127	103	12	320	258
DP3	8	140	87	9	133	73	11	239	175
DP4	4	61	44	8	151	111	9	211	169
LP1	9	143	97	9	162	125	11	288	207
LP2	9	147	105	7	104	74	9	221	167
LP3	8	176	130	9	157	107	11	240	180
LP4	6	116	87	8	113	82	8	130	95
MP1	9	210	151	9	193	150	12	404	313
MP2	9	211	128	8	254	200	10	187	138

	E13.5								
	BTX5-3	27 sections		BTX5-5	25 sections		BTX5-8	7 sections	
	counted sections	total Reelin+ cells	total Reelin+/CB1+ cells	counted sections	total Reelin+ cells	total Reelin+/CB1+ cells	counted sections	total Reelin+ cells	total Reelin+/CB1+ cells
DP1	27	590	456	25	365	251	7	75	58
DP2	26	541	404	24	308	194	7	90	68
DP3	26	569	446	25	365	255	7	64	50
DP4	23	453	348	24	285	195	7	86	59
LP1	27	483	381	25	457	313	6	65	44
LP2	27	584	439	25	397	253	4	41	29
LP3	27	497	379	25	355	238	7	67	51
LP4	26	510	386	25	474	351	6	68	52
MP1	27	1126	916	25	547	437	7	200	160
MP2	26	1444	1210	25	773	583	7	107	76

	E14.5								
	BRD6-1	22 sections		BRD6-3	13 sections		BRD6-4	15 sections	
	counted sections	total Reelin+ cells	total Reelin+/CB1+ cells	counted sections	total Reelin+ cells	total Reelin+/CB1+ cells	counted sections	total Reelin+ cells	total Reelin+/CB1+ cells
DP1	21	224	158	13	162	112	15	176	128
DP2	21	216	152	12	151	110	15	159	119
DP3	22	260	196	12	150	105	15	178	137
DP4	22	238	174	12	136	97	13	151	113
LP1	22	188	132	13	150	118	15	191	149
LP2	21	227	167	13	165	134	15	216	175
LP3	22	222	159	13	136	109	15	157	118
LP4	21	242	191	12	157	122	13	157	114
MP1	21	497	347	13	233	180	15	301	230
MP2	20	311	225	11	325	249	13	382	297

S 9 List of all collected data from cell counting of CB1 and Reelin in situ hybridization stainings.
The data set is divided in 5 big rows. Every big row contains the information of one embryonic age of 3 different animals and gives information about the counted sections per animal in total. For every animal 10 different cortical areas (DP 1-4, LP 1-4 and MP1, 2) were counted and the sheet gives information about the amount of counted sections, the number of Reelin- positive cells and the number of Reelin and CB1 coexpressing cells for every counted area.

6.2 List of figures

List of figures in supplementary information

6.3 List of tables

6.4 Acknowledgments

6.5 Curriculum vitae

6.6 Declaration/ Eidesstaatliche Versicherung

I hereby declare that I wrote the dissertation submitted without any unauthorized external assistance and used only sources acknowledged in the work. All textual passages which are appropriated verbatim or paraphrased from published and unpublished texts as well as all information obtained from oral sources are duly indicated and listed in accordance with bibliographical rules. In carrying out this research, I complied with the rules of standard scientific practice as formulated in the statutes of Johannes Gutenberg University Mainz to insure standard scientific practice.

Hiermit erkläre ich, Jennifer Sitta, geboren am 14.7.1987 in Ludwigshafen am Rhein, dass ich meine Dissertation selbstständig und unter Verwendung der angegebenen Hilfsmittel angefertigt habe. Ich habe keinen anderen Promotionsversuch unternommen und die vorliegende Arbeit wurde für keine andere Prüfung verwendet.

_____ _____

Ort, Datum (Jennifer Sitta)